Amphiphilic Block Copolymers
as Templates for Particle Formation and Positioning

Von der Fakultät für Mathematik, Informatik und Naturwissenschaften der Rheinisch-Westfälischen Technischen Hochschule Aachen zur Erlangung des akademischen Grades eines Doktors der Naturwissenschaften genehmigte Dissertation

vorgelegt von

Diplom-Ingenieur

Błażej Gorzolnik

aus Warszawa, Polen

Berichter: Universitätsprofessor Dr. rer. nat. Martin Möller

Universitätsprofessor Dr. rer. nat. Walter Richtering

Tag der mündlichen Prüfung: 12. 11. 2007

Diese Dissertation ist auf den Internetseiten der Hochschulbibliothek online verfügbar.

Table of Contents

List of abbreviations, acronyms and symbols:

α	angle of dipping
β	parameter related to particle-particle and particle-substrate interactions
δ	chemical shift
ε	porosity
μ	solution viscosity
ρ	solution density
σ	surface tension
φ	particle volume fraction
χ_{AB}	Flory Huggins interaction parameter
μCP	microcontact printing
μL	microlitre
μm	micrometre
Å	Angstrom
°C	Celsius degree
2VP	2-vinylpyridine
AFM	Atomic Force Microscopy
ATRP	Atom-Transfer Radical Polymerisation
Au	gold
$AuCl_4^-$	chloroauric anion
BCl_3	trichloroborane
$(Bu)_2Mg$	dibutyl magnesium
c	concentration
CaH_2	calcium hydrate
$[CH_3(CH_2)_7]_3Al$	trioctylaluminum
$CHCl_3$	chloroform
CH_3I	methyl iodide
chlorosilane	2,2-Dimethyl-5-(chlorodimethylsilylpropyloxymethyl)-5-ethyl-1,3-dioxane
CMC	critical micelle concentration

$CoCl_2$	cobalt (II) chloride
CTC	center-to-center distance
d	doublet
DP	degree of polymerisation
DPE	1,1-diphenylethylene
DPMK	diphenylmethyl potassium
DPN	dip pen nanolithography
EO	ethylene oxide
eV	electron volt
g	gravitational constant
h	hour or thickness of the micellar array
H_2	hydrogen
$HAuCl_4*3H_2O$	tetrachloro auric acid
HCl	hydrogen chloride
HVL	high vacuum line
HRTEM	High-Resolution Transmission Electron Microscopy
FIB	Focus Ion Beam
FT-IR	Fourier Transform Infrared Spectroscopy
ITO	thin oxide
j_e	solvent evaporation flux
j_p	micelle flux
j_w	solvent flux
J_{HH}	spin-spin coupling constant
K^+	potassium ion
KBr	potassium bromide
kHz	kilohertz
KI	potassium iodide
KOH	potassium hydroxide
l	evaporation length
L	loading
LCM	large compound micelles
$LiAuCl_4$	lithium tetrachloroaurate (III)

LiAlH$_4$	lithium aluminium hydrate
LiCl	lithium chloride
m	multiplet
mbar	millibar
MBE	Molecular Beam Epitaxy
MCVD	Metalorganic Chemical Vapour Deposition
Me$_2$SiHCl	dimethyl chlorosilane
MeOH	methanol
mg	milligram
MHz	megahertz
min	minute
mL	millilitre
Mn	number average molecular weight
Mw	weight average molecular weight
n	number of moles
N	overall degree of polymerisation
N$_2$	nitrogen
Na	sodium
NaCl	sodium chloride
Na$_2$SO$_4$	sodium sulphate
N$_i$	degree of polymerisation of block i
nm	nanometre
NMR	Nuclear Magnetic Resonance
O$_2$	oxygen
p.a.	pure for analysis
PB	poly(butadiene)
PB-*b*-PEO	poly(butadiene)-*block*-poly(ethylene oxide)
(PEO)$_2$	[poly(ethylene oxide)]$_2$
PI	poly(isoprene)
PI-*b*-P2VP	poly(isoprene)-*block*-poly(2-vinpyridine)
PI-*b*-PEO	poly(isoprene)-*block*-poly(ethylene oxide)

PMMA-*b*-PHEMA	poly(methyl methacrylate)-*block*-poly(2-hydroxyethyl methacrylate)
ppm	parts per million
PS$_2$-*b*-PEO	(polystyrene)$_2$-*block*-poly(ethylene oxide)
PS$_2$-*b*-PLLA	(polystyrene)$_2$-*block*-poly(L-lactide)
PS$_2$-*b*-PMAA	(polystyrene)$_2$-*block*-poly(methyl methacrylate)
PS$_2$-*b*-tBuMA	(polystyrene)$_2$-*block*-poly(tert-butyl methacrylate)
PS	polystyrene
PS-*b*-(PtBA)$_2$	polystyrene-*block*-[poly(*tert*-butyl acrylate)]$_2$
PS-*b*-(PAA)$_2$	polystyrene-*block*-[poly(acrylic acid)]$_2$
PS-*b*-P2VP	polystyrene-*block*-poly(2-vinpyridine)
PS-*b*-P4VP	polystyrene-*block*-poly(4-vinpyridine)
PS-*b*-(PEO)$_2$	polystyrene-*block*-[poly(ethylene oxide)]$_2$
Pt	platinum
PTFE	polytetrafluoroethylene
QDs	quantum dots
R	universal gas constant
Ref	reference
s	singlet
s-BuLi	sec-butyllithium
SCCP	solvent capillary contact printing
SEC	Size Exclusion Chromatography
SEM	Scanning Electron Microscopy
Si	silicon
SiO$_2$	silicon dioxide
SiOSi	1,3-bis-[(2,2-dihydroxymethyl)-butyloxypropyl]-tetramethyl-disiloxane
STM	Scanning Tunnelling Microscopy
t	triplet
T	temperature

t-Bu-P$_4$	1-*tert*-butyl-4,4,4-tris(dimethylamino)-2,2-bis-[tris(dimethylamino)-phosphoranylidenamino]-2λ^5,4λ^5-catenadi(phosphazene)] or phosphazene base
TEM	Transmission Electron Microscopy
T$_g$	glass temperature
THF	tetrahydrofuran
TiCl$_4$	tetrachlorotitanium
TiO	titanium oxide
TiO$_2$	titanium dioxide
Ti(OC$_3$H$_7$)$_4$	titanium (IV) isopropoxide
TLC	Thin Layer Chromatography
TMEDA	N,N,N′,N′-Tetramethylethylenediamine
UV	ultraviolet
v_c	array growth rate
v_w	substrate withdrawal rate
vol	volume
wt%	weight percent
XPS	X-ray Photoelectron Spectroscopy

Chapter 1

Introduction

1.1   Block copolymers in nanoscience and nanotechnology

Over the past two decades, nanometer-sized materials and devices have attracted large interest of many scientists and engineers; moreover, the words "nanoscience" and "nanotechnology" have captured the attention of the general public. This is because of the broad range of current and prospective applications of nanomaterials in electronics, high-density data storage, chemical sensing, drug delivery, medical diagnostic systems, nanocatalysis, etc. The main driving force that pushes research toward the investigation of materials at the nanometer and atomic scale is linked to the need, in modern technology, of miniaturizing systems and devices and of dramatically increasing their efficiency. [1-7]

There are two essentially different approaches towards nanostructures: "top-down" and "bottom-up". The former one creates small-scale structures starting from a large homogeneous material that is selectively modified by the removal or cutting down to a desired size. The latter one is based on self-organization of small components (building blocks) such as atoms or molecules into nanoscale objects. Although, the industry is still rooted in the "top-down" nanoprocessing, recent significant progress in the understanding of self-assembly processes allows supposing that the "bottom-up" techniques [8, 9] or combinations of these two methodologies [10-12] will be soon the preferred alternatives in the fabrication of nanomaterials. In the opposition to the conventional techniques that are often very expensive, time consuming, and serial processes, "bottom-up" is a cheap, simple, and parallel approach allowing construction of nanoobjects on large areas.

Self-assembly of amphiphilic block copolymers is a model example of "bottom-up" system. Block copolymers, where two or more different chains of repeating segments are linked together, segregate into distinct structures due to the incompability of the blocks.[13] Fig 1. 1 shows five types of stable bulk morphologies for a diblock copolymer.[14] The nature and the shape of the microphase-separated domains depend on the total degree of polymerization ($N = N_A + N_B$), the composition ($f = N_A/N$) and

the Flory-Huggins interaction parameter χ_{AB} (which is a measure of the incompatibility between the two blocks). Typically dimensions of the segregated domains can be tuned from 5 to more then 100 nm by changing the molecular weight of the polymer.[15]

Fig 1. 1 Schematic representations of the ordered microstructures obtained for diblock copolymer melts; from left to right: body-centered cubic packed spheres, hexagonal-packed cylinders, gyroid, hexagonally perforated layers and lamellae.[14]

The spectrum of block copolymer morphologies is by far extended via addition of a selective solvent, in which amphiphilic block copolymers form various micellar structures with one block dissolved and the other associated.[16] Although usually block copolymers form spherical micelles, by the proper design of the copolymer composition, the choice of the selective solvent, the selection of the preparation procedure and the employment of additives other structures are effortlessly obtainable (Fig 1.2). [17, 18]
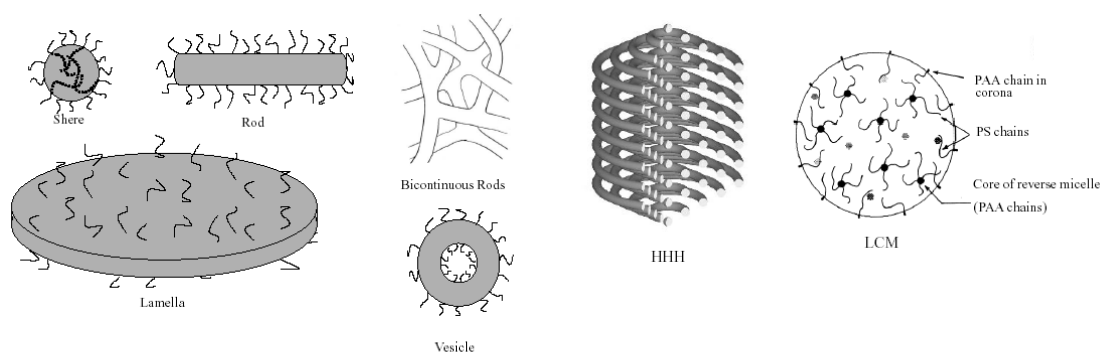

Fig 1. 2 Schematic drawings of equilibrium morphologies for PS-b-PAA amphiphilic diblock copolymer.[17] HHH refers to hexagonally packed hollow hoops morphology and LCM denotes large compound micelles.

Due to their ability to self-assembly into various nanoscaled structures, block copolymers have been widely used, both as nanoreactors and as the positioners in the fabrication of polymer/particle nanocomposites. [19, 20] They also served as templates for the mesostructured inorganic and polymer nanoporous materials obtained after the

partial or complete removal of copolymer.[21, 22] Moreover block copolymer reversed micelles were applied as nanoreactors for the synthesis of metal nanoparticles. The micelles either stabilized particles in solution or were used as structure-directing agents for nanoparticle deposition onto surfaces in a highly regular hexagonal pattern. [23]

1.2   Contents of this thesis

The goal of this dissertation has been to demonstrate that self-assembled amphiphilic block copolymers into reversed micelles are powerful and versatile tools for the synthesis as well as precise positioning of metal/metal oxide nanoparticles in regular patterns on flat surfaces or in nanofibre structures.

In the following an outline of the contents of this thesis is given:

Chapter 2 reviews the micellar approach to surfaces decorated with regular patterns of nanoparticles. The second part of the literature survey gives a brief overview on the synthesis of the block copolymers by living anionic polymerization.

Chapter 3 concerns the controlled deposition of block copolymer micelles on flat surfaces into hexagonal arrays with the special focus on the improvement of the long-range micellar order.

Chapter 4 describes attempts in the synthesis of Y shape block copolymers consisting of one poly(isoprene) block and two poly(ethylene oxide) blocks by living anionic polymerization. In addition, the synthesis of PEO four arm star polymers is reported.

Chapter 5 presents the anionic synthesis of poly(butadiene)-*b*-poly(ethylene oxide) block copolymers and their application in the controlled formation of TiO_2 nanoparticles.

Chapter 6 reports on the photo-pinning – a new method for the fabrication of nano-structured micropatterns by combining self-assembly of block copolymer micelles and conventional photolithography.

Chapter 7 concerns the low dose modification of a micellar monolayer by Focus Ion Beam for the fabrication of gold nanodots arrays on silicon substrates.

Chapter 8 is a study about the self-assembly of metal salt loaded PS-*b*-P2VP block copolymers into various micellar structures as well as their use in the electrospinning process for the fabrication of nanosized polymer fibres.

1.3   References

[1]   D. Di Ventra, S. Evoy, J. R. Heflin Jr., *Introduction to Nanoscale Science and Technology*, Klumer Academic Publishers, **2004**.

[2]   T. Ito, S. Okazaki, *Nature* **2000**, *406*, 31.

[3]   C. N. R. Rao, A. K. Cheethama, *J. Mater. Chem.* **2001**, *11*, 2887.

[4]   B. Yurke, A. J. Turberfield, A. P. Mills, F. C. Simmel, J. L. Neumann, *Nature* **2000**, *406*, 606.

[5]   Y. Cui, Q. Wei, H. Park, C. M. Lieber, *Science* **2001**, *293*, 1289.

[6]   S. M. Moghimi, A. C. Hunter, J. C. Murray, *FASEB J.* **2005**, *19*, 311.

[7]   P. Wang, *Curr. Opin. Biotechnol.* **2006**, *17*, 574.

[8]   J.-M. Lehn, *Science* **2002**, *295*, 2401.

[9]   H. Fan, K. Yang, D. M. Boye, T. Sigmon, K. J. Malloy, H. Xu, G. P. Lopez, C. J. Brinker, *Science* **2004**, *304*, 567.

[10]   J. Y. Cheng, C. A. Ross, H. I. Smith, E. L. Thomas, *Adv. Mater.* **2006**, *18*, 2505.

[11]   R. Glass, M. Möller, J. P. Spatz, *Nanotechnology* **2003**, *14*, 1153.

[12]   P. T. Hammond, *Adv. Mater.* **2004**, *16*, 1271.

[13]   A.-V. Ruzette, L. Leibler, *Nature Materials* **2005**, *4*, 19.

[14]   A. K. Khandpur, S. Foerster, F. S. Bates, I. W. Hamley, A. J. Ryan, W. Bras, K. Almdal, K. Mortensen, *Macromolecules* **1995**, *28*, 8796.

[15]   M. Lazzari, G. Liu, S. Lecommandoux, *Block Copolymers in Nanoscience*, Wiley-VCH Verlag GmbH & Co, KGaA, Weinheim, **2006**.

[16]   P. Alexandridis, R. J. Spontak, *Curr. Opin. Colloid Interface Sci.* **1999**, *4*, 130.

[17]   N. S. Cameron, M. K. Corbierre, A. Eisenberg, *Can. J. Chem.* **1999**, *77*, 1311.

[18]   I. W. Hamley, *Soft Mater.* **2005**, *1*, 36.

[19]   Y. Lin, A. Böker, J. He, K. Sill, H. Xiang, C. Abetz, X. Li, J. Wang, T. Emrick, S. Long, Q. Wang, A. Balazs, T. P. Russell, *Nature* **2005**, *434*, 55.

[20]   M. R. Bockstaller, R. A. Mickiewicz, E. L. Thomas, *Adv. Mater.* **2005**, *17*, 1331.

[21]   W. Meier, *Curr. Opin. Colloid Interface Sci.* **1999**, *4*, 6.

[22]   M. A. Hillmyer, *Adv. Polym. Sci.* **2005**, *190*, 137.

[23]   J.P. Spatz, S. Moessmer, C. Hartmann, M. Moeller, T. Herzog, M. Krieger, H.-G. Boyen, P. Ziemann, *Langmuir* **2000**, *16*, 407.

Chapter 2

Literature Overview

2.1   Inorganic cluster nanoarrays by molecular templating

2.1.1   Introduction

Metal nanoparticles or clusters are of great interest in fundamental science as well as for potential applications.[1-3] Semiconductor and noble metal nanoclusters in the nanometer size regime display interesting optical, electronic, magnetic and chemical properties that are size-dependent, *e. g.* in contrast to noble metals in bulk which are photoactive only to a small extent, nanoparticles of noble metals exhibit increased photochemical activity due to their high surface/volume ratio.[4]

Ordered arrays of particles on a substrate provide an ideal way to systematically study the effect of the particle size, shape, interparticle spacing and surrounding dielectric medium on the plasmon resonance spectra,[5-8] magnetic behaviour (interactions such as dipol-dipol) of small ferromagnetic particles [9-11] or influence of nanoparticles on the electric properties of thin metal films.[12] On the other hand investigations of individual particle properties (where lack of interactions between the particles is required) are also possible.[13-16] A surface decorated with metal clusters can be used as a well-defined mask for etching processes. In this case the surface texture contains a uniform structure covering large areas, which allows to prepare various nanostructures in large scales, but where one can also study uniformity and selectivity of etching processes.[17, 18] Another application of nanoarrays on a flat surface is a matrix for locally selective binding of different compounds and biomolecules (for instance thiols or disulfides to gold surfaces), which is of highly interest in nanotechnology applications like bio-chips, high-density data storage, etc.[19-21] Finally supported particles provide systems for model catalysis where particle size, and the support dependence can be studied.[22, 23]

There are numerous different possibilities to prepare clusters on the surface, however the large scale production of regularly distributed particles with a uniform size and shape is still a great challenge. A well-established way to fabricate quantum dots is the growth of strained islands using the Stranski-Krastanov (SK) growth method in gas phase techniques like molecular beam epitaxy (MBE) and metalorganic chemical vapor

deposition (MCVD). A number of studies have been devoted to the identification of the precise growth mechanism in different systems for example Au/Ag, Au/molybdenite, InAs/GaAs, InGalAs/GaAs, Si/Ge or Co/SiO.[24-26] Another possibility is to use strain-relief pattern deposition, where the monolayer of one material is deposited onto a substrate with a different lattice constant.[27] In this way ordered arrays of Ag and Fe on the monolayer of Cu on Pt substrate have been prepared. Several standard lithography techniques such as X-ray lithography,[28] electron-beam lithography,[29] and ion-beam lithography[30] are used in order to create nanostructures on a surface. Also different scanning probe lithography methods like scanning tunnelling microscopy (STM) technique[31, 32] or "Dip Pen" nanolithography (DPN)[33-36] can be used to selectively decorate surface with clusters. These techniques are capable of fabrication single clusters with good spatial resolution, however they are often time-consuming, expensive and not applicable to large-scale production.

Electrodeposition is a method which results in the formation of the supported quantum dots (QDs) usually in the form of aggregated nanocrystals, but also as isolated QDs.[37] Other "chemical methods" use the reactions in solutions in order to produce nanoparticles. Adjusting parameters of the process controls nucleation and growth of the clusters. To prevent agglomeration, particles are stabilized by electrostatic or steric stabilization (colloids, surfactants, polymers). [38-42]

A special technique is based on the self-assembly of diblock amphiphilic copolymers into reverse micelles in selective solvents. The block of the polymer, which is well soluble in the selective solvent, forms the shell, while the insoluble block the core of the micelle. The micelles can be then loaded with a suitable transition metal salt by protonation or complexation, and after that, deposited as a micellar monolayer onto a substrate. Subsequently the diblock copolymer is removed by means of a plasma process, which also reduces the precursor salt to the corresponding noble metal or the metal oxide nanoparticle. In this way a regular hexagonal arranged surface pattern of noble metals or a metal oxide clusters on various substrates can be generated. The size of the inorganic dots is controlled by the amount of inorganic precursor compound that has been added per micelle. The interparticle distance depends on the molecular weight of the block copolymer and film preparation.

2.1.2   The technique of preparation nanoparticles by the micellar approach

The general concept of the formation of regular nanopatterns on the surfaces is described in the following example (Fig 2. 1). Typically amphiphilic copolymer polystyrene-*block*-poly(2vinylpyridine) (PS-*b*-P2VP) is dissolved in toluene. The PS blocks are well soluble in a nonpolar solvent, whereas the P2VP blocks show poor solubility. Above the critical micellar concentration (CMC) inverse micelles are formed, where the core of the micelles consists of P2VP blocks and the PS blocks form the corona.[43-45]
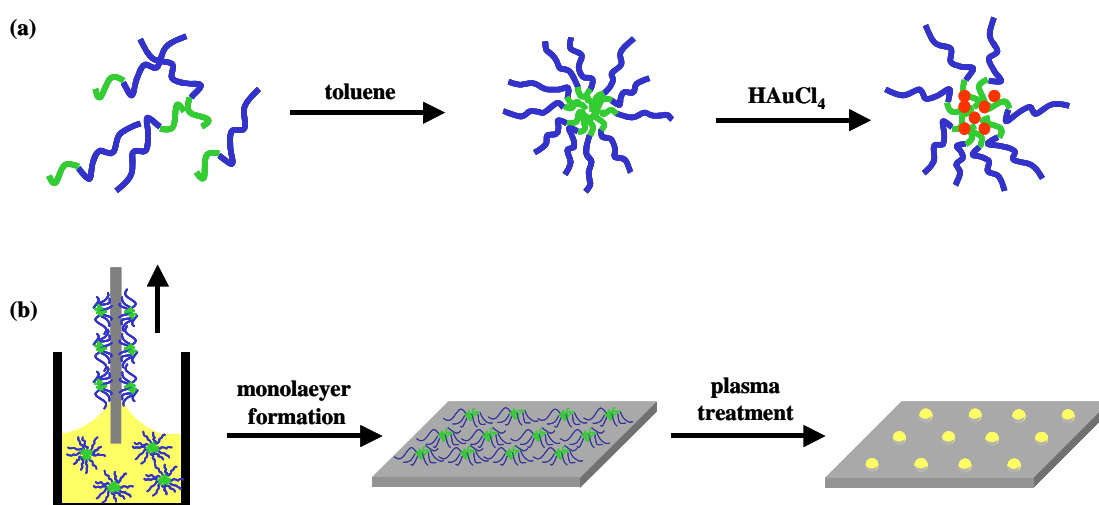

Fig 2. 1 The main steps of micellar technique (*a*) *A schematic drawing of the micelle formation of polystyrene-block-poly(2-vinylpyridine) (PS-*b*-P2VP) block copolymers in solution. The core of the micelle is loaded with a metal precursor (e.g., HAuCl₄). (b) The reverse micelles are transferred onto substrate by e.g. dip-coating. The polymer is removed and simultaneously the metal salt is reduced by applying a plasma process.*

The free electron pair of the nitrogen atom in the P2VP block is able to interact with an inorganic salt. For instance, addition of $HAuCl_4$ to the micelle solution results in an $AuCl_4^-$ ions complex bound by protonating the pyridine units.
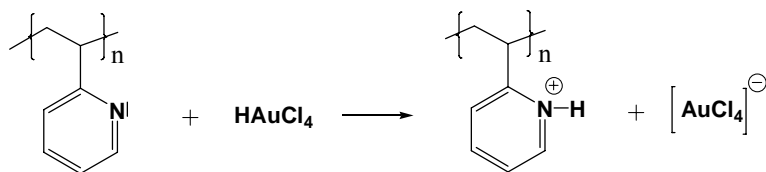
The loaded micelles are then transferred onto the surface of the desired substrate in such a way, that they form a monomicellar film. Here, several different techniques are possible: dip-coating, spin-coating or spreading a droplet on a substrate. For the formation of a monolayer, a dip-coating process was found to be the most effective. This method has several advantages: flat substrates of different sizes can be covered homogeneously over the whole surface and the distance between the deposited micelles and the regularity of the pattern can be controlled in an easy way as discussed later. In this process the substrate is dipped into the micellar solution and pulled out with a constant velocity. The formation of a monofilm of densely packed micelles is effected by long-range Van der Waals interactions and capillary forces acting between micelles during evaporation of a solvent.[45-47] Depending on the concentration of the solution and the rate at which the substrate is pulled out of the solution, micellar films of different thickness can be prepared. After the evaporation of the solvent a monolayer of loaded micelles arranged in a hexagonal pattern remains (Fig 2. 2a and c).

In the next step, a plasma process (*e.g.* oxygen, hydrogen or CF$_4$) is applied in order to transform the precursor salt sequestered in the micellar nanoreactors to metal or metal oxide particles and remove the polymer matrix. Despite the fact that other techniques could be used as well for burning off organic shell and the particle formation (*e.g.* heat treatment[48, 49] or laser ablation[50, 51]), plasma treatment is often the method of choice, because of the relatively moderate thermal conditions it generates. During the plasma process the metallic salt is reduced to single clusters and obtained particles are deposited on the surface in a pattern reflecting the previous micellar hexagonal arrangement (Fig 2. 2b and d).
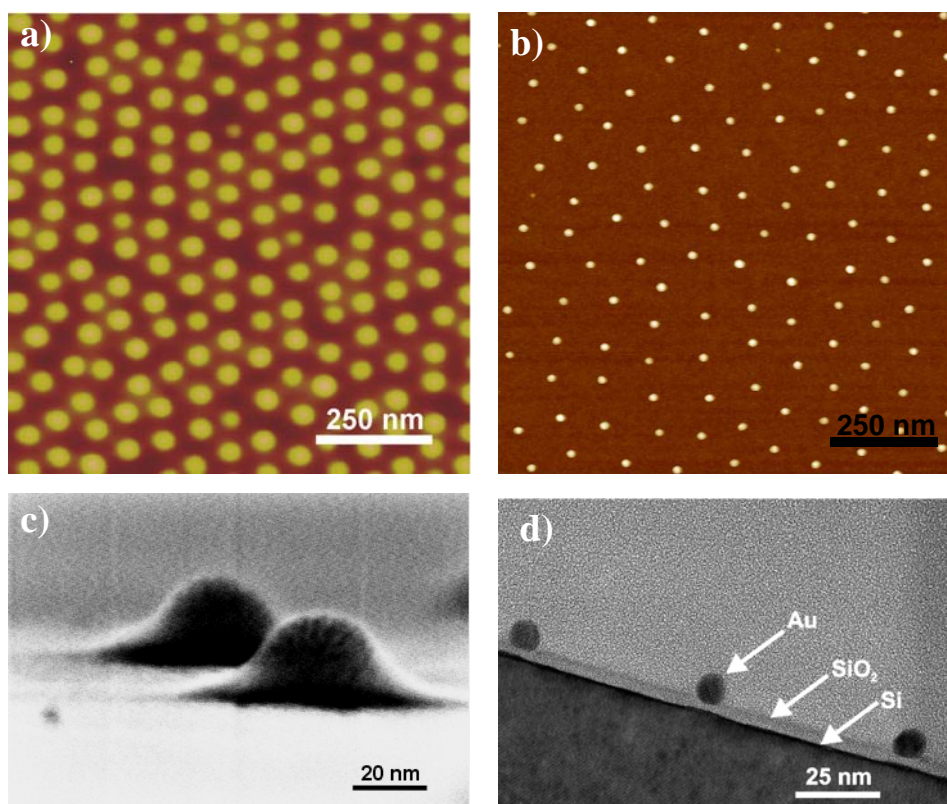
Fig 2. 2 Typical SFM topography images demonstrating well-ordered hexagonal pattern of PS-b-P2VP micelles loaded with HAuCl₄ (a) and Au particles (b), as well as corresponding high resolution SEM cross-section pictures of loaded micelles (c) and gold particles (d) deposited on Si substrate.[49] The rigid micellar cores can be clearly distinguished due to small gold particles produced during exposure to the electron beam while, the PS corona is faintly visible as a white shadow surrounding the core.

The technique of nanoparticles preparation described here is not limited to the system HAuCl$_4$ in PS-*b*-P2VP micelles. A large variety of inorganic precursor salts (resulting in broad range of metal and metal oxide particles) and block copolymers can be chosen, while at the same time various substrates are possible (*e.g.* SiO$_2$, glass, mica, diamond, etc) as it will be discussed in the subsequent sections.

2.1.3   Variation of particle size and interparticle distance

The described method gives the possibility to vary the particle size as well as the distance between the clusters. The size of resulting nanodots can be adjusted simply by the amount of the metal precursor salt added to the micellar solution (it can be expressed as the loading ratio which is defined as L = n(salt)/2VP-units)[43] or by the differing ratio of blocks (for a longer P2VP block lengths the micelles form bigger cores, which are able to incorporate more precursor salt and consequently bigger nanoparticles can be formed). The particle size can be varied between 1 and 15 nm with a very small deviation in size (typically 10 to 15%).[52-54]

The distance between the deposited clusters can be varied with the degree of polymerization of the block copolymer,[52] the dipping velocity [49, 55] or addition of PS homopolymer.[56] For example using different polymer lengths one can control the separation distance of the deposited micelles and resulting particles in range from few to hundreds of nm. Fig 2. 3 gives examples of Au nanoparticles prepared from a toluene solution of three different block copolymers PS(x)-*b*-P2VP(y) where x is the number of PS and y P2VP units in the block copolymer. Particles with separation distance of 80 nm (a), 30 nm (b) and 140 nm (c) are shown. The respective sizes of particles are 12 nm, 2 nm, and 1 nm. Independently of used copolymer the pattern shows a regular hexagonal lattice.
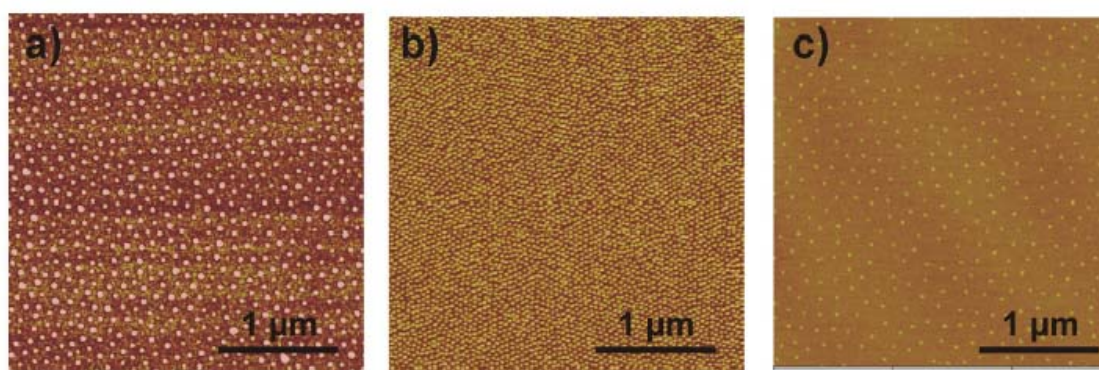
Fig 2. 3 SFM topography images of Au cluster arrays on mica substrates after the oxygen plasma treatment. The different interparticle distances are obtained by varying the lengths of the polymer blocks in the following way: (a) PS(800)-b-P2VP(860), (b) PS(325)-b-P2VP(75), and (c) PS(1700)-b-P2VP(450).[52]

The coating procedure affects the coverage of the substrate too. The corona block can be more or less stretched, with has an effect on the final distance between the particles. Fig 2. 4 shows the ability of tuning the interparticular distance of metal nanoparticles on flat surface by changing the dipping velocity. The same block copolymer (PS(1350)-b-P2VP(400)) was used in both cases.[49] In this case particles have identical size.
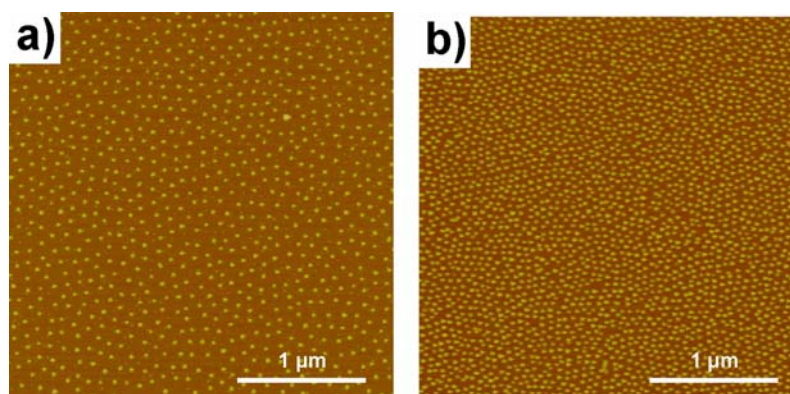

Fig 2. 4 Pattern of nanoparticles after decomposition of the polymeric shell by a plasma etching process. Samples were prepared with the dipping velocity equal to 6 mm/min (a) and 22 mm/min (b).[49]

2.1.4   The quality of the order

The micelles act as soft spheres and the formation of an ordered film is affected by the particle attraction as well as the capillary forces arising out of the solvent evaporation and contact tension. Depending on the dipping velocity, both the ordering and the center-to-center distance (CTC) can be controlled. Hartmann et al.,[49] distinguished three well-defined ordering regimes as a function of dipping velocity (see SFM images on Fig 2. 5). Only the middle regime showed a good hexagonal order. In the case of either too high or too low dipping velocities the order degenerated.

The existence of theses three regimes can be explained as follows. At low dipping speeds the film is thin and there are not enough micelles that can strongly interact with each other. As the dipping velocity increases, the thickness of the adsorbed film during the pulling process and the number of micelles per volume increase. Strong interaction between neighbouring micelles causes their hexagonal order. Further increasing the pulling speed results in decreasing distances between neighbouring micelles. The soft nature of the micelles is the reason that they are able to compress and pack closer, as the surface coverage is higher. This can be seen as decreasing the average distance between the micelles. The linear relationship between dipping velocity and the CTC distance can be found in this regime (Fig 2. 6). However, after reaching a critical point, the micelles became "too crowded" and the order is disturbed (regime III in Fig 2. 6).
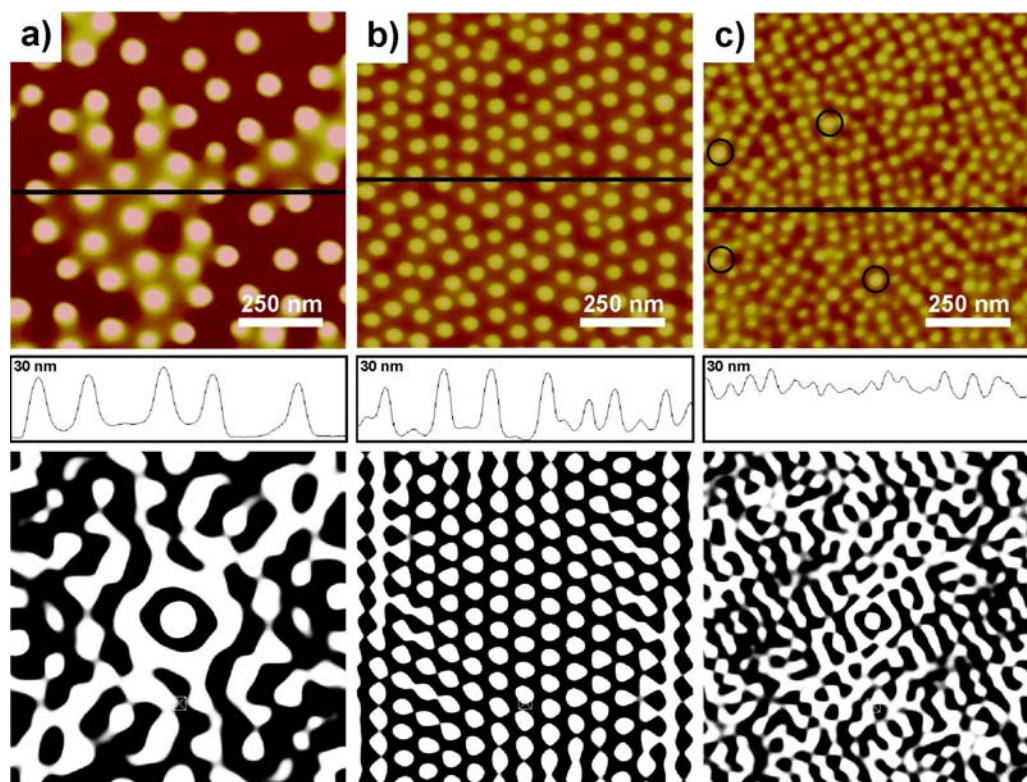
Fig 2. 5 Above: SFM height images of a regular pattern of block copolymer micelles. Inverse micelles of PS(1350)-b-P2VP(400) were deposited on a freshly cleaved mica surface at different dipping speeds. The dipping velocities were respectively: 4 mm/min (a), 16 mm/min (b) and 40 mm/min (c).

Below: Autocovariance function pictures of the corresponding SFM image. The SFM image data was correlated to itself incrementally, where two exact copies of the image data are shifted relative to one another. As a result, inherent periodic features are highlighted in real space allowing the determination of both average size and separation of features.[49]

The same three-regime transition is also observed for polymers with different molecular weight.[49] The length of PS block (forming corona) was varied while the length of P2VP block (core) was kept constant. In all cases hexagonal lattice was seen in a middle regime. The higher the molecular weight, the higher the velocity needed to form well-ordered structures.
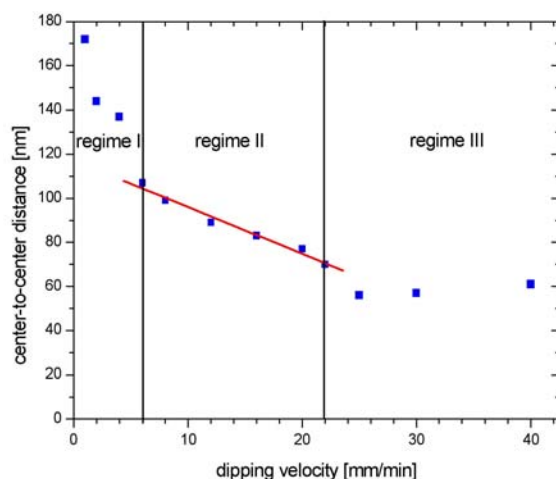
Fig 2. 6 Average distance of micelles versus dipping velocity for PS(1350)-b-P2VP(400).[49]

An interesting way of improving the hexagonal order of Au nanoparticles over large areas was achieved by the solvent annealing of not loaded PS-*b*-P4VP micellar monolayer.[57] After THF annealing, nearly perfect arranged micelles were loaded with the Au precursor salt and the polymer film was subsequently exposed to oxygen plasma producing Au nanoparticles arranged with the same long-range order.

2.1.5   The choice of the particles

The formation of nanoclusters by the micellar approach is very flexible in terms of variation of metal precursor and block copolymer. Next to the PS-*b*-P2VP loaded with HAuCl$_4$ micellar system also other precursor salts were successfully incorporated into block copolymer micelles, resulting in formation of ordered arrays of nanoparticles of elements such as Pt, Pd, Co, Ni or Ag. [52, 54]

Recently, Boyen et al. showed the formation of regularly arranged cobalt nanodots on substrates.[58] PS-*b*-P2VP micelles were loaded with CoCl$_2$. Deposition of the micelles onto the substrate followed by removal of the polymer matrix by means of oxygen plasma resulted in hexagonally ordered cobalt oxide particles. In the next step with hydrogen plasma the Co$_3$O$_4$ was reduced to pure cobalt. In the similar manner regular arrays of Fe$_{48}$Pt$_{52}$ alloy nanoparticles were fabricated.[59] The homogeneity of the alloy particles was tested by XPS and HRSEM. Most of nanodots were found to be single

domains with the small fraction of twinned particles (20-25%). Also Fe-Mo,[60] Pt-Co,[61] Au-In[62] and Au-TiO$_2$[63] Pd-Au[64] bimetallic particles were synthesized with the micellar method. While the most of bimetallic particles were prepared by simple loading corresponding precursor salts with a suitable molar ratio into the diblock copolymer micelles, the alloys of gold with In and TiO$_2$ were prepared by a post treatment of Au nanoparticles by subsequent alloying.

Using PS-*b*-PEO block copolymer micelles in which the PS block forms the corona in a selective solvent and the PEO block the core, dispersions of single Au particles were successfully prepared.[65, 66] In this case LiAuCl$_4$ was used as precursor taking the advantage of the fact that Li cations can be complexed by the polyglycol. The particle size was strictly controlled by the amount of the metal salt added to the original block copolymer solution.

Inorganic precursors such as HAuCl$_4$, LiAuCl$_4$ or CoCl$_2$ are poorly soluble in nonpolar solvents and that's why they preferentially go into the polar core of the micelle. Although metal alkoxides are well soluble in organic solvents, they can be also incorporated into micelles. Our group reported a method for the synthesis of monodisperse TiO$_2$ nanoparticles by conversion of Ti(OR)$_4$ inside PS-*b*-PEO diblock copolymer micelles.[67] The block copolymer was dissolved in toluene. An inverse micelles solution was mixed with HCl in order to create reservoirs within micelle cores. Finally, Ti(OR)$_4$ was added to the solution. The titanium alkoxides were hydrolyzed as they diffused into the core of the micelles. Conversion to TiO$_2$ nanoparticles was enhanced by thermal treatment or microwave irradiation.

The group of Cohen,[68] applied polystyrene-*b*-poly(acrylic acid) (PS-*b*-PAA) block copolymer to form micelles in toluene. However, their used slightly different technique to produce metal nanoparticles: the incorporation of a suitable inorganic salt takes place after deposition of the micelles onto the substrate, in a two-step metal loading treatment. First, the aqueous NaOH neutralizes COOH group and in a second step the transition metal ion replaces the Na$^+$ ions. Using this strategy, particles of Pb, Cu, Cd, Ag and Pd were synthesized.

Besides the so far mentioned amphiphilic block copolymers, other polymers can be used for the complexation of a variety of transition metal ions. Antonietti and coworkers

starting with polystyrene-*b*-poly(butadiene) prepared by anionic polymerization, applied polymer analogous reactions (*e.g.* epoxidation followed by opening oxirane ring with acid chloride or benzoic acid) in order to obtain different new amphiphilic block copolymers, which possess various functional groups and are able to complex or bind suitable transition metal precursors.[69, 70]

A similar approach was described using polystyrene-*b*-poly(*tert*-butyl methacrylate) block copolymer by Roescher et al.,[71] The ester groups of the poly(*tert*-butylmethacrylate) were hydrolyzed, after that resulted carboxylic side groups were converted to amide groups by reaction with pyrrolidine. Obtained in such a way, block copolymer formed stable micelles in toluene, which were loaded with Pd salt.

Table 1 gives several examples of the systems consisting of precursor salt incorporated into core of block copolymer micelles in non-polar solvent subsequently used for fabrication of metal and metal oxide particles on various substrates.

Table 1 Amphiphilic block copolymer micelles loaded with inorganic precursor salts in non-polar solvent.

Block copolymer	Precursor salt	Reference
PS-*b*-P2VP PS-*b*-P4VP	$HAuCl_4$, $AuCl_3$, $Pd(CH_3COO)_2$, Na_2PdCl_4, $K(PtCl_3C_2H_4)$, $AgNO_3$, $AgClO_4$, $Fe(NO_3)_3$, $Co(NO_3)_3$, $Ni(NO_3)_3$, $[Mo(OCOCH_3)_2]$, $CoCl_2$, $Co_2(CO)_8$, $NiCl_2$, $FeCl_3$, $ZnCl_2$ $H_2(PtCl_6)$, $MnCl_2$, $TiCl_4$	[52, 58-61, 66, 72-79]
PS-*b*-PEO	$LiAuCl_4$, $Ti(OR)_4$	[65-67]
PS-*b*-PAA	$Pb(CH_3COO)_2$, $Pb(NH_3)_4Cl$, $Cd (CH_3COO)_2$, $Ag (CH_3COO)$, $Cu(CH_3COO)_2$, $FeCl_3$	[68, 80]
Modified PS-*b*-PB (PS-*b*-PAlcohol, PS-*b*-PEster)	$HAuCl_4$, $AgNO_3$, $Cu(ClO_4)_2$, $Pd(CH_3COO)_2$, $Rh(CH_3COO)_2$, $ZnCl_2$	[69]
PS-*b*-PMAA PS-*b*-PAA	$Pd(CH_3COO)_2$, $FeCl_3$, $Pb(CH_3COO)_2$	[56, 71]
PMMA-*b*-PHEMA	$Pd(CH_3COO)_2$	[81]

2.1.6 The quality of the particle size distribution

In order to study for example the catalytic behaviour of deposited noble metal nanoclusters one has to produce samples with a regularly ordered and a narrowly size distributed particles. Recently Boyen et al. used gold nanoparticles on silica substrate to study the size dependence of their oxidation behavior under exposure to oxygen atoms.[82] After deposition of monomicelar film of PS-*b*-P2VP copolymers loaded with $HAuCl_4$ on silicon wafers, polymer matrix was removed by oxygen plasma. The arrangement of the obtained particles investigated by atomic force microscopy (AFM) exhibited hexagonal order. From AFM images Gaussian size distributions with averages diameters of 7,9 ± 1,2 nm, 2,9 ± 0,5 nm, 1,6 ± 0,3 nm and 1,3 ± 0,3 nm were observed for four different samples. Because of the small but finite size distribution of the Au particles prepared by micellar approach, additionally monodisperse Au_{55} clusters (size 1,4 nm) stabilized by PPh_3 ligand were obtained. Similarly to micellar approach, oxygen plasma treatment resulted in the removal of the ligand. X-ray photoelectron spectroscopy (XPS) measurements were then performed to investigate the chemical nature of the gold. It was found that clusters of Au_{55} (1,4 nm) exhibited extraordinary resistance against oxidation. Particles with dimensions close to Au_{55} (1,6 and 1,3 nm) contained more Au_2O_3 whereas both smaller (below 1nm) and bigger (2,9 nm and more) particles could be easily oxidized under O_2 plasma conditions.

The same micellar approach was used by Cuenya and co-workers to prepare gold clusters with different sizes in order to study the particle size and the support effect on the catalytic activity of gold nanoparticles.[83] Cluster of diameter 6,0 ± 1,5nm, 4,0 ± 1,0 nm and 1,5 ± 1,3 nm on different substrates like TO_2/Ti, SiO_2/Si, TiO_2/TiO foil and indium tin oxide on glass (ITO/glass) were investigated. However, oppositely to previous mentioned studies, they reported that clusters of sizes around 4 nm possess the lowest Au_2O_3 fraction.

2.1.7 Aperiodic patterns

The combination of a standard lithography (top-down approach) with the micellar self-assembly (bottom-up approach) allows the arrangement of nanoclusters in artificial

patterns as well as separation of single clusters in microscopic length scales.[84] The big advantage in combining these techniques lies in the significant reduction of the achievable feature size of aperiodic structures *e.g.* starting with patterned structures with sizes of 300 nm, well within the capabilities of photolithography, the combination with the micellar self-assembly results in cluster dimensions smaller   than lithography pre-patterns, leading to lines widths in the range of 10nm.[85] This is due to the fact that micelle (diameter ~200 nm) effectively acts as a positioner for the nm sized gold salt sequestered within its core.

In order to arrange nanoparticles in aperiodic structures, using the combination of the conventional lithographic technique and micellar approach the following methodology was followed. A positive resist was initially patterned via photo or e-beam lithography and in a subsequent step micelles were deposited within these template features by spin or dip-coating. Next, a suitable solvent eradicated the resist template together with those micelles sitting on top of the resist, while micelles that were in contact with the substrate remained. A plasma process reduced the precursor salt within the micelle core to metal and the organic micelles were removed, resulting in manometer sized metal particles forming artificial patterns (Fig 2. 8a, b and c).[84]

The order of particles reflected the original resist pattern *e.g.* using e-beam lithography, square arrangement Au particles on silicon substrates, separated from each other about 5 μm and 7 nm gold dots arranged in 200 μm long lines or in a circular patterns were fabricated (Fig 2. 7).[86] Similarly, using a photolithographic resist, sub-10 nm gold particles forming circular rings with diameters ranging from 1 to 20 μm were produced in a parallel process suitable for high throughput.[86] In this case after deposition of micelles in lithography-patterned resist, a plasma treatment was used to convert the loaded micelles to noble metal clusters and remove organic shell, prior to resist removal.

Direct irradiation of a monolayer of loaded micelles by e-beam simplified the approach described above (Fig 2. 8d). This process called micelle pinning, uses a monomicellar film as an e-beam negative resist. Exposure to electron beam produces crosslinked micelles, which are attached to the substrate, whereas the unmodified ones are removed by a wet lift-off technique in a subsequent step.[87] Additional treatment such as carbon

coating of micellar layer before irradiation, allowed extending this technique to non-conductive substrates *e.g.* glass or sapphire.[88]
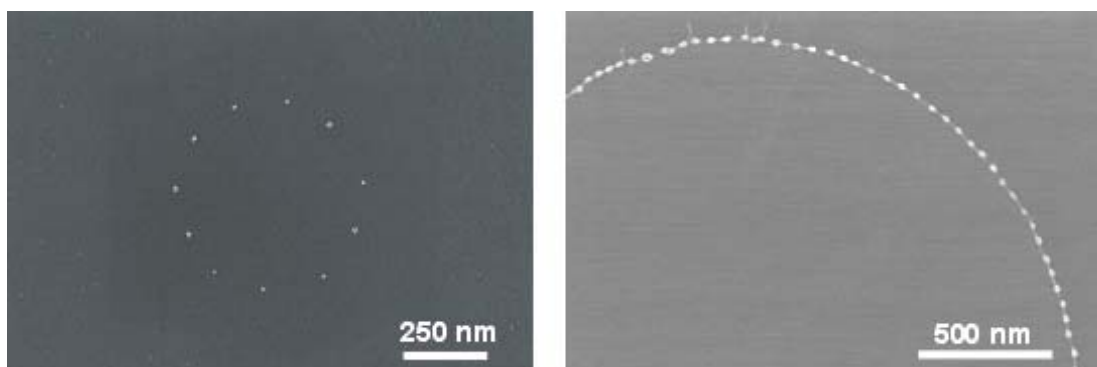

Fig 2. 7 Circular nanopatterns prepared by combination of e-beam lithography resist technique with micelle-deposition technique.[86]

Fig 2. 8 summarizes different approaches based on the combination of conventional lithography and micellar self-assembly to aperiodic patterns of nanoparticles on the surface.
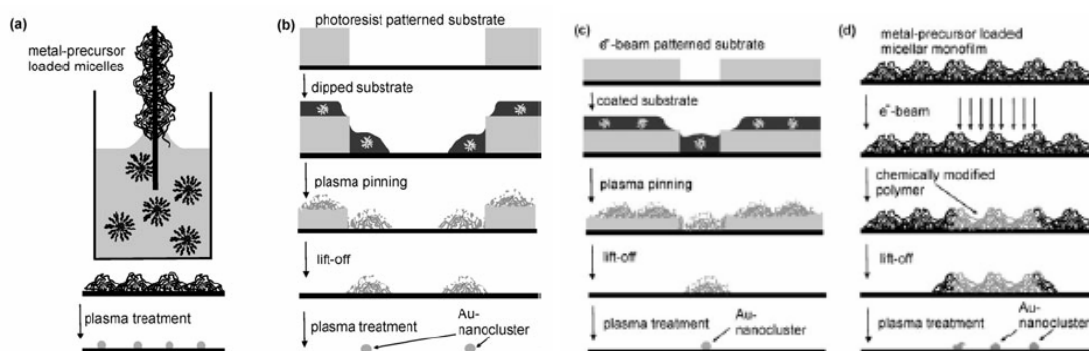

Fig 2. 8 Scheme of different approaches to nanoarrays on the surface using a) the micellar self-assembly with the combination of the pre-structuring by b) a photoresist, c) e-beam created resist or d) using a monomicellar film as an electron beam negative resist[84]

Next to standard lithography, soft lithographical pattering methods such as microcontact printing (μCP) [80, 89, 90] or solvent capillary contact printing (SCCP) [91] were combined with the micellar technique to fabricate micropatterns of nanoparticles. Using μCP method, typically a micellar film was first deposited onto a μCP stamp by spin-coating

and micelles were subsequently transferred onto a substrate by stamping procedure. Particles were generated with a plasma process. Hexagonal arrays of iron oxide nanoparticles arranged into rectangular and linear micropatterns were fabricated. However, the regularity of particle's arrays at the vicinity of the edges was disturbed as a consequence of micellar aggregation during stamping.[89] In this way also broad size-distributed (20-80 nm) and not ordered Ag particles assembled in spherical or disklike micropatterns were obtained.[90] In the SCCP technique the PDMS replica mold with microchannels was placed in contact with the monolayer of micelles. Next, a good solvent for the core-forming block, flowing through microchannels of mold selectively modified micellar layer leading (after oxygen plasma) to particles arranged in 2 or 10 μm width lines separated respectively over 4 and 10 μm.

To create connected structures such as nanowires, micellar aggregates with cylindrical morphology were envisioned.[92] The PS-*b*-P2VP block copolymer also forms crew-cut micelles when the outer soluble PS block is significantly shorter then inner insoluble P2VP block.[93] These micelles loaded with metal salt, deposited onto desired substrate and subsequently treated with plasma process served for fabrication of Au nanolines.[86] Fig 2. 9 shows continuous metal nanowires created by micellar approach when crew-cut block copolymers self-assembled into cylinders were employed as nanoreactors. Nanowires were examined for their conductivity.
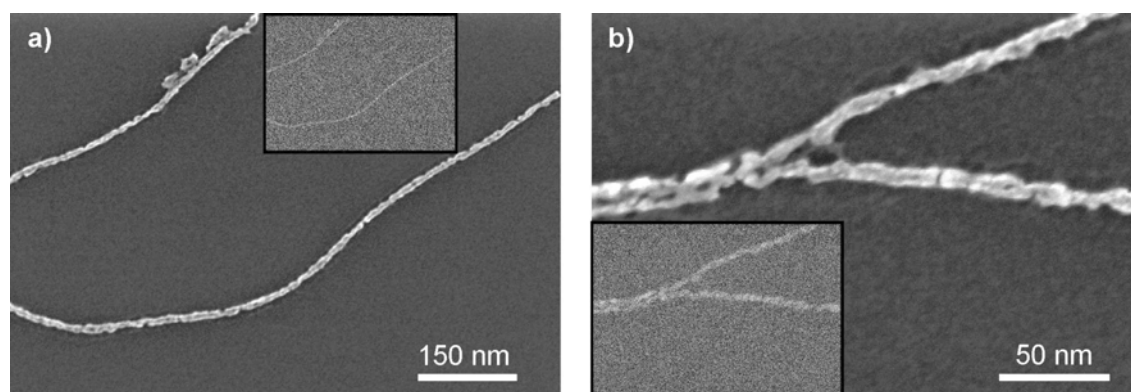

Fig 2. 9 Scanning electron microscopy pictures of continuous Au nanowires obtained from HAuCl₄ loaded PS(80)-b-P2VP(320) cylindrical micelles after O₂ plasma treatment. Insets show back scattering images of the corresponding fragment.[86]

2.1.8 Applications

Etching

A film of a diblock copolymer deposited onto a substrate can act as an etching mask and the pattern of micellar arrangement is transferred into the underlying substrate.[94] The etching rate depends on the film thickness and the polymer composition. Large etching contrasts can be achieved by loading the micelles with suitable inorganic component. As an example the monomicellar films of PS-b-P2VP block copolymer on GaAs- and InP- based semiconductor substrate were prepared.[95] The micelles with precursor salt (HAuCl$_4$) or containing single Au particle were exposed to reactive Ar-ion etching. Depending on the chemical state of gold inside the micelles, columns or pores were obtained (Fig 2. 10 and Fig 2. 11).

Fig 2. 10 Formation of columns and holes depending on the block copolymer micelles loading: with HAuCl$_4$ (left) and gold particles (right).[95]
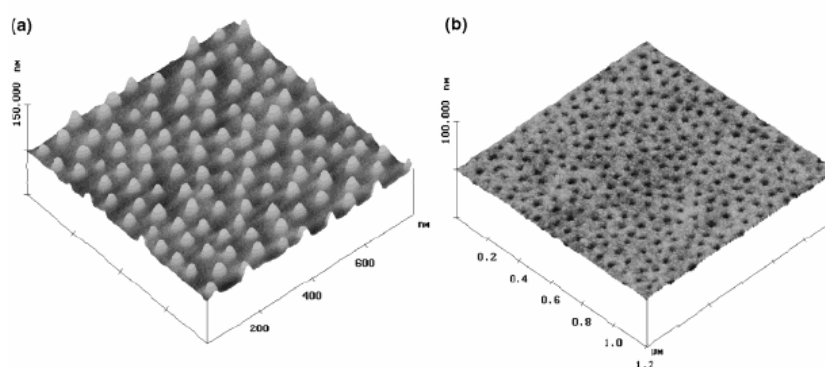

Fig 2. 11 Three-dimensional SFM images of arrays of a) islands of 25 nm height, 20 nm diameter and b) holes of 10 nm depth, 10 nm diameter separated by ca. 80 nm prepared by different micellar mask.[95]

Similarly arrays of gold nanoclusters fabricated with the micellar approach on GaAs semiconductor wafer were used as a direct mask for dry etching.[17] Regularly arranged nanocylinders with height from 20 to 90 nm were prepared. The height could be controlled by the etching conditions, whereas the diameter and the interspatial dimensions of the obtained structures were varied by the size and loading of the micelles. Koslowski et al. used described above approach to form cylindrical diamond columns on a diamond substrate.[18] In this case oxygen plasma was used to remove the polymer and reduce the Au precursor salt, leaving behind hexagonally ordered gold dots on the diamond substrate. Continuation of the plasma treatment resulted in the etching of the "naked" diamond surface where the surface decorated with gold clusters acted as a mask. Columns of 15 nm height and 10 nm diameter in a distance of 85 nm apart were obtained. In similar manner, applying strongly anisotropic Reactive Ion Etching (RIE) on silicon substrates decorated with Au particles, allowed fabrication of silicon nanopillars.[96]

This technique can be extended to the preparation of nanoporous metallic films.[97] On a top of GaAs substrate with hexagonally ordered nanocolumns gold was evaporated. The deposited gold formed a thin layer with a thickness less then height of the pillars. After removing a GaAs substrate by piranha etching, the nanoporous Au film was left free-floating and could be picked up by solid substrate *e.g.* Si wafer (Fig 2. 12)
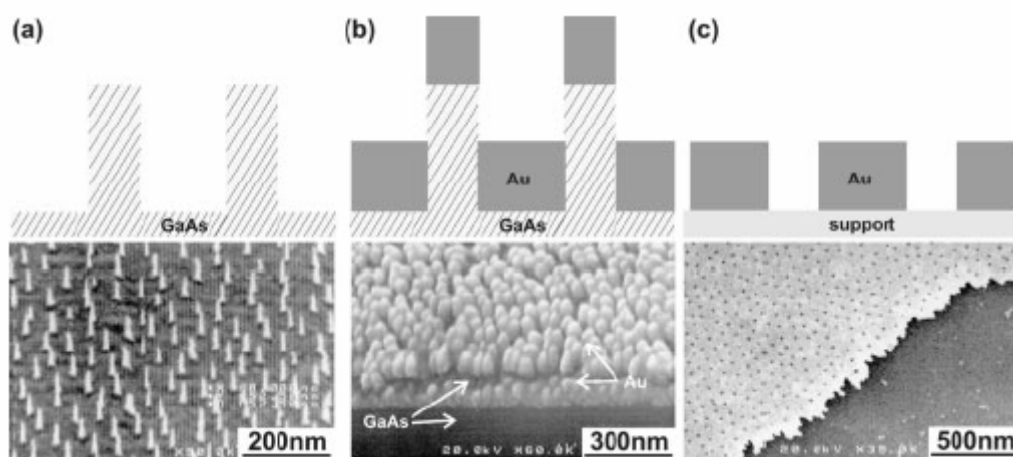
Fig 2. 12 Formation of nanoporous Au film: a) GaAs nanocolumns produced by selective ion etching of gold nanoparticle mask. b) thin film of Au deposited onto the pillar substrate. c) Au film after piranha etching.[97]

Binding

The fact, that the nanodots are not stabilized by any organic coating, makes them excellent candidates for locally selective binding of macromolecular compounds and biomolecules, where molecularly well-defined adhesive spots are separated by the desired non-adhesive regions. For instance arrays of streptavidin on a glass slide decorated with gold nanoparticles were produced.[52, 98] Gold nanoparticles arranged in ordered, two-dimensional patterns with a periodicity in the μm range were used as a substrate for selectively binding the fluorescence dyes.[21, 99, 100] The fluorescence of dyes on the patterned surface is much more intense, in comparison to the optical response of dyes adsorbed on bulk gold. Because of the separation of the Au dots a higher resolution can be achieved and standard optical techniques in order to detect fluorescence can be applied, which is of great importance for high sensitive bioanalitical applications and high-density data storage devices.

Hexagonal arranged gold nanoparticles on glass substrates were used as well-defined anchoring points for cells adhesion. [101, 102] In this case nanopatterned surface of gold clusters was first reacted with small biomolecules that were later recognized by the unique binding places localized at the surface of a cell. The long-term adhesion of cells was studied as a function of ligand distance on nanopatterned and biofunctionalized

interfaces. Furthermore, the interaction between cells and biofunctionalized surfaces was measured by the specially designed magnetic tweezers.[102]

Catalysis

Catalysis is one of the most important applications for supported metallic nanoparticles *e.g.* gold clusters on metal oxide surfaces are capable of catalyzing a wide variety of reactions like oxidation, reduction, hydro- and dehydrogenation, hydrochlorination and many others.[103, 104] Despite the success in modelling catalysis with single crystals, there is a clear need to develop models in order to study relationship among atomic structure, composition, electric properties of a surface and catalytic activity and selectivity.[105]

The micellar approach offers the chance to understand the mechanism of catalytic processes since it provides system with well-defined morphology. In this manner, Au/TiO_2 model catalyst was prepared by the micellar technique. Catalytic properties such as activity, selectivity as well as activation energy for the selective CO oxidation, have been investigated, and compared to conventionally prepared Au/TiO_2 catalyst.[49] The reaction mechanism for CO oxidation was found to be identical for both systems. The activity of the micelle-based catalyst depends on the calcination temperature. After low temperature treatment (350°C) system still contains residue of polymer shell, which affect the catalytic properties. In the range from 450 to 600°C both investigated catalytic systems have the same activity however for higher then 600°C temperatures catalyst based on micellar approach is even more active. It was proposed that more active interface between metal and substrate was formed which improve activity. The thermal stability of Au/TiO_2 system was also investigated by groups of Ziemann and Behm.[106] Cuenya et al.,[83, 107] using gold nanoparticles arrays on conducting and semiconducting substrate, reported study on catalytic activity of Au clusters for electrooxidation of carbon monoxide. They found, that clusters with the 1,5 nm size are the most active. Also other then gold metals were applied in catalysis studies. Pt and PtCo nanoparticles on carbon substrates served as a model fuel cell catalyst in electroreduction of O_2. Special emphasis was placed on examining the effect of varying interparticle distance on the voltammograms.[61] Recently, the highly regular arrays of nano-sized Au clusters on SiO_2 wafers prepared by means of self-assembly of

polyisoprene-*b*-poly(2-vinylpyridine) micelles, were employed in developing a setup for studying well-defined model compounds under catalytic relevant conditions.[108]

CNTs and nanowires

Regular arrays of metal nanoparticles on the surfaces offer a great promise as active sites for the growth of carbon nanotubes (CNTs) in the catalyst-assisted chemical vapor deposition (CVD) technique. In this method, the metal nanoparticles catalyze two processes: the carbon feedstock cracking and the nucleation of nanotubes. The micellar approach to nanoparticles as compared to traditional catalyst preparation has shown a considerable improvement in production of well-defined CNTs, by allowing a good control over diameter and density of particles. The growth of single and multi-walled CNTs using nanoarrays of gold, iron, cobalt, nickel, molybdenum and bi metallic iron-molybdenum nanoparticles prepared from PS-*b*-PVP block copolymers was successfully demonstrated. [49, 60, 80, 109] High-density arrays of iron-oxide particles, fabricated from PS-*b*-PAA micellar monolayer, allowed to grow approximately 10 μm long vertically aligned two- and free-walled CNTs. [110] Similarly, vertically grown multi-walled CNTs were produced in artificial patterns by pre-structuring micellar film with μCP technique.[80]

Group of Yi have demonstrated that gold nanoparticles prepared from PS-*b*-P2VP micelles are exceptional catalysts for growing equally distributed small-diameter silicon nanowires. [111] Furthermore, micropatterned arrays of GaN nanowires with approximately 10 nm diameter were grown on a micrometer width lines decorated with Ni nanoparticles.[91]

Fuel cells

The surface pattering of graphite with nanoparticles are of great interest for development of devices for energy storage. Graphite electrodes decorated with tin oxide particles enlarge capacity of rechargeable lithium batteries.[112] Platinum group metals are commonly used in methanol fuel cells.[113] One of the most important aspects in these processes is the proper size of the particles and high, but also homogeneous surface coverage. To increase the number of particles per surface, graphite powders

were used as substrates. Fig 2. 13 shows the pattern of gold particles, which were successfully prepared on graphite flakes using micellar approach.[49]
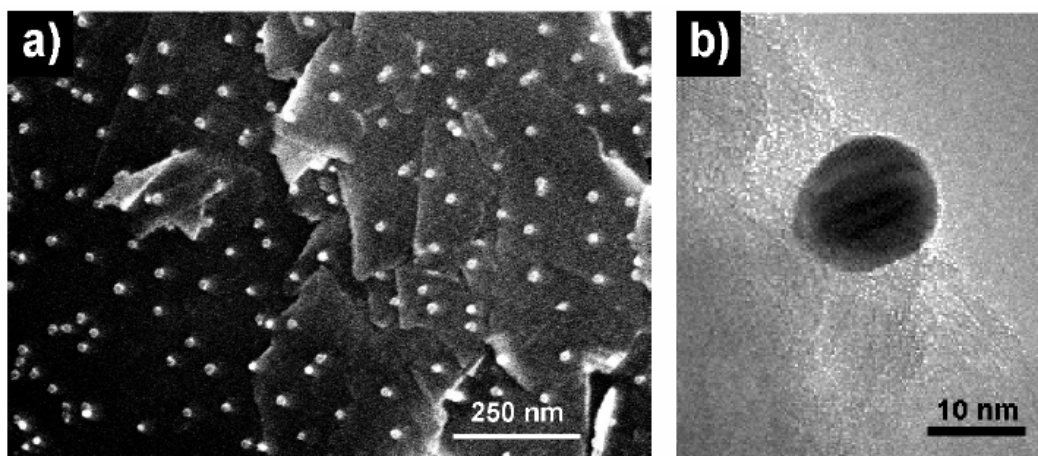

Fig 2. 13 Images of graphite flakes covered by gold nanoparticles a) scanning electron microscopy, b) transmission electron microscopy.

2.1.9   Conclusion and outlook

The micellar approach summarized here is a very efficient way to prepare surfaces decorated with patterns of nanoparticles on a large scale. The method gives control over particle size, size distribution, interparticle distance and besides allows flexibility in terms of precursor salt, block copolymer and substrate. Separation of single clusters over microns as well as different artificial micro-patterns of nanodots are possible by combining this bottom-up method with the conventional and soft lithography techniques. It is worth noting that the block copolymer micellar template approach attracts growing attention as judging by the rapidly increasing number of scientific papers published last years. Potential applications of this technique in a field of catalysis, biotechnology, nano- and microelectronics are numerous and can be tailored to many other areas.

However, the method still needs improvement (*e.g.* the order of the clusters especially the long range one has to be enhanced). Moreover there is variety of inorganic clusters, which are of potential great interest but have not been prepared by micellar deposition technique so far. Also methods for aperiodic patterns have to be further developed and

transferred to the line patterns (*e. g.* by applying crew-cut micelles). Only recently model catalysis has been performed with use of supported metal nanoparticles synthesized by the technique described here.

2.2 Block copolymers via anionic polymerization

2.2.1 Introduction

The homogeneous distribution of the metal compound over all micelles is the essential condition for the formation of well-defined particles with narrow size distribution. This is only possible when narrow-distributed block copolymers self-assembly into nearly identical micelles. So far the main techniques for the synthesis of block copolymers with predictable molecular weighs and uniform chain lengths are controlled and/or living polymerizations. Although, a significant progress was achieved in controlled/living radical polymerization techniques such as: nitroxide-mediated polymerization (NMP),[114] reversible addition-fragmentation chain transfer (RAFT)[115] and especially atom transfer radical polymerization (ATRP),[116-119] ionic (anionic, cationic and ring-opening) living polymerizations are still very frequently the methods of choice when block copolymers with very narrow polydispersities are required. Among them living anionic polymerization gives nearly monodisperse polymers and is applicable to the widest range of monomers. The first examples of controlled living anionic polymerization go back to more then 50 years ago.[120, 121]

2.2.2 Principles of anionic polymerization

Anionic polymerization proceeds via negative charged active species that are in most cases carbanions or oxanions. The chain ends comprises for electrical neutrality also counteranions (cations, which are usually alkali or alkaline earth metals *e.g.* lithium). If neither spontaneous transfer nor termination is present in the system (as it is for true living polymerizations) generally two steps can be distinguished:

1) $R^- Li^+ + M \rightarrow R\text{-}M_1^- Li^+$

2) $R\text{-}M_n^- Li^+ + M \rightarrow R\text{-}M_{n+1}^- Li^+$

The polymerization will proceed until all monomer is reacted. The active sites will remain "living" and further addition of monomer will result in additional extension of chains. The distribution of molecular weights at the late stages of living anionic polymerization is very narrow and it follows Poisson-type distribution.[122] If the initiation step is much faster then propagation steps and the exchange between different active species is very fast, the degree of polymerization is given by the ratio monomer consumed/initiator: [123]

$$DP = [\Delta M]/[I]$$

Anionic polymerization as it propagates through highly reactive negative species suffers from any protic impurities that may terminate polymerization reaction. That's why special care is required in purification of every reagent. All impurities such as moisture, oxygen, carbon dioxide and others that are able to deactivate living anions need to be excluded from the system as much as possible (usually to the level of few ppm). Several excellent reviews published by group of Bates, group of Hadjichristidis and group of Mays provide guidance through the preparation of initiators, purification and manipulations of reactants as well as polymerization procedures, using both inert atmosphere techniques and high vacuum techniques.[124-126]

The monomers polymerized by anionic polymerization are those that form stable carbanion species under polymerization conditions. The double bond has to be stabilized by the electron withdrawing substituents that enable nucleofilic attack of monomer onto active center. Any acidic monomers cannot be polymerized directly and protection of these groups is required in anionic polymerization.[127-129] Monomers that were successfully polymerized anionically include styrene plus its derivatives and dienes,[130] acrylates, and metacrylates,[131] as well as heterocycles [132] (*e.g* epoxides, lactides and siloxanes).

The most versatile initiators used in anionic polymerization are the metal organic initiators such as alkyllithium compounds. The reactivity of a metal organic compound depends upon the substituents carried by the carbanionic site, its solubility in solvent chosen and its ability to dissociate to free ions. As an example the relative reactivities in

a series of alkyllithium compounds versus the increasing degree of association is given by following relation:[133]

methyllithium > *sec*-BuLi > *i*-PrLi > *tert*-BuLi > *n*-BuLi

Alkyl lithium initiators are preferred in polymerization of styrenic and dienic monomers, however due to its high reactivity they are not suitable for *e.g.* acrylic monomers.

The second class of the initiators are the radical-anions, that results from the electron transfer reaction of an alkali metal with aromatic hydrocarbons in polar aprotic solvent. Typical example is the reaction of naphthalene with sodium in THF. Obtained radical-anion is reacting with monomer by reversible electron transfer. These radical-ionic species undergo fast dimerization (by coupling radicals) leading to bifunctional initiator. The classical example with styrene is given below:[120]
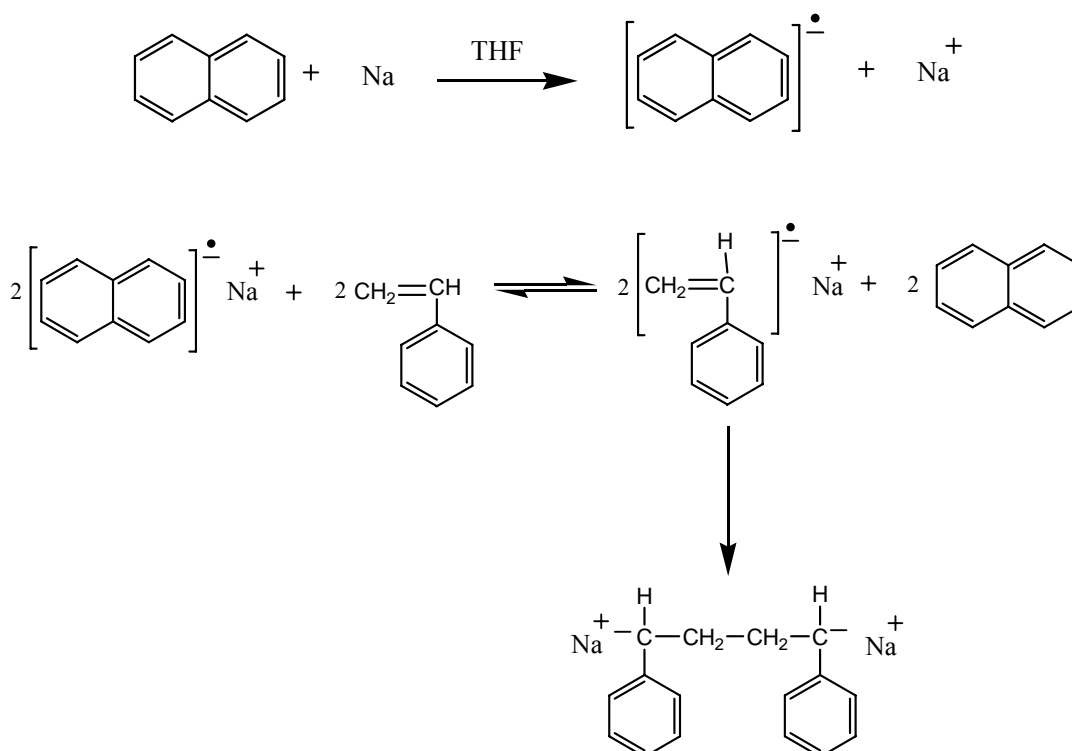
Solvents in anionic polymerizations similarly to monomers must be aprotic and free of electrophilic functions such as amino-, ester- or hydroxyl-groups. The choice of the solvent nature has a dramatic impact on the kinetics of the reaction as well as on the microstructure content (diene polymerization). In non-polar solvent the ion pairs are predominantly associated. By changing from non-polar to polar solvents, dissociation of aggregates starts leading to single contact ion pairs and solvent separated (loose) ion pairs. The solvent separated ion pairs are far more reactive then associated ions as their more easy dissociate to free ions. [134]

2.2.3   Block copolymers via anionic polymerizations

Fig 2. 14 summarizes the possible strategies towards linear block copolymers.[135] The most popular stepwise synthesis (Fig 2. 14a) allows producing diblock, triblock and multiblock copolymers with different sequence of blocks. The second route (Fig 2. 14b) involves synthesis of ω-functional homopolymers that are subsequently coupled taking advantage of the antagonist functional groups. The other routes involve switching of polymerization mechanism by the site transformation techniques (Fig 2. 14c) or using bifunctional (double-headed) initiators that are able to initiate polymerizations of two different monomers from its ends often with two diverse polymerization techniques (Fig 2. 14d).

Sequential anionic polymerization is the predominant route to well-defined linear block copolymers. Here, the terminal carbanionic site located at the chain end of the first PA block can be used to initiate the polymerization of another suitable monomer (B). If the second initiation is fast and quantitative well-defined model PA-*b*-PB diblock copolymer is prepared. The addition may be repeated leading to multi block *e.g.* PS-*b*-PI-*b*-P2VP-*b*-PtBMA-*b*-PEO pentablock copolymer was polymerized anionically by the sequential addition of five different monomers.[136] In general, monomers have to be polymerized in a certain order following the scale of reactivity (the nucleophilicity of the first block A⁻ anions should be high enough to attack the other monomer): styrene/dienes > vinylpirydines > (metha)crylates > oxiranes > siloxanes.[123]
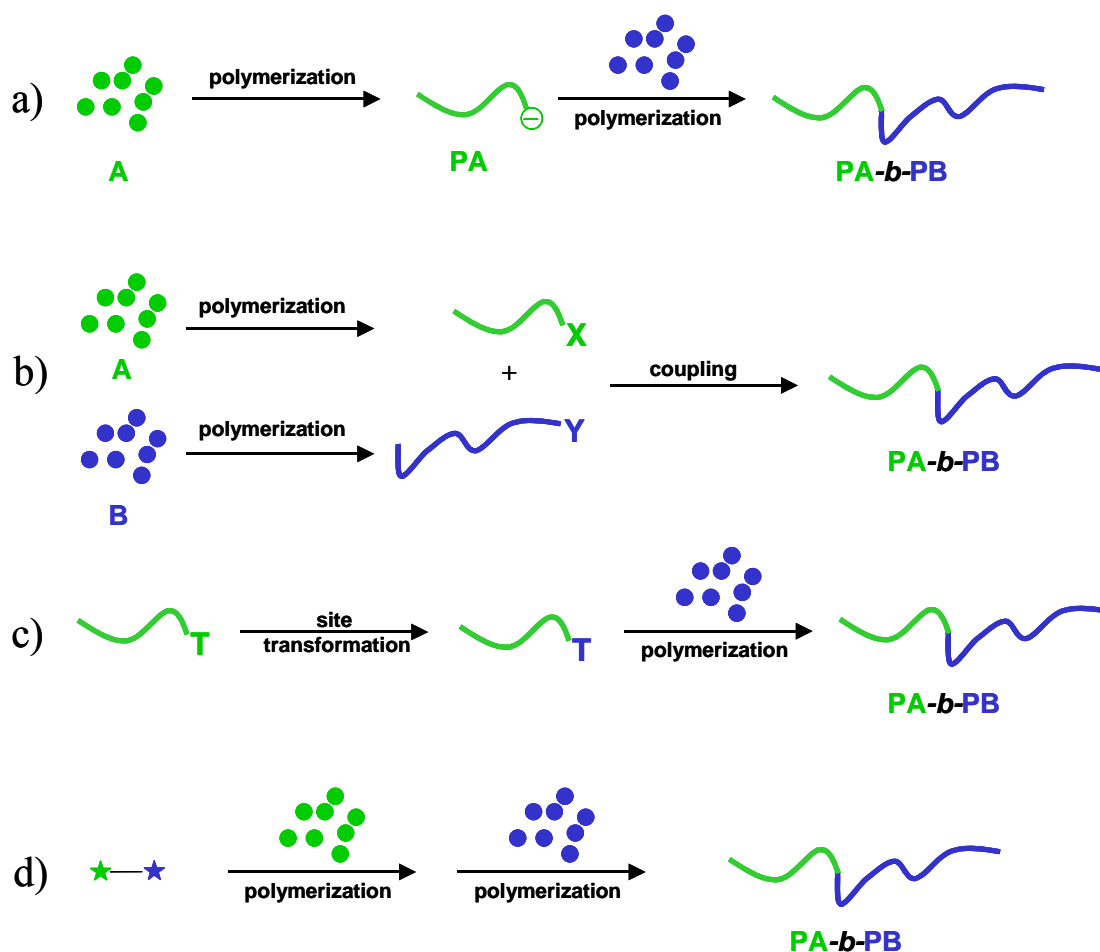
Fig 2. 14 Block copolymer synthesis: a) sequential addition of monomers; b) synthesis of linear homopolymers with functional groups followed by coupling of chains containing antagonist functions (X and Y); c) switching from one polymerization method to another; d) using dual initiator able to initiate two polymerisations.[135]

When the difference in reactivity between the first and the second monomer is very high, some side reactions may appear. In order to attenuates reactivity one can end cap living chains with diphenyl ethylene (DPE).[137-140] Because of the steric hindrance, DPE does not homopolymerize, its carbanions are less reactive then original styrene or diene carabanions, but still capable of initiating the polymerization of more electrophilic monomers.[141] An alternative method to reduce the reactivity of active centers is the addition of LiCl.[139, 142-144] It is possible to omit the "golden rule" of the scale of reactivity by chemical modification of chain ends. Following this strategy PEO-*b*-PS

and PEO-*b*-PMMA block copolymers were successfully synthesized using conversion of PEO oxanionic active ends to silyl anionic ones.[145]

Anionic polymerization give the possibility to prepare also functional polymers, where specific functional groups can be located at the one or two ends, in the center or evenly spaced along polymer chain.[146] In the synthesis of block copolymers the most interesting are ω-functional polymers that can be prepared by the reaction of living polymer with adequate termination agent. In such a way well-defined polymers with carboxyl, hydroxyl, amine, halogen, double bond and other functional groups can be prepared. The classic example of such functionalization is the carboxylation of the carbanionic living group through CO_2 addition:[147]
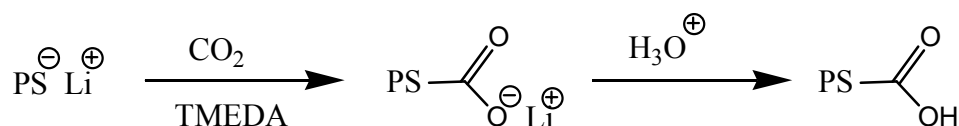
When the homopolymers are equipped with antagonist ω-functional groups well-defined block copolymers can be obtained by coupling reaction. An example of this strategy was provided by ester formation between anionically synthesized carboxylic acid terminated PS and epoxy terminal PMMA.[148] Alternatively coupling can be performed on two living polymers obtained with different polymerization mechanisms. Polystyrene-b-poly(ethyl vinyl ether) copolymers were synthesized by reacting two corresponding living homopolymers obtained by respectively living anionic and cationic polymerizations. [149]

Block copolymers that are difficult to synthesize by anionic polymerization can be sometimes straightforwardly achieved by combination of two polymerization mechanisms. The transformation of living cationic to living anionic polymerization can be realized by two-electron reduction of active cationic site. In this manner, PTHF-*b*-PCL were synthesized taking advantage of the transformation of the cationic growing center of living poly(THF) into an anionic one using samarium (II) iodide.[150] Following the transformation from anionic to ATRP, bromo-functionalized macroinitiators for ATRP were obtained by coupling with 2-bromoisobutyryl bromide

living anionic PS chains. Polymerization of methyl methacrylate leaded to PS-*b*-PMMA block copolymers.[151]

Another synthetic strategy includes dual initiators called also bifunctional or "double-headed" initiators. These initiators contain two (or more) initiation sites that are capable of initiating two (or more) polymerizations with concurrent mechanisms.[152] The advantage of this strategy towards block copolymers lies in the lack of intermediate and protection steps. PS-*b*-PCl and PMMA-*b*-PCl block copolymers were synthesized by concurrent mechanisms (anionic ROP of caprolactone and NMP of methyl methacrylate or ATRP of styrene) either in two[153] or one-step reaction.[154] Similarly, lithiopropionaldehyde dietyl acetal was used as dual initiator for preparation of polystyrene-*b*-poly(chloro-ethyl vinylether) by two-step living anionic and cationic polymerization.[155]

Anionic polymerization is a successful method to linear as well as to non-linear architectures such as star,[156-158] Y shaped block copolymers[159-161] and polymers with dendritic architectures (arborescent graft copolymers).[162, 163] Recently block copolymers with very complex and exotic architectures such as mixed arm stars,[164, 165] H-shaped, umbrella copolymers, ring-shaped block copolymers, and others were obtained.[141, 166-168]

2.2.4   Concluding remarks

Anionic polymerization provides versatile ways to produce well-defined block copolymers. Despite of the fact that anionic polymerization needs careful manipulation and special equipment (high vacuum lines, inert gas filled glove boxes, etc.), it leads to polymers with predictable molecular weighs and uniform chain lengths. Block copolymers with both linear and non-linear structures are possible by means of diverse strategies involving sequential addition of monomers, functionalization with proper group, switching between different polymerization mechanisms or dual initiators.

2.1   References

[1]   A. T. Wolde, (Ed.), *Nanotechnology Towards a Molecular Construction Kit*, STT (Study Centre for Technology Trends) Netherlands, The Hague, The Netherlands, **1998**.

[2]   A. N. Shipway, E. Katz, I. Willner, *Chem. Phys. Chem.* **2000**, *1*, 18.

[3]   R. Meyer, C. Lemire, Sh. K. Shaikhutdinov, H.-J. Freund, *Gold Bulletin* **2004**, *37*, 72.

[4]   P. V. Kamat, *J. Phys. Chem. B* **2002**, *106*, 7729.

[5]   C. Voisin, N. D. Fatti, D. Christofilos, F. Valle´e, *J. Phys. Chem. B* **2001**, *105*, 2264.

[6]   G. Schider, J. R. Kenn, W. Gotschy, B. Lamprecht, H. Ditlbacher, A. Leitner, F. R. Aussenegg, *J. Appl. Phys.* **2001**, *90*, 3825.

[7]   N. Felidj, J. Aubard, G. Levi, J. R. Krenn, G. Schidler, A. Leitner, F. R. Aussenegg, *Phys. Rev. B* **2002**, *66*, 245407.

[8]   J. P. Spatz, S. Moessmer, M. Moeller, T. Herzog, A. Plettl, P. Ziemann, *J. Lumin.* **1998**, 168.

[9]   G. Li, V. Joshi, R. L. White, S. X. Wanga, J. T. Kemp, C. Webb, R. W. Davis, S. Sun, *J. Appl. Phys.* **2003**, *93*, 7557.

[10]   S. Wirth, S. von Molnar, M. Field, D. D. Awschalom, *J. Appl. Phys.* **1999**, *85*, 5249.

[11]   H. Srikanth, E. E. Carpenter, L. Spinu, J. Wiggins, W. L. Zhou, C. J. O´Connor, *Mater. Sci. Eng., A* **2001**, *304-306*, 901.

[12]   G. Kästle, A. Schroeder, H.-G. Boyen, A. Plettl, P. Ziemann, O. Mayer, J. Spatz, M. Moeller, M. Buettner, P. Oelhafen, *Eur. J. Inorg. Chem.* **2005**, 3691.

[13]   C. Soennichsen, S. Geier, N. E. Hecker, G. von Plessen, J. Feldmann, H. Ditlbacher, B. Lamprecht, J. R. Krenn, F. R. Aussenegg, V. Z-H. Chan, J. P. Spatz, M. Moeller, *Appl. Phys. Lett.,* **2000**, *77*, 2949.

[14]   L. T. Kuhn, A. K. Geim, J. G. S. Lok, P. Hedegard, K. Ylaenen, J. B. Jensen, E. Johnson, P. E. Lindelof, *Eur. Phys. J. D* **2000**, *10*, 259.

[15]   P. Gambardella, S. Rusponi, M. Veronese, S. S. Dhesi, C. Grazioli, A. Dallmeyer, I. Cabria, R. Zeller, P. H. Dederichs, K. Kern, C. Carbone, H. Brune, *Science* **2003**, *300*, 1130.

[16] J. Mueller, C. Soennichsen, H. v. Poschinger, G. v. Plessen, T. A. Klar, J. Feldmann, *Appl. Phys. Lett.,* **2002**, *10*, 259.

[17] M. Haupt, S. Miller, K. Bitzer, K. Thonke, R. Sauer, J. P. Spatz, S. Moessmer, C. Hartmann, M. Moeller, *Phys. Stat. Sol.* **2001**, *3*, 867.

[18] B. Koslowski, S. Strobel, T. Herzog, B. Heinz, H.-G. Boyen, R. Notz, P. Ziemann, J. P. Spatz, M. Moeller, *J. Appl. Phys.* **2000**, *87*, 7533.

[19] M. Zharnikov, M. Grunze, *J. Vac. Sci. Technol. B* **2002**, *20*, 1793.

[20] A. Csaki, G. Maubach, D. Born, J. Reichert, W. Fritzsche, *Single Mol.* **2002**, *3*, 275.

[21] U. Haas, C. Thalacker, J. Adams, J. Fuhrmann, S. Riethmueller, U. Beginn, U. Ziener, M. Moeller, R. Dobrawaa, F. Wuerthner, *J. Mater. Chem.* **2003**, *13*, 767.

[22] M. Valden, X. Lai, D. W. Goodman, *Science* **1998**, *281*, 1647.

[23] J. A. Rodriguez, G. Liu, T. Jirsak, J. Hrbek, Z. Chang, J. Dvorak, A. Maiti, *J. Am. Chem. Soc.* **2002**, *124*, 5242.

[24] D. J. Eaglesham, M. Cerullo, *Phys. Rev. Lett.* **1990**, *64*, 1943.

[25] P. M. Petroff, S. P. D. Baars, *Superlattices Microstruct.* **1994**, *15*, 15.

[26] A. Javey, H. Dai, *J. Am. Chem. Soc.* **2005**, *127*, 11943.

[27] H. Brune, M. Giovannini, K. Broman, K. Kern, *Nature* **1998**, *349*, 451.

[28] J. P. Silverman, *J. Vac. Sci. Technol. B* **1997**, *15*, 2117.

[29] M. A. McCord, *J. Vac. Sci. Technol. B* **1997**, *15*, 2125.

[30] J. Melngailis, A. A. Mondelli, I. L. Berry, R. Mohondro, *J. Vac. Sci. Technol. B* **1998**, *16*, 927.

[31] D. M. Kolb, R. Ullmann, T. Will, *Science* **1997**, *275*, 1097.

[32] G. E. Engelmann, J. C. Ziegler, D. M. Kolb, *Surf. Sci.* **1998**, *275*, 1097.

[33] S. H. Hong, C. A. Mirkin, *Science* **2000**, *288*, 1808.

[34] D. S. Ginger, H. Zhang, C. A. Mirkin, *Angew. Chem. Int. Ed.* **2004**, *43*, 30.

[35] Y. Li, B. W. Maynor, J. Liu, *J. Am. Chem. Soc.* **2001**, *123*, 2105.

[36] B. W. Maynor, Y. Li, J. Liu, *Langmuir* **2001**, *17*, 2575.

[37] J. H. Fendler, (Ed.), *Nanoparticles and Nanostructured Films*, Wiley-VCH, Weinheim, **1998**.

[38] Y. Bao, M. Beerman, A. B. Pakhomov, K. M. Krishnan, *J. Phys. Chem. B* **2005**, *109*, 7220.

[39]   M. G. Warner, J. E. Hutchison, *Nat. Mater.* **2003**, *2*, 272.

[40]   L. Chitu, Y. Chushkin, S. Luby, E. Majkova, A. Satka, J. Ivan, L. Smreok, A. Buchal, M. Giersig, M. Hilgendorff, *Mater. Sci. Eng., C* **2007**, *27*, 23.

[41]   K. Niesz, M. Grass, G. A. Somorjai, *Nano Lett.* **2005**, *5*, 2238.

[42]   S. Zou, R. Hong, T. Emrick, G. C. Walker, *Langmuir* **2007**, *23*, 1612.

[43]   J. P. Spatz, S. Sheiko, M. Moeller, *Macromolecules* **1996**, *29*, 3220.

[44]   S. Moessmer, J. P. Spatz, M. Moeller, T. Aberle, J. Schmidt, W. Burchard, *Macromolecules* **2000**, *33*, 4791.

[45]   J. C. Meiners, A. Quintel-Ritzi, J. Mlynek, H. Elbs, G. Krausch, *Macromolecules* **1997**, *30*, 4945.

[46]   A. S. Dimitrov, K. Nagayama, *Langmuir* **1996**, *12*, 1303.

[47]   E. Adachi, K. Nagayama, *Langmuir* **1996**, *12*, 1836.

[48]   J. Chou, N. R. Franklin, S.-H. Baeck, T. F. Jaramillo, E. W. McFarland, *Catal. Lett.* **2004**, *95*, 107.

[49]   C. S. Hartmann, PhD thesis, (Ulm), **2003**.

[50]   G. Lengl, A. Plettl, P. Ziemann, J. P. Spatz, M. Moeller, *Appl. Phys. A* **2001**, *72*, 679.

[51]   L. Bronstein, D. Chernyshov, P. Valetsky, N. Thachenko, H. Lemmetyinen, J. Hartmann, S. Foerster, *Langmuir* **1999**, *15*, 83.

[52]   J.P. Spatz, S. Moessmer, C. Hartmann, M. Moeller, T. Herzog, M. Krieger, H.-G. Boyen, P. Ziemann, *Langmuir* **2000**, *16*, 407.

[53]   G. Kaestle, H.-G. Boyen, F. Weigl, P. Ziemann, S. Riethmueller, C. Hartmann, J.P. Spatz, M. Moeller, M. G. Garnier, P. Oelhafen, *Phase Transitions* **2003**, *76*, 307.

[54]   G. Kaestle, H.-G. Boyen, F. Weigl, G. Lengl, T. Herzog, P. Ziemann, S. Riethmueller, O. Mayer, C. Hartmann, J.P. Spatz, M. Moeller, M. Ozawa, F. Banhart, M. G. Garnier, P. Oelhafen, *Adv. Funct. Mater.* **2003**, *13*, 1.

[55]   S. Kronholz, S. Rathgeber, S Karthäuser, H. Kohlstedt, S. Clemens, T. Schneller, *Adv. Funct. Mater.* **2006**, *16*, 2346.

[56]   R. D. Bennett, A. C. Miller, N. T. Kohen, P. T. Hammond, D. J. Irvine, R. E. Cohen, *Macromolecules* **2005**, *38*, 10728.

[57] S.-H. Yun, S. I. Yoo, J. C. Jung, W.-C. Zin, B.-H. Sohn, *Chem. Mater.* **2006**, *18*, 5646.

[58] H.-G. Boyen, G. Kaestle, K. Zuern, T. Herzog, F. Weigl, P. Ziemann, O. Mayer, C. Jerome, M. Moeller, J. P. Spatz, M. G. Garnier, P. Oelhafen, *Adv. Funct. Mater.* **2003**, *13*, 359.

[59] A. Ethirajan, U. Wiedwald, H.-G. Boyen, B. Kern, L. Han, A. Klimmer, F. Weigl, G. Koastle, P. Ziemann, K. Fauth, J. Cai, R. J. Behm, A. Romanyuk, P. Oelhafen, P. Walther, J. Biskupek, U. Kaiser, *Adv. Mater.* **2007**, *19*, 406.

[60] S. Bhaviripudi, A. Reina, J. Qi, J. Kong, A. M. Belcher, *Nanotechnology* **2006**, *17*, 5080.

[61] S. Kumar, S. Zou, *Electrochem. Commun.* **2006**, *8*, 1151.

[62] H.-G. Boyen, A. Ethirajan, G. Koastle, F. Weigl, P. Ziemann, G. Schmid, M. G. Garnier, M. Bouttner, P. Oelhafen, *Phys. Rev. Lett.* **2005**, *94*, 016804.

[63] X. Li, P. Goering, E. Pippel, M. Steinhart, D. H. Kim, W. Knoll, *Macromol. Rapid Commun.* **2005**, *26*, 1173.

[64] M. V. Seregina, L. M. Bronstein, O. A. Platonova, D. M. Chernyshov, P. M. Valetsky, J. Hartmann, E. Wenz, M. Antonietti, *Chem. Mater.* **1997**, *9*, 923.

[65] J. P. Spatz, A. Roescher, M. Moeller, *Adv. Mater.* **1996**, *8*, 337.

[66] M. Moeller, J. P. Spatz, A. Roescher, S. Moessmer, S. T. Selvan, H.-A. Klok, *Macromol. Symp.* **1997**, *117*, 207.

[67] J. Spatz, S. Moessmer, M. Moeller, M. Kocher, D. Neher, G. Wegner, *Adv. Mater.* **1998**, *10*, 473.

[68] Y. Boontongkong, R. E. Cohen, *Macromolecules* **2002**, *35*, 3647.

[69] M. Antonietti, S. Foerster, J. Hartmann, S. Oestreich, *Macromolecules* **1996**, *29*, 3800.

[70] M. Breulmann, S. Foerster, M. Antonietti, *Macromol. Chem. Phys.* **2000**, *201*, 204.

[71] A. Roescher, M. Hempenius, H.-A. Klok, M. Moeller, *Acta. Polymer.* **1996**, *47*, 481.

[72] S. Klingelhoefer, W. Heitz, A. Greiner, S. Oestreich, S. Foerster, M. Antonietti, *J. Am. Chem. Soc.* **1997**, *119*, 10116.

[73]   O. A. Platonova, L. M. Bronstein, S. P. Solodovnikov, I. M. Yanovskaya, E. S. Oblonkova, P. M. Valetsky, E. Wenz, M. Antonietti, *Colloid. Polym. Sci.* **1997**, *275*, 426.

[74]   M. Antonietti, E. Wenz, L. Bronstein, M. Seregina, *Adv. Mater.* **1995**, *7*, 1000.

[75]   S. T. Selvan, T. Hayakawa, M. Nogami, M. Moeller, *J. Phys. Chem.* **1999**, *103*, 7441.

[76]   B.-H. Sohn, J.-M. Choi, S. I. Yoo, S.-H. Yun, W.-C. Zin, J. C. Jung, M. Kanehara, T. Hirata, T. Teranishi, *J. Am. Chem. Soc.* **2003**, *125*, 6368.

[77]   S. I. Yoo, B.-H. Sohn, W.-C. Zin, S.-J. An, G.-C. Yi, *Chem. Commun.* **2004**.

[78]   S.-H. Yun, B.-H. Sohn, J. C. Jung, W.-C. Zin, J.-K. Lee, O. Song, *Langmuir* **2005**, *21*, 6548.

[79]   S. Kim, F. S. Diana, P. M. Petroff, E. J. Kramer, T. Ootsu, T. Murase, *J. Polym. Sci., Part B: Polym. Phys.* **2006**, *44*, 3227.

[80]   R. D. Bennett, A. J. Hart, A. C. Miller, P. T. Hammond, D. J. Irvine, R. E. Cohen, *Langmuir* **2006**, *22*, 8273.

[81]   D. Yin, S. Horiuchi, T. Masuoka, *Chem. Mater.* **2005**, *17*, 463.

[82]   H.-G. Boyen, G. Kaestle, F. Weigl, B. Koslowski, C. Dietrich, P. Ziemann, J. P. Spatz, S. Riethmueller, C. Hartmann, M. Moeller, G. Schmid, M. G. Garnier, P. Oelhafen, *Science* **2002**, *297*, 1533.

[83]   B. R. Cuenya, S.-H. Baeck, T. F. Jaramillo, E. W. McFarland, *J. Am. Chem. Soc.* **2003**, *125*, 12928.

[84]   R. Glass, M. Möller, J. P. Spatz, *Nanotechnology* **2003**, *14*, 1153.

[85]   J. P. Spatz, V. Z.-H. Chan, S. Moessmer, F.-M. Kamm, A. Plettl, P. Ziemann, M. Moeller, *Adv. Mater.* **2002**, *14*, 1827.

[86]   M. Ott, PhD thesis, RWTH Aachen (Aachen), **2006**.

[87]   R. Glass, M. Arnold, J. Blümmel, A. Küller, M. Möller, J. P. Spatz, *Adv. Funct. Mater.* **2003**, *13*, 569.

[88]   R. Glass, M. Arnold, E. Ada Cavalcanti-Adam, J. Blümmel, C. Haferkemper, C. Dodd, J. P. Spatz, *New J. Phys.* **2004**, *6*, 101.

[89]   S.-H. Yun, B.-H. Sohn, J. C. Jung, W.-C. Zin, M. Ree, J. W. Park, *Nanotechnology* **2006**, *17*, 450.

[90] Y. Cong, J. Fu, Z. Zhang, Z. Cheng, R. Xing, J. Li, Y. Han, *J. Appl. Polym. Sci.* **2006**, *100*, 2737.

[91] W. Hwang, M.-H. Ham, B.-H. Sohn, J. Huh, Y. S. Kang, W. Jeong, J.-M. Myoung, C. Park, *Nanotechnology* **2005**, *16*, 2897.

[92] L. Cao, J. A. Massey, M. A. Winnik, I. Manners, S. Riethmueller, F. Banhart, J. P. Spatz, M. Moeller, *Adv. Funct. Mater.* **2003**, *13*, 271.

[93] J. P. Spatz, S. Moessmer, M. Moeller, *Angew. Chem. Int. Ed.* **1996**, *35*, 1510.

[94] Y. Qiao, D. Wang, J. M. Buriak, *Nano Lett.* **2007**, *7*, 464.

[95] J. P. Spatz, T. Herzog, S. Moessmer, P. Ziemann, M. Moeller, *Adv. Mater.* **1999**, *11*, 149.

[96] F. Weigl, S. Fricker, H.-G. Boyen, C. Dietrich, B. Koslowski, A. Plettl, O. Pursche, P. Ziemann, P. Walther, C. Hartmann, M. Ott, M. Möller, *Diamond Relat. Mater.* **2006**, *15*, 1689.

[97] M. Haupt, S. Miller, R. Glass, M. Amold, R. Sauer, K. Thonke, M. Moeller, J. P. Spatz, *Adv. Mater.* **2003**, *15*, 829.

[98] C. Selhuber, J. Blummel, F. Czerwinski, J. P. Spatz, *Nano Lett.* **2006**, *6*, 267.

[99] S. A. Levi, A. Mourran, J. P. Spatz, F. C. J. M. van Veggel, D. N. Reinhoudt, M. Moeller, *Chem. Eur. J.* **2002**, *8*, 3808.

[100] J. Groll, K. Albrecht, P. Gasteier, S. Riethmueller, U. Ziener, M. Moeller, *ChemBioChem* **2005**, *6*, 1782.

[101] M. Arnold, E. A. Cavalcanti-Adam, R. Glass, J. Blümmel, W. Eck, M. Kantlehner, H. Kessler, J.P.Spatz, *Chem. Phys. Chem* **2004**, *5*, 383.

[102] N. Walter, C. Selhuber, H. Kessler, J. P. Spatz, *Nano Lett.* **2006**, *6*, 398.

[103] C. Mohr, P. Claus, *Sci. Prog.* **2001**, *84*, 311.

[104] G. C. Bond, D. T. Thompson, *Gold Bulletin* **2000**, *33*, 41.

[105] D. W. Goodman, *Chem. Rev.* **1995**, *95*, 523.

[106] S. Kielbassa, A. Haebich, J. Schnaidt, J. Bansmann, F. Weigl, H.-G. Boyen, P. Ziemann, R. J. Behm, *Langmuir* **2006**.

[107] L. K. Ono, D. Sudfeld, B. R. Cuenya, *Surf. Sci.* **2006**, *600*, 5041.

[108] N. Weiher, E. Bus, B. Gorzolnik, M. Moeller, J. A. v. Bokhoven, *J. Synchrotron Rad.* **2005**, *12*, 675.

[109] S. Bhaviripudi, E. Mile, S. A. Steiner, A. T. Zare, M. S. Dresselhaus, A. M. Belcher, J. Kong, *J. Am. Chem. Soc.* **2007**, *129*, 1517.

[110] X. Liu, T. P. Bigioni, Y. Xu, A. M. Cassell, B. A. Cruden, *J. Phys. Chem. B* **2006**, *110*, 20103.

[111] J. Q. Lu, S. S. Yi, *Langmuir* **2006**, *22*, 3951.

[112] S. Park, Y. Tong, A. Wieckowski, M. J. Weaver, *Langmuir* **2002**, *18*, 3233.

[113] C. A. Bessel, K. Laubernds, N. M. Rodriguez, R. T. K. Baker, *J. Phys. Chem. B* **2001**, *105*, 1115.

[114] C. J. Hawker, A. W. Bosman, E. Harth, *Chem. Rev.* **2001**, *101*, 3661.

[115] J. Chiefari, Y. K. (Bill) Chong, F. Ercole, J. Krstina, J. Jeffery, T. P. T. Le, R. T. A. Mayadunne, G. F. Meijs, C. L. Moad, G. Moad, E. Rizzardo, S. H. Thang, *Macromolecules* **1998**, *31*, 5559.

[116] T. E. Patten, K. Matyjaszewski, *Adv. Mater.* **1998**, *10*, 901.

[117] V. Coessens, T. Pintauer, K. Matyjaszewski, *Prog. Polym. Sci.* **2001**, *26*, 337.

[118] W. Jakubowski, K. Matyjaszewski, *Angew. Chem.* **2006**, *45*, 4482.

[119] K. Matyjaszewski, W. Jakubowski, K. Min, W. Tang, J. Huang, W. A. Braunecker, N. V. Tsarevsky, *Proc. Nat. Acad. Sci. USA* **2006**, *103*, 15309.

[120] M. Szwarc, M. Levy, R. Milkovich, *J. Am. Chem. Soc.* **1956**, *78*, 2656.

[121] M. Szwarc, *Nature* **1956**, *176*, 1168.

[122] W. Lee, H. Lee, J. Cha, T.Chang, K. J. Hanley, T. P. Lodge, *Macromolecules* **2000**, *33*, 5111.

[123] M. Szwarc, *"Living Polymers and Mechanisms of Anionic Polymerization"*, Adv.Polym.Sci. 49, Springer Verlag, Berlin Heidelberg, **1983**.

[124] S. Ndoni, C. M. Papadakis, F. S. Bates, K. Almdala, *Rev. Sci. Instrum.* **1995**, *66*, 1090.

[125] D. Uhrig, J. W. Mays, *J. Polym. Sci., Part A: Polym. Chem.* **2005**, *43*, 6179.

[126] N. Hadjichristidis, H. Iatrou, S. Pispas, M. Pitsikalis, *J. Polym. Sci., Part A: Polym. Chem.* **2000**, *38*, 3211.

[127] A. Hirao, S. Loykulnant, T. Ishizone, *Prog. Polym. Sci.* **2002**, *27*, 1399.

[128] T. Ishizone, K. Okamoto, A. Hirao, S. Nakahama, *Macromolecules* **1999**, *32*, 1453.

[129] S. Loykulnant, M. Hayashi, A. Hirao, *Macromolecules* **1998**, *31*, 9121.

[130] D. Baskarana, A. H. E. Müller, *Prog. Polym. Sci.* **2007**, *32*, 173.

[131] R. Jerome, Ph. Teyssie, B. Vuillemin, T. Zundel, C. Zune, *J. Polym. Sci., Part A: Polym. Chem.* **1998**, *37*, 1.

[132] S. Penczek, M. Cypryk, A. Duda, P. Kubisa, S. Slomkowski, *Prog. Polym. Sci.* **2007**, *32*, 247.

[133] H. L. Hsieh, W. H. Glaze, *Rubber Chem. Technol.* **1970**, *43*, 22.

[134] J. Smida, M. Van Beylenb, T. E. Hogen-Esch, *Prog. Polym. Sci.* **2006**, *31*, 1041.

[135] M. Lazzari, G. Liu, S. Lecommandoux, *Block Copolymers in Nanoscience*, Wiley-VCH Verlag GmbH & Co, KGaA, Weinheim, **2006**.

[136] N. Ekizoglou, N. Hadjichristidis, *J. Polym. Sci., Part A: Polym. Chem.* **2002**, *40*, 2166.

[137] P. Guegan, J. J. Cernohous, A. K. Khandpur, T. R. Hoye, C. W. Macosko, *Macromolecules* **1996**, *29*, 4605.

[138] J. M. Yu, P. Dubois, R. Jerome, *Macromolecules* **1996**, *29*, 8362.

[139] H. Wang, M. A. Winnik, I. Manners, *Macromolecules* **2007**, *40*, 3784.

[140] G. Liu, J. Ding, S. Stewart, *Angew. Chem. Int. Ed.* **1999**, *38*, 835.

[141] R. P. Quirk, T. Yoo, Y. Lee, J. Kim, B. Lee, *Adv. Polym. Sci.* **2000**, *153*, 67.

[142] S . K. Varshney, J. P. Hautekeer, R. Fayt, R. Jerome, P. Teyssie, *Macromolecules* **1990**, *23*, 2618.

[143] R. P. Quirk, S. Corona-Galvan, *Macromolecules* **2001**, *34*, 1192.

[144] S. Pispas, N. Hadjichristidis, *Macromolecules* **2003**, *36*, 8732.

[145] T. Zundel, J. Baran, M. Mazurek, J.-S. Wang, R. Jerome, P. Teyssie, *Macromolecules* **1998**, *31*, 2724.

[146] J. Jagur-Grodzinski, *J. Polym. Sci., Part A: Polym. Chem.* **2002**, *40*, 2116.

[147] R. P. Quirk, J. Yin, L. J. Fetters, *Macromolecules* **1998**, *22*, 85.

[148] P. Guegan, C. W. Macosko, J T. Ishizone, A. Hirao, S. Nakahama, *Macromolecules* **1994**, *27*, 4993.

[149] S.Creutz, C. Vandooren, R. Jerome, P. Teyssie, *Polym. Bull.* **1994**, *33*, 21.

[150] R. Nomura, T. Endo, *Macromolecules* **1995**, *28*, 1754.

[151] M. H. Acar, K. Matyjaszewski, *Macromol. Chem. Phys.* **1999**, *200*, 1094.

[152] K. V. Bernaerts, F. E. D. Prez, *Prog. Polym. Sci.* **2006**, *31*, 671.

[153]   C. J. Hawker, J. L. Hedrick, E. E. Malmstroem, M. Trollsas, D. Mecerreyes, G. Moineau, Ph. Dubois, R. Jerome, *Macromolecules* **1998**, *31*, 213.

[154]   D. Mecerreyes, G. Moineau, P. Dubois, R. Jerome, J. L. Hedrick, C. J. Hawker, E. E. Malmstroem, M. Trollsas, *Angew. Chem. Int. Ed.* **1998**, *37*, 1274.

[155]   H. Cramail, M. Schappacher, A. Def.eux, *Polym. Adv. Technol.* **1993**, *5*, 568.

[156]   I. M . Khan, Z. Gao, K. Khougaz, A. Eisenberg, *Macromolecules* **1992**, *25*, 3002.

[157]   J. Allgaier, R. N. Young, V. Efstratiadis, N. Hadjichristidis, *Macromolecules* **1996**, *29*, 1794.

[158]   A. Avgeropoulos, Y. Poulos, N. Hadjichristidis, J. Roovers, *Macromolecules* **1996**, *29*, 6076.

[159]   A. Mavroudis, A. Avgeropoulos, N. Hadjichristidis, E. L. Thomas, D. J. Lohse, *Chem. Mater.* **2003**, *15*, 1976.

[160]   S. Gibanel, J. Forcada, V. Heroguez, M. Schappacher, Y. Gnanou, *Macromolecules* **2001**, *34*, 4451.

[161]   S. Reutenauer, G. Hurtrez, P.Dumas, *Macromolecules* **2001**, *34*, 755.

[162]   R. A. Kee, M. Gauthier, *Macromolecules* **1999**, *32*, 6478.

[163]   J. Li, M. Gauthier, *Macromolecules* **2001**, *34*, 8918.

[164]   H. Iatrou, E. Siakali-Kioulafa, N. Hadjichristidis, J. Roovers, J. Mays, *J. Polym. Sci., Part B: Polym. Phys.* **2003**, *33*, 1925.

[165]   N. Hadjichristidis, *J. Polym. Sci., Part A: Polym. Chem.* **1998**, *37*, 857.

[166]   M. Pitsikalis, S. Pispas, J. W.Mays, N. Hadjichristidis, *Adv. Polym. Sci.* **1998**, *135*, 1.

[167]   N. Hadjichristidis, M. Pitsikalis, S. Pispas, H. Iatrou, *Chem. Rev.* **2001**, *101*, 3747.

[168]   A. Hirao, M. Hayashi, S. Loykulnant, K. Sugiyama , S. W. Ryu , N. Haraguchi, A. Matsuo, T. Higashihara, *Prog. Polym. Sci.* **2005**, *30,* 111.

Chapter 3

Control of long-range ordering in block copolymer micellar monolayers

3.1   Introduction

Nanostructured surfaces can be prepared over large areas by the spontaneous self-organization of small particles. The key point in this "bottom-up" approach is to gain control over the formation of particles into the long-range ordered grains and at the same time minimize lattice defects. There are numbers of methods for patterning surfaces at the nanometer scale with particles. A simple, but rather uncontrolled way is to spray a colloidal particle suspension onto the substrate and allow the particles to deposit onto the substrate by slow evaporation of the solvent.[1-3] A more effective method is deposition by spin-coating.[4-6] In this technique a solution is spread over a fast rotating substrate. During the rapid evaporation of the solvent, the particles form hexagonal closed-packed arrays due to capillary forces until their mobility is quenched by the deficiency of the solvent. Another method to form thin layer of ordered particles is dip-coating [7-9]: a substrate is inserted into a solution and withdrawn with constant velocity. Once withdrawal is initiated and a steady-state condition is established a monolayer of closed-packed particles on the substrate is formed due to capillary forces and van der Waals interactions between the particles. Here the particles' concentration, the solvent's evaporation rate the withdrawal rate have a large influence on the density and the ordering of deposited particles.[7]

Amphiphilic block copolymers can form micelles in selective solvents.[10, 11] These micelles are composed of a relatively compact, not soluble core and a flexible corona and thus, can be considered as compressible soft spheres. Similarly to hard spheres they tend to form hexagonal ordered arrays when deposited in a form of a monolayer onto surfaces.[11-14] Furthermore, micelles can serve as nanocompartments, which can be loaded with a defined amount of an inorganic compound. A subsequent plasma treatment of the substrate, removes the polymer matrix and at the same time converts the inorganic salt to a corresponding noble metal or a metal oxide nanoparticles which maintained the same position of the micelles from which they originate. This results in a surface patterned with regular hexagonal arrays of metal or metal oxide clusters.[15-20]

Thus, gaining control on the micellar deposition process is of crucial importance with respect to the final order of the arrays on the surface.

Several groups investigated the deposition of block copolymer micelles on flat surfaces.[21-31] In most cases considerable ordering of the micelles was documented and some aspects minimizing the number of lattice defects (e.g. the withdrawal rate, the graphoepitaxy or the evaporation of a solvent) have been discussed.[14, 24] Kramer and coworkers investigated the order in a single layer of spherical domains of block copolymer melt [27-29] while Webber with his group focused on a deposition of cationic block copolymer micelles (PS-*b*-P2VPH$^+$) from aqueous solutions onto plain and patterned silicon surfaces.[30, 31] They found that both the rate of solvent evaporation and the rate of substrate withdrawal have significant impact on deposition of micelles onto substrates. The highest degree of ordering was possible when evaporation of the solvent dominated during the deposition process. According to our experience, the dip-coating procedure has proved to be the best method for the controlled growth of particle arrays over large areas.

Here we investigate the formation of monolayers of block copolymer micelles by dip-coating, focusing on the influence of the chosen selective solvent, the dipping angle and the block copolymer on the final order of the micelles deposited on silicon substrates. In order to quantify the quality of the micellar pattern, we utilized a simple and efficient method to analyse the number of defects present in the pattern.

3.2   Experimental

Materials

Toluene (Merck p.a.), xylene (Merck p.a.) and mesitylene (Merck p.a.) were dried over LiAlH$_4$ and distilled under inert gas twice. Isopropanol (Aldrich p.a.), LiAlH$_4$ (Aldrich, pallets) and acetone (Merck, technical grade) were used as received. PS-*b*-P2VP polymers (Table 3. 1) were previously synthesized in our group and the synthesis is reported elsewhere.[32] Silicon wafers were purchased from CrysTec GmbH, Berlin, Germany.

Table 3. 1Molecular weights and block lengths of the used PS-*b*-P2VP block copolymers [32]

Sample[a]	Homopolymer		Copolymer	
	Mn[a] [g/mol]	Mw/Mn[a]	Mn[a] [g/mol]	Mw/Mn[a]
PS$_{1350}$-b-P2VP$_{400}$	140 800	1.11	182 300	1.11
PS$_{1700}$-b-P2VP$_{450}$	180 200	1.09	225 400	1.13
PS$_{190}$-b-P2VP$_{190}$	19 900	1.09	40 900	1.09

[a] from SEC in $CHCl_3$ relative to narrow poly(styrene) standards

Methods

Scanning Force Microscopy (SFM) was performed with a multimode microscope equipped with a Nanoscope III controller (Digital Instruments, Veeco, Santa Barbara, U.S.A.) Investigations in the tapping mode were carried out with Si-cantilevers from Nanosensors (Weltzlar, Germany) with a spring constant of approx. 50 N/m and at a tapping frequency around 350 kHz. Image analysis was performed with the Nanoscope software (v5.12r5 Digital Instruments, Veeco, Santa Barbara, U.S.A.).

TEM: Bright field transmission electron microscopy images of the films were recorded by a Philips EM 400T microscope operating at 80 kV. In order to minimize the destructive influence of the e-beam on the sample, the intensity was kept as low as possible (second condenser lens: 50 Pt, objective lens: 30).

UV ozone treatment. Silicon wafers were treated with UV/ozone using a 40 W UV lamp (UV Technik Speciallampen GmbH; main emission 185 nm) in an oxygen stream of 350 mL/min with a sample distance of 5 mm to the lamp.

Hydrogen or *oxygen plasma* was generated by a TePla 100-E system with 100W at gas pressure of 0,25 mbar for 45 min.

Sonication Silicon wafers were sonicated using a TK 52H (Bandelin Electronic, Berlin) ultrasonic bath.

Substrate preparation

Silicon substrates were cut into pieces and cleaned by sonication in acetone, millipore water and isopropanol respectively. Activation of the surface was done by UV/ozone

treatment for 12min. Alternatively silicon substrates were exposed to oxygen plasma for 10 min.

Sample preparation

Typically a solution of the block copolymer in dry toluene was prepared with a concentration c = 5 mg/ml and mixed with 0.3 equivalent of $HAuCl_4x3H_2O$ per pyridine unit (loading 0.3) in the inert atmosphere of a Glove-Box. The mixture was stirred in the dark for at least 24 h to allow complete solubilization of the chloroauric acid in the cores of the block copolymer micelles.

Silica samples were dipped into the micellar solution and withdrawn at a constant velocity of 10 mm/min. The substrates were dipped perpendicularly to the surface of the solution except for the experiments investigating the effect of the dipping angle on the micellar order. In this case the dipping angle was changed from 45° to 135°. After withdrawal, the substrates were allowed to dry above the surface of the liquid. In order to assure comparable conditions, the dipping experiments were carried out in a closed glass-box with uniform saturation of the solvent. Once dried, the samples were analysed by means of SFM.

SFM visualisation

Large areas of the samples were scanned taking advantage of the *autocaption* function of the Nanoscope software. Nine images of the same size (2x2, 3x3 and 4x4 µm for PS(190)-*b*-P2VP(190), PS(1350)-*b*-P2VP(400) and PS(1700)-*b*-P2VP(450) respectively) were taken according to the sequence shown in Fig. 3. 1.
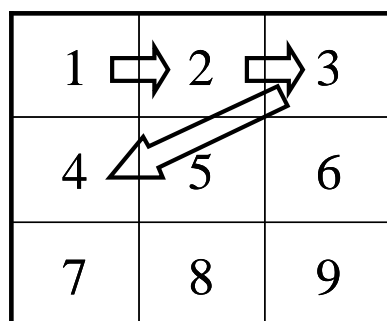

Fig. 3. 1 Scanning sequence of the autocaption function. Large areas can be scanned in this way.

Evaluation of the micellar order and determination of the distance between micelles

The micellar order was evaluated as follows. Each SFM topography image was transformed into a jpg format greyscale image and converted to a binary image using *ImageJ* software, a public domain Java image-processing software tool [W. Rasband, *ImageJ* (Imaging Software), Version 1.31., National Institutes of Health, (Bethesda), 2004]. The threshold of grey level was adjusted manually in order to identify every micelle as a white particle. Using the *paticles8plus* plugin [G. Landini *paticles8plus* plugin for *ImageJ* software, The University of Brimingham (Brimingham) 2005] each white particle was converted into a single pixel positioned in the particle's centre of mass and identified by Cartesian coordinates. The XY coordinates were transferred in form of a matrix into the Matlab software (The Mathworks Inc., *Matlab* Version 5.3.0.101083, Release 11, June 2002) and Voronoi constructions were drawn for every SFM image using a *Voronoi* function. The core-to-core distance between micelles was calculated by means of the *Delaunay Matlab* function. All calculations were done on large areas (nine pictures) and the presented data are average values for each sample. The errors were determined through evaluation of the standard deviations of the measurements.

3.3   Results and discussion

3.3.1   Dip-coating process - theoretical considerations.

Block copolymer micelles, similarly to hard spheres, form hexagonally ordered arrays when deposited in a form of a monolayer by a dip-coating process. Thus the mechanism for deposition of micelles can be considered to be similar to one proposed by Dimitrov and Nagayama for hard spheres.[7] The withdrawal procedure of the dip-coating technique is schematically illustrated in Fig. 3. 2.
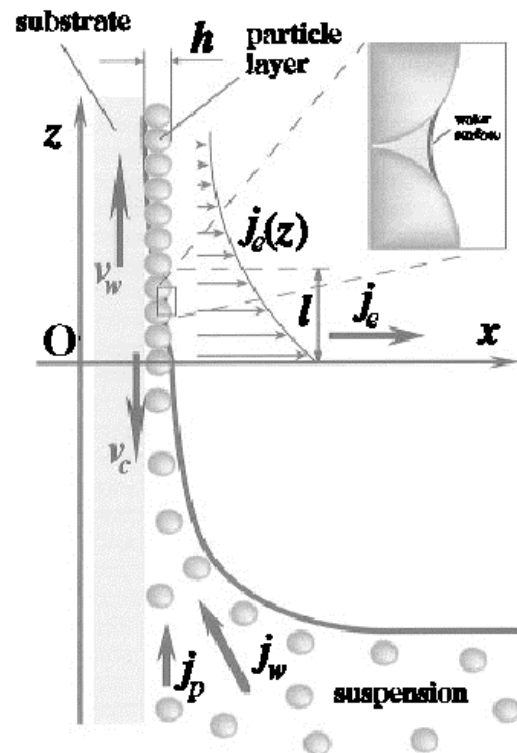
Fig. 3. 2 Schematic picture showing the particle monolayer formation by a dip-coating technique. Here, v_w denotes the substrate withdrawal rate and v_c the array growth rate; j_e, j_p and j_w is the solvent evaporation as well as the micelle and the solvent flux. The thickness of the array is described as h and l stands for evaporation length. The inset shows the menisci shape between adjacent particles.[7]

The dip-coating process leading to the regular particle monolayer begins with the formation of a thin liquid film on the surface of the substrate. Spheres are transferred from the bulk of the solution to the thin wetting film due to a convective particle flux j_p that is consequence of the solvent evaporation j_e. During the evaporation of the solvent due to thinning of the film between the neighboring spheres the curvature of the menisci is deformed which leads to a local sucking capillary pressure. The pressure gradient produces the solvent flux j_w, which carries the spheres from the bulk of the solution towards thin wetting film.

The arrangement of the particles into regular hexagonal texture starts when the thickness of the film exceeds diameter of the particles due to progressive evaporation of the solvent. The interaction between the particles confined in thin films can be

attributed to lateral capillary and electrostatic forces. The former are long-range attractive forces (the lateral component of the surface tension), which gather particles together. They are generated when the liquid surface of the menisci between the neighbouring particles is raised. This produces solvent influx from the surrounding and more spheres are transported towards the nucleus. The later forces are close-acting interparticle electrostatic repulsion. The balance between the lateral capillary and electrostatic forces determines the dense hexagonal packing.

The rate of array growth v_c as proposed by Dimitrov and Nagayama can be expressed by equation

$$v_c = \frac{\beta \, j_e l \varphi}{h(1-\varepsilon)(1-\varphi)} \tag{1}$$

where ε and h are the porosity and the height of the arrays, φ is the particle volume fraction in the solution. β is the coefficient of proportionality and depends on the particle-particle and particle-substrate interactions. For nonadsorbing particles and diluted solutions $\beta \approx 1$. Since the evaporative flux, j_e, the drying length, l, and the hydrodynamic parameter β, in eq (1) are not available experimentally, the term $\beta \, j_e l$ can be lump into a single parameter, K and the eq (1) simplifies to[33]

$$v_c = \frac{K\varphi}{h(1-\varepsilon)(1-\varphi)} \tag{2}$$

where parameter K depends on the rate of evaporation.

3.3.2   Effect of solvent on the micellar pattern.

The deposition of the micelles is controlled among other factors by the rate of evaporation of the solvent (see K parameter in equation (2)). It was found by Lin and coworkers that reducing the evaporation rate of a solvent by increasing the concentration of the non-volatile dodecanethiol ligand in toluene solution of gold particles in a simple spraying process, leads to the hexagonal structure of Au crystals over several microns.[1] Nagayama with his group observed that the control of the water

evaporation rate allows obtaining well-ordered monolayers of latex particles.[7, 34] Thus it seems reasonable to suppose that using a dip-coating technique with careful monitoring the solvent evaporation one can achieve considerable control of the spacing and ordering of block copolymer micelles. In order to decrease the rate of evaporation and as a result improve the long-range order of the micellar film we applied higher boiling solvents as selective solvents for the formation of micelles.

Two block copolymers PS(1700)-*b*-P2VP(450) and PS(1350)-*b*-P2VP(400) were dissolved with the same concentration of 5mg/ml in three different solvents: toluene, m-xylene and mesitylene (vapour pressure at 25° C : 28,4; 8,3 and 2,49 mm Hg respectively [35]).The solutions were loaded with the equivalent of 0.3 chloroauric acid molecule per pyridine unit. Subsequently SiO_2 substrates were immersed in the micellar solutions and withdrawn at a constant speed of 10 mm/min. The substrates were allowed to dry above the surface of the solution. We observed the disappearance of the residual thin film while drying. As expected, the fastest drying process occurred with toluene solutions (almost instantaneous), while the slowest drying was observed for mesitylene solutions (several seconds). SFM images of the substrates were taken and converted into Voronoi diagrams as explained in the Methods.

It has been shown that Voronoi constructions are a convenient method to estimate the regularity of a hexagonal lattice by visualization of the defects present in the pattern.[27-29, 36, 37] Voronoi diagram are obtained by drawing bonds connecting a sphere with all the neighbouring spheres around it. The perpendicular bisectors of the bonds intersect to form a polygon. The polygon has a number of sides equal to a number of nearest neighbours of the sphere in the centre. In consequence every sphere surrounded by 6 neighbours is represented by a hexagon. Pentagons and heptagons are assigned to spheres with 5 and 7 neighbours respectively.[37]

Fig. 3. 3 shows the results of such a method applied to a micellar pattern. The SFM image was digitalized and each micelle was converted into a matrix of point, each point corresponding to the centre of mass of a micelle (Fig. 3. 3 b). A voronoi diagram was subsequently constructed on the digitalized image. Usually a dislocation in the hexagonal lattice corresponds to a pair of adjacent heptagons and pentagons (Fig. 3. 3 c), however, defects in the lattice do not necessarily result in a heptagon-pentagon pair

and other combinations of heptagons and pentagons are also possible. For the simplicity the number of defects was calculated by the summation of the total number of heptagons and pentagons and then divided by two.
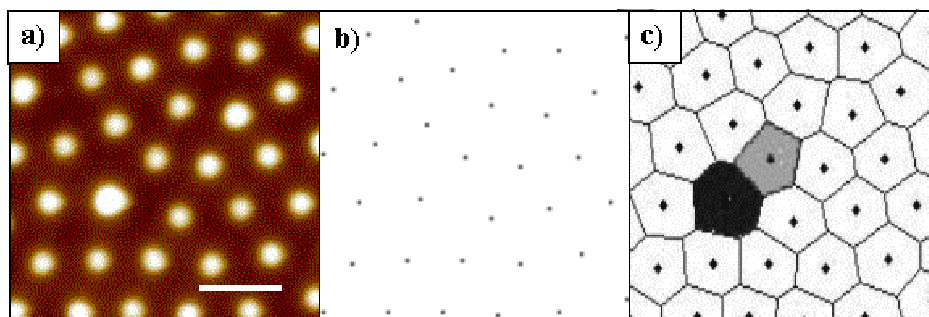

Fig. 3. 3 Principle of the conversion of SFM pictures into Voronoi diagrams. a) SFM topography image of a block copolymer micellar monolayer (scale bar 200nm); b) digitalized representation of the monolayer; c) Resulting Voronoi construction: a dislocation in the hexagonal lattice is indicated by a heptagon-pentagon pair (black and grey, respectively).

Fig. 3. 4 demonstrates typical SFM topography images and corresponding Voronoi diagrams for the PS(1700)-*b*-P[2VP(HAuCl$_4$)$_{0.3}$](450) micellar monolayers deposited on a silicon substrates from solutions in toluene, m-xylene and mesitylene. Independently of the solvent, micelles tend to form a dense hexagonal lattice. It can be observed that micelles obtained from the three different solvents slightly differ in size and hence the coverage density changes. The nature of the solvent influences the interfacial surface tension between the core and the corona resulting in different aggregation numbers of PS-*b*-P2VP micelles in toluene, xylene and mesitylene.[25] Table 3. 2 gives the average micellar height determined by *particle analysis* function (Nanoscope software). The micelles prepared in xylene are larger in height while those in mesitylene show a much broader size distribution as compared to the toluene system. For micelles obtained from a toluene solution (Fig. 3. 4 a), the SFM image and the corresponding Voronoi construction demonstrate small domains of ordered micelles that are separated by a relatively large number of defects (visible as pentagons and heptagons on the Voronoi diagram). The long-range order of the micelles is clearly improved by using the higher boiling m-xylene as selective solvent (Fig. 3. 4 b). Larger areas of hexagonal domains

are present and the number of dislocations per square micron is decreased. As expected the slower evaporation of the m-xylene prolongs the wetting of the substrate surface during the withdrawal process, allowing the micelles more time to arrange in the ordered pattern. Monolayers formed from the mesitylene solution demonstrate rather poor order with a very high number of defects (Fig. 3. 4 c). Although the least volatile mesitylene results in an even lower evaporation rate, this does not yield an increased micellar order. Apparently mesitylene is the worst medium for the PS block, among the three considered and most probably the dynamic exchange of the block copolymer molecules between different micelles is significantly disturbed. This leads to an increase of the micellar polydispersity, which drastically influences the quality of the monolayer lattice. We observed by Transmission Electron Microscopy as well as Scanning Force Microscopy, that prolonged stirring (3 weeks) does not improve the size distribution of micelles in mesitylene. This indicates that the system is still far from equilibrium.

Table 3. 2 Average height for *PS(1700)-b-P[2VP(HAuCl$_4$)$_{0.3}$](450)* **micelles deposited from three different solvents**

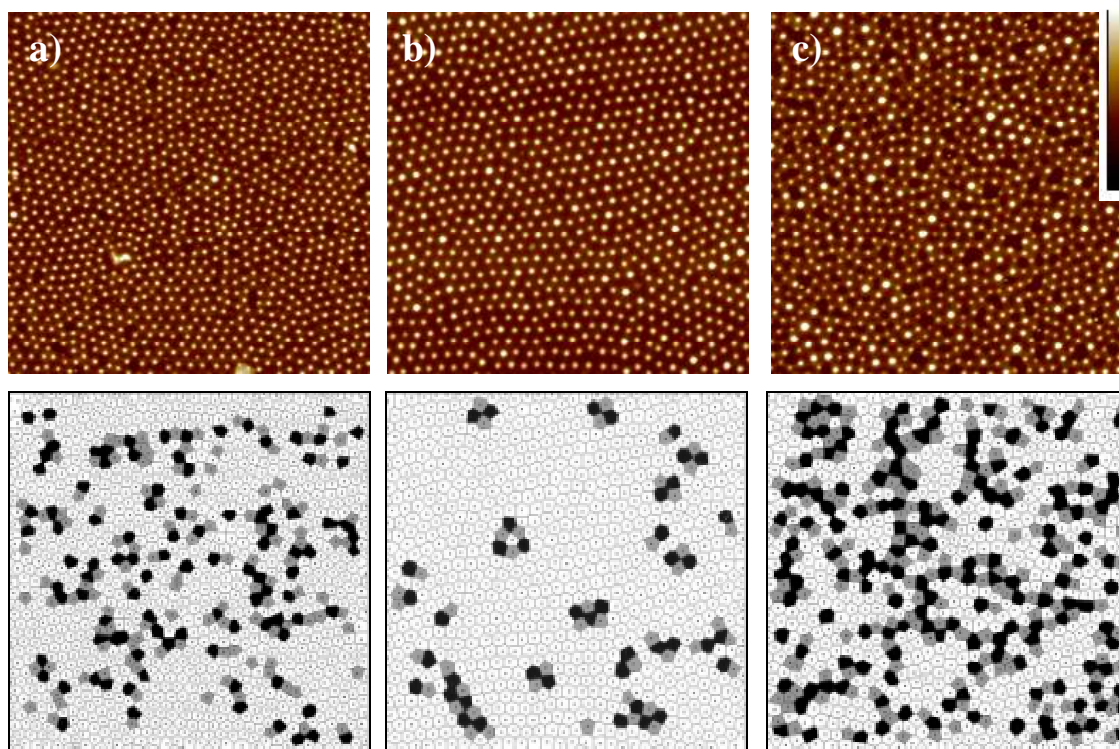| Solvent	Micellar height [nm]	σ [nm]
toluene	26	4
m-xylene	30	4
mesitylene	25	7

Fig. 3. 4 4x4 µm SFM pictures and corresponding Voronoi diagrams of PS(1700)-b-P[2VP(HAuCl₄)₀.₃](450) micellar monolayers on silica substrates obtained from a) toluene, b) m-xylene and c) mesitylene (z scale 50 nm). Defects are marked on the Voronoi diagrams.

In Fig. 3. 5 the numbers of dislocations per thousand micelles are shown as a function of the used solvent for two different block copolymers. The observed effect of the solvent on the regularity of the micellar pattern was confirmed for the gold loaded PS(1350)-b-P2VP(400) block copolymer micelles. Changing solvent from toluene to m-xylene reduces the average number of dislocations from 101 to 58 for PS(1700)-*b*-P[2VP(HAuCl₄)₀.₃](450) and from 132 to 88 for PS(1350)-*b*-P[2VP(HAuCl₄)₀.₃](400). The increase in the quality of the lattice is in a range of 43 percent for the former and 33 percent for the later micellar system. Similarly mesitylene enhances the number of defects from 65 to 40 percent dependently of the used copolymer. The solvent effect on the ordering seems to be more pronounced for the block copolymer forming bigger micelles (in our case PS(1700)-*b*-P(450)) especially when solvent is changed from toluene to mesitylene. This is most likely to be explained by two effects: 1) bigger micelles may profit more from slowing down the ordering process as they are

"kinetically slower" in achieving the final arrangement 2) the higher the molecular weight of block copolymer the slower overall polymer chain's exchange dynamics and the longer time needed to reach equilibrium state. The measurements of the micellar polydispersity in mesitylene seem to support this assumption. The size distribution from the average micellar height as estimated by the *particle analysis* function is slightly larger for PS(1700)-*b*-P[2VP(HAuCl$_4$)$_{0.3}$](450) and equal to $\sigma = 7$ whereas for PS(1350)-*b*-P[2VP(HAuCl$_4$)$_{0.3}$](400) $\sigma = 6$ nm.
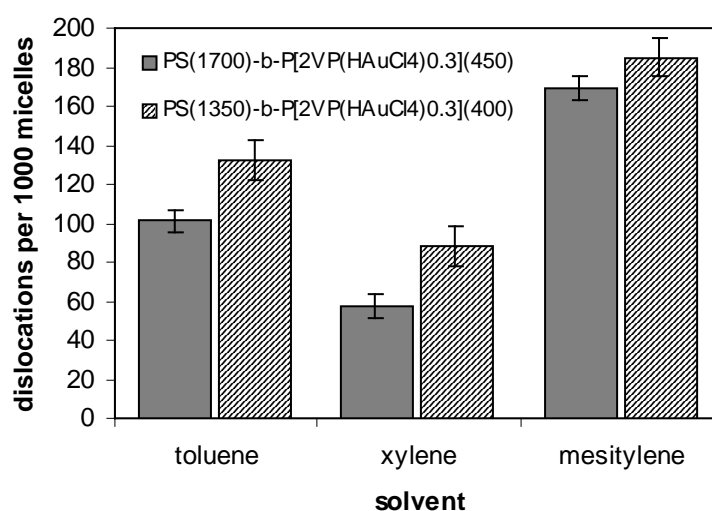
Fig. 3. 5 Dependence of the number of dislocations in hexagonal micellar lattice on selective solvent for two different block copolymer systems: PS(1700)-b-P[2VP(HAuCl$_4$)$_{0.3}$](450) and PS(1350)-b-P[2VP(HAuCl$_4$)$_{0.3}$](400).

3.3.3 Effect of dipping angle on micellar order and interdistance.

In this subsection we investigate how the variation of the dipping angle during the dip-coating process influences the micellar ordering on flat surfaces. During the dipping procedure the substrates were tilted at different angles with respect to the surface of the micellar solution, specifically at 45°, 60°, 90° 120° and 135°. SFM images of micellar monolayers deposited on silicon substrates at 45°, 90° and 135° and corresponding Voronoi diagrams are shown in Fig. 3. 6. It is clearly visible from the SFM images that the micellar interdistance changes considerably with the dipping angle, becoming smaller for larger dipping angles. The number of lattice defects per thousand micelles is shown in table 3.2 for different dipping angles. The order of the micelles does not show

a significant discrepancy if we count number of lattice defects taking into account various periodicities of micelles and calculating average numbers of displacements for tilted substrates in function of a number of micelles (Table 3. 3).
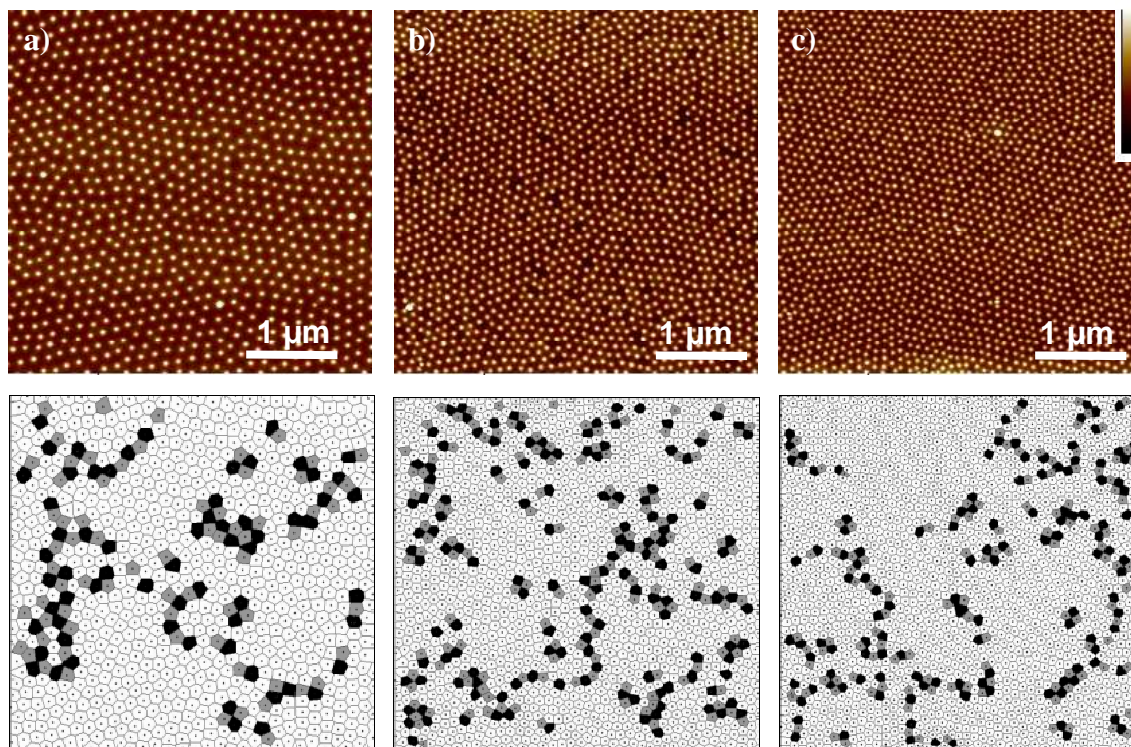

Fig. 3. 6 SFM pictures and equivalent Voronoi constructions of micellar films of PS(1700)-b-P[2VP(HAuCl₄)₀.₃](450) deposited on substrates tilted at different angles during the dipping procedure. a) 45 °, b) 90 ° and c) 135 ° with respect to the surface of the micellar solution (z scale 50 nm).

Table 3. 3 Effect of the dipping angle on the number of dislocations in the hexagonal micellar lattice.

Angle	Number of dislocations per 1000 micelles
45°	91 ± 7
60°	95 ± 8
90°	90 ± 9
120°	79 ± 8
135°	74 ± 7

Only in case of obtuse angles (120 and 135°) and corresponding high-density micellar coverage, the number of defects slightly decreases. This is due to the fact that we are dealing with the soft spheres, which can stretch or shrink depending on the conditions. Thus the micellar corona can compensate to a certain extend the effect of the higher or lower density of the micelles. However as the number of micelles increases drastically the electrostatic repulsion between neighbouring spheres plays a more important role in the lattice formation and due to lack of space freedom micelles tend to act much more like hard spheres. Fig. 3. 7 shows the dependence of the average micellar centre-to-centre distance on the dipping angle for two different polymers PS(1700)-*b*-P2VP(450) and PS(190)-*b*-P2VP(190) loaded with a gold precursor salt.
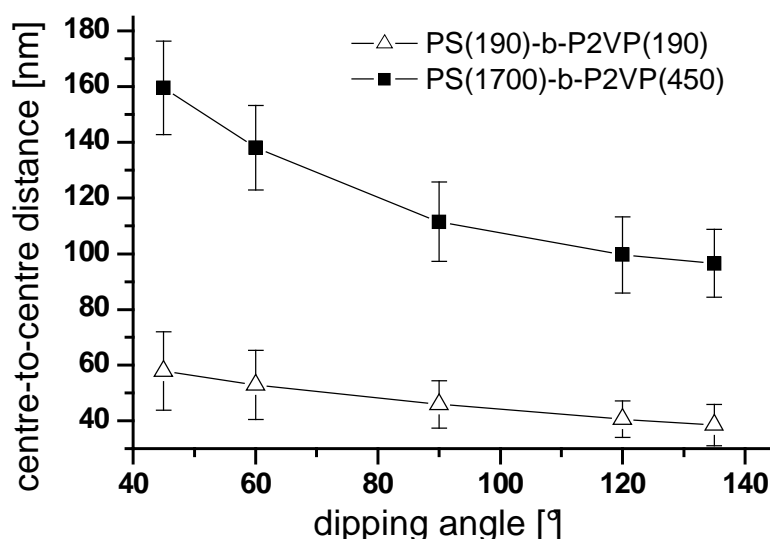
Fig. 3. 7 The micellar centre-to-centre distance in a hexagonal lattice as a function of the dipping angle for two different block copolymers: PS(1700)-b-P2VP(450) and PS(190)-b-P2VP(190) loaded with 0.3 HAuCl₄ molecules per pyridine unit.

For both polymers, it was possible to systematically change the density of the deposited micelles by varying the dipping angle, without affecting the order of the micelles. Specifically, we were able to control the interdistance of PS(1700)-*b*-P[2VP(HAuCl$_4$)$_{0.3}$](450) micelles from 95 to 160 nm and the interdistance of PS(190)-*b*-[P2VP(HAuCl$_4$)$_{0.3}$](190) from 40 to 60 nm. The elastic part of the micelle, which decides about stretching or shrinking behaviour, is the PS corona. Therefore the

longer PS block in the copolymer the larger the range in which distance between the micelles can be controlled. We believe that by tilting the samples at different angles from 45 to 135° we change the fluid meniscus as schematically depicted in Fig. 3. 8.
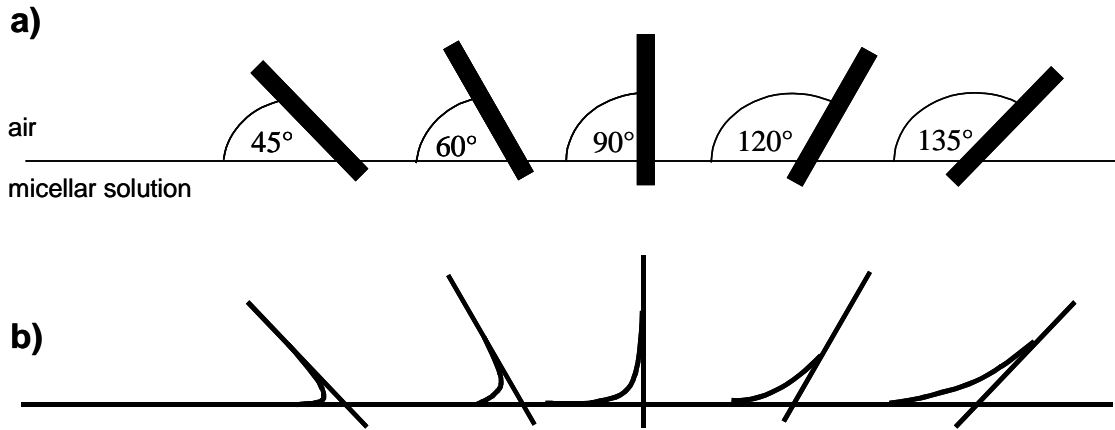

Fig. 3. 8 Deposition of micellar monolayer onto substrate under selected angles a) and corresponding contact line shapes b).

The influence of the angle on the film thickness can be explained as following. Assuming very low concentration of micelles and neglecting evaporation process during dip-coating the maximal film thickness h_∞ can be calculated from Lanadau and Levich equation [38]

$$h_\infty = 0.946 \left(\frac{\sigma}{\rho g} \right)^{1/2} Ca^{2/3} \qquad\qquad (3)$$

where σ, ρ and g stand for surface tension, solution density and gravitational constant respectively. Ca is the capillary number and is defined as

$$Ca = \frac{\mu U}{\sigma} \qquad\qquad (4)$$

where μ is the solution viscosity and U denotes the withdrawal rate. The equation (3) can be extended to substrates dip-coated under different angles with respect to the surface of the solution [38]

$$h_{\infty} = \left(\frac{\sigma}{\rho g}\right)^{1/2} \frac{1}{\sqrt{1-\sin\alpha}} \left[0.94581\,Ca^{2/3} - \frac{0.10685\cos\alpha}{1-\sin\alpha}\,Ca\right] \tag{5}$$

where α is the angle of inclination defined as the angle that the substrate makes with respect to the surface normal. By defining α as angle between substrate and the surface of the micellar solution we obtain following equation

$$h_{\infty} = \left(\frac{\sigma}{\rho g}\right)^{1/2} \frac{1}{\sqrt{1+\cos\alpha}} \left[0.94581\,Ca^{2/3} - \frac{0.10685\sin\alpha}{1+\cos\alpha}\,Ca\right] \tag{6}$$

The micellar film thickness calculated by the equation (6) as a function of inclination for the experimental withdrawal speed 10 mm/min is plotted in Fig. 3.9. (as for the pure toluene: $\sigma = 28.5 \times 10^{-3}$ N/m, $\rho = 866.9$ kg/m^3 and $\mu = 0.59 \times 10^{-3}$ sPa (20°C)[35]).
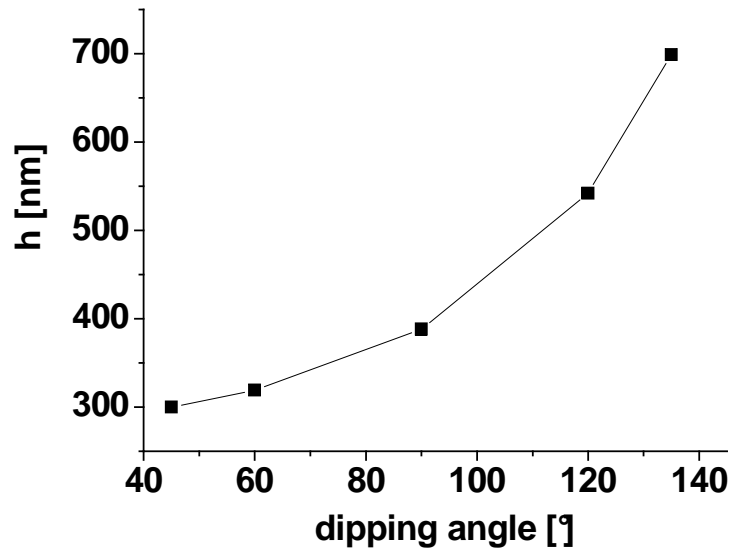

Fig. 3. 9 The calculated film thickness in a function of angle inclination.

The calculated film thickness increases with the increasing angle of inclination. Thus we may presume that sharp contact line shapes provide thinner micellar film and in consequence fewer micelles are interacting with each other leading to lower density of deposited micelles on the substrate. On the contrary tilting substrate under obtuse angles (smooth contact line shapes) increases overall amount of micelles that have to self-assemble on the substrate.

A similar reasoning was followed by Hartmann[14] to explain the changes in center-to-center distances for micellar layers deposited on substrates at different dipping velocities. A range of distances from 95 nm to 130 nm was demonstrated with the same PS(1700)-*b*-P2VP(450) block copolymer.

3.4   Conclusions

Block copolymer micelles loaded with noble metal salt can be deposited as a monolayer on flat substrates by simple dip-coating technique. Two aspects influencing the final arrangement of the micelles were studied: the choice of the selective solvent and the dipping angle. We demonstrated that micelles tend to self-organize in a lattice with fewer defects when a higher boiling solvent was exploited, provided that the solvent is still a good solvent for the corona-forming block of the copolymer. The angle between the substrate and the surface of the micellar solution during the dipping procedure had no significant effect on the ordering except for the case when substrate is dipped under obtuse angles. In this case we observed slight increase over long-range order. Changing the dipping angle proved to be a convenient and valuable tool to control the distance between the micelles without necessity of changing the block length and ratio of copolymer.

3.5   References

[1]   X. M. Lin, H. M. Jaeger, C. M. Sorensen, K. J. Klabunde, *J. Phys. Chem. B* **2001**, *105*, 3353.

[2]   B. A. Korgel, D. Fitzmaurice, *Phys. Rev. Lett.* **1998**, *80*, 3531.

[3]   S. H. Im, O. O. Park, *Langmuir* **2002**, *18*, 9642.

[4] J. C. Hulteen, D. A. Treichel, M. T. Smith, M. L. Duval, T. R. Jensen, R. P. V. Duyne, *J. Phys. Chem. B* **1999**, *103*, 3854.

[5] B.-H. Sohn, J.-M. Choi, S. I. Yoo, S.-H. Yun, W.-C. Zin, J. C. Jung, M. Kanehara, T. Hirata, T. Teranishi, *J. Am. Chem. Soc.* **2003**, *125*, 6368.

[6] J. C. Hulteen, R. P. V. Duyne, *J. Vac. Sci. Technol. A* **1995**, *13*, 1553.

[7] A. S. Dimitrov, K. Nagayama, *Langmuir* **1996**, *12*, 1303.

[8] P. Jiang, J. F. Bertone, K. S. Hwang, V. L. Colvin, *Chem. Mater.* **1999**, *11*, 2132.

[9] Z.-Z. Gu, A. Fujishima, O. Sato, *Chem. Mater.* **2002**, *14*, 760.

[10] A.-V. Ruzette, L. Leibler, *Nature Materials* **2005**, *4*, 19.

[11] A. B. R. Mayer, *Polym. Adv. Technol.* **2001**, *12*, 96.

[12] S. Moessmer, J. P. Spatz, M. Moeller, T. Aberle, J. Schmidt, W. Burchard, *Macromolecules* **2000**, *33*, 4791.

[13] J.P. Spatz, S. Moessmer, C. Hartmann, M. Moeller, T. Herzog, M. Krieger, H.-G. Boyen, P. Ziemann, *Langmuir* **2000**, *16*, 407.

[14] C. S. Hartmann, PhD thesis, (Ulm), **2003**.

[15] H.-G. Boyen, G. Kaestle, F. Weigl, B. Koslowski, C. Dietrich, P. Ziemann, J. P. Spatz, S. Riethmueller, C. Hartmann, M. Moeller, G. Schmid, M. G. Garnier, P. Oelhafen, *Science* **2002**, *297*, 1533.

[16] G. Kaestle, H.-G. Boyen, F. Weigl, G. Lengl, T. Herzog, P. Ziemann, S. Riethmueller, O. Mayer, C. Hartmann, J.P. Spatz, M. Moeller, M. Ozawa, F. Banhart, M. G. Garnier, P. Oelhafen, *Adv. Funct. Mater.* **2003**, *13*, 1.

[17] H.-G. Boyen, G. Kaestle, K. Zuern, T. Herzog, F. Weigl, P. Ziemann, O. Mayer, C. Jerome, M. Moeller, J. P. Spatz, M. G. Garnier, P. Oelhafen, *Adv. Funct. Mater.* **2003**, *13*, 359.

[18] S.-H. Yun, B.-H. Sohn, J. C. Jung, W.-C. Zin, J.-K. Lee, O. Song, *Langmuir* **2005**, *21*, 6548.

[19] B. R. Cuenya, S.-H. Baeck, T. F. Jaramillo, E. W. McFarland, *J. Am. Chem. Soc.* **2003**, *125*, 12928.

[20] C.-C. Weng, K.-F. Hsu, K.-H. Wei, *Chem. Mater.* **2004**, *16*, 4080.

[21] J. K. Cox, A. Eisenberg, R. B. Lennox, *Curr. Opin. Colloid Interface Sci.* **1999**, *4*, 52.

[22]   H. Yokoyama, T. E. Mates, E. J. Kramer, *Macromolecules* **2000**, *33*, 1888.

[23]   E. J. Kramer, *Nature* **2005**, *437*, 824.

[24]   J. Hahn, S. E. Webber, *Langmuir* **2004**, *20*, 4211.

[25]   S. Krishnamoorthy, R. Pugin, J. Brugger, H. Heinzelmann, C. Hinderling, *Adv. Funct. Mater.* **2006**, *16*, 1469.

[26]   R. A. Segalman, H. Yokoyama, E. J. Kramer, *Adv. Mater.* **2001**, *13*, 1152.

[27]   R. A. Segalman, A. Hexemer, E. J. Kramer, *Macromolecules* **2003**, *36*, 6831.

[28]   R. A. Segalman, A. Hexemer, R. C. Hayward, E. J. Kramer, *Macromolecules* **2003**, *36*, 3272.

[29]   R. A. Segalman, A. Hexemer, E. J. Kramer, *Phys. Rev. Lett.* **2003**, *91*, 196101.

[30]   J. Hahn, S. E. Webber, *Langmuir* **2003**, *19*, 3098.

[31]   J. Hahn, S. E. Webber, *Langmuir* **2004**, *20*, 1489.

[32]   S. Moessmer, PhD thesis, University of Ulm (Ulm), **1999**.

[33]   B. G. Prevo, O. D. Velev, *Langmuir* **2004**, *20*, 2099.

[34]   N. D. Denkov, D. Velev, P. A. Kralchevsky, I. B. Ivanov, H. Yoshimura, K. Nagayamat, *Langmuir* **1992**, *8*, 3183.

[35]   D. R. Lide, *Handbook of Chemistry and Physics*, 75th ed., CRC Press, **1994**.

[36]   A. H. Marcus, S. A. Rice, *Phys. Rev. E* **1997**, *55*, 637.

[37]   F. P. Preparata, M. I. Shamos, *Computational Geometry*, Springer, New York, **1985**.

[38]   A. A. Darhuber, S. M. Troian, J. M. Davis, S. M. Miller, *J. Appl. Phys.* **2000**, *88*, 5119.

Chapter 4

Synthesis of branched copolymers

4.1   Introduction

Anionic polymerization is among the best tools for the synthesis of tailor-made polymers with controllable molecular weight and narrow polydispersity. This powerful technique offers methods for the controlled manipulation of macromolecular architecture and not only simple block copolymers, but also polymers with complex architectures such as multi-block polymers, star polymers, star-block copolymers, graft copolymers, and miktoarm star copolymers can be successfully prepared by living anionic polymerization.[1-7] However, there are still only a few references about Y shape copolymers (also called AB$_2$-type or miktoarm). The reason for this may lie in their preparation, which requires a multi-step synthesis.

The first synthesis of a Y shape copolymer was described by Teyssie et al.[8] Polystyrene-*block*-[poly-(ethylene oxide)]$_2$ [PS-*b*-(PEO)$_2$] was obtained by end-capping a living polystyryl carbanion by a naphthalene derivative followed by polymerization of ethylene oxide using naphthalene sodium radical ion as the initiator. Recently, Gnanou and co-workers synthesized in several steps styrene-functionalised PS-b-(PEO)$_2$ macromonomers using anionic polymerization in combination with protecting group chemistry. These copolymers were used as reactive surfactants in emulsion polymerization [9] and also as steric stabilizers for dispersion polymerization.[10] An interesting route based on a double addition-elimination reaction of polystyryl Li or K on a specific 1,1-diphenylethylene derivative leading to PS$_2$-PEO, PS$_2$-PLLA, PS$_2$-PMAA and PS$_2$-tBuMA Y shape copolymers, respectively, was reported by the group of Dumas.[11] Other pathways to miktoarm copolymers involve reactions with chlorosilane derivatives [12-14] or non-polymerizable linking agents. [5, 15] Recently, also cationic[16] and atom-transfer radical polymerization (ATRP) [17-20] were successfully applied in the synthesis of AB$_2$ type polymers. For example polystyrene-*block*-[poly(*tert*-butyl acrylate)]$_2$ [PS-(PtBA)$_2$] Y-shaped block copolymers were synthesized by ATRP using a multistep route involving protecting group

chemistry.[20] Hydrolysis of the *tert*-butyl groups led to the formation of amphiphilic PS-(PAA)$_2$ Y-shaped block copolymers.

It is well known that block copolymers similarly to low molecular weight surfactants can self-organize into micelles if they are dissolved in a selective solvent for one of the polymer block.[21, 22] The parameters of the micelles such as overall size, core and shell dimensions, microstructure, aggregation number and other properties are influenced by chemical nature, molecular weight of the blocks, solvent-block interactions, concentration, temperature and also architecture of the copolymer. Recently, it was found that the Y shape block copolymers consisting of two identical blocks covalently linked to the third one show different micellar behaviour compared to the simple AB block copolymers.[16, 23, 24]

Here we report on our attempts in the synthesis of an AB$_2$ block copolymer where block A is hydrophobic (poly(isoprene)) and block B hydrophilic (poly(ethylene oxide)). Two synthetic pathways were explored. The first route was based on the combination of anionic polymerization with protection chemistry whereas the second one consisted of a sequential two-step anionic synthesis. Additionally, we report on the preparation of poly(ethylene oxide) four arm star polymers.

4.2   Experimental

Materials

Ethylene oxide (Messer, 2.8) was purged through columns filled with CaH$_2$ and molecular sieves (pore size 4Å), respectively. Isoprene was dried over CaH$_2$ then distilled under inert gas over Na. Toluene (Merck, p.a.), benzene (Merck, p.a.), and tetrahydrofuran (THF) (Merck, p.a.) were dried over LiAlH$_4$ and distilled twice under inert gas, n-hexane (Merck, p.a.) dried over CaH$_2$ and distilled under N$_2$. Trimethylolpropane allyl ether (Aldrich 98%), 2,2-dimethoxypropane (Aldrich 98%) and 1,1-diphenylethylene (DPE) (Aldrich, 97%) were distilled under inert gas atmosphere. p-Toluenesulfonic acid monohydrate (Aldrich, 98%), KI (Fluka, 99%), NaCl (Aldrich, p.a.), Na$_2$SO$_4$ (Fluka, p.a., anhydrous), Me$_2$SiHCl (Aldrich, 98%), divinyltetramethyldisiloxane platinum (PC072) (ABCR, 3-3,5% platinum), s-BuLi (Aldrich, 1.3 mol/l in cyclohexane), (Bu)$_2$Mg (Aldrich, 1.0 mol/l in heptanes), CaH$_2$

(Fluka, p.a.), LiAlH$_4$ (Aldrich, pallets), acetic acid (Fluka, p.a.), N,N,N′,N′-tetramethylethylenediamine (TMEDA) (Fluka, 99%), diphenylmethane (Fluka, p.a.), naphthalene (Aldrich), acetone (Merck, technical grade), and petrol ether (Merck, technical grade) were used as received.

Methods

All polymerizations were performed in the high vacuum line or in N$_2$ atmosphere inside a Glove Box.

Size Exclusion Chromatography (SEC). The molecular weight of polymers was determined in Freon or chloroform at room temperature using Waters microstyragel columns (pore size 10^5, 10^4, 10^3 Å). Detection was performed on a differential refractometer (Waters model 410) and a differential viscometer (Viscothek model H502, SEC-Win software). Elution volumes were converted to the molecular weights based on calibration with narrow polydispersity PI or PS standard samples.

^{1}H-NMR spectra were performed in CDCl$_3$ (99,8%, Deutero GmbH) on a Bruker DRX 400 spectrometer at 400 MHz.

Fourier Transform Infrared Spectroscopy (FT-IR) spectra were recorded on a Bruker IFS 113V spectrometer. Samples were prepared as KBr pellets.

Thin layer chromatography (TLC) was carried out on silica gel plates (Merck, DC-Alufolien Aluminiumoxid 150 F$_{254}$).

Synthesis
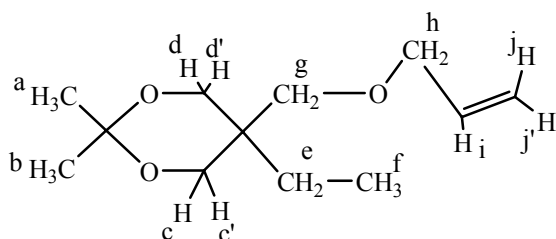
II

2,2-Dimethyl-5-ethyl-5(allyloxymethyl)-1,3-dioxane (**II**). p-Toluenesulfonic acid monohydrate (92 mg) was added to a mixture of 2-(allyloxymethyl)-2-ethyl-1,3-

propanediol (9.2 g, 53 mmol) and 2,2-dimethoxypropane (97.8 ml) and stirred at RT. After 1.5 hours the solution was shaken with fresh aqueous 5% sodium bicarbonate solution (7ml), then saturated aqueous solution of NaCl (25 ml) was added and the mixture was again shaken. After removal of the lower aqueous layer the organic phase was again washed with 25 ml of NaCl solution and separated. The organic layer was dried over Na_2SO_4, filtered and the solvent evaporated at 40 °C/40 mbar. This yielded 11.2 g colourless oil. Distillation at 50 °C/2 mbar gave 9.3 g (82% yield) of an oil. ^{1}H NMR ($CDCl_3$, δ in ppm) 0.79 (t, $3H^f J_{HH}$= 3.8 Hz), 1.33 (q, $2H^e J_{HH}$= 7.2 Hz), 1.37 (s,s, $3H^a$ and $3H^b J_{HH}$= 7.2 Hz), 3.46 (s, $2H^g$), 3.61 (dd, $2H^{cd}$ and $2H^{c'd'} J_{HH}$= 10.0 and 17.6 Hz), 3.95 (m, $2H^h$), 5.18 (m, H^j and $H^{j'}$), 5.87 (m, $2H^i$)
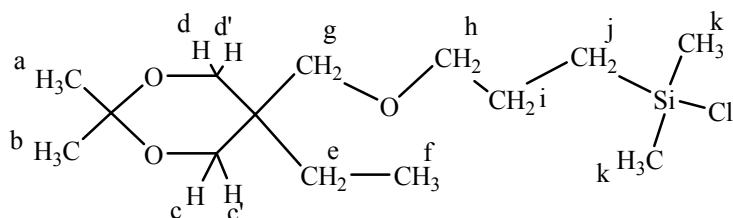
III

2,2-Dimethyl-5-(chlorodimethylsilylpropyloxymethyl)-5-ethyl-1,3-dioxane (**III**). A mixture of compound **II** (6.3 g, 29.4 mmol), dimethylchlorosilane (8 ml, 73.0 mmol), n-hexane (15 ml) and a solution of divinyltetramethyldisiloxane platinum (PC072, ABCR, 3-3,5% platinum; 30 μl) in xylene was stirred at 30 °C for 16 hours. The reaction progress was controlled by TLC in $CHCl_3$. Distillation at 60 °C /$3*10^{-2}$ mbar gave 6.8 g (81% yield) of a colourless oil. ^{1}H NMR ($CDCl_3$, δ in ppm) 0.36 (s, $6H^k$), 0.78 (m, $3H^f$ and $2H^j$), 1.33 (q, $2H^e J_{HH}$= 7.2 Hz), 1.37 (d, $3H^a$ and $3H^b J_{HH}$= 7.2 Hz), 1.63 (m, $2H^i$), 3.37 (t, $2H^h J_{HH}$= 7.6 Hz), 3.40 (s, $2H^g$), 3.60 (dd, $2H^{cd}$ and $2H^{c'd'} J_{HH}$= 11.8 and 30.0 Hz).

III'
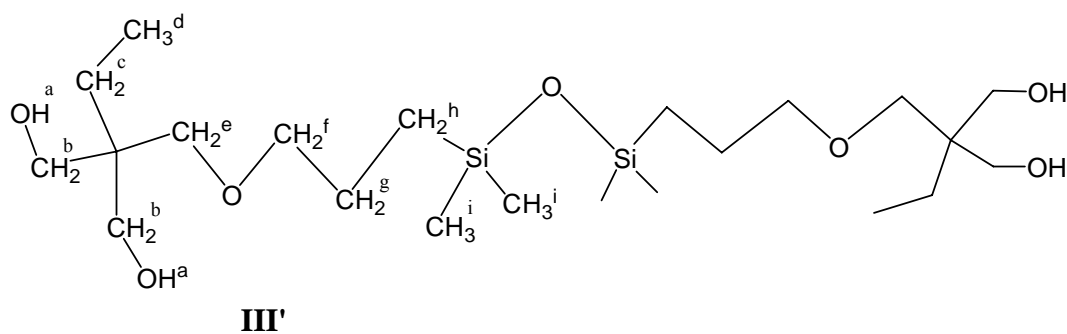
1,3-bis-[(2,2-dihydroxymethyl)-butyloxypropyl]-tetramethyl-disiloxane (**III'**). A mixture of compound **III** (2.5 g, 8.2 mmol), H_2O (1 ml) and HCl (0.5 ml, 37%) was stirred in a 10 ml flask for 10h. After that the solvent was evaporated at 30 °C giving 2.3 g (92% yield) of colourless oil. The product (**III'**) of the reaction was freeze-dried several times with anionic-pure benzene and dried in vacuo (ca. 10^{-5} mbar) overnight. ^{1}H NMR (CDCl_3, δ in ppm) 0.05 (s, 12H[i]), 0.45 (m, 4H[h]), 0.78 (m, 6H[d]), 1.31 (q, 4H[c] J_{HH}= 7.2 Hz), 1.63 (m, 4H[g]), 3.37 (t, 4H[f] J_{HH}= 7.6 Hz), 3.40 (s, 4H[e]), 3.60 (dd, 4H[b]J_{HH}= 11.8 and 30.0 Hz). FT-IR 3150-3600 (broad, –OH), 1000-1150 (Si-O-Si).

Preparation of Y-shape copolymers – first route

Prior to the polymerization experiments isoprene was dried over Bu_2Mg and condensed to the calibrated ampoule using high vacuum techniques. Chlorosilane **III** was purified first using the long spinning band column in order to distil-off unsaturated impurities then distilled twice by "kugelrohr distillation" and transferred to the Glove Box. Toluene was purified over s-BuLi/DPE, condensed to the flask and also transferred to the Glove Box. Typically, the polymerization procedure proceeded as follows: 40 ml of toluene and 2.78 g (40.85 mmol) isoprene were given to the reaction flask at –78 °C. After several minutes 0.86 ml (0.98 mmol) s-BuLi were added to the mixture. The solution was allowed to stir for some minutes and the temperature was increased to 25 °C. The development of the yellow colour evidenced the formation of carbanionic living species. Polymerization was allowed to proceed several hours. After completed reaction excess of chlorosilane **III** was added to the living anions. The yellow colour of the mixture disappeared immediately. The solution was stirred for some time depending on the experimental conditions. After that the polymer was precipitated twice in methanol, dried under vacuum and analysed by ^{1}H NMR and SEC. The following step -

splitting the protection group - was performed in toluene or THF by acetic acid, HCl or BCl$_3$, respectively. Typically 0.5g of polymer was dissolved in 5 ml of solvent and the acidic reagent was added in amounts from 20 µl to 3 ml depending on the experiment. The reaction was controlled by ^{1}H NMR. The polymer was isolated from the reaction mixture by precipitation in methanol and dried several times with the freeze-drying technique.

The polymerization of ethylene oxide from deprotected hydroxyl groups was carried out with diphenylmethyl potassium (DPMK), which was synthesized according to ref [25]. To the solution of 1 g (0.308 mmol) polyisoprene in 60 ml THF, 0.2 ml of DPMK in THF (0.911mol/l) was added dropwise until a slight reddish colour persisted. Subsequently, 0.4 ml (8 mmol) EO was added. The mixture was warmed up to room temperature and stirred for 48h. The living anions were quenched with 1 ml acetic acid. The product of the reaction was precipitated in hexane and methanol. Obtained different fractions were analysed by ^{1}H NMR and SEC.

Preparation of Y-shape copolymers – second route

Prior to the polymerization experiments THF was purified over s-BuLi/DPE, condensed to the valve-equipped flask, and transferred to the Glove Box. Solutions of allyl ether and diphenylmethyl potassium were prepared in THF. Typically, to the mixture of 40 ml THF and 3.88 ml solution of allyl ether **I** in THF (0.45 mol/l) 3.85 ml of diphenylmethyl potassium in THF (0.911 mol/l) were added dropwise. After addition a slight orange colour developed. The mixture was stirred several minutes. Afterwards the desired amount of EO was added. The colour vanished after 15-20 minutes, indicating the presence of oxoanions. The polymerization was carried out 48h at room temperature. The viscosity of the reaction mixture increased after 8h and after one day a bright green colour appeared. The living anions were quenched with excess of KI (5.25 mmol). The Polymer was then isolated by precipitation in diethyl ether, dried and characterized by ^{1}H NMR and SEC.

The (PEO)$_2$ polymer with protected OH groups was used as an macroinitiator for the polymerization of isoprene. Prior to the reaction (PEO)$_2$ was freeze-dried 4 times with anionic-pure benzene and dried under vacuum at the high vacuum line (HVL) for 24h. 1.59 mmol of poly(ethylene oxide) were dissolved in 5 ml toluene or THF in the flask

cooled down to 0 °C. Several drops of TMEDA and 0.026 mmol s-BuLi were added to the solution. Upon addition of the initiator an orange-pink colour developed. 0.15g (2.35 mmol) isoprene was introduced to the reactor and the mixture was stirred for 3h. Living anions were quenched with methanol. The polymer was precipitated with petholether and methanol. The different obtained fractions were characterised by ^{1}H NMR and SEC.

Preparation of four arm star EO polymers

Prior to the polymerization experiments THF was purified over s-BuLi/DPE, condensed to the valve-equipped flask, and transferred to the Glove Box. Disiloxane **III′** (190 mg, 0.5 mmol) was dissolved in 50 ml of THF. The solution was cooled down to −78 °C and 2.2 ml of diphenylmethyl potassium solution in THF (0.911 mol/l) were added dropwise in order to activate the OH groups. After 15 minutes EO (2.033 g, 46 mmol) was condensed from the ampoule. The polymerization was carried out 48h at room temperature. After termination with acetic acid and precipitation in petrol ether the isolated polymer was characterised by ^{1}H NMR and SEC.

4.3 Results and discussion

Two pathways were explored for the synthesis of Y shape block copolymer built up from two identical hydrophilic PEO chains, which are covalently linked to a hydrophobic PI chain. The first route (Fig. 4. 1) consisted of the synthesis of linear poly(isoprene) quenched with a chlorosilane compound, deprotection of the hydroxyl groups acting as initiators for the polymerization of EO. The second route (Fig. 4. 2) was based on the polymerization of ethylene oxide from the hydroxyl groups of allyl ether leading to the formation of two PEO chains with double bond functionality in the centre of the molecule and subsequent polymerization of isoprene.
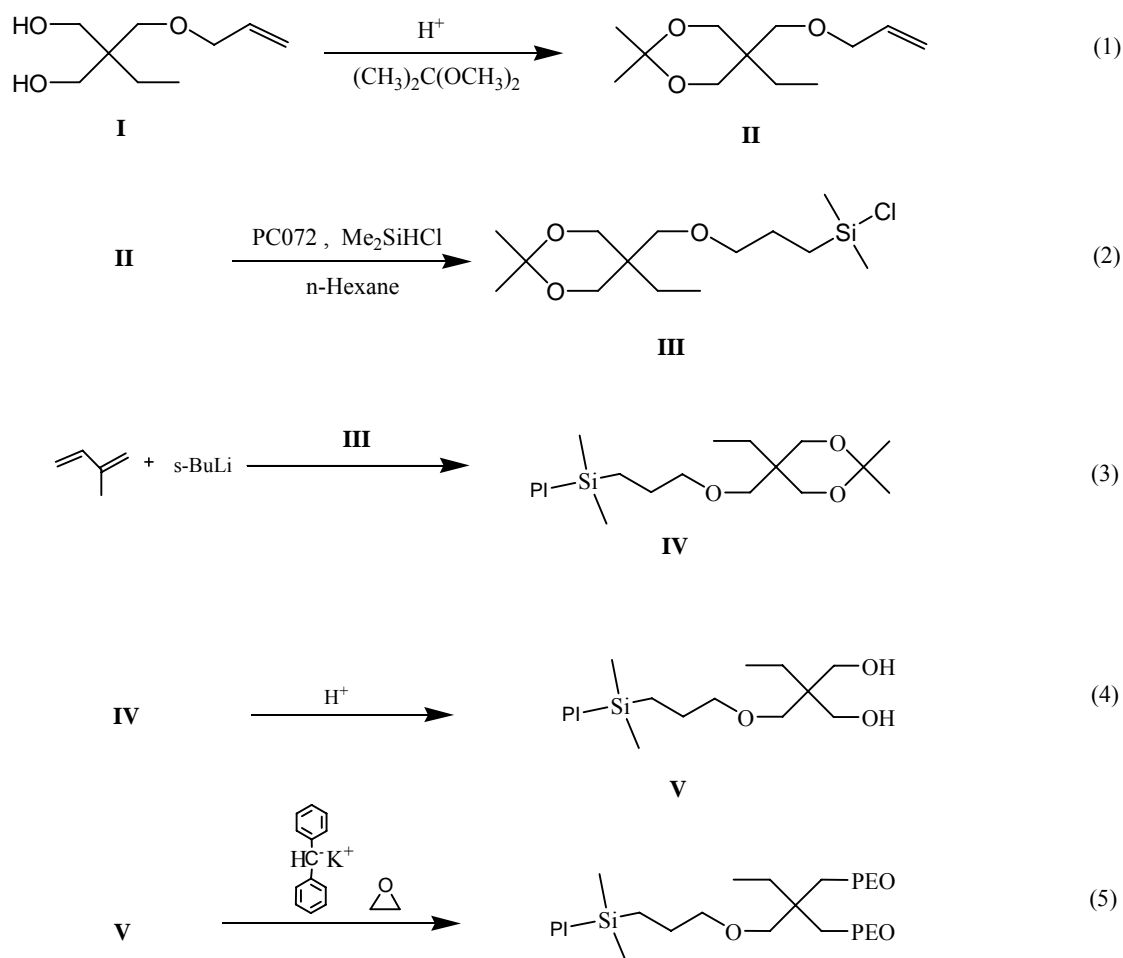
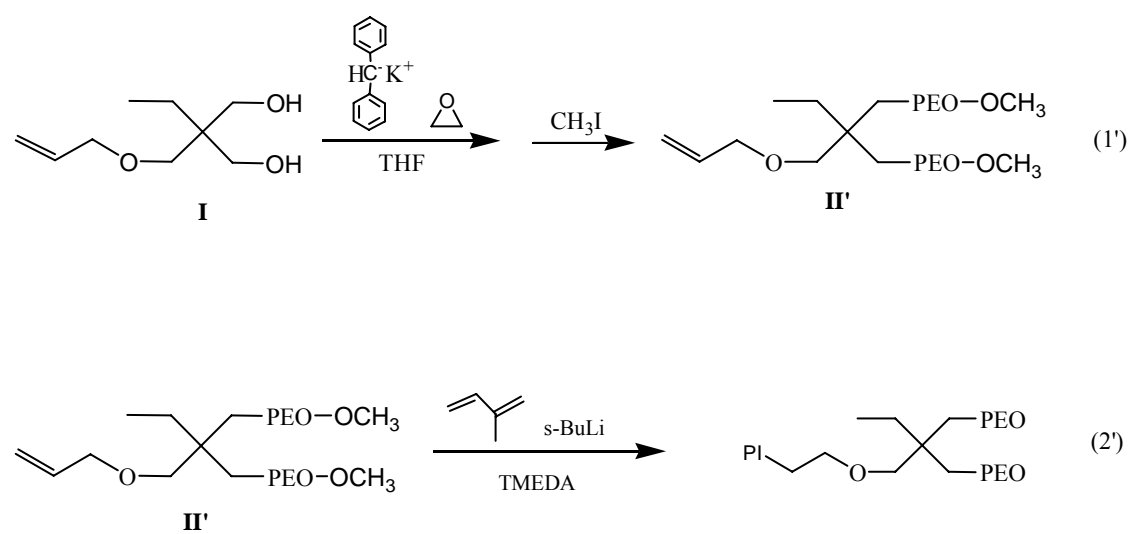*Fig. 4. 1 Synthetic pathway of Y-shape copolymers via route 1*

Fig. 4. 2 Synthetic pathway of Y-shape copolymers via route 2

Synthesis of Y shape PI-b-PEO₂ via route 1

The hydroxyl groups in allyl ether **I** were protected in the reaction with 2,2-dimethoxypropane (Fig. 4. 1, eq. 1).[26, 27] The obtained cyclic ketal **II** was subsequently reacted with dimethylchlorosilane via hydrosilylation under Pt-catalysis (Fig. 4. 1, eq 2). [28, 29] The achieved chlorosilane **III** was carefully purified and dried in order to quench efficiently the living anionic species of polyisoprene. The purification of the chlorosilane compound was difficult mostly because of its sensitivity to moisture and the high boiling point. After several attempts it was possible to remove unsaturated impurities by distilling them off with a spinning band column and subsequently purify chlorosilane **III** by means of "kugelrohr distillation". (For the spectra see Fig. 4. 3a)

The anionic polymerization of isoprene was initiated with s-BuLi by the rapid addition of the desired amount of Li initiator to the monomer in toluene. The solution turned immediately yellow indicating the formation of living isoprenyl carbanions. After the complete conversion, living anions were reacted with an excess of chlorosilane **III**. Upon the addition the colour disappeared instantly. Samples after the precipitation have been characterized with SEC and ^{1}H NMR (Table 4. 1 and Fig. 4. 3b). There is a good agreement between the targeted molecular mass and the one, which was obtained from the GPC characterization. Furthermore, the obtained polyisoprene samples exhibited very narrow molar mass distributions. Independently of the ratio of quenching agent **III** the functionalisation of the polyisoprene samples was very close to 100%. However, upon stirring the mixture after the reaction of chlorosilane with the living anions for an additional week at room temperature, we have observed in the ^{1}H NMR spectra partial disappearance of signals from the end group. This indicates side reactions, which could be associated with the presence of LiCl that functions as powerful nucleophile in aprotic solvents.[30] From NMR analysis one can conclude that for this experiment only 60% of the living anions were functionalised.

Table 4. 1 Characteristics of poly(isoprene) terminated with silane obtained via route 1

Sample[a]	[isoprene]/ [s-BuLi]	[chlorosilane]/ [s-BuLi]	Mn[b] [g/mol]	Mw/Mn[b]	Yield of functionalisation[c] [%]	Yield[d] [%]
PI$_{44}$	44	1.5	3250	1.10	94	93
PI$_{43}$	42	7	3160	1.10	99	91
PI$_{43}$[e]	42	7	3140	1.10	61	89
PI$_{170}$	154	2.5	11760	1.18	98	92

[a] block lengths calculated from SEC taking into account the mass of silane end group as 226 g/mol
[b] obtained from SEC in CHCl$_3$ relative to narrow polyisoprene standards
[c] calculated from ^{1}HNMR taking the ratio of the area of the signal corresponding to the protons of the isoprene double bonds (I$_1$ (–C=CH) of the 1,4-adduct at 5.05-5.20 ppm and I$_2$ (–C=CH$_2$) of the 3,4-adduct 4.65-4.80 ppm) to that of the peaks arising from protons of the cyclic ketal functionality in the silane end group (I$_3$ (–O–CH$_2$) at 3.55-3.70 ppm): Yield of functionalisation = [(M$_n$-226)/68]/[4(I$_1$+I$_2$/2)/(I$_3$/2)] 100%
[d] after precipitation
[e] mixture after quenching carbanions with chlorosilane which was kept on stirring for one week.

The isolated poly(isoprene) with the ketal functionality was treated in acidic conditions in order to deprotect the hydroxyl groups (Fig. 4. 1 eq. 4). The product of the reaction was analysed by ^{1}H NMR. We determined the efficiency of the reaction through disappearance of proton signals associated with the protecting group (see doublet a, b at 1.35-1.4 ppm on Fig. 4. 3 b). In the model compound (chlorosilane **III**) the removal of the protection group could be easily achieved under mild conditions (using acetic acid). In the case of polyisoprene **IV**, regardless of the applied experimental conditions (solvent, time and acidic reagent) the protection group could not be fully removed. Table 4.2 gives the experimental conditions and the yield of cleavage. Acetic acid as well as 1M HCl failed to cleave completely the ketal function under our experimental conditions, whereas stronger reagents (conc. HCl or BCl$_3$) led to side reactions (disappearance of the signals of the protons of the whole end group. This can be explained by the cleavage of the ether bond during the splitting reaction. The carbon-oxygen bond is relatively stable, however, it is possible to split it for instance with concentrated hydrohalic acids. Rather high temperature is required for this reaction. The boron chloride is even a stronger splitting agent for the ether bond.[30] Other possibilities for the disappearance of signals from the end groups such as 1)

hindering of the signals in NMR due to some molecular interactions and 2) co-precipitation of chlorosilane together with polymer were excluded by additional experiments.
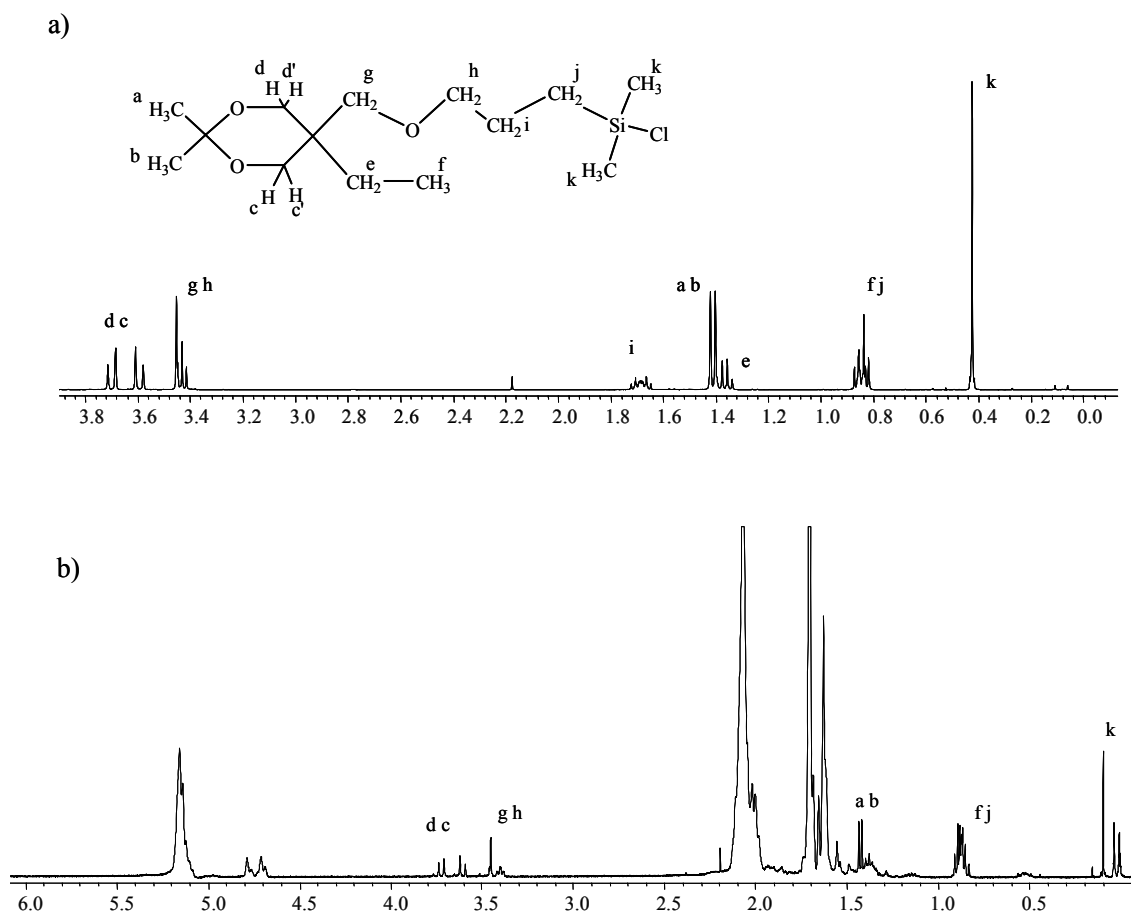
a)

b)

*Fig. 4. 3 ^{1}H NMR spectra in CDCl$_3$ of chlorosilane **III** a) and polyisoprene coupled with silane end group IV b).*

Table 4. 2 Splitting conditions for silane terminated poly(isoprene)

Sample[a]	Cleavage reagent	Solvent	Reaction time [h]	Yield of cleavage[b] [%]
PI_{44}	Acetic acid	Toluene	3	0
PI_{44}	Acetic acid	Toluene	12	0
PI_{44}	1M HCl	THF	12	~10
PI_{170}	37% HCl	THF	3	-
PI_{170}	BCl_3	THF	0,5	-

[a] block lengths calculated from SEC taking into account the mass of silane end group as 226 g/mol
[b] estimated from ^1H NMR taking into account the disappearance of the doublet at 1.35-1.4 ppm corresponding to two methyl groups and shift of the signals corresponding to the protons of the cyclic ketal in the silane end group ($-O-CH_2$ 3.55-3.70)

The polyisoprene macromonomer with the best results (partial cleavage) upon reaction with 1M HCl in THF was then used for further investigations. From ^1H NMR analysis it was estimated that the splitting of the protecting group was successful only in 10%. Special care was taken for the purification and drying of polyisoprene **V**. Protic impurities can induce homopolymerization of ethylene oxide yielding to a complex mixture of block copolymer and homopolymers. The two hydroxyl groups were deprotonated with diphenylmethyl potassium and used to grow two poly(ethylene oxide) chains. We have chosen diphenylmethyl potassium (DPMK) as an initiator for the polymerization of EO instead of the s-BuLi/t-BuP$_4$ system which is widely explored in our group,[31, 32] because of its red coloration in THF. Thus it was possible to titrate deprotected OH groups of polyisoprene **V** by slow drop wise addition of DPMK initiator to the mixture till the slight reddish colour developed. From the addition of the initiator we could conclude that not more then 30% of the living chains were equipped with OH groups. After the complete conversion of EO, living anions were terminated with acetic acid. Several precipitation steps were performed, in order to isolate Y-shape block copolymer from the complicated mixture. The obtained product was composed of poly(isoprene) as well as poly(ethylene oxide) homopolymers and most probably very small amounts of poly(isoprene)-*block*-[poly(ethylene oxide)]$_2$. Because of the problems with the synthesis of the AB$_2$ block polymer via route 1, especially difficulties

in the purification of chlorosilane **III** and problems with the deprotection reaction we proposed an alternative synthetic route for the preparation of Y-shaped copolymers.

Synthesis of Y shape PI-b-PEO$_2$ via route 2

The hydroxyl groups in allyl ether **I** were deprotonated with diphenylmethyl potassium and two poly(ethylene oxide) blocks were grown. The living anions were terminated with methyl iodide (eq 1') resulting in methoxy end groups. Table 4. 3 and Fig. 4. 4 show the characteristics of the obtained poly(ethylene oxide) macromonomers with the double bond functionality. The molar masses of PEO macromonomers determined by SEC and ^{1}H NMR analysis were found in good agreement with expected values.

Table 4. 3 Characteristics of poly(ethylene oxide) with double bond functionality obtained from route 2

Sample[a]	[EO]/ [K$^+$DPM]	Mn[b] [g/mol]	Mn[c] [g/mol]	Mw/Mn[c]	Funcionalisation[d]	Yield[e] [%]
(PEO$_{40}$)$_2$ 59	50	4480	3540	1.3	95	81
(PEO$_{48}$)$_2$ 78	48	4010	4200	1.16	99	94

[a] block lengths calculated from SEC in CHCl$_3$ relative to narrow poly(ethylene oxide) standards
[b] calculated from the signals of the protons at the double bond of the allyl ether (I$_1$ (CH$_2$=) at 5.05-5.25 ppm) and of protons of PEO (I$_2$ (CH$_2$O) 3,6 ppm): Mn$_{PEO}$ = 44(2I$_2$/4I$_1$) assuming 100% initiation by the hydroxy groups
[c] obtained from SEC in CHCl$_3$ relative to narrow poly(ethylene oxide) standards
[d] calculated from the signal of the protons at the double bond of the allyl ether (I$_1$ (CH$_2$=) 5.05-5.25 ppm) and of protons of the methoxy group (I$_2$ (CH$_3$O–) 3.35ppm): Funcionalization = (6I$_1$/2I$_2$) 100%
[e] after precipitation

From the amount of the K initiator consumed in order to activate OH groups we know that both hydroxyl groups were initiated. From the ratio of the methoxy end groups to the double bond one - calculated from ^{1}H NMR of the obtained polymer - and from the sharpness of the signal arising from protons of the CH$_3$O– group, it can be concluded that both EO chains were growing equally. However, we do not have proof for it.

The (PEO)$_2$ sample with the higher degree of functionalization was carefully dried with several freeze-melting cycles and used in further polymerization of isoprene (eq. 2'). The initiation of the double bond was analysed by ^{1}H NMR and monitored by

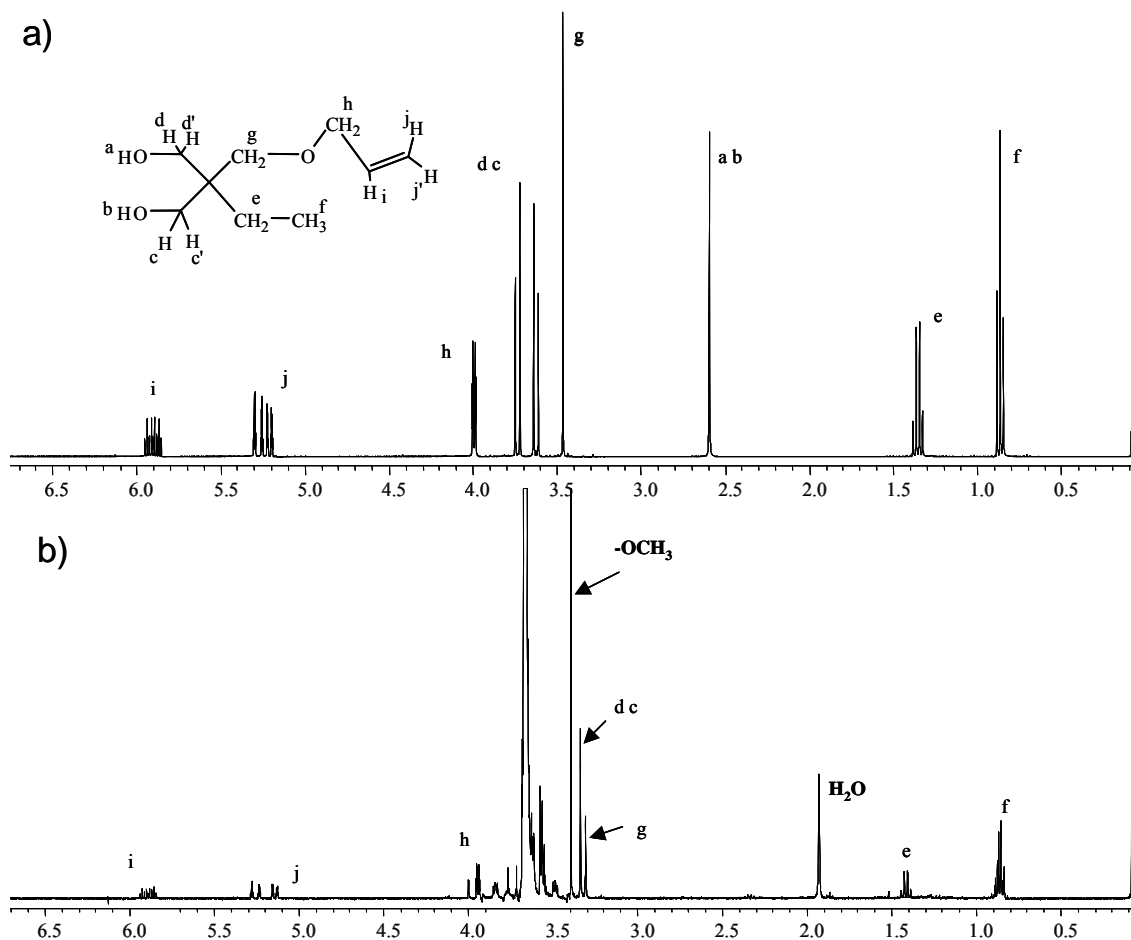disappearance of signals of double bond protons. The reaction conditions are shown in Table 4. 4.

*Fig. 4. 4 ^{1}H NMR spectra in CDCl$_3$ of allyl ether **I** a) and poly(ethylene oxide) II' with the double bond functionality b)*

Regardless of the experimental conditions (solvent, amount of s-BuLi, addition of TMEDA, and time of the reaction) very poor initiation of the double bond and no isoprene propagation from the active centre was observed under our experimental conditions. The addition of very large amounts of s-BuLi (as compared to macroinitiator) resulted in the slow disappearance of signals corresponding to protons from the double bond, however no polymer grown from the active centre. Addition of tetramethylenediamine (TMEDA) or changing the solvent to THF did not improve initiation. It can be associated with the strong aggregation of living anions and the low solubility of EO in an aprotic solvent. Furthermore we observed that the polymer upon

exposure to the sunlight for several weeks developed slide yellow-green coloration. This indicates the presence of iodide traces, which could additionally disturb the reaction with the Li initiator.

Table 4. 4 Formation of macroinitiator from PEO$_2$ polymer

Exp.	Sample[a]	[s-BuLi] / [P(EO)$_2$]	Solvent	Time [h]	TMEDA	Colour	Initiaton[b]	PI homopolymer
				0.1	–	orange	50%	–
1	**(PEO$_{48}$)$_2$ 93**	10	Toluene	2	–	orange	100%	–
				5	–	orange	100%	+
2	**(PEO$_{48}$)$_2$ 96**	2	Toluene	2	+	orange	55%	+
3[c]	**(PEO$_{48}$)$_2$ 86**	2	THF	1	–	–	~5%	+

[a] block lengths calculated from SEC in CHCl$_3$ relative to narrow poly(ethylene oxide) standards
[b] calculated from the signals of the protons at the double bond of the allyl ether (I$_1$ (CH$_2$=) 5.05-5.25 ppm) and of protons of the methoxy group (I$_2$ (CH$_3$O–) 3.35ppm): Initiation = 100%[1– (6I$_1$/2I$_2$)]
[c] reaction at -78°C

Synthesis of 4 arm PEO star polymer

Chlorosilane **III** was successfully applied in the synthesis of EO star polymers (Fig. 4. 5). The synthetic pathway was based on the controlled hydrolysis of chlorosilane **III** to the corresponding siloxane **III"** and subsequent polymerization of ethylene oxide from the hydroxyl groups of the siloxane (reaction 2"). The hydrolysis of chlorosilane **III** to siloxane (SiOSi) **III''** was performed by water under acidic conditions. During this step also the hydroxyl groups were deprotected. The product of the reaction was examined by ^{1}H NMR and IR spectroscopy.
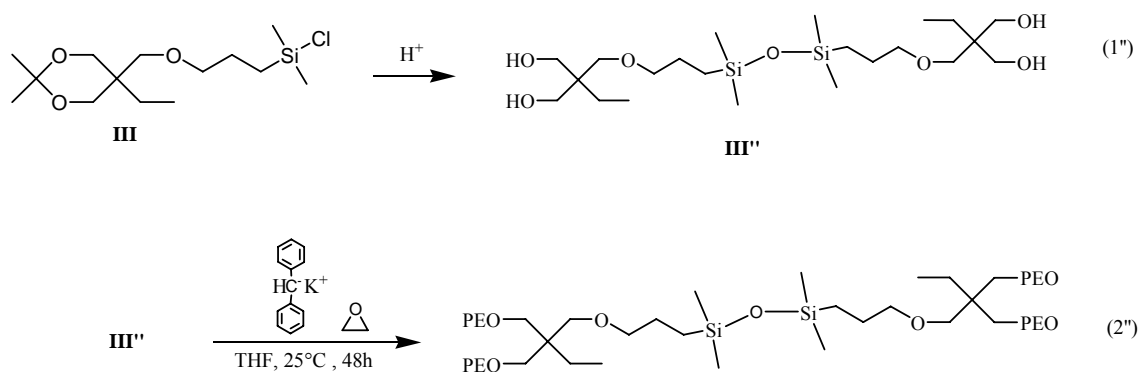
(1")

(2")

Fig. 4. 5 Synthetic pathway of 4 arm poly(ethylene oxide).

The SiOSi compound was used after careful purification as a macroinitiator for EO polymerization. Also here the potassium initiator was added till a slight colour persisted indicating complete deprotonation of the hydroxyl groups. Table 4. 5 summarizes the data of the synthesized star polymers.

Table 4. 5 Reaction entries, molecular weights, polydispersities for 4 arm star PEO

Sample[a]	[EO] / [K$^+$DPM]	Mn[b] [g/mol]	Mn[c] [g/mol]	Mw/Mn[c]	Yield[d] [%]
(PEO$_{43}$)$_4$ 81	67	11400	7500	1.25	80
(PEO$_{28}$)$_4$ 106	26	4400	5000	1.15	90

[a] block lengths calculated from SEC in CHCl$_3$ relative to narrow poly(ethylene oxide) standards

[b] calculated from the signals of the protons at the methyl group of siloxane (I$_1$ (-CH$_3$) at 0.70-0.85 ppm) and of protons of PEO (I$_2$ (CH$_2$O) 3,6 ppm): Mn$_{PEO}$ = 44(6I$_2$/4I$_1$) assuming 100% initiation by the hydroxy groups

[c] obtained from SEC in CHCl$_3$ relative to narrow poly(ethylene oxide) standards

[d] after precipitation

^{1}H NMR and corresponding SEC data in the case of second entry are in good agreement demonstrating efficient control over the polymerization. However, the obtained molecular weights are relatively broadly distributed for anionic polymerization.

4.4   Conclusion

Our attempts in the synthesis of Y shape block copolymers containing covalently linked two identical PEO blocks with one PI block were not successful regardless of the applied pathway. In the case of the first route, coupled poly(isoprene) with very good yield functionalisation by silane was obtained. However, independently of the applied experimental conditions the second part (splitting the protection group of the hydroxyl groups) was not successful. Acetic acid as well as 1M HCl failed to cleave completely the ketal function, whereas concentrated HCl or BCl_3 led to side reactions.

Using the second route we showed that the polymerization of ethylene oxide could be initiated and EO polymer can be grown from hydroxyl groups of allyl ether leading to two PEO chains with double bond functionality. It was not possible to determine whether the chains grew equally fast at both ends, although there is no indication or reason that one active side would react, whereas the other stays dormant. We found that under our experimental conditions we are not able to effectively initiate the double bond functionality in $(PEO)_2$ polymer or grow isoprene chains from it. We presume that this could be due to reaction of the initiator with residual CH_3I and solubility problems of the living anions.

Comparing the two approaches of the Y shape copolymer synthesis, the first route seems to be more promising in terms of producing well-defined block copolymers. As we already showed most of the steps such as: synthesis of poly(isoprene), its coupling with silane and EO polymerization from OH groups were successful. The method requests modifications such as replacement of the protection group to easier leaving one. Applying a better separation procedure of the complicated polymer mixture can also improve this technique.

4.5   References

[1]   M. Pitsikalis, S. Pispas, J. W.Mays, N. Hadjichristidis, *Adv. Polym. Sci.* **1998**, *135*, 1.

[2]   N. Hadjichristidis, *J. Polym. Sci., Part A: Polym. Chem.* **1998**, *37*, 857.

[3]   N. Hadjichristidis, M. Pitsikalis, S. Pispas, H. Iatrou, *Chem. Rev.* **2001**, *101*, 3747.

[4]   A. Hirao, M. Hayashi, T. Higashihara, *Macromol. Chem. Phys.* **2001**, *202*, 3165.

[5]   A. Hirao, M. Hayashi, S. Loykulnant, K. Sugiyama , S. W. Ryu , N. Haraguchi, A. Matsuo, T. Higashihara, *Prog. Polym. Sci.* **2005**, *30*, 111.

[6]   J. Li, M. Gauthier, *Macromolecules* **2001**, *34*, 8918.

[7]   D. M. Knauss, T. Huang, *Macromolecules* **2003**, *36*, 6036.

[8]   H. Ba-Gia, R. Jerome, P. Teyssie, *J. Polym. Sci., Part A: Polym. Chem.* **1980**, *18*, 3483.

[9]   S. Gibanel, J. Forcada, V. Heroguez, M. Schappacher, Y. Gnanou, *Macromolecules* **2001**, *34*, 4451.

[10]   S. Gibanel, V. Heroguez, J. Forcada, Y. Gnanou, *Macromolecules* **2002**, *35*, 2467.

[11]   S. Reutenauer, G. Hurtrez, P.Dumas, *Macromolecules* **2001**, *34*, 755.

[12]   A. Mavroudis, A. Avgeropoulos, N. Hadjichristidis, E. L. Thomas, D. J. Lohse, *Chem. Mater.* **2003**, *15*, 1976.

[13]   H. Iatrou, E. Siakali-Kioulafa, N. Hadjichristidis, J. Roovers, J. Mays, *J. Polym. Sci., Part B: Polym. Phys.* **2003**, *33*, 1925.

[14]   I. M . Khan, Z. Gao, K. Khougaz, A. Eisenberg, *Macromolecules* **1992**, *25*, 3002.

[15]   R. P. Quirk, Y. J. Kim, *J. Polym. Prepr. (Am. Chem. Soc., Div. Polym. Chem.)* **1996**, *37*, 643.

[16]   J. Yun, R. Faust, L. S. Szilagyi, S. Keki, M. Zsuga, *Macromolecules* **2003**, *36*, 1717.

[17]   Y. Cai, S. P. Armes, *Macromolecules* **2005**, *38*, 271.

[18]   Y. Cai, C. Burguiere, S. P. Armes, *Chem. Commun.* **2004**, 802.

[19]   S. Peleshanko, R. Gunawidjaja, J. Jeong, V. V. Shevchenko, V. V. Tsukruk, *Langmuir* **2004**, *20*, 9423.

[20]   R. Francis, B. Lepoittevin, D. Taton, Y. Gnanou, *Macromolecules* **2002**, *35*, 9001.

[21]   J.P. Spatz, S. Moessmer, C. Hartmann, M. Moeller, T. Herzog, M. Krieger, H.-G. Boyen, P. Ziemann, *Langmuir* **2000**, *16*, 407.

[22]   S. Moessmer, J. P. Spatz, M. Moeller, T. Aberle, J. Schmidt, W. Burchard, *Macromolecules* **2000**, *33*, 4791.

[23]   S. Pispas, N. Hadjichristidis, I. Potemkin, A. Khokhlov, *Macromolecules* **2000**, *33*, 1741.

[24]   D. J. Pochan, S. P. Gido, S. Pispas, J. W. Mays, A. J. Ryan, J. P. A. Fairclough, I. W. Hamley, N. J. Terrill, *Macromolecules* **1996**, *29*, 5091.

[25]   S. Moessmer, PhD thesis, University of Ulm (Ulm), **1999**.

[26]   J Hannah, R. L. Tolman, J. D. Karkas, R. Liou, H. C. Perry, A. K. Field, *J. Heterocycl. Chem.* **1989**, *26*, 1261.

[27]   P. Koscienski, C. Yeates, *J. Chem. Soc. Perkin Trans.* **1985**, 1879.

[28]   M. Kira, T. Hino, H. Sakurai, *J. Am. Chem. Soc.* **1992**, *114*, 6697.

[29]   S. Riethmueller, PhD thesis, University of Ulm (Ulm), **2002**.

[30]   M. V. Bhatt, S. U. Kulkarni, *Synthesis* **1983**, *4*, 249.

[31]   B. Esswein, A. Molenberg, M. Moeller, *Macromol. Symp.* **1996**, *107*, 331.

[32]   B. Esswein, M. Moeller, *Angew. Chem.* **1996**, *108*, 703.

Chapter 5

Formation of uniform TiO₂ nanoparticles by means of block copolymer micelles as nanoreactors

5.1   Introduction

Nanoparticles exhibit unique properties, which differ from the ones of bulk materials, because of quantum size effects and large surface area.[1, 2] Nanostructured titanium dioxide (TiO₂) attracts significant attention in the field of photocatalysis,[3, 4] photonic crystals, optical emission and sensing,[5, 6] because of its optical and catalytic properties.

Various chemical routs towards the formation of TiO₂ nanostructures have been reported. Gold-titanium core-shell particles were obtained by complexation of titanium precursor with a positive polyelectrolyte.[7] Bullen and co-workers prepared TiO₂ nanoparticle arrays using a nanosphere lithography technique.[8] Porous nanostructured titanium oxide networks were created e.g. by TiO₂ nanoparticle infiltration in a polymer gel template.[4] Mesoporus silica-titania thin films were obtained combining the self-assembly of metal oxide-coordinated surfactant [9] or block copolymers [10-12] and sol-gel processing.

Amphiphilic block copolymers self-organized into reversed micelles can be used as nanoreactors for the formation of metal and metal oxide nanoparticles with controlled size and interdistance when deposited on a surface.[13] Antonietti and co-workers synthesized polymer-titanium oxide nanocomposites using self-assembly of poly(styrene)-*block*-poly(methylmethacrylic acid) into micellar structures.[14] The group of Russell have reported formation of cylindrical nanodomains of PS-*b*-PEO block copolymer oriented parallel to the silicon surface.[15] The PEO domains in the polymer were selectively swollen by H₂O and subsequently exposed to TiCl₄ resulting in the formation of titanium oxide dots stabilized by the block copolymer. Recently arrays of titanium oxide nanoparticles on silicon substrate were fabricated using a micellar monofilm of PS-*b*-P2VP [16] or PS-*b*-P4VP [17] as a template. The particles were utilized subsequently as seeds to grow TiO₂ nanoneedles.[17, 18] Spatz et al combined PS-*b*-PEO micelles with microwave techniques for the formation of titanium particles arranged in hexagonal arrays.[19] Although the authors successfully produced TiO₂ nanoparticles, we

believe it is possible to significantly improve the order of the particles deposited on a substrate by employing a copolymer like poly(butadiene)-*block*-poly(ethylene oxide). Exchanging the corona-forming block into polydiene provide more plasticity to the system during self-organization of the micelles into monolayer.

In this chapter we report on the synthesis of poly(butadiene)-*block*-poly(ethylene oxide) and poly(isoprene)-*block*-poly(ethylene oxide) polymers by anionic polymerisation and the implementation of poly(butadiene)-*block*-poly(ethylene oxide) for the preparation of titanium dioxide nanoparticles. The morphology and chemical composition of the obtained nanoparticles were investigated by TEM and XPS respectively.

5.2   Experimental

Materials

Ethylene oxide (Messer, 2.8) was purged through columns filled with CaH_2 and molecular sieves (pore size 4Å). Butadiene (Messer-Griesheim, stabilized) was purged through columns filled with sodium on aluminium oxide and molecular sieves (pore size 4Å). Isoprene (Aldrich, stabilized) was dried over CaH_2 then distilled under inert gas over Na. Toluene (Merck p.a.) and tetrahydrofuran (THF) (Merck p.a.) were dried over $LiAlH_4$ and distilled twice under inert gas. Na (Aldrich, technical grade), s-BuLi (Aldrich 1.3 mol/l in cyclohexane), phosphazene base t-Bu-P_4 (Fluka purum, ~1.0 M in n-hexane), Bu_2Mg (Aldrich, 1.0 mol/l in heptanes), CaH_2 (Fluka p.a.), $LiAlH_4$ (Aldrich, pallets), acetic acid (Fluka, p.a.), acetone (Merck, technical grade), and petrol ether (Merck, technical grade) were used as received.

Methods

All polymerisations were performed in a high vacuum line.

Size Exclusion Chromatography (SEC). The molecular weight of polymers was determined in freon or chloroform at room temperature using Waters microstyragel columns (pore size 10^5, 10^4, 10^3 Å). Detection was performed on a differential refractometer (Waters model 410) and a differential viscometer (Viscothek model

H502, SEC-Win software). Elution volumes were converted to the molecular weights based on the calibration with narrow polydispersity PI or PS standard samples.

¹H-NMR spectra were performed in CDCl$_3$ (99,8%, Deutero GmbH) on a Bruker DRX 400 spectrometer at 400 MHz.

X-ray Photoelectron Spectroscopy (XPS) measurements were carried out in an Ultra Axis™ spectrometer, (Kratos Analytical, Manchester UK). The samples were irradiated with monoenergetic Al K$_{\alpha1,2}$ radiation (1486.6 eV) and the spectra were taken at a power of 144 W (12 kV x 12 mA). The aliphatic carbon (C-C, C-H) at a binding energy of 285 eV (C 1s photoline) was used to determine the charging.

Microwave treatment. Micellar solutions were treated with a MLS 1200 Microwave laboratory system with the frequency of 2,45 GHz (MLS GmbH) at a power of 200W.

TEM: Bright field transmission electron microscopy images of the films were recorded by a Philips EM 400T microscope operating at 80 kV. In order to minimize the destructive influence of the e-beam on the sample, the intensity was kept as low as possible (second condenser lens: 50 Pt, objective lens: 30).

Synthesis of PB-b-PEO and PI-b-PEO

Prior to polymerisation exact amount of pre-purified THF, ethylene oxide and butadiene (or isoprene) were dried in a high vacuum line over Bu$_2$Mg. Dienes and ethylene oxide were distilled under the high vacuum into ampoules equipped with PTFE valves. THF was distilled directly into the reaction flask. Subsequently the monomer was condensed from the ampoule to the reactor. The calculated amount of s-BuLi was introduced and a deep yellow colour of the mixture developed. The synthesis was carried out in THF at -78°C. After 3-5 hours a small amount of ethylene oxide was condensed to the reaction flask to cap the living polymer. The yellow colour disappeared almost instantly and the solution became colourless. After stirring for additional 20 minutes the sample was taken, in order to determine molecular weight and molecular weight distribution of the first block. Subsequently t-Bu-P$_4$ was introduced and the rest of EO was added to the reaction mixture. The polymerisation of the second block was performed at 35°C for 48 hours. At the end of the reaction the solution had a deep blue colour. After termination

with acetic acid and precipitation in cold acetone, the polymer was isolated and characterized by means of ^{1}H NMR and SEC. ^{1}H NMR (CDCl$_3$, δ in ppm): 1.0-1.2 (broad, -C$\underline{H}_2$-CH(R)-CH=CH$_2$), 1.9-2.1 (broad, C$\underline{H}_2$-CH=CH-C$\underline{H}_2$- and CH$_2$=CH-C$\underline{H}$-), 3,6-3,8 (broad, -CH$_2$-O-), 4.8-5.0 (broad, CH$_2$=), 5.3-5.7 (broad, –CH=C). The poly(butadiene) microstructure was calculated from resonance peak at 4.8-5.0 ppm and at 5.3-5.7 ppm. The PEO content in the block copolymers was calculated from the signals of the protons at 3.6-3.8 ppm and 4.8-5.0 ppm.

Substrate preparation

Silicon substrates were cut into pieces and cleaned by sonication in acetone, milipore water and isopropanol respectively. Activation of the surface was done by UV/ozone treatment for 12 min.

Samples preparation

Typically a solution of the block copolymer in dry toluene was prepared with a concentration c = 5 mg/ml and mixed with 0.5 equivalent of HCl per ethylene oxide unit (loading 0.5). The mixture was stirred for 2 days to allow complete solubilization of the hydrochloric acid in the cores of the block copolymer micelles, subsequently the micelles were loaded with titanium isopropoxide (loading 0.5) and the solution was stirred for additional 2 days. The solution was treated in a microwave unit at power of 200 Watt for 30 minutes in order to support the formation of TiO$_2$ particles.

Thin films for Transmission Electron Microscopy were prepared by putting a drop of the micellar solution onto a carbon coated copper grid, which was in direct contact with a soaking tissue to remove the excess of the solution.

Silica samples for XPS analysis were dipped and withdrawn from the micellar solution with a constant velocity of 10 mm/min. The covered substrates were allowed to dry above the surface of the liquid.

5.3   Results and discussion

Polymerisation of PB-b-PEO and PI-b-PEO block copolymers

The conventional way of preparation of the PB-*b*-PEO or PI-*b*-PEO block copolymers proceeds in two steps and involves replacement of the lithium conterion with potassium.[20, 21] The reason for such procedure is to avoid the association of the living PEO chain ends with Li^+ ions, which form ion pairs that terminate the chain propagation. We have chosen the one-pot synthesis employing alkyllithium compound together with an extremely strong phosphazene base t-Bu-P_4 that preserves the living character of the growing polymer chains by pushing the equilibrium towards free anions.[22-24]

The anionic polymerisation of diene was initiated with s-BuLi by the rapid addition of the Li initiator to the monomer solution in THF (Fig. 5. 1). The temperature during the initiation was kept at –78°C in order to preserve the living character of the polymerisation and prevent possible side reactions. Upon addition of initiator, the solution turned immediately canary yellow indicating the formation of living carbanions. After the complete conversion (3-5h), living anions were reacted with ethylene oxide (Fig. 5. 1, eq. 2) and the yellow colour disappeared. Only one monomer unit was incorporated to the living chain as a result of using lithium conterion. Subsequently the stechiometric amount of phosphazene base t-Bu-P_4 and the rest of EO were added and the temperature was raised to 35°C. Polymerisation of the second block was allowed to proceed for 48 hours. After one day a deep blue colour developed. The reaction was terminated by addition of a small amount of acetic acid. The block copolymers were characterized by means of ^1H NMR and SEC.
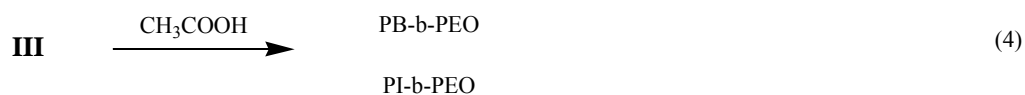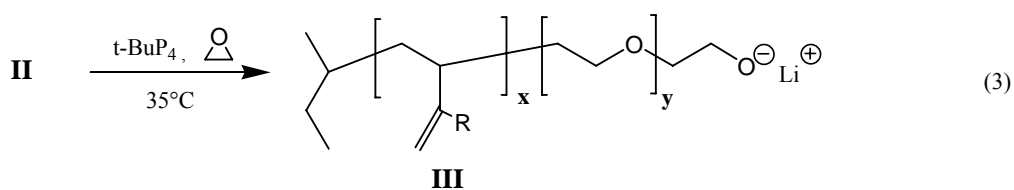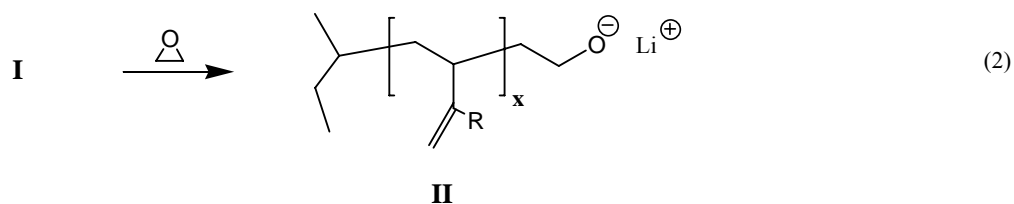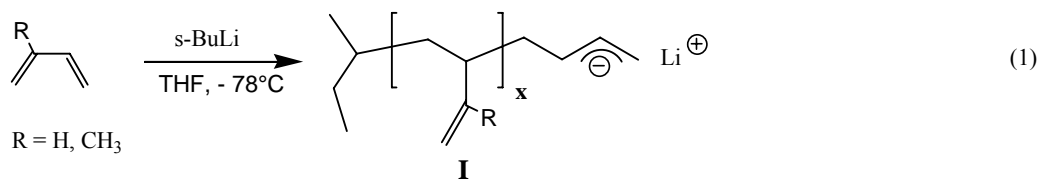
*Fig. 5. 1 Synthetic pathway to PB-*b*-PEO and PI-*b*-PEO block copolymers with s-BuLi and t-Bu-P₄ base as an initiating system.*

Table 5. 1 lists the entries for the PB-*b*-PEO and PI-*b*-PEO block polymerisations:

Table 5. 1 Reaction entries for PB-*b*-PEO and PI-*b*-PEO polymerisations

Sample	Polymer[a] PI(PB)$_x$-*b*-PEO$_y$	n isoprene or butadiene [mmol]	n EO [mmol]	n s-BuLi [mmol]	V THF [ml]
PB$_{175}$-*b*-PEO$_{65}$ 26	175-65	228	88	1,3	150
PI$_{155}$-*b*-PEO$_{140}$ 30	155-140	100	90	0,65	100
PB$_{200}$-*b*-PEO$_{160}$ 33	200-160	200	160	1	150
PB$_{400}$-*b*-PEO$_{100}$ 40	400-100	120	30	0,3	120
PB$_{200}$-*b*-PEO$_{210}$ 44	200-210	80	85	0,4	100
PB$_{400}$-*b*-PEO$_{425}$ 45	400-425	80	85	0,2	50

[a] DP of the block copolymer aimed at by the monomer/initiator ratio

Table 5. 2 summarized the characteristics of the obtained block copolymers:

Table 5. 2 Molecular weights, polydispersities and block lengths of synthesized PB-*b*-PEO and PI-*b*-PEO copolymers

Sample[a]	Homopolymer		Copolymer				
	Mn[b] [g/mol]	Mw/Mn[b]	Mn[b] [g/mol]	Mw/Mn[b]	Yield[c] [%]	PB(PI)/ PEO[d]	PI(PB)$_x$-*b*-PEO$_y$
PB$_{175}$-*b*-PEO$_{65}$ 26	10000	1,11	10060	1,10	86	5,3	185-35
PI$_{155}$-*b*-PEO$_{140}$ 30	1840	1,20	13400	1,13	45	0,12	27-230
PB$_{200}$-*b*-PEO$_{160}$ 33	5370	1,25	15980	1,15	60	0,48	100-210
PB$_{400}$-*b*-PEO$_{100}$ 40	29800	1,07	30230	1,08	83	7,89	550-70
PB$_{200}$-*b*-PEO$_{210}$ 44	11600	1,08	27120	1,07	85	0,81	215-265
PB$_{400}$-*b*-PEO$_{425}$ 45	21300	1,20	53960	1,10	90	0,78	390-500

[a] DP of the block copolymer aimed at by the monomer/initiator ratio
[b] from SEC in CHCl₃ relative to narrow poly(styrene) standards
[c] after precipitation
[d] ratio poly(butadiene) or poly(isoprene) to poly(ethylene oxide) obtained by ¹H NMR
[e] DP of the block copolymer calculated from the ratio between blocks and the Mn for PB(PI) obtained by SEC

The composition of the first block was determined by ^{1}H NMR analysis (89% 1,2- and 11% 1,4- adduct for PB and 28% 1,2-, 61% 3,4-, and 11% 1,4-addition in case of PI).

TiO₂ nanoparticles synthesis

Poly(diene)-*block*-poly(ethylene oxide) polymers in toluene were employed as micellar nanoreactors. Titanium (IV) isopropoxide was loaded into the micellar core where the titanium is coordinated with the ethylene oxide units.[9] The $Ti(OC_3H_7)_4$ can be hydrolysed in presence of water or HCl.[6, 11] However, Ti alkoxides are rather soluble in organic solvents, therefore controlled hydrolysis of metal oxide particles in micellar nanoreactors was difficult to achieve and the formed particles had a very broad size distribution (Fig. 5. 2).
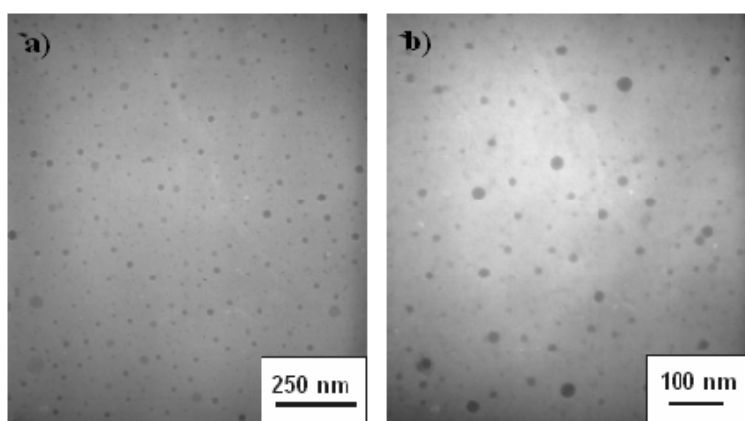
Fig. 5. 2 TEM images of titanium oxide nanoparticles after hydrolysis of titanium isopropoxide with HCl, cast from micellar solution onto carbon coated grids a) and b)

For this reason a modified approach towards TiO_2 nanoparticles was followed [19] (Fig. 5. 3): the micelles were first loaded with HCl and subsequently, after two days of stirring when the aqueous HCl had been uptaken by the core of the micelles, the titanium precursor salt was introduced to the system. The $Ti(OC_3H_7)_4$ was hydrolysed to small titanium particles as soon as it reached the HCl-filled core of the micelles. The particles were difficult to detect with the available TEM. The formation of the TiO_2

particles was further supported by the microwave treatment, which acts on the water present in the core of the block copolymer micelles.
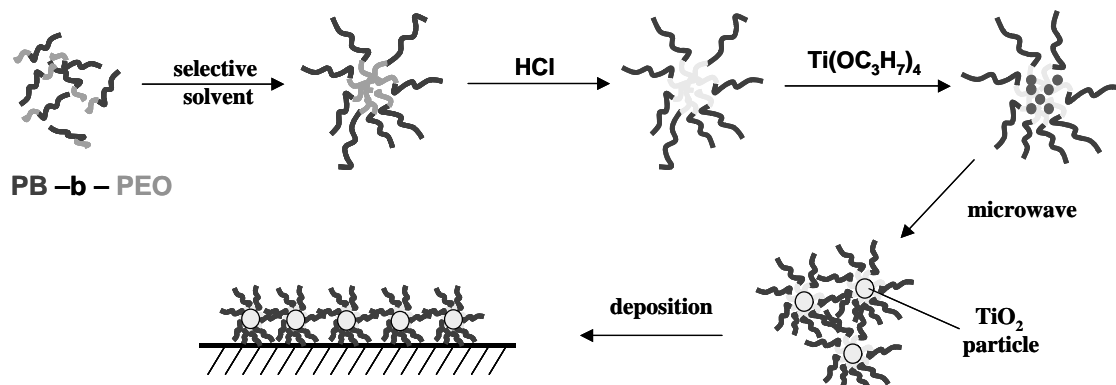
Fig. 5. 3 Formation of TiO₂ nanoparticles using poly(butadiene)-block-poly(ethylene oxide) copolymer micelles as template.

In order to suppress formation of particles the micellar solution was treated in a microwave oven at a power of 200 W for 30 minutes. During the treatment the temperature of the solution slightly increased.

Fig. 5. 4 shows Transmission Electron Micrographs of the TiO₂ particles embedded in a monomicellar film of PB(400)-*b*-PEO(425) block copolymer cast on a copper grid from a solution after microwave treatment. The image shows quasi-hexagonal order of metal oxide particles with relatively narrow size distribution. By measurements on 80 particles, it was determined that the particles diameter was 11+/- 4 nm and the particles interdistance approximately 40nm. The order of the particles over large areas was clearly improved with respect to what shown in [19]. This is most likely due to the presence of poly(butadiene) in the corona of the micelles instead of poly(styrene). Because of its low Tg, PB provides more plasticity to the system during self-organization into regular arrays when deposited on surfaces as monomicellar layer.
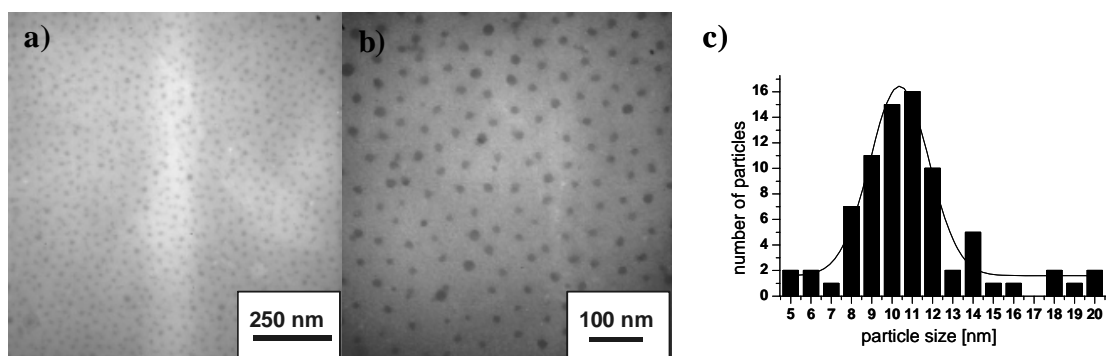
Fig. 5. 4 TEM images of block copolymer stabilized titanium oxide nanoparticles, cast from solution onto carbon coated grids a) and b); c) particle size distribution (n=80)

In order to identify the chemical composition of titanium nanoparticles XPS measurements were performed. Various oxides can be easily distinguished from the Ti 2p XPS spectrum.[8, 25, 26] In the case of TiO_2, peaks at approximately 459.0 and 464.6 eV are assigned to $Ti_{2p3/2}$ and $Ti_{2p1/2}$. Fig. 5. 5 shows the Ti 2p spectrum of Ti nanoparticles/polymer composite deposited on a silicon substrate. The shape and the spin-orbit splitting of the Ti 2p emission peaks are characteristic of titanium dioxide; also maxima of the signal at 464,775 and 458,981 eV respectively are in very good agreement with literature data.[8, 25, 26] (the observed BEs were referenced to the C 1s photoemission line at 285.0 eV).
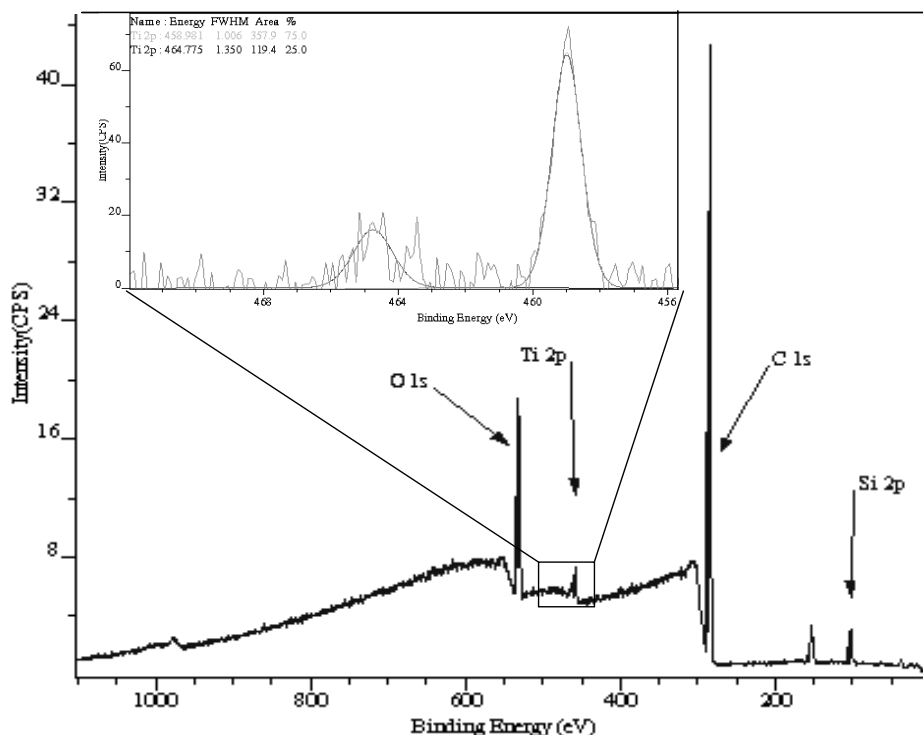
Fig. 5. 5 XPS Ti₂ₚ spectrum of titanium oxide nanoparticles/block copolymer composite after microwave treatment and subsequent deposition of micelles on a silicon oxide surface.

5.4   Conclusions

A series of block copolymers with narrow polydispersities consisting of poly(butadiene) with poly(ethylene oxide) block were prepared by one-step living anionic polymerisation. These polymers were successfully utilized for the preparation of mono-dispersed titanium oxide particles. It was demonstrated that titanium clusters stabilized by the block copolymer micelles can be deposited in a hexagonal order onto flat substrates and that the order was significantly improved with respect to Spatz at all.[19] From XPS analysis, the nature of the particles was confirmed to be pure TiO₂. By exposing the monomicellar film to plasma, the polymer template will be removed leaving on the substrate naked TiO2 clusters preserving the same order of the micelles. [16, 17, 19]

5.5   References

[1]   A. B. R. Mayer, *Polym. Adv. Technol.* **2001**, *12*, 96.

[2]   A. N. Shipway, E. Katz, I. Willner, *Chem. Phys. Chem.* **2000**, *1*, 18.

[3]   J. Theurich, M. Lindner, D. W. Bahnemann, *Langmuir* **1996**, *12*, 6368.

[4]   D. G. Shchukin, J. H. Schattka, M. Antonietti, R. A. Caruso, *J. Phys. Chem. B* **2003**, *107*, 952.

[5]   B. C. O'Regan, F. Lenzmann, *J. Phys. Chem. B* **2004**, *108*, 4342.

[6]   S. Jeon, P. V. Braun, *Chem. Mater.* **2003**, *15*, 1256.

[7]   K. S. Mayya, D. I. Gittins, F. Caruso, *Chem. Mater.* **2001**, *13*, 3833.

[8]   H. A. Bullen, S. J. Garrett, *Nano Lett.* **2002**, *2*, 739.

[9]   N. Huesing, B. Launay, D. Doshi, G. Kickelbick, *Chem. Mater.* **2002**, *14*, 2429.

[10]   P. Yang, D. Zhao, D. I. Margolese, B. F. Chmelka, G. D. Stucky, *Chem. Mater.* **1999**, *11*, 2813.

[11]   P. C. A. Alberius, K. L. Frindell, R. C. Hayward, E. J. Kramer, G. D. Stucky, B. F. Chmelka, *Chem. Mater.* **2002**, *14*, 3284.

[12]   M. Groenewolt, T. Brezesinski, H. Schlaad, M. Antonietti, P. W. Groh, B. Ivan, *Adv. Mater.* **2005**, *17*, 1158.

[13]   J.P. Spatz, S. Moessmer, C. Hartmann, M. Moeller, T. Herzog, M. Krieger, H.-G. Boyen, P. Ziemann, *Langmuir* **2000**, *16*, 407.

[14]   N. Steunou, S. Foerster, P. Florian, C. Sancheza, M. Antonietti, *J. Mater. Chem.* **2002**, *12*, 3426.

[15]   D. H. Kim, S. H. Kim, K. Lavery, T. P. Russell, *Nano Lett.* **2004**, *4*, 1841.

[16]   X. Li, K. H. A. Lau, D. H. Kim, W. Knoll, *Langmuir* **2005**, *21*, 5212.

[17]   C.-C. Weng, K.-F. Hsu, K.-H. Wei, *Chem. Mater.* **2004**, *16*, 4080.

[18]   C.-C. Weng, C.-P. Chen, C.-H. Ting, K.-H. Wei, *Chem. Mater.* **2005**, *17*, 3328.

[19]   J. Spatz, S. Moessmer, M. Moeller, M. Kocher, D. Neher, G. Wegner, *Adv. Mater.* **1998**, *10*, 473.

[20]   M. A. Hillmyer, F. S. Bates, *Macromolecules* **1996**, *29*, 6994.

[21]   J. Allgaier, A. Poppe, L. Willner, D. Richter, *Macromolecules* **1997**, *30*, 1582.

[22]   B. Esswein, A. Molenberg, M. Moeller, *Macromol. Symp.* **1996**, *107*, 331.

[23]   B. Esswein, M. Moeller, *Angew. Chem.* **1996**, *108*, 703.

[24]   S. Foerster, E. Kraemer, *Macromolecules* **1999**, *32*, 2783.

[25]   J. M. Mckay, V. E. Henrich, *Surf. Sci.* **1984**, *137*, 463.

[26]   G. Liu, W. Jaegermann, J. He, V. Sundstroem, L. Sun, *J. Phys. Chem. B* **2002**,
        106, 5814.

Chapter 6

Nano-structured micropatterns by combination of block copolymer self-assembly and UV photolithography[*]

6.1 Introduction

Metal and metal oxide nanoparticles arranged in periodic and aperiodic patterns on a surface enable systematic studies on nanoparticle interactions such as magnetic and electronic coupling and energy transfer [1, 2] but are also of interest for potential applications ranging from the production of nanoscale electronics,[3-5] data storage,[6, 7] biosensors and analytical devices.[8, 9] Key specifications for the dots are the control over the size, the monodispersity, the spatial order and the precise positioning on the surface.

Commonly, sub-micron structures are fabricated via well-established photo-lithography [10] where the minimal feature size is restricted by the resist sensitivity and the used wavelengths. Other novel top-down techniques like X-ray,[11] electro-beam,[12] focused ion beam[13] or "Dip Pen" lithography[14] satisfy the quest for smaller dimensions although they are serial techniques, not suitable for structuring of large areas.

Self-assembly in contrast to lithographic top-down methods can easily build nanostructures with the resolution of few nanometers e.g. block copolymers form a rich variety of nanoscale periodic patterns.[15, 16] A large range of fabrication approaches based on block copolymers is present in literature, demonstrating the potential of these materials. Using the self-organisation of amphiphilic block copolymers to micelles, nanoparticles can be patterned at the surface of the substrate.[17, 18] Micelles are used as nanoreactors for particle formation by loading them with a suitable metal or metal oxide precursor, depositing as a monolayer onto a substrate and treating the monolayer by a plasma process that reduces the precursor salt to the corresponding noble metal or metal oxide nanoparticles and removes the polymer matrix. The obtained particles maintain the same hexagonal packing of the micelles. This approach is very flexible in terms of variation of metal precursor, block copolymer and substrate material. The size of the clusters is adjusted in the range from 1 to 15 nm, while the interparticle distance can

---

reach up to 200 nm.[19-21] Self-organization allows massive parallel processing in the nanometer and sub-nanometer regime, however this method is restricted to preparation periodic patterns and artificial structures are not accessible in this way.

Aperiodic structures of nanoscale ordered nanoobjects can be realized by combining self-organization of macromolecules on the nanometer scale and fabrication of larger-scale structures by "top-down" techniques.[22-25] The capability of pre-structured surfaces to direct the self-assembly of metal precursor loaded block copolymer micelles has been demonstrated by using breath figures [26] and e-beam resist or photoresist patterns defined by lithographic techniques.[27-29] Soft lithography has been employed for microcontact printing of block copolymer micellar monolayers,[29] microfluidics dispensing copolymer solutions on surfaces [30] and modification of micellar films by capillary contact printing.[31] So far the guidance or confinement of the copolymer solutions in predefined topological structures has resulted in patterns of micelles that show non-uniformity in terms of micellar position and sizes,[30] aggregation of micelles in the vicinity of pattern edges [30, 32] or geometries restricted to single chains of nano-objects.[28] These issues can be overcome by a method we recently proposed, based on the chemical modification by e-beam lithography of a micellar monolayer for the creation of arrays of metal and metal oxide nanodots.[33] However, this approach requires expensive equipment, high energy doses and it is not suitable for nonconductive substrates, unless additional treatment is carried out.[34] Moreover, e-beam patterning is a time-consuming serial process not suitable for large areas.

In this chapter we propose a photo-pinning method for the fabrication of nano-structured micropatterns as a low cost and easy combination of block copolymer self-assembly and photolithography. The method is simple, parallel and allows patterning of large areas on conductive as well as nonconductive substrates. It uses the self-assembled micellar film as a very thin (<50 nm), light curable resist that carries already the compound to be deposited. We demonstrate the potential of the method when a block copolymer with the corona block containing unsaturated bonds is used as resist. Specifically, we report on the synthesis of the photocrosslinkable poly(isoprene)-*b*-poly(2vinylpyridine) (PI-*b*-P2VP) amphiphilic block copolymer by anionic polymerization and we show its capability to self-organize into reverse micelles when dissolved in a selective solvent.

With the photo-pinning method, it is possible to obtain arrays of nanodots with only a single layer lithographic process, without any additional metal deposition, minimizing the needed steps and in consequence the chance of defects in the resulting structures.

6.2   Experimental

Materials

Isoprene (Aldrich, p.a.) was dried over CaH_2 then distilled under inert gas over Na. 2-Vinylpyridine (Aldrich, p.a.) was purified by distillation under inert gas, first over potassium hydroxide, then over calcium hydride. Toluene (Merck, p.a.), methanol (Merck, p.a.) and tetrahydrofuran (THF) (Merck, p.a.) were dried over $LiAlH_4$ and distilled under inert gas twice. 1,1-diphenylethylene (DPE) (Aldrich, 97%) was dried over CaH_2 and distilled under inert gas atmosphere. Vinyltriethoxysilane (ABCR GmbH, Karlsruhe, Germany) and (3-acryloxypropyl)trimethoxysilane (ABCR GmbH, Karlsruhe, Germany) were filtered. Hydroxylamine (Aldrich, 50 wt.% in H_2O), $HAuCl_4x3H_2O$ (Fluka, purum), s-BuLi (Aldrich, 1.3 mol/l in cyclohexane), Bu_2Mg (Aldrich, 1.0 mol/l in heptanes), CaH_2 (Fluka, p.a.), KOH (Merck, technical grade), Na (Aldrich, technical grade), isopropanol (Aldrich, p.a.), $LiAlH_4$ (Aldrich, pallets), acetone (Merck, technical grade), and petrol ether (Merck, technical grade) were used as received. PS_{1350}-*b*-$P2VP_{400}$ block copolymer (Mn = 18.2 kg/mol; Mw/Mn = 1.1) polymer was previously synthesized in our group.[35] Silicon wafers were purchased from CrysTec GmbH, Berlin, Germany.

PI-b-P2VP synthesis

Prior to the polymerization procedure, prepurified isoprene was dried over $(Bu)_2Mg$ and condensed into a calibrated ampoule equipped with a PTFE valve using high vacuum techniques. Prepurified 2VP was dried by stirring in a high vacuum line (HVL) over CaH_2 and subsequently over trioctylaluminum. It was then condensed into a flask equipped with PTFE valve. Similarly, toluene and THF were purified in a HVL over s-BuLi/DPE and condensed into flasks. Ampoules and flasks with chemicals were then transferred into a nitrogen filled Glove-Box (MBraun) equipped with a n-heptane cooling bath where the polymerization procedure was carried out. Toluene was

introduced to a reaction flask at -78°C. Subsequently isoprene was transferred from the ampoule directly to the reaction flask. After several minutes s-BuLi was added to the mixture. The development of a yellow colour evidenced the formation of carbanionic living species. The solution was allowed to stir for few minutes and subsequently the temperature was raised up to 25°C. After the reaction was completed (3-5 hours) the flask was cooled down again to -78°C and an aliquot of the polymer solution was taken and analysed by SEC in order to determine the molecular weight and the molecular weight distribution of the first block. Afterwards THF was introduced to the solution followed by the addition of few drops of 1,1–diphenylethylene (DPE) to the living anions. Upon addition of DPE the yellow colour of the mixture changed immediately to deep red. The solution was stirred for 10 minutes and a calculated amount of 2VP was added dropwise to the reaction flask by means of a syringe. The solution was stirred for additional 15 minutes and living anions were terminated with few drops of methanol. The polymer was precipitated in cold acetone, isolated and characterized by means of ^{1}H NMR and SEC. ^{1}H NMR (CDCl$_3$, δ in ppm): 1.55-2.20 (broad, -CH$_3$ 3,4- and 1,4-addition, -CH$_2$ 1,4- addition and -C$\underline{H}_2$C$\underline{H}$(C$_5$H$_4$N)), 4.65-4.85 (broad, =CH$_2$ 1,2- and 1,4- addition), 5.0-5.1 (broad, =CH- 1,4- addition), 6.2-7.1 (broad, aromatic protons except the H atom in o-position to the N atom), 8,05-8,15 (broad, aromatic H atom in o-position to the N atom). The polyisoprene microstructure was calculated from the resonance peak at 5.0-5.1 ppm and the doublet at 4.65-4.85 ppm. The 2VP content in the block copolymers was determined from integrals over the aromatic protons at 8,05-8,15 ppm and protons at the double bond of PI (5.0-5.1 ppm).

Analysis

Size Exclusion Chromatography (SEC). The molecular weight of polymers was determined in chloroform at room temperature using Waters microstyragel columns (pore size 10^5, 10^4, 10^3 Å). Detection was performed on a differential refractometer (Waters model 410) and a differential viscometer (Viscothek model H502, SEC-Win software). Elution volumes were converted to the molecular weights based on calibration with narrow polydispersity PI standard samples.

^{1}H-NMR spectra were performed in CDCl$_3$ (99,8%, Deutero GmbH) on a Bruker DRX 400 spectrometer at 400 MHz.

Transmission Electron Microscopy (TEM). Bright field transmission electron microscopy images of the films were recorded by a Philips EM10 or EM 400T microscope operating at 100 kV. In order to minimize the destructive influence of the e-beam on the sample, the intensity was kept as low as possible (second condenser lens: 50 Pt, objective lens: 30).

Scanning Electron Microscopy (SEM) was performed with a Hitachi model S2000N and a Zeiss Supra 35VP scanning electron microscope operating at voltages from 3 to 15 kV and working distances from 5 to 10 mm.

Scanning Force Microscopy (SFM) was performed with a Nanoscope III from Digital Instruments (Veeco, Santa Barbara, US) microscope. Investigations in the tapping mode were carried out with Si-cantilevers from Nanosensors (Weltzlar, Germany) with a spring constant of approx. 50 N/m and at a tapping frequency around 350 kHz. Images were edited with Nanoscope software (v5.12r5 Digital Instruments, Veeco, Santa Barbara, US).

Light Microscopy was performed by means of an Axioplan Imaging microscope (Carl Zeiss, Göttingen, Germany).

Methods

Solution preparation. Typically 0.5 wt% solution of the block copolymer in dry toluene was prepared and mixed with 0.3 equiv of $HAuCl_4x3H_2O$ per pyridine unit. The mixture was stirred in the dark for at least 24 h to allow complete solubilization of the gold acid in the cores of the block copolymer micelles.

Sample preparation. Silicon wafers were cut into pieces, cleaned and functionalised with silanes self-assembled monolayers. Cleaning was done by sonication in acetone, milipore water and iso-propanol respectively. The surface was subsequently activated by 12 min UV/ozone treatment by 40W-UV lamp (UV-Technik Speziallampen GmbH Germany; λ = 185 nm) in oxygen stream of 350 mL/min with a sample distance of 5 mm to the lamp. The substrates were then transferred into nitrogen filled Glove-Box and immersed in a 0.6 wt% solution of vinyltriethoxysilane or (3-acryloxypropyl)trimethoxysilane in dry toluene for 2 h. Afterwards the substrates were thoroughly rinsed with a fresh solvent and stored in dry toluene in the dark. The

functionalised substrates were dipped into the micellar solution and withdrawn at a constant speed of 10mm/min.

The *TEM* samples were prepared by putting a drop of the micellar solution onto a SiO_2 coated 400 mesh copper grid (Plano, Marburg, Germany), which was put into contact with a soaking tissue to remove excess solution.

Photochemical modification. Irradiation of the samples was performed in ambient air with a standard low-pressure laboratory UV lamp (Dr. Gröbel UV-Elektronik GmbH, Germany; λ= 254 nm; measured intensity: 0.4 mW/cm^2 at a distance of 10 cm) through TEM grids (Plano, Marburg, Germany) or photolithographic masks. Typical irradiation conditions were 1 to 45 min, 1 to 10 cm lamp-sample distance. The photolithography masks consisted of chromium lines on UV transparent fused silica (Lithosil Q1, Schott Lithotec AG, Jena, Germany): one mask consisted of 25 μm wide lines separated by 30 μm windows; a second mask consisted of 4 series of lines with different widths (10, 5, 2 and 1 μm).

Lift-off process. This step was performed by immersion in toluene. Usually after one hour of immersion, the majority of the polymer was removed from the substrate however we allowed immersion times typically of several hours. The process can be significantly shortened by additional ultrasonication (TK 52H ultrasonic bath; Bandelin Electronic, Berlin).

Plasma treatment. Hydrogen plasma was created in a custom-made microwave etcher. Typical conditions were: 300 W; 0.096 mbar; 0.5 h.

Gold seeding. Electroless deposition of gold in the presence of Au clusters acting as seeds for the reduction of gold salt was done as follows. Substrates decorated with gold particles were cleaned with acetone, isopropanol and millipore water respectively before being immersed in an aqueous solution containing hydroxylamine (0.02 mmol). Subsequently, an aqueous solution of $HAuCl_4$ (0.02 wt%) was added and the mixture was allowed to stir typically for 3 min. The substrates were then cleaned with water and acetone, and blow-dried with nitrogen.

6.3   Results and discussion

6.3.1   Synthesis of PI-*b*-P2VP block copolymers by anionic polymerization

Currently there are two possible approaches via anionic polymerization to PI-*b*-P2VP block copolymers with a high content of the 1,4- microstructure, predicted molecular weights and low molecular weight distributions.[36, 37] In the first one isoprene is polymerised in a non-polar solvent such as hexane with a lithium compound as an initiator. After the synthesis of the first block, a polar solvent is added into the mixture and 2-vinylpyridine is polymerised.[36] This method requires a slow addition of 2VP and low temperatures. The alternative procedure is based on the sequential anionic polymerization of isoprene and 2–vinylpyridine in benzene using s-BuLi as an initiator in the presence of lithium chloride.[37] However in this case controlled polymerization is only possible with very efficient stirring and precisely controlled temperature (6-8 °C) of the mixture during addition of 2-vinyl pyridine. Furthermore, a rapid quenching of the living reaction immediately after addition of the vinyl monomer is necessary to obtain a well-defined polymer. These inconveniences make the method somewhat difficult to handle. Taking this into account we propose the following approach to PI-*b*-P2VP block copolymers (Fig 6. 1). The anionic polymerization of isoprene was initiated at −78 °C by the rapid addition of the desired amount of s-BuLi to the monomer solution in toluene. Yellow coloration of the solution indicated the formation of living isoprene anions. Subsequently the temperature was raised to 20 °C and the mixture was allowed to stir for 3-4 hours. After the polymerization of the first block was completed, the reaction flask was cooled again to −78 °C and THF was added to the mixture in order to change the solvent into tetrahydrofuran/toluene mixture (~90/10, vol/vol) and ipso facto provide a suitable medium for the vinylpyridine. Afterwards a few drops of 1,1-diphenylethylene (DPE) were introduced. Upon addition the colour of the mixture immediately changed to deep red. The living chains were reacted with DPE in order to avoid side reactions due to the high reactivity of isoprene carbanions. Because of steric hindrance, DPE does not homopolymerise and only one unit is incorporated into the main backbone (Fig 6. 1 eq. 2). The diphenyl methyl carbanions that result are less reactive than the diene carbanions but still efficient to initiate the 2VP polymerization.[38] Next the calculated amount of 2VP was added dropwise to the

reaction flask. The reaction was allowed to proceed only for several minutes since the polymerization of 2-vinylpyridine is almost instantaneous under these conditions.[39] The living chains were terminated with methanol. Block copolymers were precipitated in cold acetone, isolated and characterized by means of ^{1}H NMR and SEC.
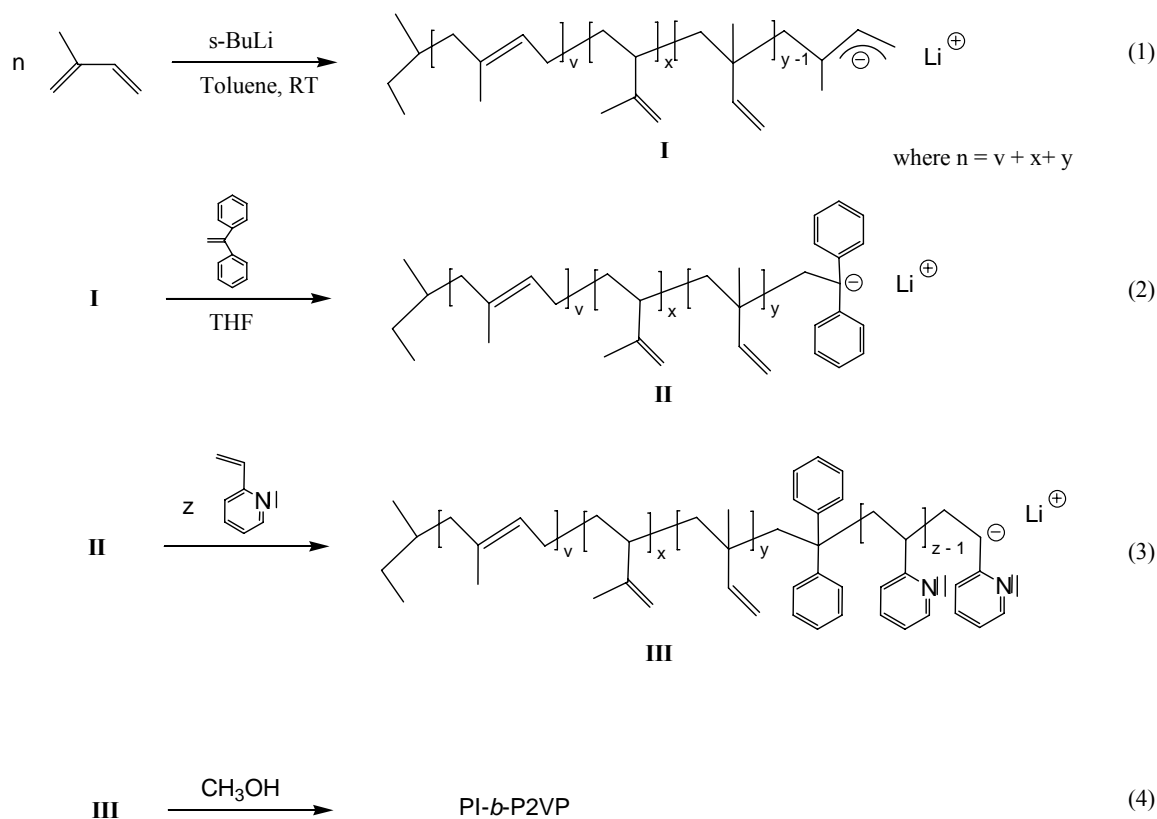

Fig 6. 1 Schematic illustration of the synthesis of PI-b-P2VP.

The reaction entries and characterization data of the copolymers are listed in the Table 6. 1 and Table 6. 2 below.

Table 6. 1 Reaction entries for PI-*b*-P2VP copolymers

Sample	Polymer[a] PI$_x$-P2VP$_y$	n isoprene [mmol]	n 2VP [mmol]	n s-BuLi [mmol]	V Toluene/THF [ml]
PI$_{325}$-*b*-P2VP$_{395}$ 64	325-330	59.60	57.80	0.18	20/160
PI$_{325}$-*b*-P2VP$_{110}$ 65	325-90	58.80	16.40	0.18	20/160
PI$_{775}$-*b*-P2VP$_{565}$ 113	815-500	57.05	35.00	0.07	20/160
PI$_{600}$-*b*-P2VP$_{555}$ 114	600-460	55.00	41.30	0.09	20/160
PI$_{65}$-*b*-P2VP$_{845}$ 115	60-605	4.00	42.50	0.07	6/60
PI$_{1210}$-*b*-P2VP$_{390}$ 117	1250-330	88.00	23.10	0.07	30/270
PI$_{570}$-*b*-P2VP$_{310}$ 1A	540-260	59.62	28.30	0.11	20/160

[a] DP of the block copolymer aimed at by the monomer/initiator ratio

Table 6. 2 Molecular weights, polydispersities and block lengths of synthesized PI-*b*-P2VP copolymers

Sample[a]	Homopolymer		Copolymer		
	Mn[b] [g/mol]	Mw/Mn[b]	Mn[b] [g/mol]	Mw/Mn[b]	Yield[c] [%]
PI$_{325}$-*b*-P2VP$_{395}$ 64	22000	1.19	38700	1.08	93
PI$_{325}$-*b*-P2VP$_{110}$ 65	22000	1.19	29100	1.12	96
PI$_{775}$-*b*-P2VP$_{565}$ 113	52700	1.05	46700	1.09	97
PI$_{600}$-*b*-P2VP$_{555}$ 114	40800	1.04	43500	1.11	93
PI$_{65}$-*b*-P2VP$_{845}$ 115	4600	1.07	42500	1.06	89
PI$_{1210}$-*b*-P2VP$_{390}$ 117	82400	1.10	93100	1.16	87
PI$_{570}$-*b*-P2VP$_{310}$ 1A	38800	1.06	73500	1.16	91

[a] block lengths calculated from GPC of the first block and ^{1}H NMR of the copolymer

[b] from SEC in CHCl$_3$ relative to narrow poly(isoprene) standards

[c] after precipitation

We have obtained block copolymers with the high content of 1,4- microstructure in the poly(isoprene) block (from NMR analysis 92 %). The copolymers have relatively narrow polydispersity and their molecular masses are in good agreement with the aimed values.

6.3.2   Formation of PI-*b*-P2VP monomicellar film

It is well known that polymer chains above the glass temperature (Tg) are mobile and free to change the shape, while below the Tg, the chains are "frozen" and only a bend stretching is possible. We propose that polystyrene (Tg = 100 °C) can be substituted with poly(isoprene) (Tg = –60 °C for high 1,4– configuration)[40] and that poly(isoprene)-*b*-poly(2vinylpyridine) (PI-*b*-P2VP) reversed micelles can be employed for the formation of highly regular arrays of particles. One can expect that utilizing a polymer far above its Tg will facilitate the organisation of micelles into arrays of even higher order compared to those obtained with a higher Tg polymer.

Poly(isoprene)-*block*-poly(2vinylpyridine)   similarly   to   polystyrene-*block*-poly(2vinylpyridine) self-assembles into reverse micelles when dissolved in a selective solvent, The micelles can be loaded with a metal precursor salt and self-organise into a regular lattice when deposited onto flat surfaces. Fig 6. 2a shows a transmission electron micrograph of the regular arrangement of gold loaded PI-*b*-P2VP micelles. The dark contrast in the TEM image is due to the presence of tiny gold particles located in the cores of amphiphilic micelles (Fig 6. 2a inset). These ultrasmall Au particles are formed by irradiation of the gold salt by the e-beam during imaging. Fig 6. 2 b) and c) show typical SEM and SFM topography images monolayers of PI-*b*-P2VP micelles loaded with chloroauric acid and deposited on a silicon oxide substrate.
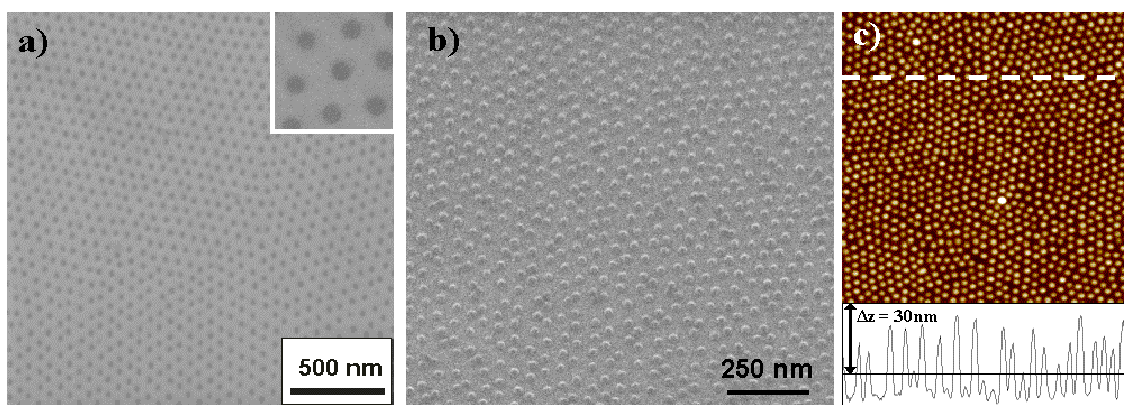
Fig 6. 2 PI(775)-b-P[2VP(HAuCl$_4$)$_{0.3}$](565) micellar monolayer deposited on a SiO$_2$ substrate. a) TEM image, b) SEM image and c) 2x2 μm SFM topography image.

In order to quantify the quality of the micellar pattern, we utilized the same method as described in detail in chapter 3.[41] Fig 6. 3 demonstrates a typical SFM topography image and the equivalent Voronoi diagram for a monolayer of PI(775)-*b*-P[2VP(HAuCl$_4$)$_{0.3}$](565) micelles. An average 63 ± 9 dislocations per 1000 micelles was determined by analyzing nine SFM images
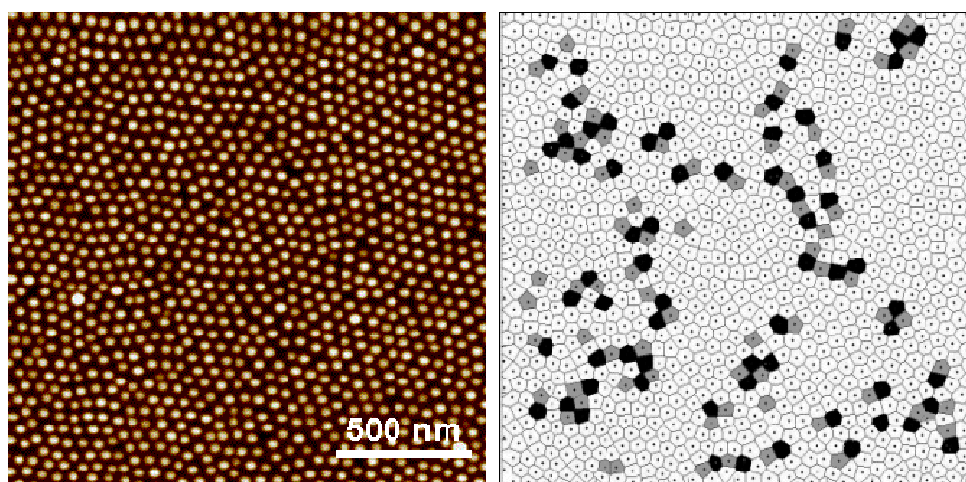
Fig 6. 3 SFM picture and corresponding Voronoi construction of a PI(775)-b-P[2VP(HAuCl$_4$)$_{0.3}$](565) micellar monolayer deposited on a silica substrate from a toluene solution.

PI(775)-*b*-P[2VP(HAuCl$_4$)$_{0.3}$](565) micelles with poly(diene) forming corona self-organise in a more regular lattice as compared with the best polystyrene-*b*-

poly(2vinylpyridine) block copolymer: PS(1700)-*b*-P[2VP(HAuCl$_4$)$_{0.3}$](450) (101 $\pm$ 5 dislocations per 1000 micelles).[41] It can be explained by the higher mobility of such micelles particularly at the very end of the evaporation process, while PS-*b*-P2VP micelles were already placed and not able to move due to the deficiency of the solvent.

PI-*b*-P2VP copolymers is a good alternative to PS-*b*-P2VP for nanoparticle formation and substrate decoration, however, it has to be mentioned that due to its ability to crosslink, it has to be handle and stored very carefully. In fact, if the polymer is partially crosslinked the dynamic exchange of the block copolymer chains among micelles is dramatically disturbed and the micellar polydispersity increases. As a result, the overall organization of the micelles on the surface is significantly hindered. Fig 6. 4 demonstrates the SFM high image of the PI(775)-*b*-P[2VP(HAuCl$_4$)$_{0.3}$](565) micelles deposited onto SiO$_2$ substrate. In this case micellar solution was prepared from partially crosslinked block copolymer (crosslinking density was very low, hardly detectable by SEC analysis).
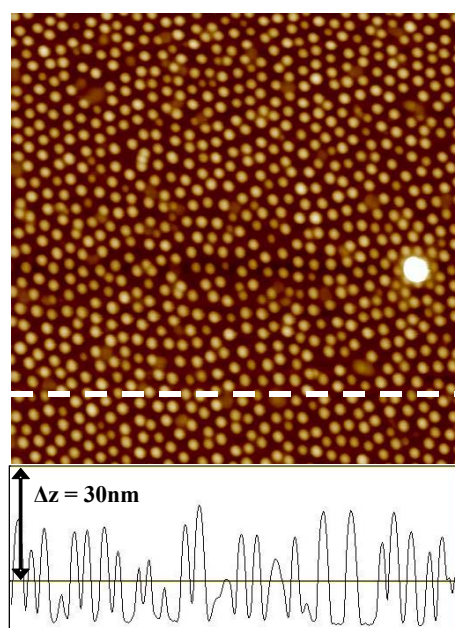
Fig 6. 4 2x2 µm SFM topography image of PI(775)-b-P[2VP(HAuCl$_4$)$_{0.3}$](565) micellar monolayer deposited on a SiO$_2$ substrate showing the effect of the unintentional PI block partial crosslinkage on the micellar pattern quality.

6.3.3   Photo-pinning

The photo-pinning method is schematically shown in Fig 6. 5. A monolayer of block copolymer micelles loaded with a metal precursor salt in their cores is formed on a substrate by dip coating. UV light exposure through an appropriate mask causes selective cross-linking of the block copolymer. By subsequently placing the substrate in a suitable solvent that eradicates the non-modified polymer, the pattern present on the mask is reproduced on the surface. Finally, the metal salt is transformed to the metal nanodots and the remaining organic matrix is removed by means of plasma treatment.
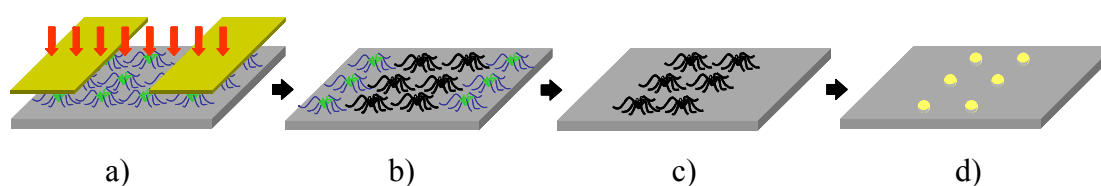
Fig 6. 5 Scheme presenting the photo-pinning method for the formation of nanoparticles arrays on surfaces. a) A monolayer of metal loaded micelles is formed on a substrate and irradiated by UV light through a mask; b) the selective irradiation causes the crosslinking of the polymer molecules in the irradiated areas; c) a solvent lift-off step removes the non modified polymer leaving on the surface only micelles arranged according to the pattern present on the mask; d) a H_2 plasma treatment reduces the salt in the core of the micelles and removes the remaining organic matrix. This step results in the formation of arrays of Au nanoclusters.

The key point of the photo-pinning method is the capability of generating radicals during the irradiation process. The realization of the pattern is most efficient with a block copolymer where the corona block contains unsaturated bonds e.g. poly(isoprene). Crosslinking can be further supported by functionalization of the substrate with a vinyl or acryl silane monolayer. As an example silicon substrates pre-functionalised with (3-acryloxypropopyl)trimethoxysilane were dip-coated in 5 mg/ml solution of poly(isoprene(775))-*b*-poly([2vinylpyridine(HAuCl$_4$)$_{0.3}$](565)) in toluene. The coated substrates were subsequently exposed to UV light (λ = 254 nm) for 35 min at a distance of 10 cm from the lamp, either through Transmission Electron Microscopy grids (Fig 6. 6b) or through photolithography masks realized with deep UV transparent

quartz (Fig 6. 6c-d). The light exposure was kept at low energy level in order to achieve the crosslinking of the polymer and at the same time to avoid the reduction of the Au precursor salt to noble metal (the problem of the gold reduction due to over exposure is outlined in subsequent chapter). The micelles were crosslinked and tightly bounded to the substrate. The non-irradiated areas were lifted-off by immersion in toluene. If the lift-off was not facilitated by ultrasonication, up to several hours were necessary to achieve a clear, well-defined pattern. The brighter areas in the pictures represent the irradiated regions containing micelles, while the dark ones correspond to naked regions of the substrate. Pattern transfer to the micellar monolayer over large areas is demonstrated in Fig 6. 6d. The pictures illustrate four fragments of a sample, which was irradiated through a mask with diminishing dimensions of vertical lines and inter distances. The width of the obtained lines changes form 10 to approx. 2 µm.
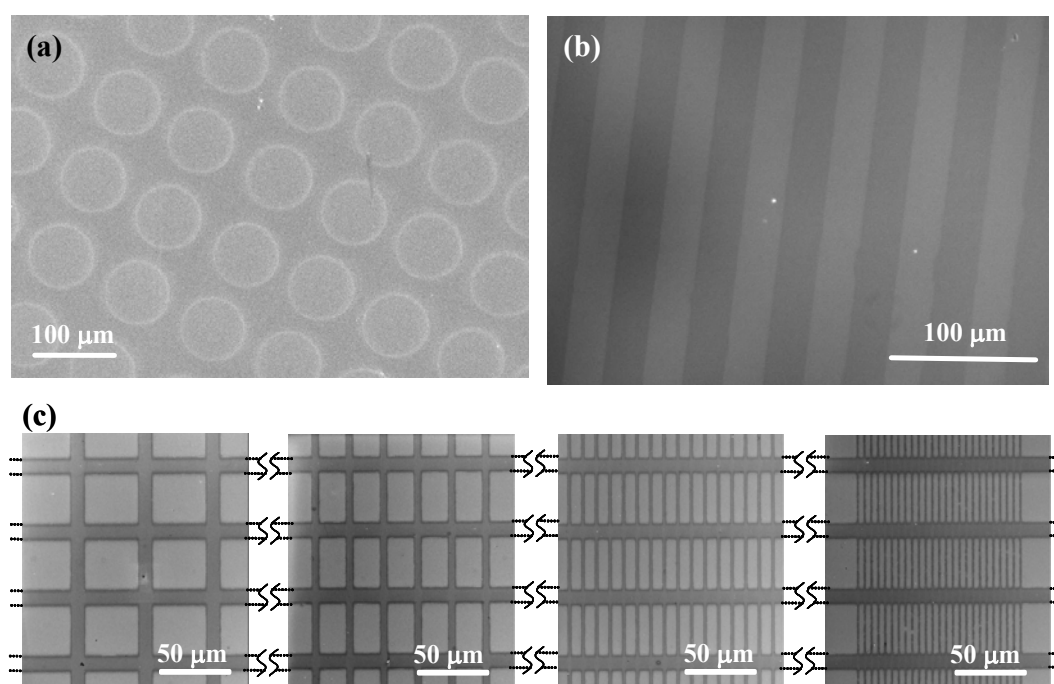
Fig 6. 6 Large area patterns of loaded block copolymer micelles after selective irradiation and lift-off: a) and c) SEM, b) optical microscope images. PI(775)-b-P[2VP(HAuCl₄)₀.₃](565) micellar monolayers on (3-acryloxypropopyl)trimethoxysilane functionalized silica substrates were irradiated (λ=254nm) through a TEM grid a) or lithography masks with linear b) and chequer c) patterns.

Fig 6. 7 shows Scanning Force Micrographs of the striped pattern prepared with PI(570)-*b*-P[2VP(HAuCl$_4$)$_{0.3}$](310) block copolymer on a vinyl silane modified substrate. The substrate was irradiated through a lithography mask consisting of 25 μm wide chromium lines separated by 30 μm on UV transparent glass. As it can be seen in the large area scan (Fig 6. 7a), the pattern present on the mask is accurately transferred to the micellar layer and the average cross section below the image confirms the dimensions of the mask pattern. The sharpness of the borderlines is evaluated by the higher magnification SFM image and can be seen as a smooth transition area with a width of ca. 500 nm (Fig 6. 7b). Two further images (Fig 6. 7c and d) show an optimum contrast between the non-irradiated area (no micelles) and the irradiated area (closed packed micelles); the inset of Fig 6. 7d shows the Fourier transformation of the hexagonal micellar pattern.
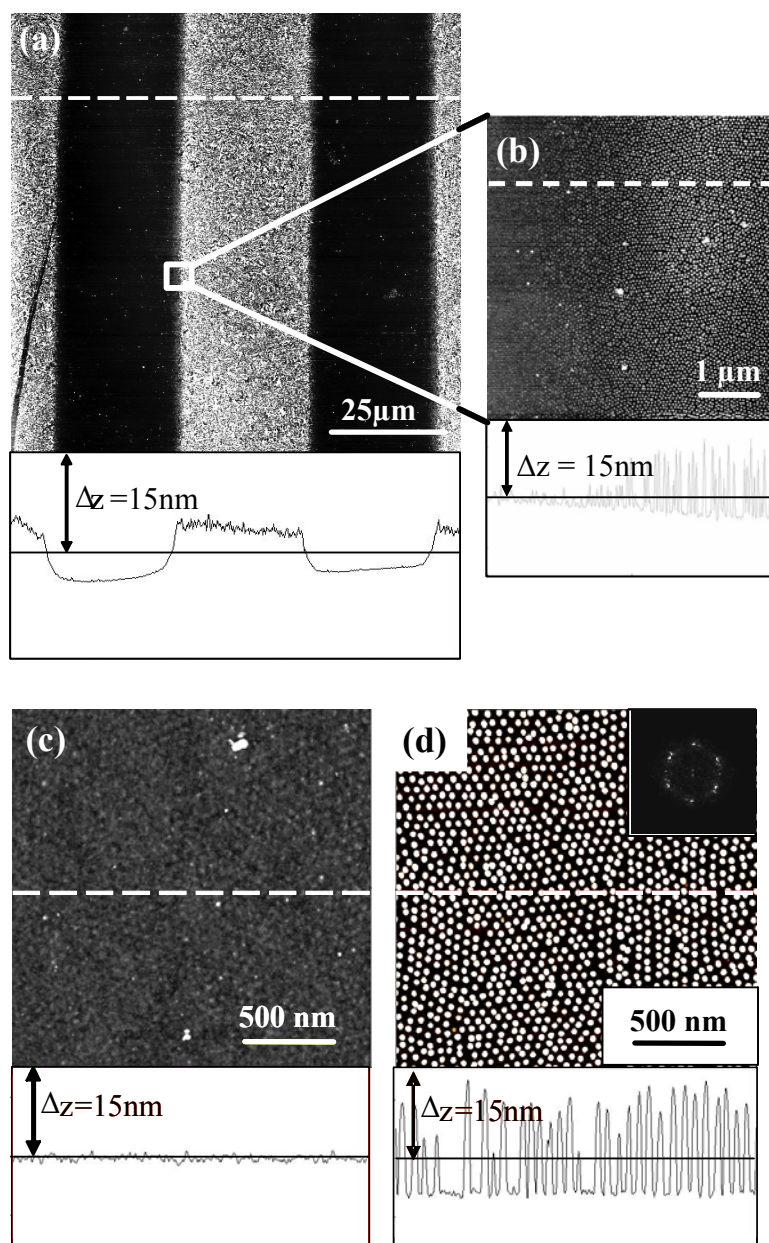
Fig 6. 7 SFM pictures of a striped pattern of PI(570)-b-P[2VP(HAuCl₄)₀.₃](310) micellar monolayer on silica substrate after UV irradiation through a lithography mask and lift-off in toluene of the non-irradiated areas of the layer. The silica was functionalized with a vinyltriethoxysilane. The sample was exposed for 35 minutes at 10 cm distance from the lamp (λ=254nm). a) large area SFM picture, b) 5x5 µm scan of the boundary area, c) and d) 2x2 µm scans show the bare substrate and one covered with micelles respectively. The inset on the right side shows the Fourier transformation of the micellar pattern.

Impurities or polymer residue, that do not carry the inorganic load (visible as white spots on the SFM pictures), have no influence on the entire process and are removed by the subsequent plasma treatment. In the present study the broadness of the boundary area depends on scattering of the UV light, which is consequence of a non-parallel light beam and a non-perfect adherence of the mask to the surface of the irradiated sample. All experiments were carried out without clean room facilities and the presence of dust particles could not be excluded. Taking this into account good transfer of the pattern was achieved.

In order to obtain Au clusters from the micelles remaining on the surface, the sample was exposed to hydrogen plasma (300W; 0.096 mbar; 0.5 h). During this process the polymer matrix was removed and at the same time one gold nanoparticle was created from each micelle. Fig 6. 8 illustrates SEM images of hexagonal arrays of gold clusters arranged in 30 μm lines on a SiO_2 substrate. Due to the small cluster size in combination with the large scan area the contrast of the image is rather poor, however the striped structure is clearly visible. In the irradiated area 2 ± 1 nm single Au clusters (Fig 6. 8c) were deposited on the surface in a pattern templating the hexagonal arrangement of micelles. The distance between the gold clusters is determined by the molecular weight of the PI(570)-*b*-P2VP(310) block copolymer and was found to be approx. 50 nm.
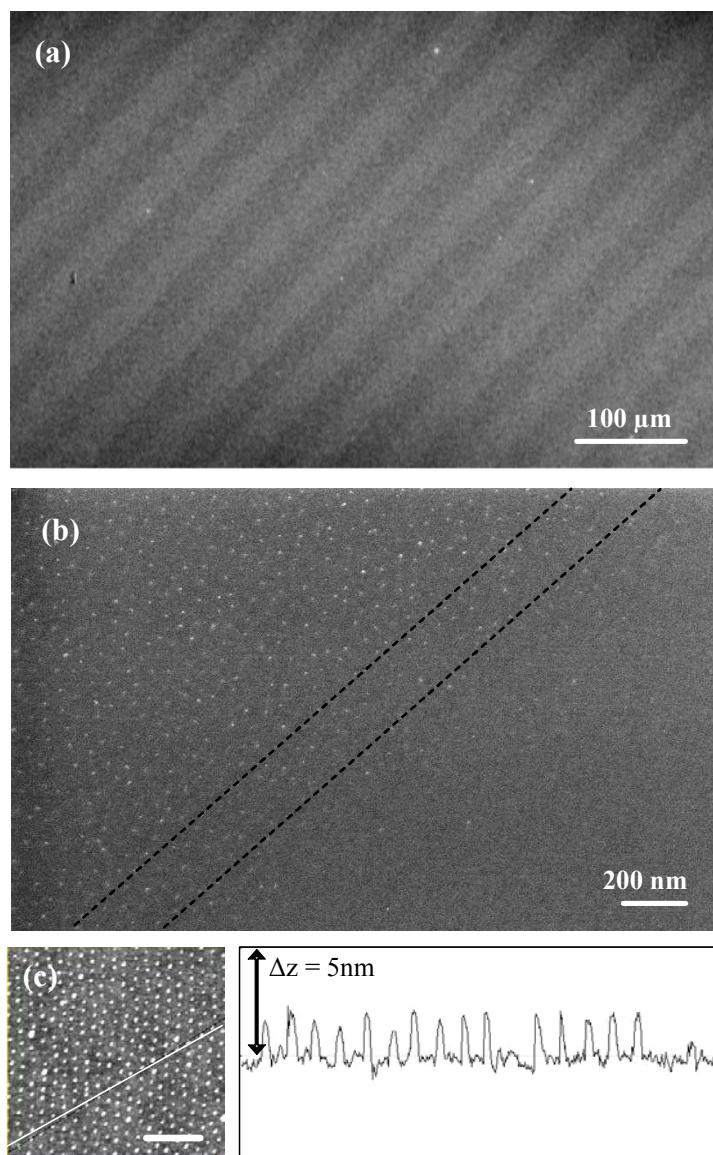
Fig 6. 8 SEM and SFM images of gold nanodots arranged in a linear pattern on a silicon substrate. Au dots were obtained by hydrogen plasma treatment of PI(570)-b-P[2VP(HAuCl$_4$)$_{0.3}$](310) micellar monolayer patterned by photo-pinning: a) SEM image with brighter stripes representing the gold clusters arrays, b) SEM of the border between irradiated and non-treated areas, c) SFM image of the dots with cross-section (scale bar 250 nm).

For pattern visualisation purposes, metalization of the nano-structured lines was performed by electroless deposition of gold. The sample decorated with 30 μm white lines of gold clusters shown in Fig 6. 8 was immersed in an aqueous solution of

hydroxylamine and chloroauric acid for 3 min. The Au nanodots present on the surface served as seeds for deposition of gold and a thin polycrystalline film of Au was formed in the decorated areas only (Fig 6. 9). The inset on the right side shows the SEM picture of the gold line border. The height of lines measured with the SFM was found to be around 25 nm (Fig 6. 9c).
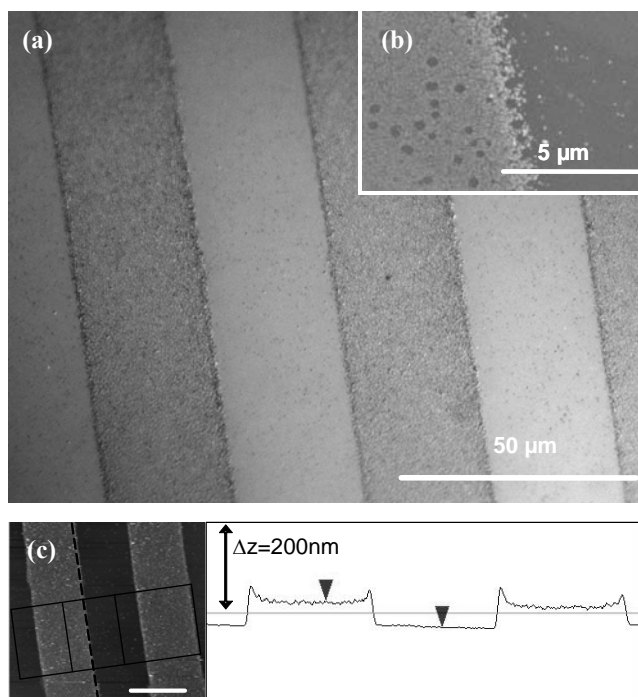
Fig 6. 9 Gold lines on silicon substrate obtained by Au electroless deposition using patterned gold clusters as seeds. a) light microscopy picture, b) SEM image of he Au line border and c) SFM image with average cross-section (scale bar 25μm).

The photo-pinning approach presented here is less efficient if the substrate is not pretreated by a vinyl (or acryl) silane. Employing bare SiO_2 instead of a silane-modified substrate demanded approximately a twice-longer time of UV exposure to crosslink the polymer sufficiently and bind it to the surface of the substrate. Also metal loaded nanofilms of micelles from polymers that do not possess chemical groups, which can be easily crosslinked under UV exposure, can be photo structured. We were able to photo-pin to the surface gold loaded polystyrene-*b*-poly(2vinylpyridine) with the pre-functionalization of the surface by vinyl silane and the addition of UV active

compounds such as benzophenone (Fig 6. 10a and b respectively). However, no optimization attempts were made on the PS-*b*-P2VP system. It must be noted, that the conditions of irradiation were much stronger (longer times of irradiation at shorter distances) and the edges of the resultant patterns in both cases were less defined as compared to the experiments with the PI-*b*-P2VP block copolymer. As it can be seen, the pattern present on the mask was more accurately transferred to the underlying micellar layer in the case of the sample prepared on the pre-functionalized substrate, while the sample with benzophenone addition gave rather poor results. The one possible explanation is the more homogeneous distribution of photoactive sites (vinyl groups) chemically bounded to the substrate in the former case, in opposite to rather mobile and for this reason differing in the local concentration photo-crosslinker in latter case.
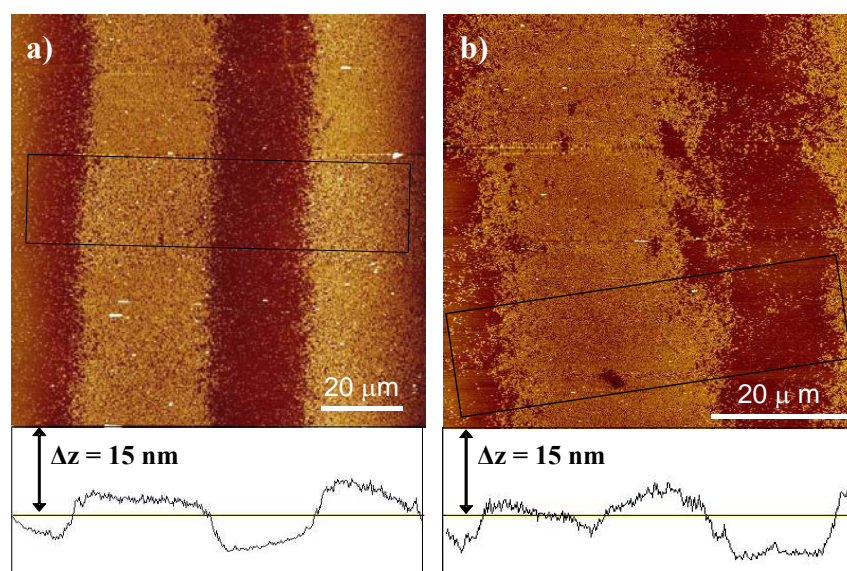
Fig 6. 10 SFM pictures of a striped pattern of PS(1350)-b-P[2VP(HAuCl₄)₀.₃](450) micellar monolayer on silica substrate after UV irradiation through a lithography mask and lift-off in toluene of the non-irradiated areas of the layer. The samples were exposed for 60 minutes at 1 cm distance from the lamp (λ=254nm). a) the silica was functionalized with a vinyltriethoxysilane, b) before deposition benzophenone was added to the micellar solution (3 wt% in respect to the block copolymer).

6.4   Conclusions

Series of PI-*b*-P2VP block copolymers have been prepared by living anionic polymerization. These copolymers were subsequently used in fabrication of Au nanoparticles on flat surfaces. We also developed the photo-pinning method for the fabrication of metal nano-structured micropatterns by combining self-assembly of block copolymer micelles and photolithography. The method utilizes block copolymers that are able to crosslink under the exposure of UV light such as poly(isoprene)-*b*-poly(2vinylpyridine) and can be extended to saturated polymers e.g. polystyrene-*b*-poly(2vinylpyridine), if a photoinitiator is added and surface attachment is facilitated by a silane monolayer. The photo-pinning approach is a simple, parallel process, which allows patterning of large areas on conductive and non-conductive substrates in aperiodic and designed micro- and nanopatterns. It is compatible with the common MEMS techniques and suitable for wide range of applications especially in the fabrication of biosensors, electronic and optical devices. Although the quality of the transferred patterns reported here is limited to micron resolution it is obvious that the resolution can be improved further simply by using standard lithography equipment not available for the experiments reported here. Further experiments taking advantage of such equipment are needed to explore the resolution limits of the proposed photo-pinning method. It should be noted that the diameter of one single micelle can be easily tuned in the range 30-200 nm by the choice of the block copolymer molecular weight. [17] The upper limit of this range is within the same length scale as the resolution obtainable by photolitography on a ultrathin resist layer that can be modified by deep UV, like the one proposed here. E-beam and Focus Ion Beam writing has demonstrated that even single micelles can be cut through [42-44] and that the sharpness of the border between the micelle covered and bare surface is ultimately given by the size of the micelles.

6.5 References

[1] G. Li, V. Joshi, R. L. White, S. Wang, J. T. Kemp, C. Webb, R. W. Davis, *J. Appl. Phys.* **2003**, *10*, 7557.

[2] C. Sönnichsen, S. Geier, N. E. Hecker, G. von Plessen, J. Feldmann, H. Diltbacher, B. Lamprecht, J. R. Kernn, F. R. Aussenegg, V. Z.-H. Chan, J. P. Spatz, M. Möller, *Appl. Phys. Lett.* **2000**, *77*, 2949.

[3] Y. Chang, C. W. Lin, H. H. Hsu, J. H. Fang, S. J. Lin, *J. Electrochem. Soc.* **2004**, *151*, C81.

[4] H. P. Fong, Y. Wu, Y. Y. Wang, C. C. Wan, *J. Electron. Mater.* **2003**, *32*, 9.

[5] E. Suhir, *Microelectron. J.* **2000**, *31*, 839.

[6] D. A. Thompson, I. S. Best, *IBM J. Res. Dev.* **2000**, *44*, 311.

[7] V. Skumryew, S. Stoyanov, Y. Zhang, G. Hadjipanayis, D. Givord, J. Nogues, *Nature* **2003**, *423*, 850.

[8] M. Arnold, E. A. Cavalcanti-Adam, R. Glass, J. Blümmel, W. Eck, M. Kantlehner, H. Kessler, J. P. Spatz, *ChemPhysChem* **2004**, *5*, 383.

[9] A. Csáki, G. Maubach, D. Born, J. Reichert, W. Fritzsche, *Single Mol.* **2002**, 275.

[10] T. Ito, S. Okazaki, *Nature* **2000**, *406*, 1027.

[11] J. P. Silverman, *J. Vac. Sci. Technol. B* **1997**, *15*, 2117.

[12] M. K. Corbierre, J. Beerens, R. B. Lennox, *Chem. Mater.* **2005**, *17*, 5774.

[13] J. Melngailis, A. A. Mondelli, I. L. Berry, R. Mohondro, *J. Vac. Sci. Technol. B* **1998**, *16*, 927.

[14] C. A. Mirkin, D. S. Ginger, H. Zhang, *Angew. Chem. Int. Ed.* **2004**, *43*, 30.

[15] A. V. Ruzette, L. Leibler, *Nat. Mater.* **2005**, *4*, 19.

[16] M. J. Fasolka, A. M. Mayes, *Annu. Rev. Matter. Res.* **2001**, *31*, 323.

[17] J. P. Spatz, S. Mössmer, C. Hartmann, M. Möller, T. Herzog, M. Krieger, H.-G. Boyen, P. Ziemann, B. Kabius, *Langmuir* **2000**, *16*, 407.

[18] S. Mößmer, J. P. Spatz, M. Möller, T. Aberle, J. Schmidt, W. Burchard, *Macromolecules* **2000**, 4791.

[19] H.-G. Boyen, G. Kästle, U. Zürn, T. Herzog, F. Weigl, P. Ziemann, O. Mayer, C. Jerome, M. Möller, J. P. Spatz, M. G. Garnier, P. Oelhafen, *Adv. Fun .Mater.* **2003**, *13*, 359.

[20] J. Spatz, S. Möbmer, M. Möller, M. Kocher, D. Neher, G. Wegner, *Adv. Mater.* **1998**, *10*, 473.

[21] G. Kästle, H.-G. Boyen, F. Weigl, G. Lengl, T. Herzog, P. Ziemann, S. Riethmüller, O. Meyer, C. Hartmann, J. P. Spatz, M. Möller, M. Ozawa, F. Banhart, M. G. Garnier, P. Oelhafen, *Adv. Funct. Mater.* **2003**, *13*, 1.

[22] J. C. Love, L. A. Estroff, J. K. Kriebel, R. G. Nuzzo, G. M. Whitesides, *Chemical Reviews* **2005**, *105*, 1103.

[23] A. Goelzhaeuser, W. Eck, W. Geyer, V. Stadler, T. Weimann, P. Hinze, M. Grunze, *Adv. Mater.* **2001**, 806.

[24] P. Du, M. Li, K. Douki, X. Li, C. B. W. Garcia, A. Jain, D.-M. Smilgies, L. J. Fetters, S. M. Gruner, U. Wiesner, C. K. Ober, *Adv. Mater.* **2004**, *16*, 953.

[25] M. Li, K. Douki, K. Goto, X. Li, C. Coenjarts, D. M. Smilgies, C. K. Ober, *Chem. Mater.* **2004**, *16*, 3800.

[26] S. A. Levi, A. Mourran, J. P. Spatz, F. C. J. M. van Veggel, D. N. Reinhoudt, M. Moeller, *Chem. Eur. J.* **2002**, *8*, 3808.

[27] J. P. Spatz, V. Z.-H. Chan, S. Moessmer, F.-M. Kamm, A. Plettl, P. Ziemann, M. Moeller, *Adv. Mater.* **2002**, *14*, 1827.

[28] R. Glass, M. Möller, J. P. Spatz, *Nanotechnology* **2003**, *14*, 1153.

[29] S.-H. Yun, B.-H. Sohn, J. C. Jung, W.-C. Zin, M. Ree, J. W. Park, *Nanotechnology* **2006**, *17*, 450.

[30] T. Deng, Y.-H. Ha, J. Y. Cheng, C. A. Ross, E. L. Thomas, *Langmuir* **2002**, *18*, 6719.

[31] W. Hwang, M.-H. Ham, B.-H. Sohn, J. Huh, Y. S. Kang, W. Jeong, J.-M. Myoung, C. Park, *Nanotechnology* **2005**, *16*, 2897.

[32] S.-H. Yun, B.-H. Sohn, J. C. Jung, W.-C. Zin, M. Ree, J. W. Park, *Nanotechnology* **2006**, *17*, 450.

[33] R. Glass, M. Arnold, J. Blümmel, A. Küller, M. Möller, J. P. Spatz, *Adv. Funct. Mater.* **2003**, *13*, 569.

[34] R. Glass, M. Arnold, E. Ada Cavalcanti-Adam, J. Blümmel, C. Haferkemper, C. Dodd, J. P. Spatz, *New J. Phys.* **2004**, *6*, 101.

[35] S. Moessmer, PhD thesis, University of Ulm (Ulm), **1999**.

[36] H. Watanabe, M. Tirrell, *Macromolecules* **1993**, *26*, 6455.

[37] R. P. Quirk, S. Corona-Galvan, *Macromolecules* **2001**, *34*, 1192.

[38] M. Szwarc, *"Living Polymers and Mechanisms of Anionic Polymerization"*, Adv.Polym.Sci. 49, Springer Verlag, Berlin Heidelberg, **1983**.

[39] M. Fisher, M. Szwarc, *Macromolecules* **1970**, *3*, 23.

[40] F. Fontaine, C. Morland, C. Noel, L. Monnerie, B. Erman, *Macromolecules* **1989**, *22*, 3348.

[41] see Chapter 3 of this thesis.

[42] R. Glass, M. Arnold, E. A. Cavalcanti-Adam, J. Blümmel, C. Haferkemper, C. Dodd, J. P. Spatz, *New J. Phys.* **2004**, *6*, 101.

[43] P. Mela, B. Gorzolnik, M. Bückins, A. Mourran, J. Mayer, M. Moeller, *Small* **2007**, *3*, 1368.

[44] see Chapter 7 of this thesis.

Appendix to Chapter 6

In this appendix two very important aspects of the irradiation step influencing the quality of final patterns fabricated by the photolipinning method are addressed: 1) a distance between the photolithography mask and the micellar resist as well as 2) a distance between the source of the UV light and the mask. As it will be shown, both issues are crucial for precise transfer of desired patterns from mask to the micellar resist.

Effect of gaps between mask and substrate

Fig 6a. 1 illustrates the influence of increasing distance between a mask and a resist during contact photolithography on the quality of a transferred pattern. In the ideal case, the mask is in intimate contact with the photoresist providing a well-defined light intensity profile on the resist. Hence, produced objects (after developing porocess that in case of negative resist is simply dissolving the unexposed part of the resist) precisely match with the mask pattern. (Fig 6a. 1a). However, due to the resist surface roughness or impurities between the surface of the resist and mask such as particles, the distance between photolithography mask and resist may increase. Upon enlarging the gap, light diffraction generates a gradient of the light intensity that significantly broadens the regions to be exposed effecting final image resolution. Consequently, the resist after developing results in sloped sidewalls (Fig 6a. 1b, c and d) or in extreme cases, where the gap reach several microns, the control over transmitted pattern is completely lost (Fig 6a. 1e, f and g).
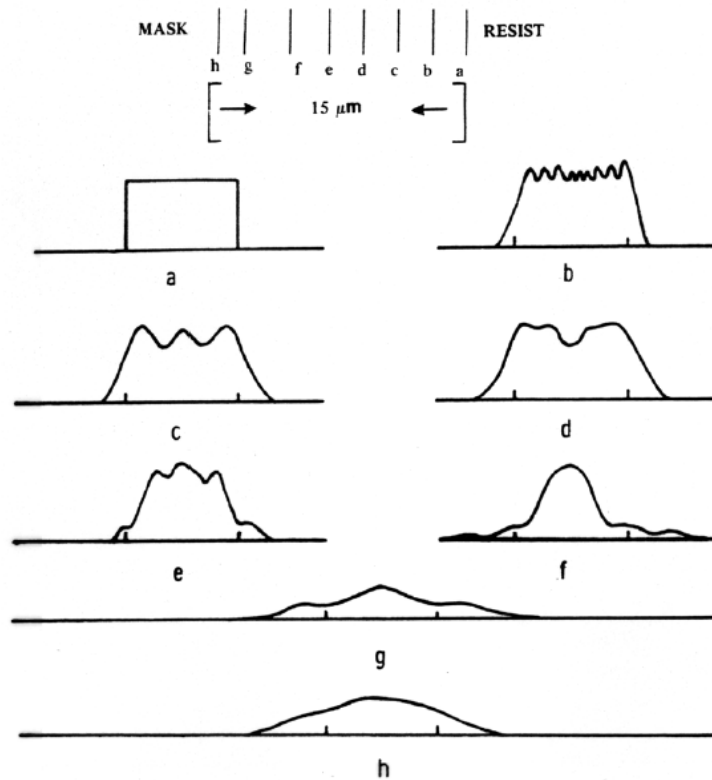
Fig 6a. 1 The decrease in image quality (and hence resolution) noted here affects contact lithography in which particulates or other problems have caused there to be some distance between mask and substrate.[1]

Fig 6a. 2 shows the effect of mask-sample gap as observed with our photo-pinning system. The good contact between mask and micellar layer during irradiation step provided accurate transfer of the pattern to the micellar resist (Fig 6a. 2a), while poor mask-sample contact resulted in significant broadening of the demanded dimensions of the mask pattern (Fig 6a. 2b).
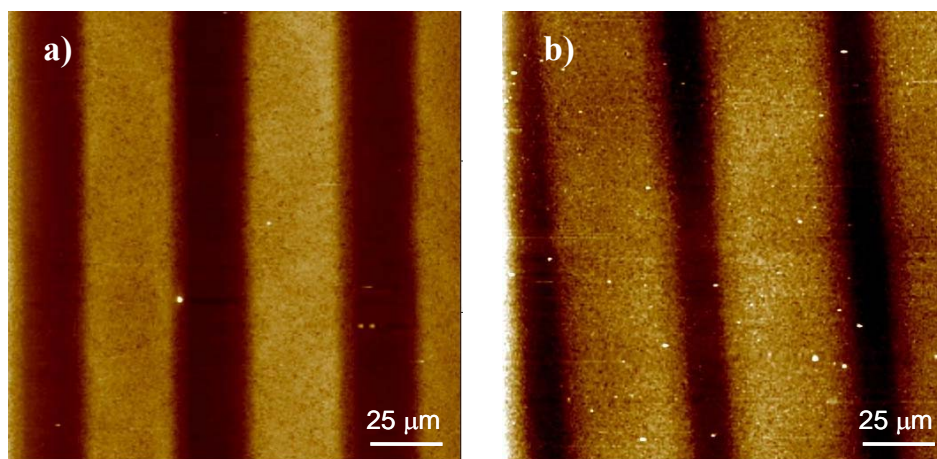
Fig 6a. 2 SFM pictures of the striped pattern after UV irradiation and toluene lift-off. Pictures are representative for a good (a) and a poor (b) mask-sample contact during transferring the pattern from the lithography mask onto a PI(570)-b-P[2VP(HAuCl₄)₀.₃](310) micellar monolayer. The samples were exposed for 5 minutes at 1 cm distance between the mask and the light source (λ=254nm).

Effect of distance between source of light and mask

A non-parallel UV light beam we used, also affected resolution of our photopininig method. The simple tube-shaped lamp without any alignment equipment produces light that penetrates in all directions, that's why the distance between the source of UV radiation and the mask is influencing the parallelism of UV light (the larger the distance, the "more parallel" light). However, we have to remember that the intensity of light is inversely proportional to the square of the distance from the light source and higher distances demand extremely long times of irradiation. We found out that in our experiments, the optimum gap between the UV lamp and samples is around 10 cm (Fig 6a. 3a). As expected, decreasing the distance slightly broadens the pinned micellar lines and expands the gradient at boundary between the irradiated and non-irradiated regions (Fig 6a. 3b).
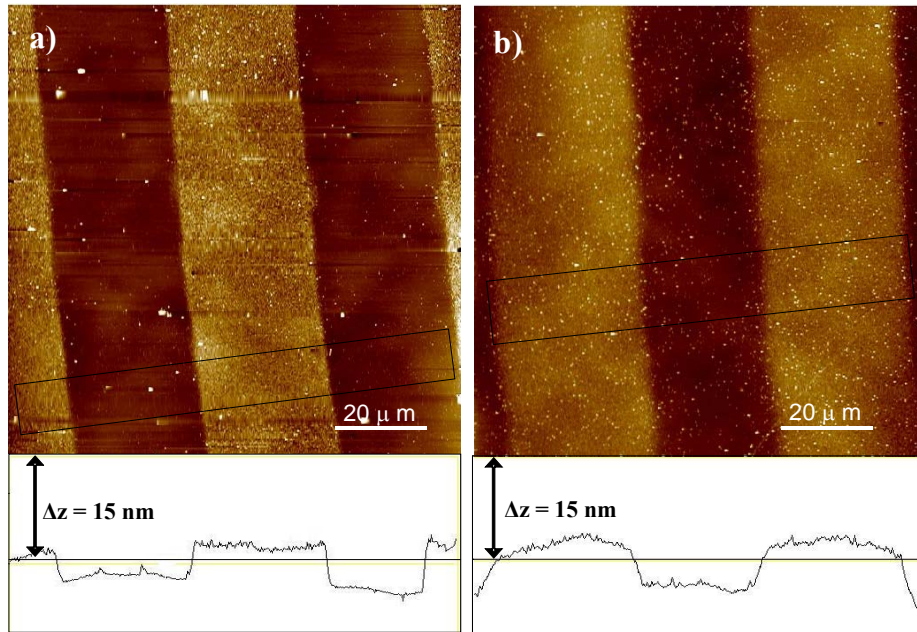
Fig 6a. 3 SFM pictures demonstrating the effect of the distance between the mask and the light source ($\lambda=254nm$) on the quality of the transferred pattern onto a PI(570)-b-P[2VP(HAuCl$_4$)$_{0.3}$](310) micellar monolayer during UV irradiation. a) 10 and b) 1 cm the lamp-to-mask spacing.

The negative effects caused by the non-perfect mask adherence and the non-parallel UV light beam could be partially overcome by increasing the exposure time followed by the stronger lift-off procedure. However, it has to be noted that at the same time, prolonged exposure enlarges the dimensions of crosslinked regions, and more important, it also increases light absorption in the micellar resist, reducing the precursor salt to metal particles.

References

[1]   W. M. Moreau, *"Semiconductor Lithography: Principles, Practices, and Materials. Microdevices"*. New York: Plenum Press, **1988**

Chapter 7

Low ion dose FIB modification of monomicellar layers for the creation of highly ordered metal nanodots arrays[*]

7.1   Introduction

There is continuous interest in the fabrication of substrate supported metal and metaloxide nanostructures for applications in fields of technology such as molecular electronics, biosensors, and material science.[1-5] Specifically, gold nanodots are of interest for their optical, conductive and catalytic properties.[6-9] Different approaches have been followed for the creation of controlled patterns of gold nanoparticles and nanowires on surfaces, either by preparing the particles in solution and then depositing them on a surface, or by generating the structure directly on the surface. In the first case fabrication of defined aperiodic patterns requires local control of the deposition of the particles, [10, 11] typically achieved by photoresist technology.[12] In the second case particle formation must be effected with local control. Here particle size, size uniformity and interparticle distances are critical issues.

There are examples for both approaches where an electron beam has been used either to define chemical patterns for the guided adsorption of solution synthesized particles,[13] or for the direct modification of films of premade nanoparticles or of gold solutions.[14, 15] We have previously shown that highly regular patterns of metal and metal oxide nanodots on surfaces can be obtained by using self-assembly of block copolymer micelles with metal precursor salts sequestered in their cores. [16] Under the right conditions, the micelles self assemble on the surface in hexagonal patterns. Subsequent plasma treatment reduces the metal salt and removes the copolymer leaving metal nanodots which preserve the same regular pattern of the micelles. In order to create aperiodic patterns of gold nanodots, we used the micellar layer as e-beam negative resist.[17] Because the resist already contains the functionality goal of the patterning, it is possible to create arrays of nanodots with a single layer lithographic process, minimizing the needed steps and therefore the chance of defects in the resulting structures.

Although e-beam proved to be a successful choice for direct lithography of the micellar layer, there are limitations because of the very high doses that were needed in order to pin the irradiated micelles effectively to the substrate. In detail, these are electrostatic charging and the concurrent beam deflection, slow writing rates and a limitation in the choice of the substrate. Here focused ion beam (FIB) is an interesting and in some cases superior alternative. A focused ion beam system has proven to be a versatile tool for micro and nano device prototyping. FIB systems can be used for imaging, high resolution milling and direct modification of a resist layer and self-assembled monolayers.[18, 19] Furthermore, commercially available focused ion beam (FIB) systems have reached a similar resolution as electron beam systems. Because of the higher mass of ions with respect to electrons, in FIB lithography the momentum of the ions is higher at lower velocity and therefore the energy transfer is better. Consequently, lower doses are required than in e-beam lithography to introduce crosslinking in an organic thin film.[20] Problems typical for e-beam lithography like low resist sensitivity, back scattering and proximity effects, can be minimized.[21, 22] FIB has also the potential to pattern magnetic materials with better resolution than e-beam.[23] Furthermore, because the energy transfer is very efficient, localization of the FIB induced material modification is high and high writing speeds can be achieved when FIB is used for direct lithography. For high resolution patterning, the lower doses required by FIB (and therefore the shorter writing time), cannot be compensated by the higher currents available in e-beam lithography (i.e. higher dose in the same writing time) because high intensity e-beam irradiation suffers from electrostatic charging at the expenses of the resolution. Taniguchi and coauthors concluded that the writing speed of FIB is expected to be 50 times faster in the case of lithography on spin-on-glass (SOG) resists.[24]

In this chapter we report the low dose modification of a micellar monolayer by FIB for the fabrication of gold nanodots arrays on silicon substrates.

7.2   Experimental

Materials

PS(1350)-b-P2VP(400) block copolymer (Mn = 18.2 kg/mol; Mw/Mn = 1.1) polymer was previously synthesized in our group. Toluene (Merck p.a.) was dried over $LiAlH_4$ and distilled. $HAuCl_4x3H_2O$ (Fluka, purum) was used as received. Silicon wafers were purchased from CrysTec GmbH, Berlin, Germany.

Analysis

SFM imaging. A Nanoscope III scanning probe microscope (Digital Instruments, Veeco, Santa Barbara, U.S.A.) was used with silicon cantilevers Si-cantilevers (Nanosensors, Neuchatel, Switzerland) resonating at approx. 350 kHz. Images were edited with Nanoscope software (v5.12r5 Digital Instruments, Veeco, Santa Barbara, U.S.A.).

HRSEM imaging: A Zeiss Supra 35VP microscope was used.

Light Microscopy was performed by means of an Axioplan Imaging microscope (Carl Zeiss, Göttingen, Germany). Contrast enhancement of the images was done with the Femtoscan software (Advanced Technologies Center, Russia).

Raman Microscopy. These experiments were performed with a WITec alpha 300R Raman microscope (WITec GmbH, Ulm, Germany) to acquire Raman spectra and images of the sample in air. The sample was illuminated with a frequency doubled Nd:YAG Laser maximum power of 50 mW at 532 nm excitation. The data were acquired at a scan speed of 0.1 s per pixel with a diffraction-limited spatial resolution of ~360 nm. The spectrum was measured using a Peltier-cooled CCD detector, and the spectrometer was operated in the backscattering geometry. A 100× objective was used for selecting the area of interest. Images which represent the distribution of peak intensity over a selected spectral region were calculated by integration of the Raman spectra over that spectral region (WITec Project software, ver.1.88, WITec GmbH, Ulm, Germany).

Methods

Layer formation. 0.5wt % solution of PS(1350)-*b*-P2VP(400) in dry toluene were prepared and mixed with 0.5 equiv of $HAuCl_4x3H_2O$ per pyridine unit. The mixture was stirred in the dark for 24 h to allow complete solubilization of the gold acid in the cores of the block copolymer micelles. Silicon substrates were dipped into this solution and withdrawn at a constant speed (10 mm/min). Prior dipping, the silicon substrates were cleaned by ultrasonication in acetone, water, isopropanol (5 minutes each solvent) and dried under nitrogen flow.

FIB writing. Focused Ion Beam direct writing was done on a FEI Strata FIB 205 (FEI Company, Eindhoven, NL) system. The gallium ion beam energy was set to 30 keV. The patterns consisted of lines with 0.5 µm width and 20 µm length. They were written with 20 µm long single pass lines in raster mode, with 50 % overlap. The width of the single pass line was dependent on the ion current value. The ion dose of the beam is calculated by dividing the beam current by the ''area'' of the beam ($\pi d^2/4$). The diameter d is approximately the half-width of the Gaussian, as estimated from the resolution and the width of the lines written. The beam currents of 1 pA and 10 pA correspond to spot sizes of 6 and 20 nm, respectively. The ion beam doses in the irradiated arrays were calculated from the total number of ions obtained by multiplying the nominal beam currents with the exposure times and dividing it through the exposed area.

Solvent lift-off. The samples were immersed in toluene for 10 hours.

Plasma treatment. Hydrogen plasma was generated in a home-built etcher by means of a magnetron. Typical conditions were: 300W; 0.096mbar; 0.5h.

7.3   Results and discussion

Fig 7. 1 presents the different steps of the direct FIB lithography process to deposit nanoclusters with nanometer accuracy.

monolayer   FIB   development   Plasma treatment
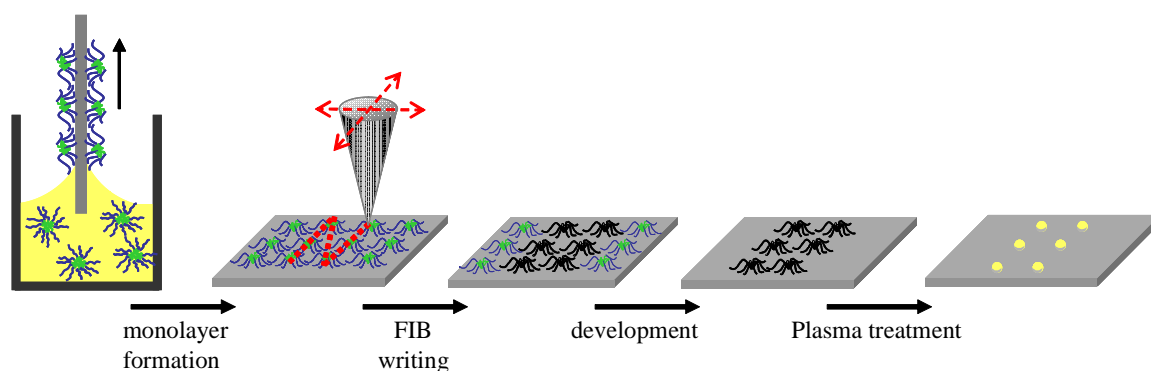formation   writing

Fig 7. 1 Schematic of the process steps for the formation nanodots of arrays: micellar film formation, FIB writing and layer development, deposition of clusters and removal of the polymer by plasma.

The method comprises three steps: i) deposition of the micellar monolayer incorporating an organic compound in their cores ii) FIB writing of predefined patterns and layer development in solvent iii) H_2 or O_2 plasma treatment of the remaining layer. The method is generally suitable for deposition of noble and non noble metal dots and also for oxidic particles of various compositions. Here we report the low dose modification of a micellar monolayer by FIB for the fabrication of gold nanodots arrays on silicon substrates.

Lithographic patterns consisting of sets of 25 lines with 0.5 µm width and 20 µm length were realized with three different settings in terms of dwell time and ion current (Table 7. 1) on a monolayer of polystyrene-*block*-poly(2-vinylpyridine), PS-*b*-P2VP, micelles loaded with chloroauric acid. Care was taken that the patterns were placed in unirradiated areas from which e.g. no ion-beam induced SE-images were acquired before or after patterning. The three different irradiation conditions were employed on adjacent areas of the micelle-coated wafer, which were subsequently exposed to the same lift off and plasma treatment. Conditions 2 and 3 were chosen in such a way that both resulted in an ion dose 10 times lower as for condition 1, but adjusted by either

lowering the total beam current or the total exposure time, respectively. Thus for the same total ion dose, a dose rate dependence could be revealed.

Table 7. 1 FIB writing conditions and heights of unmodified and FIB modified micelles.

	Ion current [pA]	Dwell time [us]	Beam diameter [nm]	Ion dose [ions/cm^2]	Micellar height [nm]	
					Before	After
Condition 1	10	10	~20 nm	$1 \cdot 10^{15}$	27± 5	10± 3
Condition 2	1	10	~6 nm	$1 \cdot 10^{14}$	27± 5	21± 4
Condition 3	10	1	~20 nm	$1 \cdot 10^{14}$	26± 6	20± 4

All tested FIB conditions resulted in a decrease of the thickness of the irradiated polymer, as shown in the SFM images of Fig 7. 2 where the darker color corresponds to micelles with lower height.

condition 1

10 pA, 10 μs

condition 2

1 pA, 10 μs

condition 3

10 pA, 1 μs
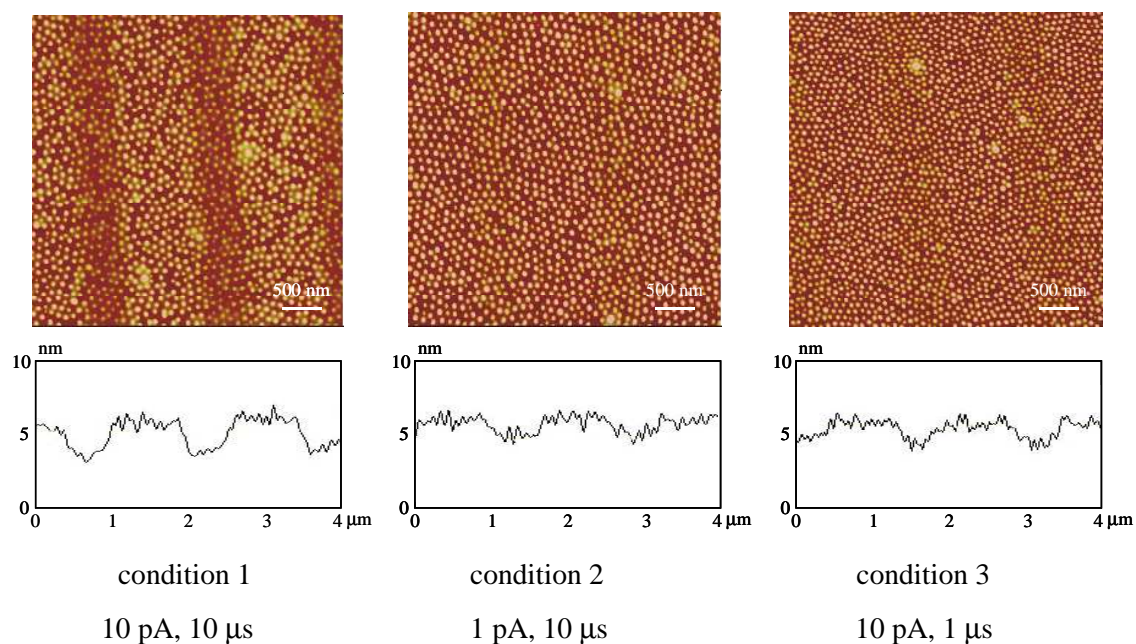
Fig 7. 2 SFM images and average height profiles of the micellar monolayer after FIB modification. Darker color corresponds to lower height. The average height profiles were determined on areas of approx 4x8 μm. Scale bar: 500 nm.

Analysis of the height profile in the SFM pictures revealed that condition 1 caused the strongest ablation reducing the micelles' height from approx. 27 nm to 10 nm (Table 7. 1), while the lower ion doses of conditions 2 and 3 resulted in a decrease in the height of the film of approx. 6 nm.

Fig 7. 3 shows a scanning force micrograph of micelles that were ion bombarded with the highest dose (condition 1). It is clearly depicted that the ablation was most effective at the location of the core of the micelles where the heavy gold ions were located. We had observed a similar effect earlier when we used such monolayers of gold loaded micelles as an etching mask for argon sputtering and it was explained by the improved energy transfer to the heavy atoms.[25]
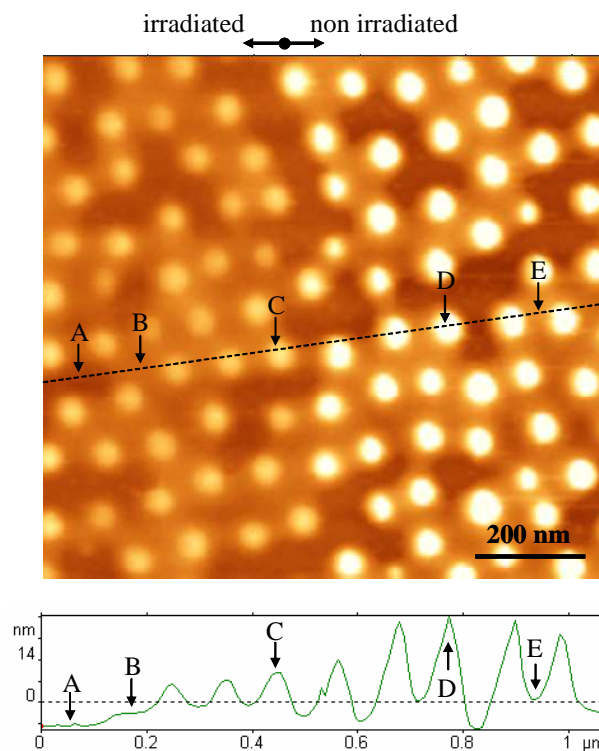
Fig 7. 3 SFM micrograph of the border between irradiated (left) and non irradiated (right) areas of a micellar layer exposed to the ion dose of condition 1. The height profile refers to the line drawn on the micrograph. A represents the naked substrate; heights B and E correspond to the irradiated and non irradiated PS layer, respectively; heights C and D compare the effect of the ion bombardment on the core of the micelles.

The damage to the micellar core can be such that the gold is shot out of the core of the irradiated micelles and redeposited elsewhere. This can be seen in the HRSEM images obtained after solvent lift off of the non irradiated polymer (Fig 7. 4, lower panel) where the bright spots in between the irradiated micelles can be assigned to redeposited gold. For the highest used dose of condition 1, a significant amount of gold was found not only in between irradiated micelles, but also in between irradiated lines. The HRSEM images of the upper panel (Fig 7. 4) show that for the highest dose, the polymer layer was not completely removed in the areas close to the written pattern, while the lift-off was successful for the other writing conditions. This indicates that in the strongest condition, unavoidable stray ions already modified the polymer in areas not directly exposed to the beam so that it resisted the solvent lift-off.

condition 1

10 pA, 10 µs

condition 2

1 pA, 10 µs

condition 3

10 pA, 1µs
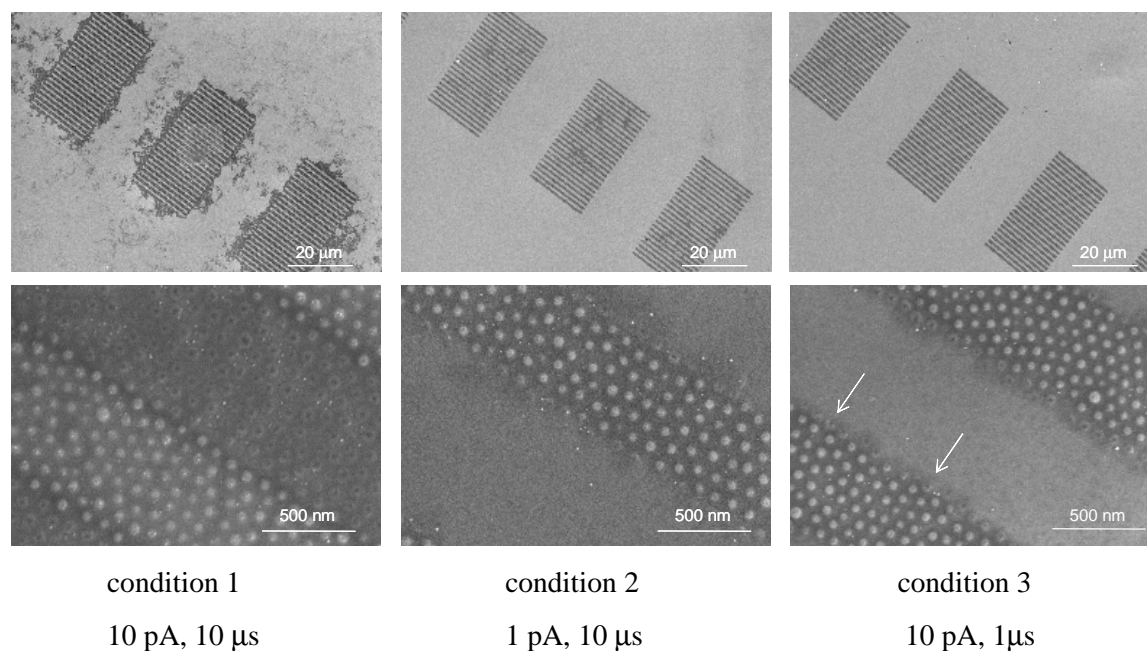
Fig 7. 4 HRSEM images of the patterns after toluene lift-off. The arrows indicate micelles that were cut through by the focused ion beam.

The arrows in Fig 7. 4 point to single micelles that are cut through by the ion beam. The sharpness of the pattern border is, therefore, given by the size of the micelles. This can be tuned by choosing the lengths of the PS and P2VP blocks.[16]

Hydrogen plasma treatment of the samples fully reduced the gold inside the micelles and combusted the remaining polymer, leaving arrays of gold nanodots on the surface (Fig 7. 5). The HRSEM images demonstrate that in the case of the high dose irradiation (condition 1) several small Au clusters were deposited per micelle at the locus of the micelle. We believe that at the highest ion dose, the gold salt was already reduced and the preformed particles could not fuse to a single particle during the plasma treatment. Formation of a single fused cluster per micelle was, however, favoured in the case of the lower irradiation dose (conditions 2 and 3) when the plasma acts on the polymer bound gold salt. The single gold particles were deposited according to the hexagonal packing of the micelles, i.e. the mesomorphic order was maintained as confirmed by the Fast Fourier Transformation of the SFM images (Fig 7. 5, lower panel).

condition 1

10pA, 10μs

condition 2

1pa, 10μs

condition 3

10pA, 1μs
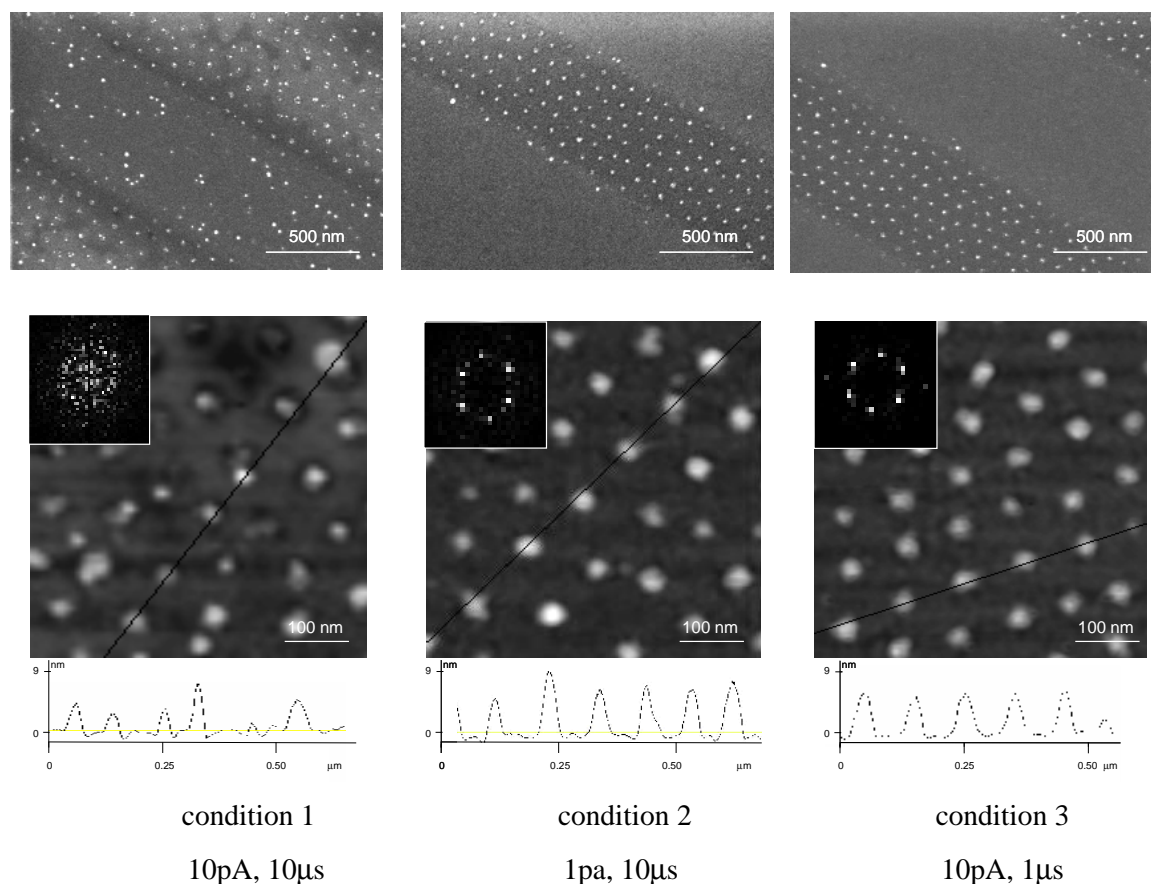
Fig 7. 5 FIB generated gold dots patterns after hydrogen plasma: HRSEM images (upper panels) and AFM images (lower panels) for different FIB settings.

The height profile analysis of the SFM images shows that the gold nanodots of the patterns irradiated with conditions 2 and 3 are uniform in height (approx. 7 nm) comparable to the height of nanodots obtained on a control substrate that was not irradiated (approx 8 nm, not shown). No significant differences were found for the arrays and individual Au particles formed under conditions 2 and 3, indicating that the formation process only depends on the total ion dose and does not show any significant dependence on the local beam current or exposure time. With respect to the results obtained by e-beam pinning,[17] we used doses up to three orders of magnitude lower. Within our first investigation, we have observed that even ion doses lower than 10^{14} ion/cm^2 can be used for the successful modification of the micellar monolayer (not shown). For conditions 2 and 3, only few ill deposited gold particles are found, mostly located near to the border between irradiated and non irradiated areas, while uncontrolled deposition of gold particles in the non irradiated areas, where the micelles were removed by the lift off process in the case of high energy irradiation (condition 1) is demonstrated by the HRSEM images.

Ion doses of 10^{15} ions/cm^2 and higher are too strong for the micellar layer and result in a disordered deposition of gold particles with broad size distribution. Furthermore, the SEM picture of the pattern obtained with the highest ion dose (Fig 7. 5, upper panel) shows an inversed contrast in the silicon background with respect to that obtained with weaker conditions. We attribute this effect to ion implantation or even substrate amorphization caused by the high doses during irradiation. Gallium ion implantation is the explanation Huey and Langford [26] proposed for the 1 nm protrusion they measured in a silicon substrate irradiated with 10^{15} ion/cm^2, while no topography changes were detected with doses of 10^{13} ion/cm^2. Ion doses in the range of 10^{15} ion/cm^2 and even lower are seldom used for FIB nanofabrication. On our substrates irradiated with a 10^{14} ion/cm^2 dose, we could measure 1 nm protrusions by SFM. Under a light microscope, the nanodot arrays obtained with such dose are extremely bright and easy to detect (Fig 7. 6) both in bright field and dark field.
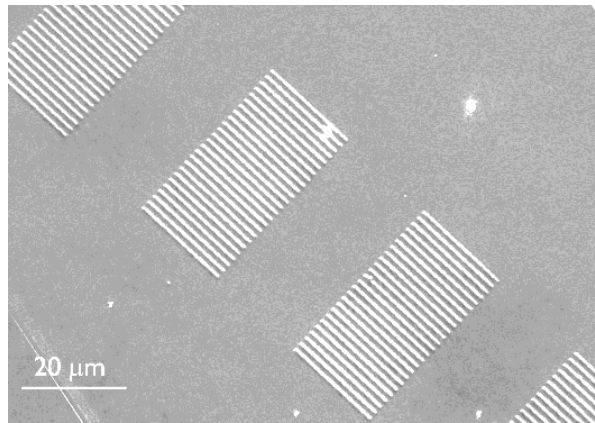
Fig 7. 6 Optical micrograph (dark field) of FIB generated patterns of gold nanodots (after hydrogen plasma). The used dose was 10^{14} ion/cm^2. The bright areas correspond to those irradiated by FIB, where the gold nanodots are located.

The optical contrast observed on the FIB written samples has to be attributed to the surface modifications induced by the ion bombardment. In fact, no optical contrast has been observed on samples only partially covered with dots of the same size and separation distance (not shown), prepared by dip-coating only half of the surface, without any Ga ion irradiation. The scattering due to the particle plasmons is not strong enough to be detected in the far field by our microscope set-up, in agreement with earlier observations that only larger particles could easily be imaged in dark field, because the scattering intensity is proportional to the volume of the nanoparticles. [7, 27]

In control experiments in which we wrote structures by FIB in plain silicon covered by a layer of native silicon oxide (about 2 nm thick), we could clearly observe optical contrast for the patterns realized with 10^{14} ion/cm^2 creating 1 nm protrusions (Fig 7. 7) both in dark field and bright field.
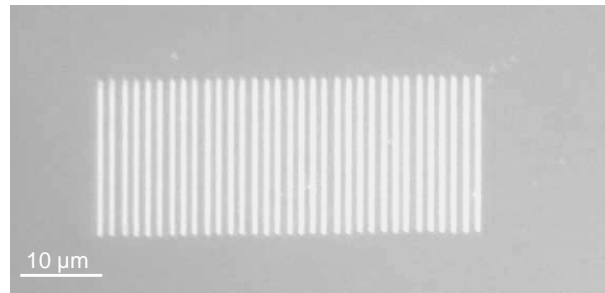
Fig 7. 7 Optical micrograph (dark field) of FIB generated patterns on plain silicon. The used dose was 10^{14} ion/cm^2.

Even patterns written with an ion dose as low as 10^{13} ion/cm^2 still showed optical contrast, although less evident (Fig 7. 8). With this dose, no changes in topography could be detected by SFM, in agreement with the study of Huey and Langford. [26]
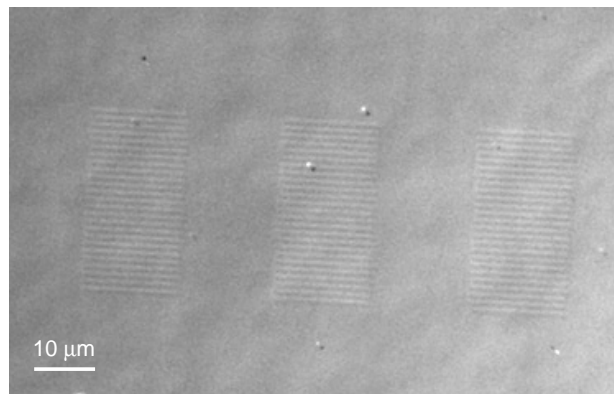

Fig 7. 8 Optical micrograph (differential interference contrast) of FIB generated patterns on plain silicon with a dose of 10^{13} ion/cm^2.

Spectral analysis by means of a confocal Raman microscope (WITec GmbH, Ulm, Germany) confirmed the silicon modification by ion bombardment showing broad bands not present in the Raman spectrum of unmodified silicon [28] and a sharp decrease (~ 60%) of the peak at 520 cm^{-1} which is the signature of crystalline silicon (Fig 7. 9). The intensity of the Raman scattering is closely related to the crystalline structure of a material and decreases with local damage of the structure. [29, 30]
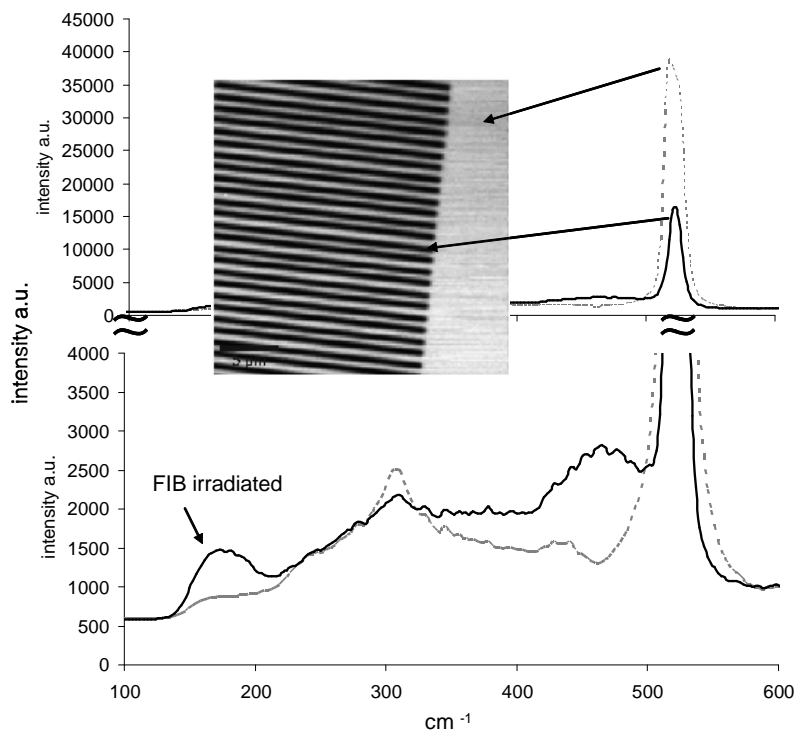
Fig 7. 9 Average Raman spectra of FIB irradiated (continuous line) and non irradiated (dotted line) silicon substrate. The inset shows the image generated by integration of the collected spectra over the spectral region from 490 to 550 cm^{-1}.

The modification is associated with altered physical and optical properties, like the refractive properties. Ion beam implantation is well known to enable controlled and, in the case of FIB, laterally resolved changes in materials by modifying their structure, introducing defects and impurity atoms. [31] Indeed, by FIB irradiation of the micellar layer, we obtained the combination of two optical elements, i.e. the plasmon active gold dots and the underlying grid consisting of a periodic modulation of the refractive index. So far with our optical set-up, we could not determine whether and to which extend there might be an interaction between the two elements, resulting in the alteration of either the optical properties of the gold dots or of those of the grating. To the best of our knowledge, the optical contrast induced by low dose FIB writing in a silicon substrate detected by light microscopy has not been reported in literature. The contrast shown in micrograph of Fig 7. 7 clearly demonstrates the potential of the FIB usage for optical data storage.

Recently, the optical modification effect induced by the Ga ion implantation in hydrogenated amorphous silicon carbide films has been proposed for possible applications in the area of high-density optical data storage [32, 33] and the controlled creation of lattice defects in crystalline SiC by Be^+ FIB has been exploited to laterally confine surface phonon polaritons without altering the chemical composition of the surface. [34] These authors showed infrared near-field images of patterns of modified crystalline SiC, demonstrating the first subwavelength scale phonon photonic structure.

7.4 Conclusions

We have shown that low dose FIB irradiation is a successful method for the formation of lateral resolved micro and nanopatterns in combination with a metal salt (here gold) loaded micellar monofilm as a direct deposition resist. Notably, it provides a new concept to obtain the combination of two different functional elements: the metal and metal oxide identities generated from the resist and the grating induced in the substrate. The beam locally crosslinks and pins the micelles onto the substrate without compromising their structural integrity, so that, after plasma treatment, hexagonally ordered gold dots result on the surface. The micellar resist is up to 3 orders of magnitude more sensitive to Ga ions than to electrons. The use of low doses opens up the possibility for efficient locally controlled patterning also on non-conductive substrates. The simultaneous creation of an optically functional grating decorated by gold nanodots gives a first obvious advantage of making the nanodot patterns easy to detect by conventional light microscopy. This can be of interest for the creation of diffraction based biosensors. [35] The optical properties of noble metal nanoparticles have been extensively studied [36, 37] and exploited for assays relying not only on (large) ensembles of particles [38, 39] but also on single nanoparticles [40] in an attempt to create a new class of chemosensors and biosensors. Raschke and coworkers showed that even the changes in the scattering spectrum of single gold nanoparticles interacting with biomolecules are large enough to be detected. [40] Furthermore, surfaces with precisely controlled peptide densities can be created by functionalizing nanodots fabricated with the micellar approach as in this study.[5]

7.5   References

[1]   V. Skumryew, S. Stoyanov, Y. Zhang, G. Hadjipanayis, D. Givord, J. Nogues, *Nature* **2003**, *423*, 850.

[2]   G. Li, V. Joshi, R. L. White, S. X. Wanga, J. T. Kemp, C. Webb, R. W. Davis, S. Sun, *J. Appl. Phys.* **2003**, *93*, 7557.

[3]   M. E. Franke, T. J. Koplin, U. Simon, *Small* **2006**, *2*, 36.

[4]   S. Chah, M. R. Hammond, R. N. Zare, *Chemistry & Biology* **2005**, *12*, 323.

[5]   M. Arnold, E. A. Cavalcanti-Adam, R. Glass, J. Blümmel, W. Eck, M. Kantlehner, H. Kessler, J.P.Spatz, *Chem. Phys. Chem* **2004**, *5*, 383.

[6]   M.-C. Daniel, D. Astruc, *Chem. Rev.* **2004**, *104*, 293.

[7]   C. Soennichsen, S. Geier, N. E. Hecker, G. von Plessen, J. Feldmann, H. Ditlbacher, B. Lamprecht, J. R. Krenn, F. R. Aussenegg, V. Z-H. Chan, J. P. Spatz, M. Moeller, *Appl. Phys. Lett.,* **2000**, *77*, 2949.

[8]   K. C. Grabar, R. G. Freeman, M. B. Hommer, M. J. Natan, *Anal. Chem.* **1995**, *67*, 735.

[9]   M. Valden, X. Lai, D. W. Goodman, *Science* **1998**, *281*, 1647.

[10]   T. Deng, Y.-H. Ha, J. Y. Cheng, C. A. Ross, E. L. Thomas, *Langmuir* **2002**, *18*, 6719.

[11]   S. A. Levi, A. Mourran, J. P. Spatz, F. C. J. M. van Veggel, D. N. Reinhoudt, M. Moeller, *Chem. Eur. J.* **2002**, *8*, 3808.

[12]   J. P. Spatz, V. Z.-H. Chan, S. Moessmer, F.-M. Kamm, A. Plettl, P. Ziemann, M. Moeller, *Adv. Mater.* **2002**, *14*, 1827.

[13]   P. M. Mendes, S. Jacke, K. Critchley, J. Plaza, Y. Chen, K. Nikitin, R. E. Palmer, J. A. Preece, S. D. Evans, D. Fitzmaurice, *Langmuir* **2004**, *3766*.

[14]   M. K. Corbierre, J. Beerens, R. B. Lennox, *Chem. Mater.* **2005**, *17*, 5774.

[15]   H. G. Craighead, L. M. Schiavone, *Appl. Phys. Lett.,* **1984**, *48*, 1748.

[16]   J.P. Spatz, S. Moessmer, C. Hartmann, M. Moeller, T. Herzog, M. Krieger, H.-G. Boyen, P. Ziemann, *Langmuir* **2000**, *16*, 407.

[17]   R. Glass, M. Arnold, J. Blümmel, A. Küller, M. Möller, J. P. Spatz, *Adv. Funct. Mater.* **2003**, *13*, 569.

[18]   S. Reyntjens, R. Puers, *J. Micromech. Microeng.* **2001**, *11*, 287.

[19]   E. T. Ada, L. Hanley, S. Etchin, J. Melngailis, W. J. Dressik, M.-S. Chen, J. M. Calvert, *J. Vac. Sci. Technol. B* **1995**, *13*, 2189.

[20]   L. Calcagno, *Nucl. Instrum. Methods B* **1995**, *105*, 63.

[21]   K. Arshak, M. Mihov, A. Arshak, D. McDonagh, D. Sutton, S. B. Newcomb, *J. Vac. Sci. Technol. B.* **2004**, *22*, 189.

[22]   A. A. Tseng, *Small* **2005**, *1*, 924.

[23]   S. Khizroev, D. Litvinov, *Nanotechnology* **2004**, *15*, R7.

[24]   J. Taniguchi, K. Koga, Y. Kogo, I. Miyamoto, *Microelectron. Eng.* **2006**, *83*, 940.

[25]   J. P. Spatz, T. Herzog, S. Moessmer, P. Ziemann, M. Moeller, *Adv. Mater.* **1999**, *11*, 151.

[26]   B. D. Huey, R. M. Langford, *Nanotechnology* **2003**, *14*, 409.

[27]   E. Dulkeith, T. Niedereichholtz, T. A. Klar, J. Feldmann, G. von Plessen, D. I. Gittins, K. S. Mayya, F. Caruso, *Phys. Rev. B* **2004**, *70*, 205424.

[28]   M. M. Khayyat, G. K. Banini, D. G Hasko, M. m. Chadhri, *Appl. Phys. Lett.,* **2003**, *36*, 1300.

[29]   S. Nakashima, M. Hangyo, *IEEE J. Quantum Electron.* **1989**, *25*, 965.

[30]   J. C. Bourgoin, I. F. Morhange, R. Besseman, *Rad. Effects* **1974**, *22*, 205.

[31]   P. D. Townsend, *Rep. Prog. Phys.* **1987**, *50*, 501.

[32]   L. Bischoff, J. Teichert, S. Kitova, T. Tsvetkova, *Vacuum* **2003**, *69*, 73.

[33]   T. Tsvetkova, O. Angelov, M. Sendova-Vassileva, D. Dimova-Malinovska, L. Bischoff, G. J. Adriaenssens, W. Grudzinski, J. Zuk, *Vacuum* **2003**, *70*, 467.

[34]   N. Ocelic, R. Hillenbrand, *Nat. Mater.* **2004**, *3*, 606.

[35]   P. M. St John, R. Davis, N. Cady, J. Czajka, C. A. Batt, H. G. Craighead, *Anal. Chem.* **1998**, *70*, 1108.

[36]   P. Mulvaney, *Langmuir* **1996**, *12*, 788.

[37]   A. N. Shipway, E. Katz, I. Willmyer, *Chem. Phys. Chem.* **2000**, *1*, 18.

[38]   P. Englebienne, *Analyst* **1998**, *123*, 1599.

[39]   P. Englebienne, A. V. Hoonaker, M. Verhas, *Analyst* **2001**, *126*, 1645.

[40]   G. Raschke, S. Kowrik, T. Franzl, C. Soennichsen, T. A. Klar, J. Feldmann, A. Nichtl, K. Kuerzinger, *Nano Lett.* **2003**, *7*, 935.

Chapter 8

Nanofibres electrospun from block copolymer micellar solutions

8.1 Introduction

One-dimensional polymer nanoarchitectures such as nanofibres have attracted considerable attention because of their unique magnetic, electronic, optical and surface properties. [1-9] Nanofibres have shown remarkable potential applications in fundamental studies as well as in nanocatalysis, nanoelectronics, tissue scaffolds production and drug delivery systems. [1, 8, 10-16]

Electrostatic spinning also known as electrospinning is a versatile process for producing fibres in the nanometer range. Differently from other methods such as drawing,[17] template synthesis,[18] "nanofibre seeding" [19] or self-assembly,[20, 21] it produces nanofibers with remarkably long lengths and uniform diameters and can be scaled-up to an industrial process.[1, 10]

Electrospinning occurs when a suspended droplet of a polymer melt or solution is charged with a high voltage. Upon a critical electric potential, the electrostatic force at the surface of the fluid overcomes the surface tension and a fine polymer jet is ejected. Due to chain entanglements of the polymer the charged jet does not break into droplets but is elongated and accelerated towards a counter electrode. As the jet travels, it dries and finally electrically charged solid nanofibres are deposited. [1, 10, 22] The morphology of the fibres depends on the polymer solution parameters (polymer molecular weight, solution concentration, used solvent) and the process parameters (strength of applied electric field, deposition distance, temperature, humidity, etc.). [2, 5, 13, 23]

Although electrospinning is an old process (the first patent on this technique was awarded in 1934)[24] only recently this method has attracted rapidly growing interest. A wide range of polymers has been successfully electrospun, including biodegradable polymers, [12, 13, 25] conducting polymers,[26] polymer blends, [6, 23] mixtures of polymers with inorganic materials [2, 3, 7, 8, 27-30] and polymers with implemented proteins.[14, 15] Fabrication of porous,[31, 32] ribbon-like [33, 34] and hollow fibres [25, 35] has been reported. In addition several methods for the collection of aligned fibres have been developed

lately.[35-39]   In literature there are only few reports on electrospinning of block copolymers. Typically block copolymers are electrospun as a solution in a good solvent [6, 12, 40] or as a melt [13]. The observed microphase separation is very weak and appears only locally.[6, 32, 40] This is due to the fact that the kinetics of the spinning process (rapid solvent evaporation) is fast in comparison to the timescale of spontaneous self-assembly and that a strong deformation during the electrospinning process occurs. Post production annealing above Tg facilitates the microphase separation, but care has to be taken to maintain the fibre integrity.[41] This problem can be overcome by the so-called coaxial spinning with an inorganic compound that forms a thermally stable core of the nanofibres and that can be safely removed in a subsequent step.[42]

To the best of our knowledge, there are no reports where amphiphilic block copolymers are spun from solution in a selective solvent. Only recently group of Long reported the spinning process of amphiphilic phospholipid wormlike micelles from nonpolar solvent. In this chapter we investigate the morphology of fibres obtained from solutions of amphiphilic block copolymers in selective solvents, where core shell nanostructures are present. We also investigate the possibility of incorporating metal nanoparticles in the fibres using the micellar nanoreactor concepts explained in previous chapters.[43]

We start by studying the self-assembly of metal salt loaded PS-*b*-P2VP block copolymers into worm-like micelles and discussing factors influencing their morphology changes from spheres to cylinders.

8.2   Experimental

Materials

Styrene (Aldrich, p.a.) and 2-Vinylpyridine (2VP) (Aldrich, p.a.) were purified by distilling under inert gas, first over potassium hydroxide, then over calcium hydride. Toluene (Merck, p.a.), mesitylene (Merck, p.a.), methanol (Merck, p.a.) and tetrahydrofuran (THF) (Merck, p.a.) were dried over $LiAlH_4$ and distilled twice under inert gas. Sec-BuLi (Aldrich, 1.3 mol/L in cyclohexane), $(Bu)_2Mg$ (Aldrich, 1.0 mol/L in heptanes), $[CH_3(CH_2)_7]_3Al$ (Aldrich, 25 wt% in hexanes), CaH_2 (Fluka, p.a.), KOH (Merck, technical grade), $LiAlH_4$ (Aldrich, pallets), LiCl (Fluka p.a.), $HAuCl_4*3H_2O$ (Fluka), hydrazine (Fluka, anhydrous 1 M solution in THF) and petrol ether (Merck,

technical grade) were used as received. PS-*b*-P2VP block copolymers were synthesized elsewhere [44, 45] or were prepared as described below by living anionic polymerization (reaction entries are specified in Table 8. 1). Table 8. 2 gives the characteristic of synthesized PS-*b*-P2VP polymers. PI-*b*-P2VP block copolymers were prepared by anionic synthesis. [46]

Table 8. 1 Reaction entries for PS-*b*-P2VP polymerizations

Sample	Polymer[a] PS$_x$-*b*-P2VP$_y$	n styrene[mmol]	n 2-vinylpyridine [mmol]	n s-BuLi [mmol]	V THF [ml]
PS$_{1100}$-*b*-P2VP$_{2650}$	530-2090	27.7	108.9	0.052	180
PS$_{1030}$-*b*-P2VP$_{3500}$	710-3200	23.08	104.1	0.0325	125

[a] DP of the block copolymer aimed at by the monomer/initiator ratio

Table 8. 2 Molecular weights and block lengths of synthesized PS-*b*-P2VP block copolymers

Sample[a]	Homopolymer		Copolymer		
	Mn[a] [g/mol]	Mw/Mn[a]	Mn[a] [g/mol]	Mw/Mn[a]	DP$_{P2VP}$/DP$_{PS}$ [b]
PS$_{1100}$-*b*-P2VP$_{2650}$	120 000	1.08	360 600	1.18	2.4
PS$_{1030}$-*b*-P2VP$_{3500}$	108 300	1.1	430 000	1.21	3.4

[a] from SEC in CHCl$_3$ relative to narrow poly(styrene) standards

[b] block copolymer ratio obtained from ^{1}H NMR in CDCl$_3$

PS-b-P2VP Synthesis

All manipulations were performed in a high vacuum line (HVL) and under inert atmosphere of nitrogen inside a Glove-Box (Unilab, Mbraun GmbH, Garching, Germany).

Prior to the polymerization experiments, prepurified styrene and 2VP were dried in a HVL stirring over CaH$_2$ and trioctylaluminum respectively and condensed to flasks equipped with stopcocks. Flasks with the monomers were transferred into the Glove-Box and stored in the fridge (-25°C). The drying procedure was similar for THF. In this case prepurified solvent was stirred in the HVL over s-BuLi with few drops of DPE,

condensed to a flask equipped with a PTFE valve and finally transferred into the Glove-Box. The polymerization was carried out at −78 °C in a flask immersed in a n-heptane cooling bath, inside the Glove-Box. To the THF filled flask LiCl (2 molar fold excess in relation to the calculated living chain ends) and styrene were introduced. After several minutes s-BuLi was added to the mixture. The development of the orange-yellow colour evidenced the formation of carbanionic living species. The mixture was allowed to stir for 2 hours and a small aliquot of the polymer solution was taken and terminated with methanol. The sample was analysed by SEC in order to determine molecular weight and molecular weight distribution of the first block. Afterwards a calculated amount of the second monomer was added dropwise to the reaction flask by means of a syringe. The colour of the mixture immediately changed from orange-yellow to red. The solution was stirred for additional 15 to 30 minutes and living anions were terminated with few drops of methanol. The polymer was precipitated in petrol ether, isolated and characterized by means of ^{1}H NMR and SEC. ^{1}H NMR (CDCl$_3$, δ in ppm): 1.38-2.40 (broad, C$\underline{H}_2$C$\underline{H}$(C$_6$H$_5$) and -C$\underline{H}_2$C$\underline{H}$(C$_5$H$_4$N)), 6.2-7.1 (broad, aromatic protons except the H atom in o-position to the N atom), 8.05-8.15 (broad, aromatic H atom in o-position to the N atom). The 2VP content in the block copolymers was calculated from integrals over the aromatic protons.

Analysis

Size Exclusion Chromatography (SEC). The molecular weight of polymers was determined in chloroform at room temperature using Waters microstyragel columns (pore size 10^5, 10^4, 10^3 Å). The detection was performed on a differential refractometer (Waters model 410) and a differential viscometer (Viscothek model H502, SEC-Win software). Elution volumes were converted to the molecular weights based on calibration with narrow polydispersity PS standard samples.

^{1}H-NMR spectra were performed in CDCl$_3$ (99,8%, Deutero GmbH) on a Bruker DRX 400 spectrometer at 400 MHz.

TEM: Bright field transmission electron microscopy images of the micellar films and electrospun fibres were recorded by a Philips EM10 or EM 400T microscope operating at 100 kV. In order to minimize the destructive influence of the e-beam on the sample,

the intensity was kept as low as possible (second condenser lens: 50 Pt, objective lens: 30).

Scanning Force Microscopy (SFM) was performed with a Nanoscope III from Digital Instruments microscope (Veeco, Santa Barbara, U.S.A.). Investigations in the tapping mode were carried out with Si-cantilevers from Nanosensors (Weltzlar, Germany) with a spring constant of approx. 50 N/m and at a tapping frequency around 350 kHz.

Methods

Solution preparation

Solutions of the block copolymers in dry toluene or/and mesitylene were prepared with concentrations in the range of 0.1-0.5 wt% and subsequently mixed with molar equivalents of $HAuCl_4*3H_2O$ per pyridine unit (range L = 0.1-0.9) in the inert atmosphere of the Glove-Box. Solutions for the electrospinning experiments were prepared with higher concentrations (typically from 2 to 12 wt%). All solutions were stirred in the dark for at least 48 h to allow complete solubilization of the chloroauric acid in the cores of the block copolymer micelles.

Gold salt reduction

The reduction of the gold salt to obtain metal nanoparticles in the electrospun fibres was performed either before or after the electospinning process. In the first case a 10 fold excess of hydrazine with respect to the chloroauric acid was added to the micellar solution. In the latter case, the electrospun fibres were exposed to hydrazine vapours for few seconds. All reduction experiments were performed inside the Glove-Box.

Electrospinning

Fibres were produced in a custom-made electrospinning box that ensured stable and safe experimental conditions. The electrospinning set-up consisted of a syringe pump equipped with a syringe containing a micellar solution, a stainless steal needle connected to the negative pole of a voltage source and a grounded SEM stub serving as collector (Fig 8. 1). The distance between the needle and the collector was varied between 5 and 35 cm. The micellar solution was pumped via a syringe pump to the

spinneret with a flow from 0.02 to 0.5 mL/h and the voltage was changed in the range 10 - 40 kV. Fibres were collected onto aluminium foil covered SEM stubs. To facilitate TEM analysis copper TEM grids were carefully fixed to the stub with a carbon tape, so that fibres could be directly collected on the grids.

Electrospinning experiments were carried under ambient temperature and humidity conditions.
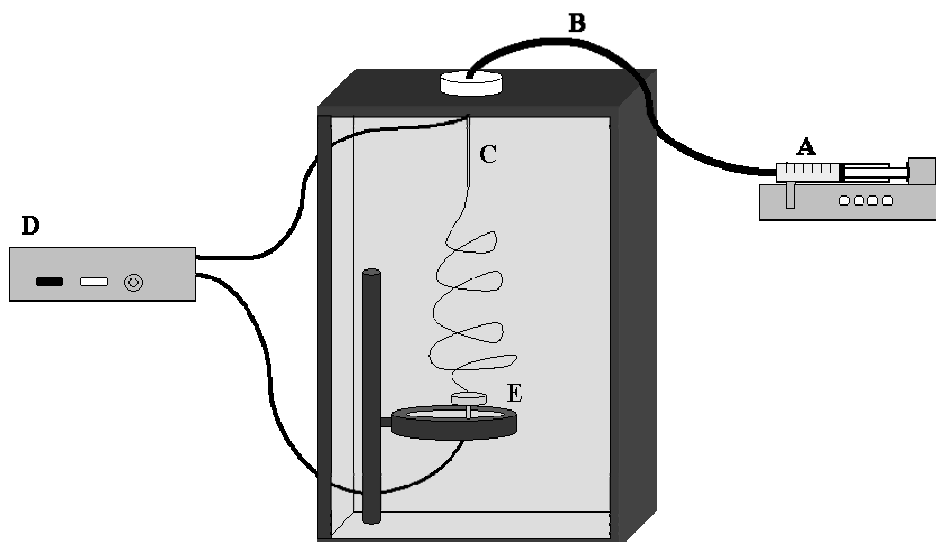

Fig 8. 1 Schematic drawing of the experimental set-up used in the electrospinning experiments. A micellar solution from a syringe (A) is pumped through a Teflon tube (B) to a needle (C) connected to a high voltage supply (D). The produced fibres are collected on a target consisting of a SEM stub (E).

8.3   Results and discussion

8.3.1   Micellar morphologies

Amphiphilic block copolymers dissolved in a selective solvent tend to self-organize into micellar aggregates.[47] On the basis of the volume fraction of the constituent components, the number of segments in the copolymer and the Flory-Huggins interaction parameter, the existence of different morphologies like spherical, cylindrical, gyroid and lamellar, can be predicted.[48]

In previous chapters we restricted ourselves to the use of copolymers where the corona-forming block was significantly longer than the core-forming one, resulting in spherical

micelles. Here we show that other morphologies such as cylindrical or worm-like micelles, bicontinuous rods and vesicles, are also attainable (see Fig 8. 2 from A to D respectively) when the insoluble P2VP core block is significantly longer than the outer soluble PS or PI block and the so-called crew-cut micelles are formed.

Various morphologies were reported by the group of Eisenberg[49-51] for poly(styrene)-*block*-poly(ethylene oxide) (PS-*b*-PEO) and poly(styrene)-*block*-poly(acrylic acid) (PS-*b*-PAA) copolymers in aqueous solutions. It was shown that both morphology and kinetic stability of crew-cut copolymer micelles depend strongly on the preparation technique, polymer-related properties (such as total molecular weight of polymer, ratio between constituent blocks) and on solution conditions (pH, ionic strength, solvent polarity). In reports from our group, it has been shown that crew-cut PS-*b*-P2VP and PS-*b*-PEO block copolymers dissolved in selective solvent for PS and loaded with an appropriate inorganic salt, form elongated structures or vesicles, and that the cylindrical micellar morphology offers an interesting way to fabricate metal nanowires.[52]
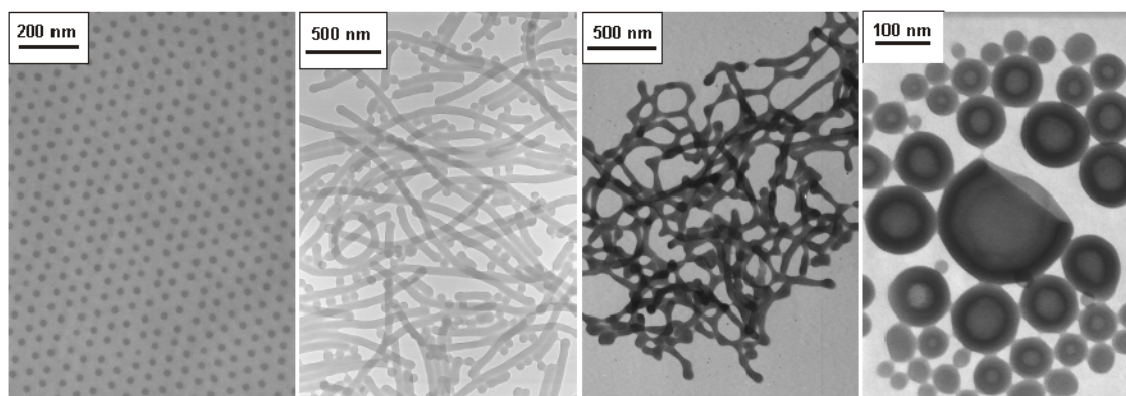
A: PI(775)-b-P2VP(565)   B: PS(1030)-b-P2VP(3500) C: PS(500)-b-P2VP(1400)   D: PI(65)-b-P2VP(845)

Fig 8. 2 Transmission electron micrographs of different micellar morphologies obtained from poly(styrene)- and poly(isoprene)-block-poly(2vinylpyridine) copolymer solutions. A: 0.5 wt% in toluene, $HAuCl_4*3H_2O$ loading (L) = 0.3; B: 0.5 wt% in toluene/mesitylene (60:40, vol/vol), L = 0.3; C: 0.25 wt% in mesitylene, L = 0.3; D: 0.5 wt% in toluene, L = 0.3.

In the following subsections we report on the crew-cut copolymers and their ability to form worm-like architectures. We focused on the influence of the polymer composition

and the choice of the selective solvent on the formation of cylindrical structures. A discussion on the effect of the polymer concentration on the transformation of crew-cut micelles from spheres to cylinders can be found in chapter 8 of ref [44].

Effect of the composition of the polymer (P2VP/PS ratio, Mw) on the block copolymer morphology

Several crew-cut PS-*b*-P2VP block copolymers with different ratio between the degrees of polymerization of the two constituent blocks (DP_{P2VP}/DP_{PS}) were dissolved in toluene with the concentration of 0.5 wt% and treated with the 0.3 equivalent of chloroauric acid per pyridine unit (Table 8. 3). The solutions were dropped onto TEM grids and investigated by TEM.

Table 8. 3 Degree of polymerization and block ratio for investigated crew-cut PS-*b*-P2VP block copolymers

Block copolymer	DP_{PS}[a]	DP_{P2VP}[b]	DP_{P2VP}/DP_{PS}[b]
PS$_{35}$-*b*-P2VP$_{200}$	35	200	5.7
PS$_{80}$-*b*-P2VP$_{320}$	80	320	4.0
PS$_{180}$-*b*-P2VP$_{700}$	180	700	3.9
PS$_{110}$-*b*-P2VP$_{280}$	110	280	2.5
PS$_{550}$-*b*-P2VP$_{1400}$	550	1400	2.5
PS$_{360}$-*b*-P2VP$_{560}$	360	560	1.6
PS$_{560}$-*b*-P2VP$_{660}$	560	660	1.2

[a] from SEC relative to narrow poly(styrene) standards

[b] from SEC of the first block and ^{1}H NMR of block copolymer

Fig 8. 3 presents the transmission electron micrographs of thin films of PS-*b*-P2VP block copolymers, ordered with decreasing DP_{P2VP}/DP_{PS} ratio for block copolymers. The cores of the micelles appear as dark areas in the TEM images because of the reduction upon electron beam irradiation of the gold salt sequestered in their cores. For the first three block copolymers (Fig 8. 3a-c) with relatively long P2VP block in

comparison to PS block ($DP_{P2VP}/DP_{PS} \geq 3.9$) both worm-like and spherical micelles are present. If the ratio $DP_{P2VP}/DP_{PS} \leq 2.5$ (Fig 8. 3d-h) only spherical micelles can be observed.

In Fig 8. 3a, b and c one can observe merging spherical micelles to more favourable in this case worm-like structures. The observation of these phenomena is possible due to the fast evaporation of the solvent, which freezes the non-equilibrium system in a solution. Although the cylindrical micelles are thermodynamically more favourable the kinetics of sphere-to-cylinder transition is slow as compared to the rapid solvent evaporation during the deposition process.

Fig 8. 3 d and e show two parts of the same sample (PS(110)-*b*-P2VP(280)) with necklace and honeycomb structures. These micelles possess short PS block and that's why steric hindrance between micelles is reduced. In consequence they tend to aggregate forming common coronas and leading to necklace structures (Fig 8. 3d) or honey comb structures (Fig 8. 3e). It indicates that this is the length of the corona-forming block that drives the merging of the micelles. Direct comparison between two crew-cut polymers PS(110)-*b*-P2VP(280) and PS(500)-*b*-P2VP(1400) (Fig 8. 3d and f respectively) with the same block ratio 2.5 seems to confirm this assumption. Micelles of the former block copolymer follow agglomeration, while of the later one self-organize into hexagonal structure.

The data shown so far demonstrate that the sphere-to-cylinder transition take place only for crew-cut micelles build from copolymers with DP_{P2VP}/DP_{PS} block ratio grater then 3.9. There are three components of the free energy that may contribute to the micellar transition: the interfacial area between PS and P2VP block, core-chain stretching and corona-chain repulsion. Ott in his PhD thesis,[53] compared intrinsic micellar parameters (such as number of aggregation, degree of core block stretching, average surface area per copolymer chain at the core/corona interface and the coronal chain density on the interface surface) for different spherical and cylindrical micelles. He found out, that only density (the number of terminal grafted corona chains per unit area) significantly varies between spheres and cylinders, while other parameters remain constant. This indicates that micellar morphology is predominantly driven by the interphacial energy component, while the stretching and repulsion contributions are of minor importance in this case.
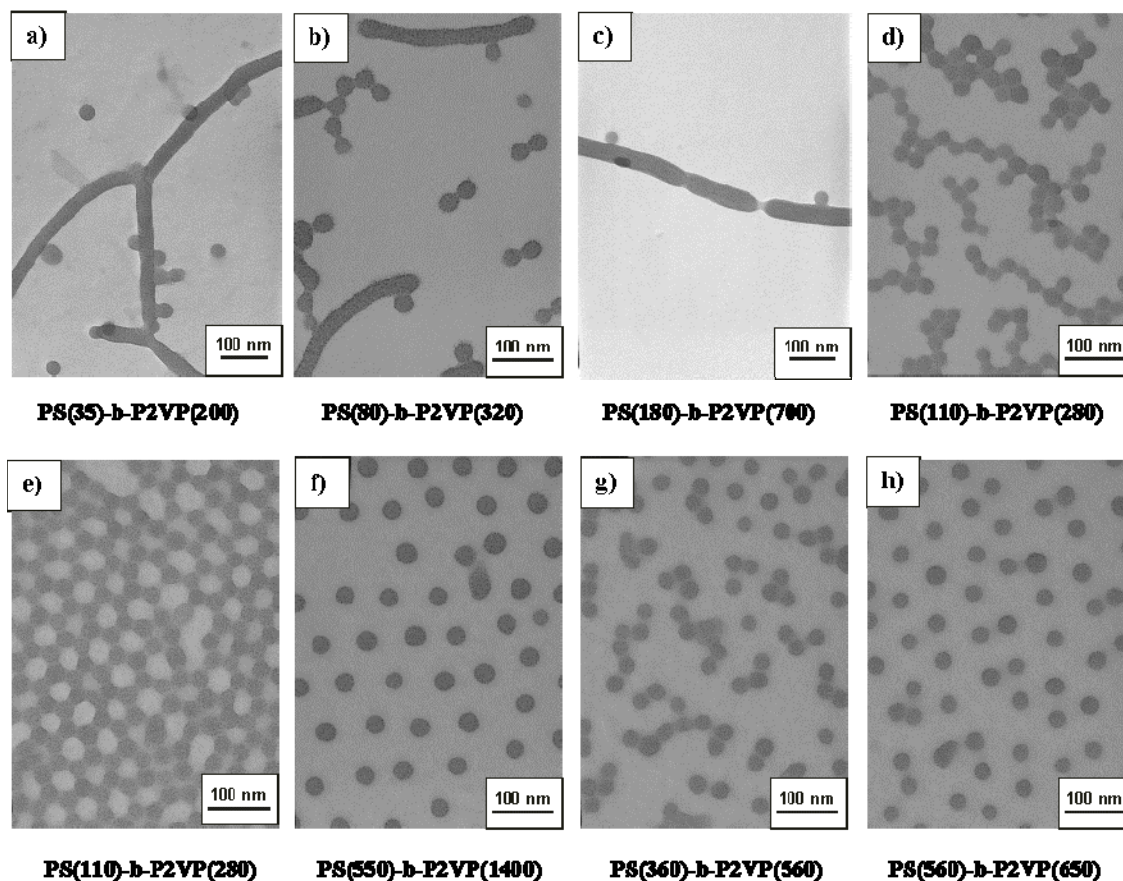
Fig 8. 3 TEM micrographs of crew-cut micelles of PS-b-P2VP block copolymers showing the influence of the block ratio and total molecular weight on the micellar morphology.

Effect of the solvent on the block copolymer morphology

PS-*b*-P2VP block copolymer with various compositions were dissolved in toluene or in mesitylene with the concentration of 0.5 wt% and loaded with the equivalent of 0.5 $HAuCl_4$ per pyridine unit. Fig 8. 4 shows TEM micrographs of PS-*b*-P2VP block copolymer micelles deposited onto TEM grids from solutions in both solvents. If the medium is toluene (Fig 8. 4 upper panel) majority of block copolymers self-assembly into spherical micelles, except for the crew-cut PS(80)-*b*-P2VP(320) ((DP_{P2VP}/DP_{PS}) = 4.0) forming cylindrical structures. When the block copolymers are dissolved in mesitylene (Fig 8. 4 lower panel) the first block copolymer (PS(1350)-*b*-P2VP(400)) with the long corona-forming block and the short core-forming one, still self-organizes exclusively into spherical micelles but for the symmetric PS(800)-*b*-P2VP(860) both spherical and elongated structures coexist. The two crew-cut polymers self-organize

into bicontinuous structures, where cylinders are no more separate, but they form interconnected architectures. It is also worth mentioning that in each case, the sizes of the micellar cores are bigger in mesitylene then in toluene, for the same block copolymer.

The observed transition sphere-to-cylinder for block copolymers with ratio DP_{P2VP}/DP_{PS} ≥ 3.9 in toluene is shifted to symmetric copolymers, when mesitylene is the selective solvent. It indicates that the nature of the solvent has significant effect on the morphology changes of block copolymer micelles. For the polymers forming in toluene crew-cut micelles (PS(500)-*b*-P2VP(1400) and PS(80)-*b*-P2VP(320)) there is an additional transition to bicontinuous rodlike aggregates. This transition is independent of the fact whether crew-cut polymer has formed spherical or elongated micelles in toluene.

PS(1350)-*b*-P2VP(400)   PS(800)-*b*-P2VP(860)   PS(500)-*b*-P2VP(1400)   PS(80)-*b*-P2VP(320)
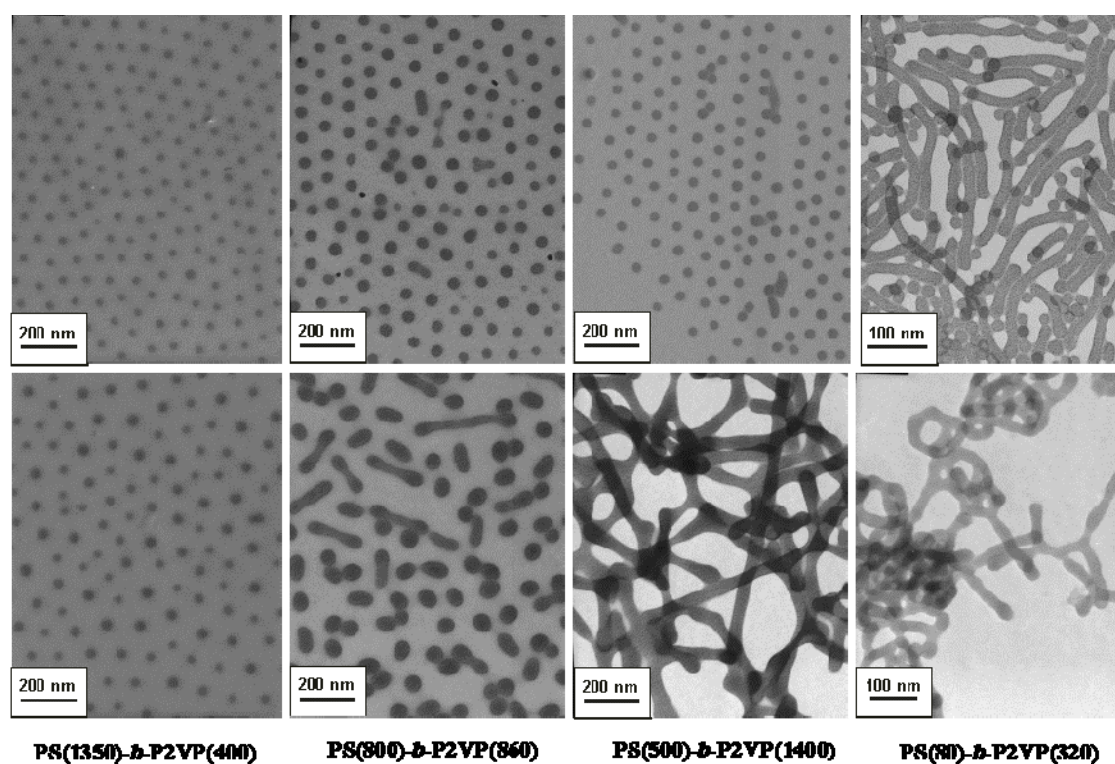
Fig 8. 4 Influence of the solvent on the formation of cylindrical micelles. TEM micrographs of PS-b-P2VP block copolymer micelles prepared in toluene (above) and in mesitylene (below). The copolymers are ordered with the increasing ratio (N_{P2VP}/N_{PS}) from left to right.

Morphology changes are driven by the solvent-corona and solvent-core interactions. While the first one is responsible for the repulsion of the corona chains, the second is related to the degree of stretching inside the micellar core. The strength of the polymer-solvent interaction is given by the Flory-Huggins parameter that is related to the solubility parameter δ and the dielectric constant ε.[54] Table 8. 4 shows characteristic values of these parameters for polystyrene homopolymer and both solvents. Polystyrene is a non-polar polymer and its miscibility with a solvent can be estimated from comparison between solubility parameters of PS and the solvent. In general substances that have closer values mix better. Based on the comparison between the solubility parameters of PS and both solvents we may conclude, that toluene is a slightly better medium for the polystyrene and provides slightly stronger PS-solvent interaction. In this case spherical micelles are preferentially formed. On the other hand, protonated with chloroauric acid P2VP chains are quite polar and the polymer-solvent interaction should be rather estimated from the polarity of the solvent. Higher ε for mesitylene indicates stronger interaction of core forming chains and the solvent. In consequence more solvent is present in the core of the micelles and P2VP chains are more stretched as observed by bigger sizes of micellar cores. These two factors induce morphology changes from spheres to cylinders.

Table 8. 4 Some physical parameters of polymers and solvents

Component	Solubility parameter δ[55]$[MPa^{1/2}]$	Dielectric constant ε[56]
polystyrene	16.6 - 20.2	2.4 - 2.6
poly(2VP/AuCl$_4$)	-	-
toluene	8.9	2.4
mesitylene	8.8	3.4

Here we have shown that by simple changing the nature of the solvent we can tune the morphology of the micellar aggregates and as exemplified, promote formation of the worm-like architectures even in the case of symmetric block copolymers, which

self-organize exclusively to spherical micelles when dissolved in toluene. Furthermore, upon changing the solvent, cylinders were transformed into bicontinuous structure with is the intermediate morphology between cylinders and vesicles.

8.3.2   Nanofibres obtained by electrospinning of micellar solutions

In order to obtain stable jet and consequently form uniform fibres, various process conditions (flow rate, spinneret-collector distance and applied voltage) were adjusted for each polymer solution.

Nanofibres from spherical micelles

We started our electrospinning studies with the relatively high molecular weigh polystyrene-*block*-poly(2vinylpyridine) (PS(3300)-*b*-P2VP(270)) in toluene. Micellar solutions with concentrations ranging from 2 to 12 wt% with and without incorporation of a gold salt were electrospun. The results for the two systems were similar: concentrations lower than 3 wt% yielded only the formation of polymer particles and no fibres were obtained, concentration higher than 6 wt% were two viscous to be successfully electrospun, concentrations in the range 3 – 6 wt% were successfully used for the formation of uniform and beaded fibres. Typically fibres with average diameter ranging from 80 to 400 nm were obtained. Frequently two populations of fibres could be seen: a main population with diameters of several hundreds of nanometers and a second population with diameters below 100 nm. These two populations resulted from the two (or more) jets arising from spinneret at the same time. Upon optimisation of the spinning conditions relatively homogeneous nanofibres could be obtained. Representative transmission electron micrographs of nanofibres spun from loaded and non-loaded block copolymer solutions are presented in the top and bottom part of Fig 8. 5 respectively.
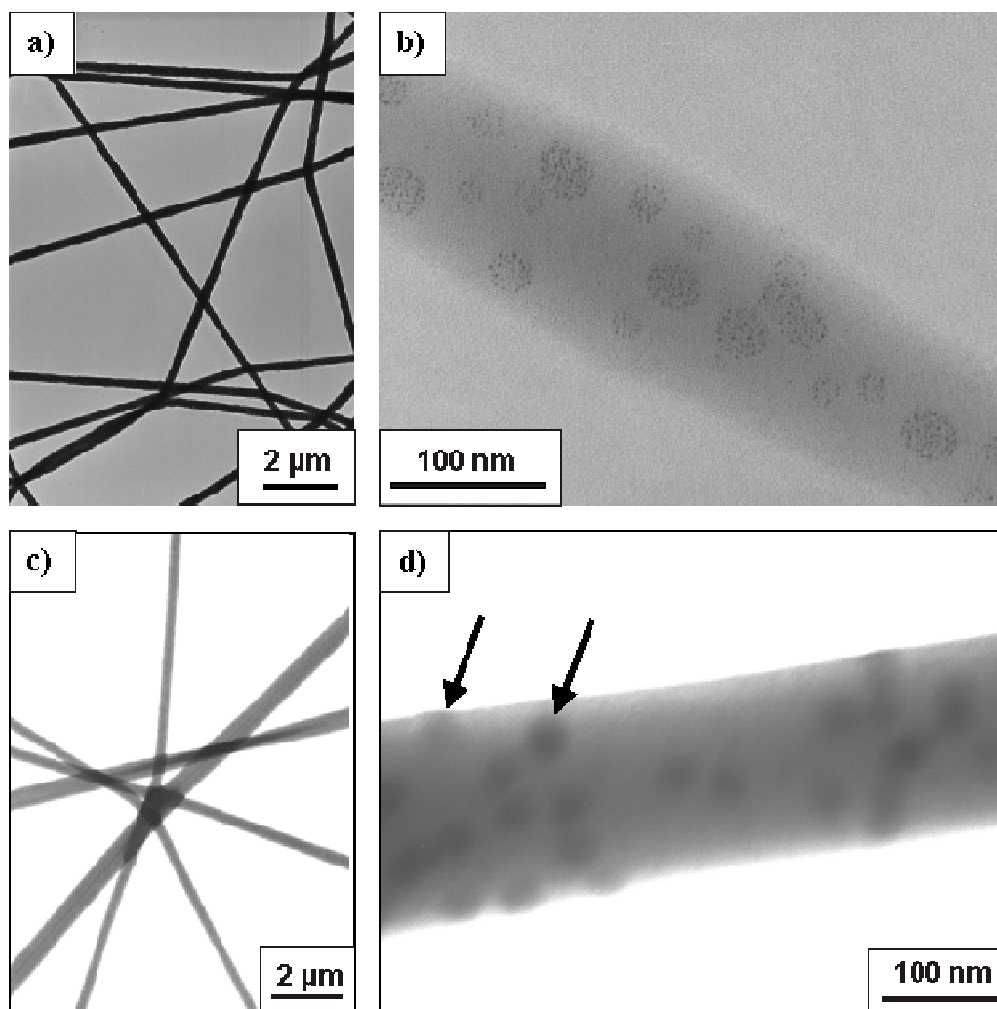
Fig 8. 5 TEM images of electrospun fibres made from the HAuCl₄ loaded (above) and non-loaded (below) PS(3300)-b-P2VP(270) micellar solution. Conditions used: concentration 3.5 wt%; loading 0.3 L; voltage 20.0 kV flow rate 0.3 mL/h; distance 25 cm. Before imaging the non-loaded fibres were stained by the exposure to I₂ vapours. Arrows indicate cores of the micelles.

The internal structure of the fibres spun from a HAuCl₄-loaded solution is depicted in the TEM image in Fig 8. 5b. Dark regions in the image are associated with the cores of the micelles were the ultra small Au particles are located. The micellar structures are homogeneously distributed along the fibre and present a variation in the micellar cores' size. Possible explanations for the origin of this size variation could be the partial disintegration of the micellar structures due to the loss of some of the polymer chains (these chains could be involved in the formation of the fibre giving rise to

entanglements) and the strong elongating deformation appearing during the electrospinning process. It is also possible that the micellar solution had not yet reached full equilibrium when it was used for electrospinning.

Fig 8. 5d shows TEM photography of single nanofibre fabricated from 3.5 wt% PS(3300)-*b*-P2VP(270) block copolymer micellar solution without loading. The nanofibres were exposed to I_2 vapours that selectively reacted with nitrogen functionality increasing the contrast in bright field electron microscopy imaging so that the dark regions on TEM images were identified as P2VP domains. As can be observed the integrity of core-shell structures is preserved and regularly dispersed micelles similar to those loaded with inorganic are visible. This brings us to the conclusion that the presence of the gold salt does not have a critical influence on the morphology of the fibres and that the micellar structures are kinetically stable enough to be spun without additional inorganic stabilization.

Furthermore, by the comparison between loaded and not loaded solutions we can conclude that the absence of inorganic salt (that should decrease conductivity and in consequence the spinability) has a minor influence on the electrospinning process and produced fibres from spherical micelles.

Nanofibres with gold particles

Fig 8. 6 demonstrates two alternative approaches for the formation of fibres with embedded nano-sized gold particles. In the first route, the fibres are electrospun from solution of $HAuCl_4$ loaded micelles and subsequently exposed to hydrazine vapours. The second strategy is based on the reduction of the inorganic salt in solution and the subsequent electrospinning of the solution containing already gold particles stabilized by micelles.
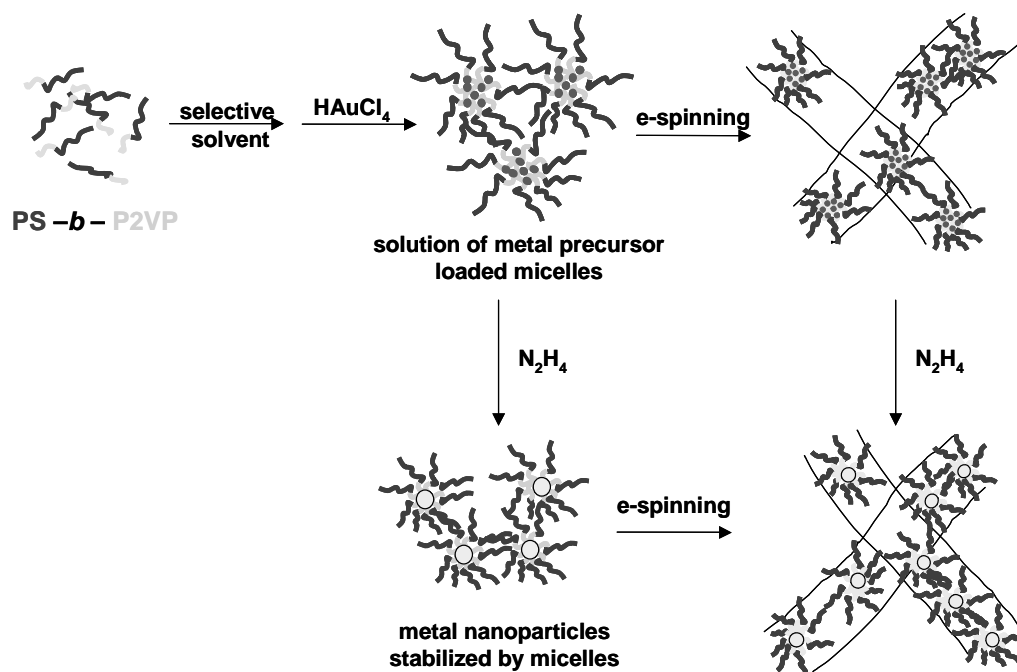
Fig 8. 6 Illustration of two alternative approaches towards nanofibres with gold nanoparticles: reduction of the gold before or after the spinning process.

Fig 8. 7 shows Transmission Electron Micrographs of nanofibres with gold particles produced following the first strategy. Rather polydispersed particles were formed (Fig 8. 7b and c). This can be explained by the fact that the reducing agent needs to diffuse through the block copolymer (while penetrating the fibre interior) and is not able to simultaneously initiate reduction of gold salt. Furthermore, it is worth noting that upon exposure to hydrazine holes on the surface of the fibres appear, indicating the aggressive influence of hydrazine on P2VP blocks. Thus, diverse local concentration of the reducing agent and swelling of the pyridine core (introducing the mobility of small gold particles) by hydrazine results in high polydispersity of particles. Although, the hydrazine reduction method on as-spun fibres, produced rather unsatisfactory results, it has to be stated that this process was not optimised and the goal may be achieved by other, more homogeneous reduction techniques such as heat treatment or UV exposure.
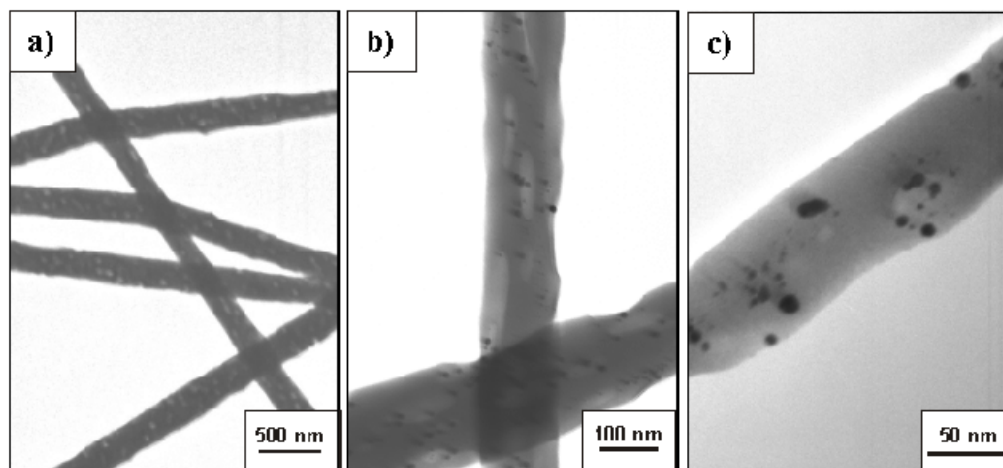
Fig 8. 7 Representative TEM images of electospun PS-b-P2VP fibres containing Au nanoparticles by the reduction on as-spun fibres method a), b) and c).

In the second "reduction first" approach, a 3.5 wt% toluene solution of the chloroauric salt loaded micelles was rapidly mixed with a 10 fold excess of anhydrous hydrazine. Upon mixing an instantaneous colour change from yellow to red occurred. This change corresponds to the formation of single gold particles in the cores of the micelles as reported by Spatz. Interestingly, contrary to what described in [57], it was not necessary to neutralize the excess of hydrazine with acid in order to prevent the nanoparticles coagulation: even after several hours no coupling between the micellar-stabilized particles was detected, most likely because of the very high viscosity of the micellar solution that prevents agglomeration of the gold particles.

Fig 8. 8 shows TEM pictures of fibres spun from the solution: 12 nm gold nanoparticles are visible within the polymer fibres. Fig 8. 8d shows the histogram of particle size distribution.
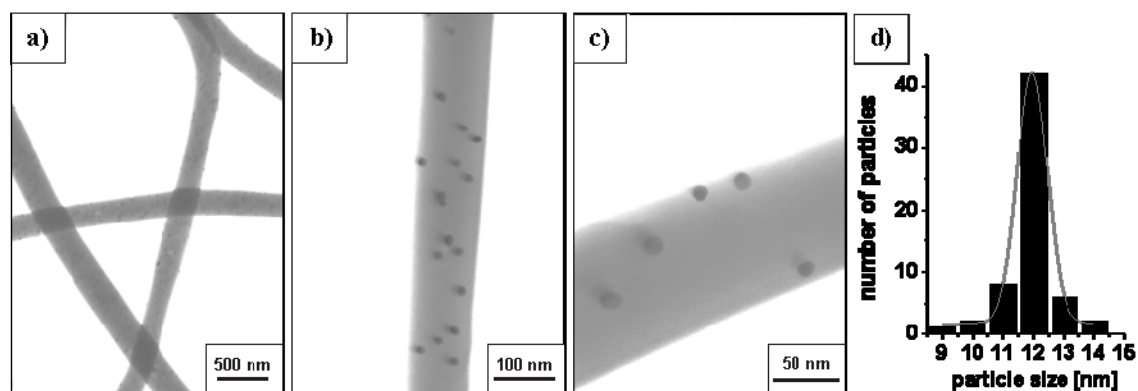
Fig 8. 8 TEM micrographs of nanofibres prepared by "reduction first" approach (a-c) and corresponding size profile of gold particle (d) (n=60, σ=0.81). The loss in picture sharpness visible on the high magnification images (b and c) is a consequence of vibrations of the analysed fibre upon electron beam exposure during TEM imaging.

Nanofibres from crew-cut micelles

Two sets of crew-cut PS-*b*-P2VP block copolymers were subjected for the electrospinning experiments:

1) block copolymers with low molecular weight and $DP_{P2VP}/DP_{PS} \geq 3.9$ that formed cylindrical micelles in toluene (PS(70)-*b*-P2VP(380), PS(80)-*b*-P2VP(320) and PS(180)-*b*-P2VP(700)),

2) block copolymers with relatively high molecular weight and $DP_{P2VP}/DP_{PS} = 2.4$ and 3.4 that had to be dissolved in a mixture of toluene and mesitylene to form cylindrical micelles (PS(1100)-*b*-P2VP(2650) and PS(1050)-*b*-P2VP(3500) respectively).

In the case of the short block copolymers regardless of the experimental conditions employed, it was not possible to successfully spin these solutions. Due to low molecular weight (possibly not satisfactory to built entanglement couplings), spinning resulted only in particles for both non-loaded and loaded solutions.

The first investigated high molecular weight block copolymer (PS(1100)-*b*-P2VP(2650)) with the ratio DP_{P2VP}/DP_{PS} equal to 2.4 forms exclusively spherical micelles when dissolved in toluene. In order to shift the equilibrium towards cylindrical

structures we applied different toluene/mesitylene mixtures as the selective solvent. However, increasing amount of mesitylene in the mixture, at the same time enhances difficulties with polymer solubility if the concentration of copolymer was kept at high levels necessary for spinning experiments. Furthermore, mesitylene as higher boiling solvent longer evaporates during e-spinning process that may have negative effect on spinability. The optimal 50/50 (vol/vol) composition of solvents gave combination of cylinders and spheres for this block copolymer.

Fig 8. 9 shows particles and nanofibres formed upon spinning with various conditions of loaded and non-loaded PS(1100)-*b*-P2VP(2650) micellar solutions. Fig 8. 9a indicates that only particles arrived from electrospinning process even at the concentration of 6 wt%. The particles have very characteristic "half-sphere" shape with several concaves on the surface. The interesting particle's shape could be explained by the sample post treatment before SEM analysis. The SEM is performed under high vacuum and particles may collapse upon reaching analytical conditions. However, the fact that some small particles are inside the bigger ones, allows supposing that the half-sphere shape is rather created already during journey of polymer material against counter electrode, before the particles reach the collector. The characteristic shape of the particles may be related to phase separation phenomena and the difference in evaporation speed between both solvents. Upon significant increase of micellar concentration to 10 wt%, particles connected via fibre (as shown on Fig 8. 9b and c) could be produced. Further optimisation of spinning conditions (increasing of voltage to 35 kV) resulted in beaded fibres with concaves. However, achievement of regular and smooth nanofibres was not possible in our experimental conditions.

Typically addition of ions improves the conductivity that helps fibres to be formed.[1] In our case, when the PS(1100)-*b*-P2VP(2650) solution was loaded with chloroauric acid surprisingly no fibres could be produced even at the concentration of 10 wt%. We attributed this to different state of the block copolymer molecules self-organizing into micelles. There is a dynamic equilibrium between free molecules and chains associated into micellar structures. While in the case of the non-loaded solution, micelles are relatively easy exchanging polymer molecules between each other and some of the free single chains could still contribute to the formation of fibres, addition of inorganic salt shifts the equilibrium towards micelles and also significantly increases the stability of

the micelles. This effect is negligible for spherical micelles, but much more pronounced for the crew-cut micelles, where the PS soluble block is short in the comparison to the not soluble P2VP - forming rigid core of the micelle.
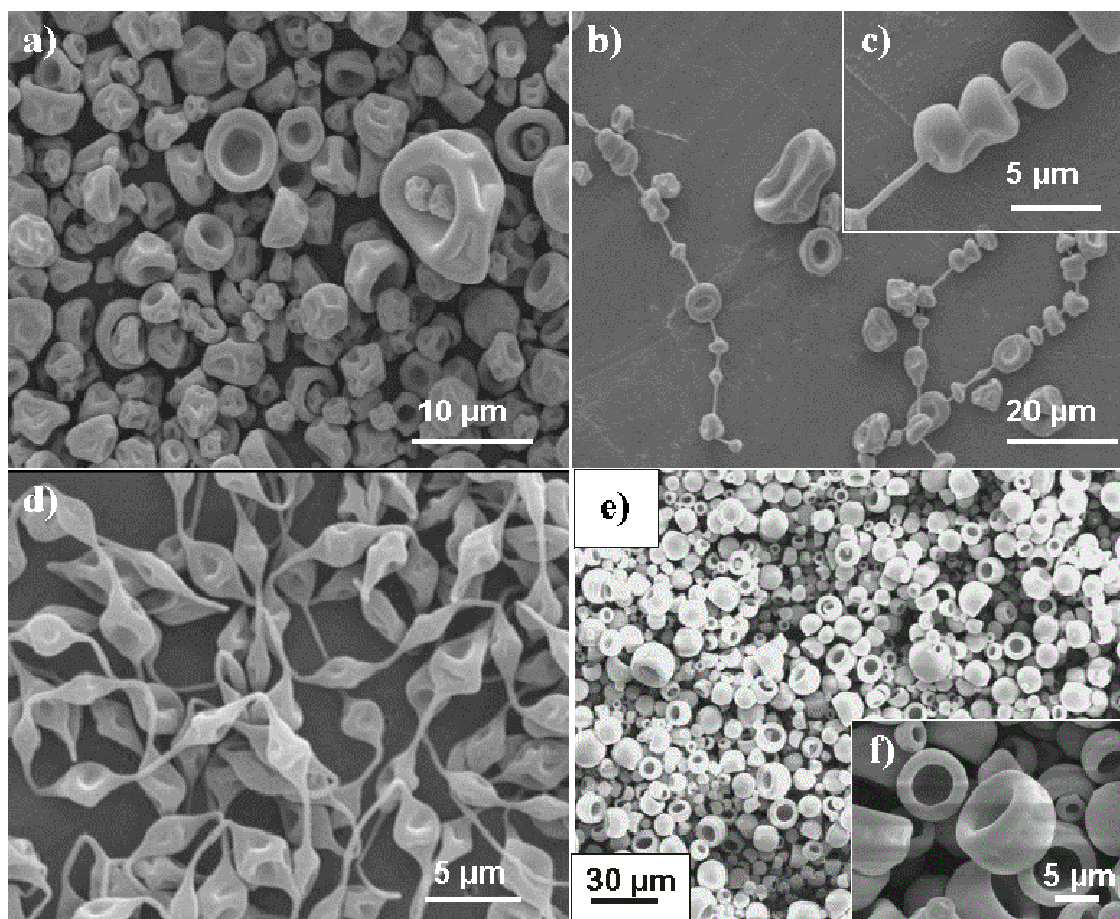

Fig 8. 9 SEM pictures showing particles and nanofibres obtained from electrospinning of non-loaded (a-d) and loaded (e and f) PS(1100)-b-P2VP(2650) micellar solution in the mixture toluene/mesitylene (50/50 vol/vol); conditions: (a) 6 wt%, 0.05 mL/h, 20 kV; (b) and (c) 10 wt% ; (d) 35kV, (e) and (f) 10 wt%, 0.3 L, 0.05mL/h, 20kV.

Similarly to PS(1100)-*b*-P2VP(2650), exclusively particles were formed when the solutions of the PS(1050)-*b*-P2VP(3500) block copolymer was loaded and submitted to electrospinning (Fig 8. 10a). Due to relatively high molecular mass of block copolymer consequently micelles with big dimensions could be easy observed under SEM even under low magnifications. Fig 8. 10b indicates that polymer particles consisted of cylindrical micelles. Also very long cylindrical micelles are visible in a droplet of

micellar solution Fig 8. 10c. Upon increasing concentration to 10wt% only some particles connected with fibres were fabricated Fig 8. 10.

As we already discussed, crew-cut micelles with the relatively short PS blocks are hardly contributing to the entanglements of single chains and the high viscosity is rather attributed to overlapping cylinders. At this point we may also drive very important conclusion that the PS-*b*-P2VP cylinders are not providing itself strong enough entanglements to build fibres.
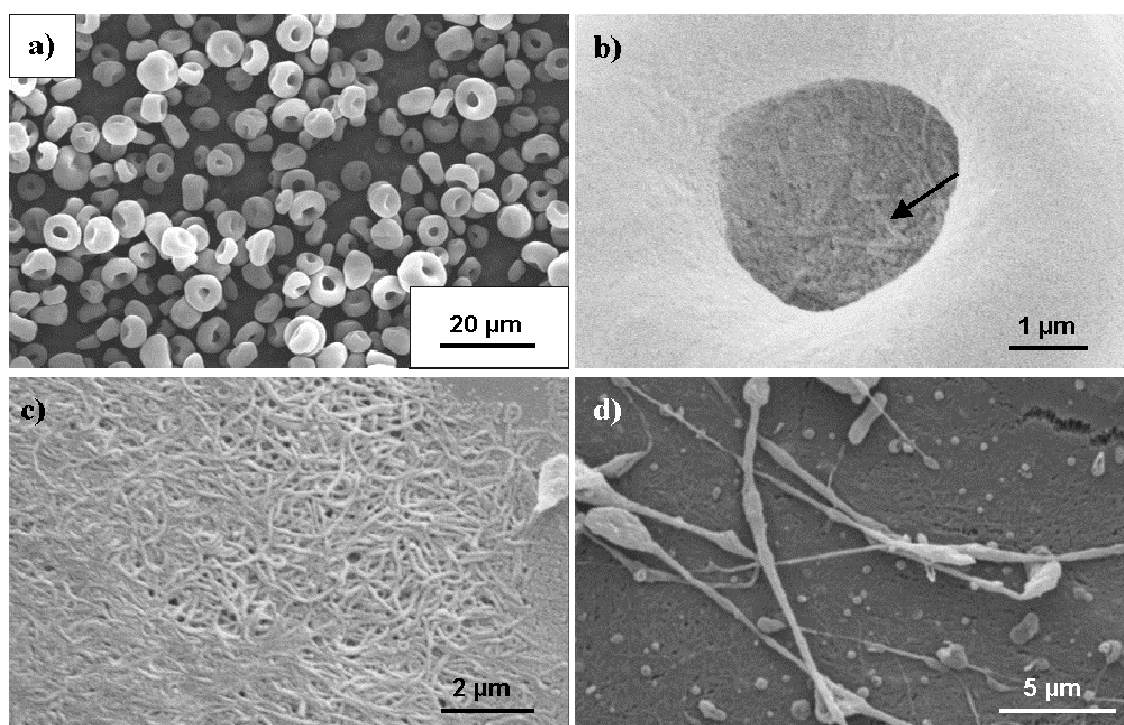

Fig 8. 10 Scanning electron micrographs of crew-cut PS(1050)-b-P[2VP(HAuCl₄)₀.₃](3500) micelles in toluene after electrospinning. a) particles obtained from spinning with conditions: 6 wt%; 0.3 L; 20.0 kV; 0.05 mL/h; 20 cm, b) a single particle with cylindrical micelles, c) a droplet of micellar solution showing jumble of cylindrical micelles, d) few fibres obtained upon increasing the concentration to 10 wt% (0.3L, 30 kV, 0.02 mL/h and 20 cm).

In order to overcome the problem of spinability, the block copolymers forming crew-cut micelles were electrospun together with the high molecular weight PS homopolymer that provided the necessary number of entanglements.

In the case of the low molecular weight crew-cut copolymers, 5 wt% PS(70)-*b*-P2VP(380) micellar solution was mixed with different amounts of PS(37500) homopolymer. In order to increase viscosity and form fibres, it was necessary to add at least 20 wt% of polystyrene (in respect to the block copolymer). Fig 8. 11 shows the micrographs with the as spun fibres. Fibres with average diameter ranging from 80 to 350nm were produced (Fig 8. 11a). Fig 8. 11b and c demonstrate the higher magnification images taken from different parts of the same stub. While on the first inset (Fig 8. 11b) a population of rather smooth and uniform thin fibres is revealed, the second one (Fig 8. 11c) demonstrates characteristic holes on the surface of the thicker fibre, appearing due to phase separation of the high molecular weight polystyrene and the block copolymer. Fig 8. 11d shows the image of a small-diameter fibre with embedded micellar structures. The micellar deformation along fibre axis may be attributed to an elongation either during spinning process or upon electron irradiation while the imagining.
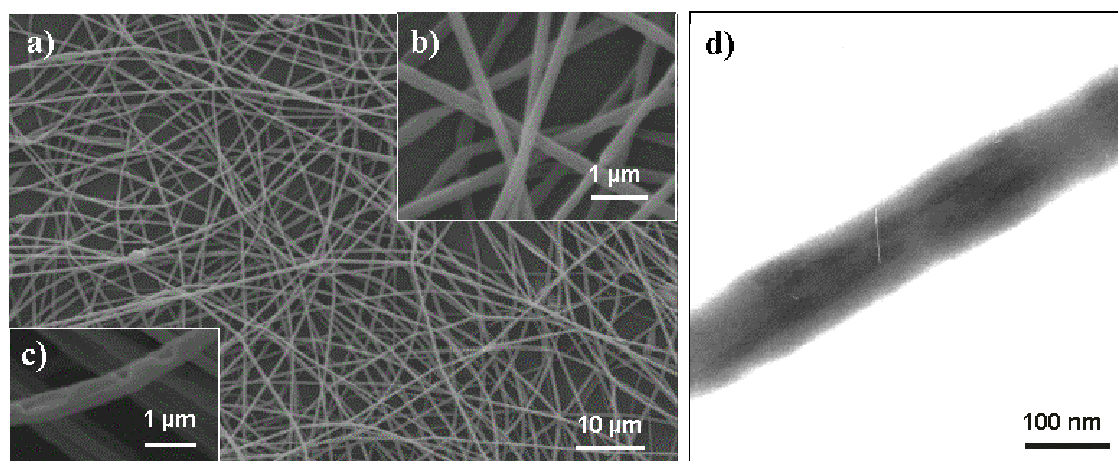
Fig 8. 11 SEM (a- c) and TEM (d) images of as-spun fibres obtained from the mixture of PS(70)-b-P2VP(380) block copolymer micellar solution loaded with chloroauric acid and the high molecular polystyrene. Conditions: 0.3 L; 30.0 kV; 0.2 mL/h; 20 cm.

Fig 8. 12 shows the influence of PS homopolymer quantity in the PS(1050)-*b*-P[2VP(HAuCl$_4$)$_{0.3}$](3500) micellar solution on fabricated nanofibres. Addition of 0.25 wt% PS to 10 wt% solution of block copolymer resulted in connected particles and beaded fibres (Fig 8. 12a and b), whereas 0.5 wt% of homopolymer gave rather smooth fibres (Fig 8. 12c, d and e).
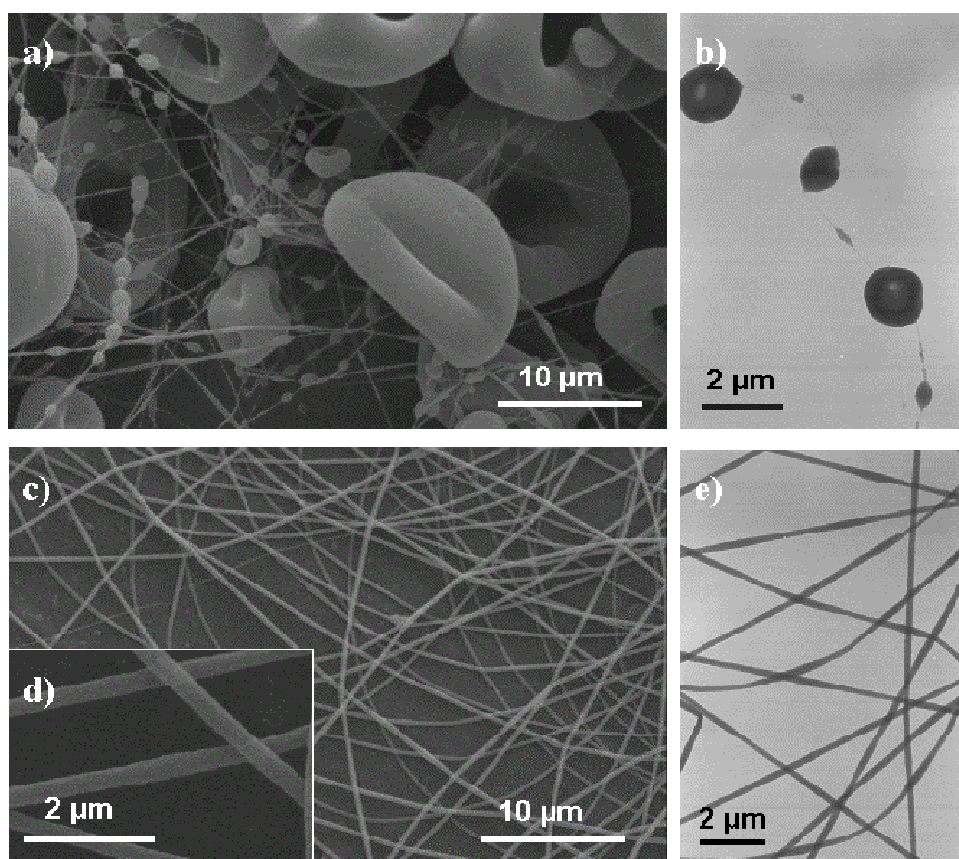

Fig 8. 12 Images of nanofibres prepared by electrospinning from micellar solutions of PS(1050)-b-P[2VP(HAuCl$_4$)$_{0.3}$](3500) block copolymer with addition of 0.25 wt% (upper panels) and 0.5 wt% (lower panels) of PS(37500) in toluene/mesitylene (50/50 vol/vol) mixture. a), c) and d) SEM images; b) and e) TEM pictures.

By simple variation of solvent composition different micellar morphologies could be obtained and incorporated into the internal structure of electrospun fibres. Fig 8. 13 shows TEM micrographs of nanofibres spun from 10 wt% micellar solution of PS(1050)-*b*-P2VP(3500) copolymer blended with the 0.5 wt% of PS(37500) in the two different toluene/mesitylene mixtures (50/10 and 50/50 by volume).

If the selective solvent consisted from the toluene/mesitylene mixture with the volume ratio 50/10, fibres with spherical micelles connected with each other and aligned along the fibre were obtained. Fig 8. 13a demonstrates TEM image, where the alignment of the spherical micelles in a fibre may be clearly seen. Fig 8. 13b and c show a fibre build from a row of micelles. Due to large dimensions of the polymer spheres the resultant fibre displays kind of "corn morphology". Fig 8. 13d shows the solution used for spinning, when diluted and casted on the TEM grid. As expected micelles arrange into necklace structures forming common coronas but keeping the cores still well separated.

When the mesitylene content was increased to 50/50 by volume, mainly cylindrical micelles were formed and incorporated into internal structure of the fibres when subjected to electrospinning. Fig 8. 13e shows the SEM image with fibre morphology demonstrating homogeneously distribution and excellent alignment of the cylinders along the nanofibre. In addition to fibres with diameters of hundreds of nanometers, thin nanofibres were sometimes found. Fig 8. 13f and g show a fibre with exactly one cylindrical micelle incorporated into a fibre. Fig 8. 13h show TEM image of the diluted solution casted on the TEM grid. Mainly cylindrical micelles could be found.
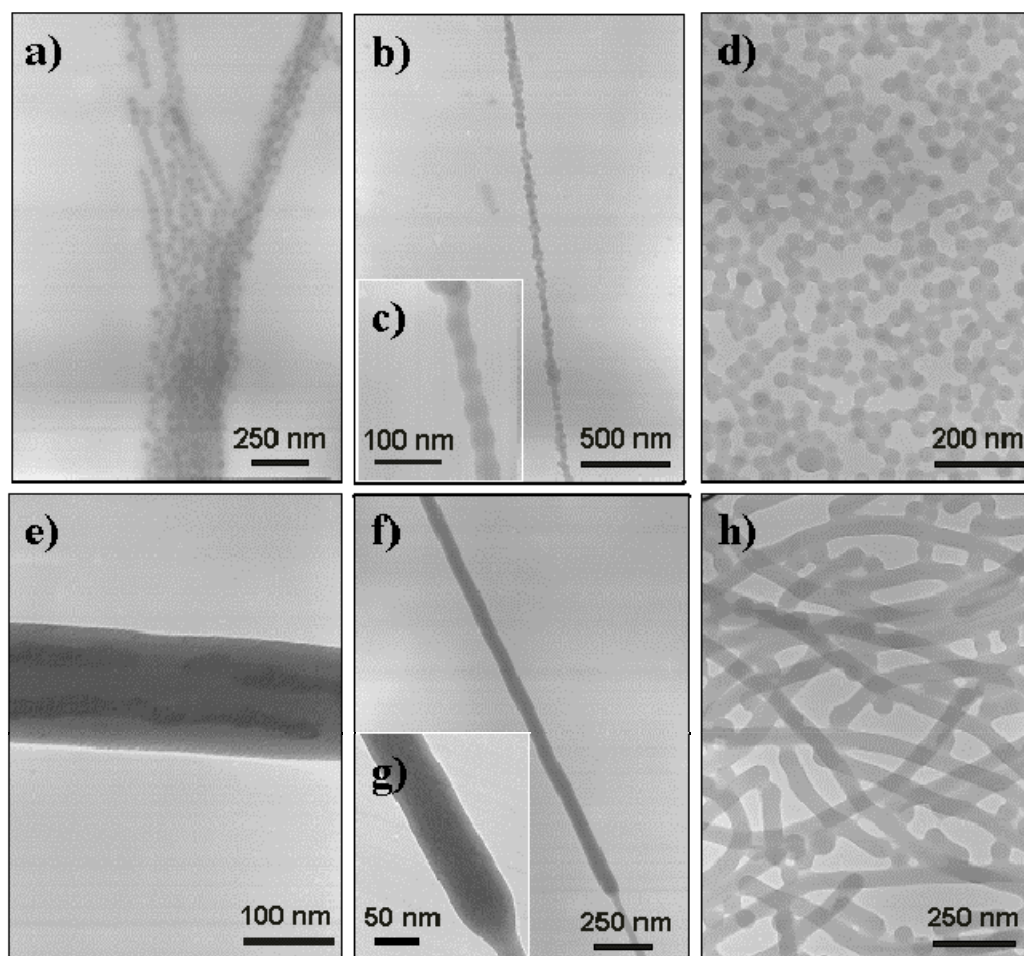
Fig 8. 13 TEM micrographs of nanofibres spun from micellar solution of PS(1050)-b-P[2VP(HAuCl₄)₀.₃](3500) crew-cut copolymer blended with a high molecular mass polystyrene in toluene/mesitylene mixtures: (50/10 vol/vol) (above) and (50/50 vol/vol) (below), as well as corresponding micellar films formed on a substrate, casted from these solutions (d and h respectively). a) TEM image showing alignment of the spherical micelles in a fibre, b) and c) pictures showing fibre with a "corn morphology" build from a row of micelles, d) monolayer of spherical crew-cut micelles after casting from a diluted micellar solution on the carbon coated TEM grid, e) image showing the homogeneously distribution and excellent alignment of the cylinders along the nanofibre f) a fibre with exactly one cylindrical micelle incorporated into structure g) higher magnification picture showing one of the ends of the worm-like micelle, h) corresponding TEM image of the diluted solution casted on the TEM grid showing a population of mainly cylindrical micelles.

8.4   Conclusions

Different structures can be obtained from amphiphilic block copolymers such as poly(styrene)-*block*-poly(2vinylpyridine) or poly(isoprene)-*block*-poly(2vinylpyridine) simply by varying the block ratio or selective solvent. For the PS-*b*-P2VP block copolymers dissolved in toluene we found the experimental value of the ratio between blocks ($DP_{P2VP}/DP_{PS} \geq 3.9$), which favours transition from spheres to cylindrical micelles. We demonstrated, that the conversion to cylindrical structures can be also enhanced by the alteration of the selective solvent. Upon changing medium from toluene to mesitylene even symmetric block copolymers form worm-like micelles.

We have shown for the first time that electrospinning of the PS-*b*-P2VP block copolymer micellar solutions leads to polymer fibres. Starting from micellar solutions, nanosized fibres (50 - 300 nm) with uniformly distributed spherical and cylindrical PS-*b*-P2VP structures could be produced. However, while in the first case, polymer self-assembled into spherical micelles provided enough numbers of entanglements to form fibres, in the second one when dealing with cylindrical structures, our attempts were not successful regardless of the applied block copolymer and experimental conditions. Thus, addition of high molecular PS homopolymer was necessary to obtain appropriate number of entanglements and form smooth and uniform nanofibres. The surface and the morphology of the produced fibres were characterized by different microscopy techniques (SEM, SFM and TEM). Furthermore, taking advantage of micellar nanoreactors we have produced PS-*b*-P2VP fibres with homogeneously distributed 12 nm gold nanodots, demonstrating the capability for incorporating monodisperse metal or metal oxide nanoparticles into internal structure of block copolymer fibres.

8.5   References

[1]   S. Ramakrishna, K. Fujihara, W. E. Teo, T. C. Lim, Z. Ma, *An Introduction to Electrospinning and Nanofibers*, World Scientific, Singapore, **2005**.

[2]   M. Wang, H. Singh, T.A. Hatton, G. C. Rutledge, *Polymer* **2004**, *45*, 5505.

[3]   Y. Hong, D. Li, J. Zheng, G. Zou, *Langmuir* **2006**, *22*, 7331.

[4]   A. Babel, D. Li, Y. Xia, S. A. Jenekhe, *Macromolecules* **2005**, *38*, 4705.

[5]   S. Madhugiri, A. Dalton, J. Gutierrez, J. P. Ferraris, K. J. B. Jr., *J. Am. Chem. Soc.* **2003**, *125*, 14531.

[6]   M. Ma, R. M. Hill, J. L. Lowery, S. V. Fridrikh, G. C. Rutledge, *Langmuir* **2005**, *21*, 5549.

[7]   G.-M. Kim, A. Wutzler, H.-J. Radusch, G. H. Michler, P. Simon, R. A. Sperling, W. J. Parak, *Chem. Mater.* **2005**, *17*, 4949.

[8]   P. Viswanathamurthi, N. Bhattarai, H. Y. Kim, D. R. Lee, *Nanotechnology* **2004**, *15*, 320.

[9]   S. T. Tan, J. H. Wendorff, C. Pietzonka, Z. H. Jia, G. Q. Wang, *Chem. Phys. Chem.* **2005**, *6*, 1461.

[10]   D. Li, Y. Xia, *Adv. Mater.* **2004**, *16*, 1151.

[11]   Y. Dzenis, *Science* **2004**, *304*, 1917.

[12]   H. Jiang, D. Fang, B. S. Hsiao, B. Chu, W. Chen, *Biomacromolecules* **2004**, *5*, 326.

[13]   P. D. Dalton, K. Klinkhammer, J. Salber, D. Klee, M. Moeller, *Biomacromolecules* **2006**, *7*, 686.

[14]   S. Y. Chew, J. Wen, E. K. F. Yim, K. W. Leong, *Biomacromolecules* **2005**, *6*, 2017.

[15]   P. Ye, Z.-K. Xu, J. Wu, C. Innocent, P. Seta, *Macromolecules* **2006**, *39*, 1041.

[16]   S. R. Bhattarai, N. Bhattarai, H. K. Yi, P. H. Hwang, D. I. Cha, H. Y. Kim, *Biomaterials* **2004**, *25*, 2595.

[17]   T. Ondarcuhu, C. Joachim, *Europhys. Lett.* **1998**, *42*, 215.

[18]   H. Li, Y. Ke, Y. Hu, *J. Appl. Polym. Sci.* **2005**, *99*, 1018.

[19]   X. Zhang, W. J. Goux, S. K. Manohar, *J. Am. Chem. Soc.* **2004**, *126*, 4502.

[20]   G. Liu, L. Qiao, A. Guo, *Macromolecules* **1996**, *29*, 5508.

[21]   C. Wu, M. Li, S. C. M. Kwan, G. J. Liu, *Macromolecules* **1998**, *31*, 7553.

[22]   M. M. Hohman, M. Shin, G. Rutledge, M. P. Brenner, *Phys. Fluids* **2001**, *13*, 2201.

[23]   P. Wutticharoenmongkol, P. Supaphol, T. Srikhirin, T. Kerdcharoen, T. Osotchan, *J. Polym. Sci., Part B: Polym. Phys.* **2005**, *43*, 1881.

[24]   A. Formhals, US Patent, 1,975,504, **1934**.

[25] Y. Z. Zhang, J. Venugopal, Z.-M. Huang, C. T. Lim, S. Ramakrishna, *Biomacromolecules* **2005**, *6*, 2583.

[26] Y. Zhou, M. Freitag, J. Hone, C. Staii, J. A. T. Johnson, Nicholas J. Pinto, A. G. MacDiarmid, *Appl. Phys. Lett.,* **2003**, *83*, 3800.

[27] H. Dai, J. Gong, H. Kim, D. Lee, *Nanotechnology* **2002**, *13*, 674.

[28] J.-M. Lim, J. H. Moon, G.-R. Yi, C.-J. Heo, S.-M. Yang, *Langmuir* **2006**, *22*, 3445.

[29] H. Liu, J. B. Edel, L. M. Bellan, H. G. Craighead, *Small* **2006**, *2*, 495.

[30] T. Shang, F. Yang, W. Zheng, C. Wang, *Small* **2006**, *2*, 1007.

[31] J. T. McCann, M. Marquez, Y. Xia, *J. Am. Chem. Soc.* **2006**, *128*, 1436.

[32] T. Ruotsalainen, J. Turku, P. Heikkila, J. Ruokolainen, A. Nykanen, T. Laitinen, M. Torkkeli, R. Serimaa, G. ten Brinke, A. Harlin, O. Ikkala, *Adv. Mater.* **2005**, *17*, 1048.

[33] L. Huang, R. A. McMillan, R. P. Apkarian, B. Pourdeyhimi, V. P. Conticello, E. L. Chaikof, *Macromolecules* **2000**, *33*, 2989.

[34] A. Koski, K. Yim, S. Shivkumar, *Materials Letters* **2004**, *58*, 493.

[35] W. E. Teo, S. Ramakrishna, *Nanotechnology* **2006**, *17*, R89.

[36] A. Theron, E. Zussman, A. L. Yarin, *Nanotechnology* **2001**, *12*, 384.

[37] W. E. Teo, M. Kotaki, X. M. Mo, S. Ramakrishna, *Nanotechnology* **2005**, *16*, 918.

[38] W. E. Teo, S. Ramakrishna, *Nanotechnology* **2005**, *16*, 1878.

[39] P. D. Dalton, D. Klee, M. Moeller, *Polymer* **2005**, *46*, 611.

[40] H. Fong, D. H. Reneker, *J. Polym. Sci., Part B: Polym. Phys.* **1999**, *37*, 3488.

[41] V. Kalra, P. A. Kakad, S. Mendez, T. Ivannikov, M. Kamperman, Y. L. Joo, *Macromolecules* **2006**, *39*, 5453.

[42] V. Kalra, S. Mendez, J. H. Lee, H. Nguyen, M. Marquez, Y. L. Joo, *Adv. Mater.* **2006**, *18*, 3299.

[43] M. G. McKee, J. M. Layman, M. P. Cashion, T. E. Long, *Science* **2006**, *311*, 353.

[44] S. Moessmer, PhD thesis, University of Ulm (Ulm), **1999**.

[45] J. P. Spatz, S. Moessmer, M. Moeller, *Angew. Chem. Int. Ed.* **1996**, *35*, 1510.

[46] see Chapter 6 of this thesis.

[47]   S. Moessmer, J. P. Spatz, M. Moeller, T. Aberle, J. Schmidt, W. Burchard, *Macromolecules* **2000**, *33*, 4791.

[48]   M. Lazzari, G. Liu, S. Lecommandoux, *Block Copolymers in Nanoscience*, Wiley-VCH Verlag GmbH & Co, KGaA, Weinheim, **2006**.

[49]   L. Desbaumes, A. Eisenberg, *Langmuir* **1999**, *15*, 36.

[50]   L. Zhang, A. Eisenberg, *Macromolecules* **1999**, *32*, 2239.

[51]   K. Yu, A. Eisenberg, *Macromolecules* **1998**, *31*, 3509.

[52]   M. Ott, **2005**.

[53]   M. Ott, PhD thesis, RWTH Aachen (Aachen), **2006**.

[54]   C. M. Hansen, *Hansen Solubility Parameters: a User's Handbook*, CRC Press, Boca Raton, **2000**.

[55]   J. Brandrup, E. H. Immergut, *Polymer Handbook*, 3rd ed. ed., Wiley, New York, **1989**.

[56]   D. R. Lide, *Handbook of Chemistry and Physics*, 75th ed., CRC Press, **1994**.

[57]   J.P. Spatz, S. Moessmer, C. Hartmann, M. Moeller, T. Herzog, M. Krieger, H.-G. Boyen, P. Ziemann, *Langmuir* **2000**, *16*, 407.

Summary

In this thesis amphiphilic block copolymers were successfully applied as templates for the controlled formation and defined positioning of metal/metal oxide nanoparticles in periodic and artificial patterns on flat surfaces as well as in polymer nanofibre structures.

After a brief introduction to the formation of inorganic cluster nanoarrays by micellar templating and to the synthesis of block copolymers by anionic polymerisation in **Chapter 2**, **Chapter 3** describes the controlled deposition of block copolymer micelles on flat surfaces. Amphiphilic polystyrene-*b*-poly(2-vinylpyridine) copolymers dissolved in various organic solvents were loaded with chloroauric acid and deposited by dip-coating technique onto SiO_2 substrates. Under the right dipping conditions, the micelles form spontaneously a closed monofilm with hexagonal order. Emphasis was placed on the influence of the selective solvent and the dipping angle on the long-range order of the micelles. Block copolymer monolayers were carefully characterised by scanning force microscopy (SFM) and the regularity of the hexagonal lattice was quantified as the number of dislocations present for a given number of micelles. The dislocations were identified by transforming the collected SFM images into Voronoi diagrams. The study shows that micelles self-organize in a lattice with fewer defects when a higher boiling solvent is used as selective solvent, provided that the solvent is still a good medium for the corona-forming block of the copolymer. By selecting the appropriate solvent, the number of dislocations present in the hexagonal lattice of the micellar layer was decreased up to 40 %. The angle between the substrates and the solution surface during the dip-coating process had no considerable effect on the long-range order, however it proved to be of crucial importance for the tuning of the micellar separation distance. The interdistance of long-corona micelles were varied from 95 to 160 nm and the interdistance of short corona micelles from 40 to 60 nm.

Chapter 4 deals with the synthesis of branched block copolymers. Two strategies were developed in order to obtain Y shape copolymers containing one poly(isoprene) block and two poly(ethylene oxide) blocks covalently linked. The first route was based on the combination of anionic polymerization with protection chemistry. The second approach,

consisted of a sequential two-step anionic synthesis. Our attempts to obtain AB_2-type block copolymers were not successful regardless of the applied pathway, even though intermediate products such as end functional poly(isoprene) (first route) and two PEO chains with double bond functionality (second route) were straightforwardly obtained. Additionally, we report on the successful preparation of poly(ethylene oxide) four arm star polymers.

The formation of poly(butadiene)-*b*-poly(ethylene oxide) block copolymer micelles in solution and their ability to act as nanoreactors for the controlled generation of TiO_2 nanoparticles is demonstrated in **Chapter 5**. First, a series of well-defined PB-*b*-PEO block copolymers have been synthesized by living anionic polymerization. Block copolymers with the expected stereochemistry and narrow molecular mass distributions were prepared using s-BuLi together with a strong phosphazene base (t-Bu-P_4) as an initiating system. The PB-*b*-PEO polymers formed micelles in toluene with a core consisting of PEO blocks and a corona from PB chains. These micelles were successfully utilized for the preparation of hexagonal ordered, mono-dispersed, pure titanium dioxide particles.

Chapter 6 and **Chapter 7** are directed to the controlled arrangements of micelles and subsequently nanoparticles in artificial patterns on flat substrates. This is achieved by the combinations of "top-down" and "bottom-up" approaches: a self-assembled monolayer of hexagonally ordered block copolymer micelles loaded with a metal precursor salt is used as a resist for lithography. Solvent development of the monolayer after selective exposure results in the removal of the unmodified polymer only. In this way, desired patterns of micelles are left on the surface. Subsequent plasma treatment reduces the metal salt and removes the organic polymer completely, yielding a single metal nanoparticles per micelle at the place of the micelles's core, i.e., in the same pattern of the micelles. Two different energy sources were used to selective modify and pin the micelles to the substrate: UV light (photo-pinning method described in Chapter 6) and a Focused Ion Beam (FIB direct writing described in Chapter 7).

The photo-pinning method works optimally with block copolymers, such as poly(isoprene)-*b*-poly(2vinylpyridine) (PI-*b*-P2VP), that are able to crosslink under the exposure to UV light. Hence, a series of photocrosslinkable PI-*b*-P2VP amphiphilic

block copolymer were synthesized by living anionic polymerization. However, it was shown that the photo-pinning method can be extended also to saturated polymers *e.g.* polystyrene-*b*-poly(2vinylpyridine), if a photoinitiator is added and surface attachment is facilitated by a silane monolayer.

The photo-pinning approach offers all the advantages of photolithography: it is a simple and parallel process, which allows patterning of large areas on conductive and non-conductive substrates.

Chapter 7 shows that patterns of nanometer dimensions can be obtained by low-dose FIB structuring of block copolymer micellar monolayers. FIB writing is an interesting and in some cases superior alternative to e-beam writing for very precise micro-nano device prototyping. As the micellar resist is up to 3 orders of magnitude more sensitive to Ga ions than to electrons, low ion dose FIB pinning opens the possibility of patterning of non-conductive substrates. Noteworthy, even at rather low ion doses the silicon surface was modified so that the irradiated and thus the gold decorated areas became visible by conventional light microscopy.

The two developed methods are compatible with the common MEMS techniques and suitable for wide range of applications especially in the fabrication of biosensors, electronic and optical devices.

Chapter 8 presents the formation of nanofibers by electrospinning of block copolymer solutions. Besides the spherical micelles described in previous chapters, crew-cut micelles were used. Their self-assembly in solution into cylindrical structures was investigated and the relation between system parameters (ratio between constituent blocks, molecular weight of block copolymers, used selective solvent) and the resulting micellar morphologies discussed.

Nanofibers were successfully electrospun from toluene solutions of spherical micelles of PS-*b*-P2VP loaded with a gold precursor salt. In the case the salt was reduced to metallic gold by exposing the fibers to hydrazine vapours, embedded polydispersed Au particles were formed, whereas reduction of the salt by addition of anhydrous hydrazine in the micellar solution prior to the spinning process, resulted in homogeneously distributed, monodispersed gold nanoparticles in the electrospun nanofibers. Electospinning of the cylindrical micellar solutions led to the formation of nanofibers only

upon addition of PS homopolymer to the solution. Potentially, nanofibres with incorporated cylindrical micelles loaded with gold can serve for the fabrication of metal nanowires, which are attractive, easy-to-handle building blocks for optical and electronic devices.

Acknowledgement

I would like to sincerely thank Dr. Kim-Ho Phan, Dirk Grafahrend and Stefan Rütten for carrying out the SEM measurements.

I am grateful to all my laboratory and office colleagues for their open and enthusiastic working atmosphere. Many thanks go in particular to: Sylwia, Krystyna, Priya, Carla, Elvira, Ana, Julia, Nicole, Heidrun, Melanie, Kristina, Yayun, Marian, Sascha, Jürgen and Peter.

All co-workers at the OC III department as well as at DWI and ITMC, for the inspiring collaboration and the non-scientific activities we did together, have my appreciation.

I would like to cordially thank my parents and my brother for their interest in my work and encouragement.

Finally, I own my loving thanks to my wife Agata, for her love and patience during the entire Ph.D. period. Without her unconditional support and understanding, I would not be where I am today. I also thank my six-month old son Artur for giving me the most wonderful moments of my life.

Curriculum Vitae

Name: **Błażej Gorzolnik**

Date and place of birth: 3.05.1976 Warszawa

Educational Background:

05.2001-02.2006	Ph.D. in Chemistry, *Supervisor:* Prof. Dr. Martin Moeller *Title of Thesis:* "Amphiphilic Block Copolymers as Templates for Particle Formation and Positioning"
05.2001- 10.2003	University of Ulm, Department of Organic Chemistry III /Macromolecular Chemistry (Germany)
11.2003-02.2006	Institute of Technical and Macromolecular Chemistry at RWTH Aachen, (Germany)
1995-2000	M.S. in Chemical Technology Technical University of Gliwice, Department of Chemistry, Faculty: Organic Chemical Technology (Poland); *Supervisor:* Dr. Zbigniew Stec *Title of Thesis:* „Research on Obtaining Dihydroperoxy 2,6-diisopropylnaftalene by Oxidation of 2,6-diisopropylnaftalene"
1991-1995	Secondary School No 2 in Racibórz (Poland)

Employment:

since 05.2006	*Researcher* in Institut de Chimie et des Matériaux Paris-Est (ICMPE), Equipe Systemes Polymeres Complexes, Thiais (France)
11.2003-02.2006	*Research Assistant* at the Institute of Technical and Macromolecular Chemistry at RWTH Aachen (Germany)
05.2001- 10.2003	*Research Assistant* at the University of Ulm, Department of Organic Chemistry III/ Macromolecular Chemistry (Germany)
01-04.2001	*Service, Sale and Promotion Specialist* in PREVAC Sp z o.o. -Precision and Vacuum Technology, Rogów (Poland)

Publications:

P. Mela, B. Gorzolnik, M. Bückins, A. Mourran, J. Mayer, M. Moeller "Low ion dose FIB modification of monomicellar layers for the creation of highly ordered metal nanodots arrays." *Small* (2007). 3, 1368.

X. Zhu, M. A. Scherbina, A. V. Bakirov, B. Gorzolnik, S. N. Chvalun, U. Beginn, M. Möller "Methacrylated Self-Organizing 2,3,4-Tris(alkoxy)benzenesulfonate – a New Concept towards Ion Selective Membrane"- *Chem. Mater.* (2006). 18, 4667.

B. Gorzolnik, P. Mella, M. Moeller "Nano-structured micropatterns by combination of block copolymer self-assembly and UV photolithography" - *Nanotechnology* (2006). 17, 5027.

N. Weiher, E. Bus, B. Gorzolnik, M. Moeller and J.A. van Bokhoven "An *in-situ* and *operando X*-ray absorption spectroscopy set-up for measuring sub-monolayer model and powder catalysts"– *J. Synchrotron Rad.* (2005). 12, 675–679.

Patent:

P. Mela, M. Mott, J. Spatz, B. Gorzolnik, M. Moeller "Photochemical method for manufacturing nanometrically surface decorated substrates" **EP 1760527**

Presentations:

"Design of mesoporous materials with controlled porosity and functionality from nanostructured diblock copolymers" 234th ACS National Meeting, Boston (USA) 19-23. 08. 2007;

"Functional nanoporous materials from ordered block copolymers" POLYNANOCAT meeting, Thiais (France) 5-6.11.2006;

"Micellar Formation of Gold Nanoparticles - Effect of the Solvent", POLYNANO meeting CSEM Neuchatel (Switzerland), 1-3.10.2003;

"Synthesis of Block Copolymers and Deposition of Nanodots", POLYNANO meeting, University of Twente, Enschede (Nederland) 10-11.04.2003;

"Synthesis of Linear and Branched Block Copolymers via Anionic Polymerisation" POLYNANO meeting, Hersonissos, (Greece), 4-5.03.2002